CRANFIELD UNIVERSITY

MAHADI ABD MURAD

AN INTEGRATED STRUCTURAL HEALTH MONITORING
APPROACH TO COMPOSITE-BASED PIPELINE REPAIR

SCHOOL OF ENGINEERING
Offshore, Process and Energy Engineering Department

PhD (Full Time)
Academic Year: 2008-2011

Supervisor: Professor Feargal Brennan

June 2011

CRANFIELD UNIVERSITY

SCHOOL OF ENGINEERING
Offshore, Process and Energy Engineering Department

PhD (Full Time)

Academic Year: 2008-2011

MAHADI ABD MURAD

AN INTEGRATED STRUCTURAL HEALTH MONITORING
APPROACH TO COMPOSITE-BASED PIPELINE REPAIR

Supervisor: Professor Feargal Brennan

June 2011

This thesis is submitted in partial fulfilment of the requirements for the
degree of PhD

ABSTRACT

One of the most common problems in the structural integrity of industrial pipelines is external corrosion. Composite materials have been accepted as a repair option to restore the original strength of the effected damaged section but the approach to analyse how well the composite repair has influenced the stress and strain distributions between the reinforced steel and the reinforcing composite is yet to be determined. This approach is required since it can increase the confidence level among pipeline operators or manufacturers in terms of the composite repair solution that they have chosen or offered.

The aim of this study was to develop an integrated approach that could provide a complete methodology to assess the integrity of pipeline systems, especially in quantifying the level of reinforcement provided by the repair in the elastic working region. This cannot be achieved by the traditional method that only relies on classical mechanics derived from strength of materials and compatibility relations. To fulfil this aim, efforts included the simulation of a fibre glass composite repair system using finite element analysis (ABAQUS) software, design and fabrication of the pressure and temperature test rig, installation of fibre glass composite material, and data acquisition.

The arc-shaped notch defect that has never been studied before was chosen in the study of stress concentration and bonding integrity of the composite repair system and further validated experimentally using the test rig. The numerical results of this work demonstrated different stress concentration values as the arc-shaped defect size increased. With a proper test plan, the optimum repair system that contains variable lengths of the arc-shaped defect and different lengths as well as thicknesses of the composite material was achieved in the stress distribution study. The bonding integrity via strain distribution study was further validated experimentally. The experimental pressure test results showed some good agreement, especially in the hoop load transfer and limitations of the simulation works were adequately addressed. The experimental temperature results managed to show how the thermal strain behaved in the anisotropic Triaxial Woven Fibre composite repair system.

This approach is useful for a better acquisition of information that enables the diagnosis and prognosis of the pipeline repair system prior to installation on site. The novelty of this technique is in its ability to analyse the load transfer in a composite repair system in a more efficient way which can save time and cost.

ACKNOWLEDGEMENTS

TABLE OF CONTENTS

LIST OF FIGURES

LIST OF TABLES

NOMENCLATURES

ACFM	Alternating Current Field Measurement
ACPD	Alternating Current Potential Drop
ACORES	Association of Composite Repair Suppliers
AFC	Active Fibre Composite
ASCM	Alternating Current Stress Measurement
CHESS	Composite Hull Embedded Sensor System
CFRP	Carbon Fibre Reinforced Polymer
CPU	Central Processing Unit
CTE	Coefficient of Thermal Expansion
DCPD	Direct Current Potential Drop
DMA	Dynamic Mechanical Analysis
DSV	Differential Scanning Calorimetry
EB-IMP	Engineering-Based Integrity Management Programme
EFPI	Extrinsic Fabry Perot Interferometer
FBG	Fibre Bragg Grating
FE	Finite Element
FEM	Finite Element Method
GF	Gauge Factor
GFRP	Glass Fibre Reinforced Polymer
HSE	Health and Safety Executive
ILI	In-Line Inspection
K_t^h	Hoop Stress Concentration Factor
K_t^a	Axial Stress Concentration Factor
K_t	Theoretical Stress Concentration
L	Composite Repair length
MFC	Macro-Fibre Composite
MFL	Magnetic Flux Leakage
NDE	Non Destructive Examination
NDT	Non Destructive Test
NPS	Nominal Pipe Size
OFDR	Optical Frequency Domain Reflectometry
OFS	Optical Fibre Sensor
OPS	Office of Pipeline Safety
OTDR	Optical Time Domain Reflectometry
P	Composite Repair Thickness
PDE	Partial Differential Equation
PLC	Programmable Logic Controller
POD	Probability of Detection
POS	Probability of Sizing
PRI	Pipeline Repair Index
PVC	Polyvinyl Chloride
PVDF	Polyvinylidene Fluoride
RBI	Risk Based Inspection

RSG	Rectangular Strain Gauge
RVE	Representative Volume Element
SCADA	Supervisory Control and Data Acquisition
SCC	Stress Corrosion Cracking
SCF	Stress Concentration Factor
SCFR %	Percentage of Stress Concentration Factor Reduction
SIMdex	Structural Integrity Monitoring Index
S-T-C	Self-Temperature-Compensation
SHM	Structural Health Monitoring
SIF	Stress Intensity Factor
SIM	Structural Integrity Monitoring
SRA	Structural Reliability Analysis
σ_{max}	Maximum Stress at the Defect
σ_{nom}	Nominal Stress away from the Defect
ε	Strain
TG	Thermogravimetry
TDR	Time Domain Reflectometry
TMA	Thermomechanical Analysis
TWF	Triaxial Woven Fabric
v_f	Fibre Volume Fraction
V_f	Volume Percent for Reinforcement Content
V_m	Volume Percent for Matrix Content
W	Notch Length
w_f	Weight of Fibre
w_m	Weight of Matrix
W_m	Weight Percent for Matrix Content
XFEM	Extended Finite Element Method

1 INTRODUCTION

One of the most common problems in the structural integrity of industrial pipelines is external corrosion. This external corrosion is normally driven by two factors, namely the environment and the age of the pipeline itself. So, much effort has been put in by many companies, individuals and others in upholding the integrity of these ageing pipelines and solving the external corrosion problem. The key success to realising the extension of pipeline life with proper protection is counting on a systematic strategy on how to develop and implement integrity management programmes by each pipeline operator. Based on the data generated by the inspection programme for instance, an operator can go forward and make decisions related to the current and future integrity of a pipeline, remaining life assessment, and appropriate preventative maintenance and inspection activities to maintain the design plan for the pipeline.

The four components namely Assessment, Monitoring, Mitigation, and Life Extension are shown in Figure 1.1 and they provide the means to develop a comprehensive integrity management programme and meet specific needs and situations for each pipeline operator and pipeline system. One of the important criteria to ensure the success of this integrity management programme is to know how the repair of the pipeline has been evaluated. Composite materials, for example, have been accepted as a repair option to restore the original strength of the effected damaged section, but the approach to analyse how well the composite repair has influenced the stress and strain distributions under the influence of internal pressure and temperature between the reinforced steel and the reinforcing composite is yet to be determined. Hence, this integrity management really needs a good approach that can increase the confidence level among the pipeline operators and manufacturers.

An integrated Structural Health Monitoring approach in composite based pipeline repair is novel because it provides an overview of the whole pipeline integrity management programme. For example, the nature of the defect is properly assessed and then further explored using the finite element method. ABAQUS software has been used in this simulation work and the data acquisition of strain measurement was carried

out using the Compact Rio system with Labview software, together with strain gauges. Real time monitoring and data acquisition are able to provide the diagnosis and prognosis of the structural system at any given time. If the repair is not able to restore the damage, then the related pipe shall be mitigated immediately. Otherwise, the integrity management programme will then focus on the life extension programme which can contribute to more cost savings for pipeline operators.
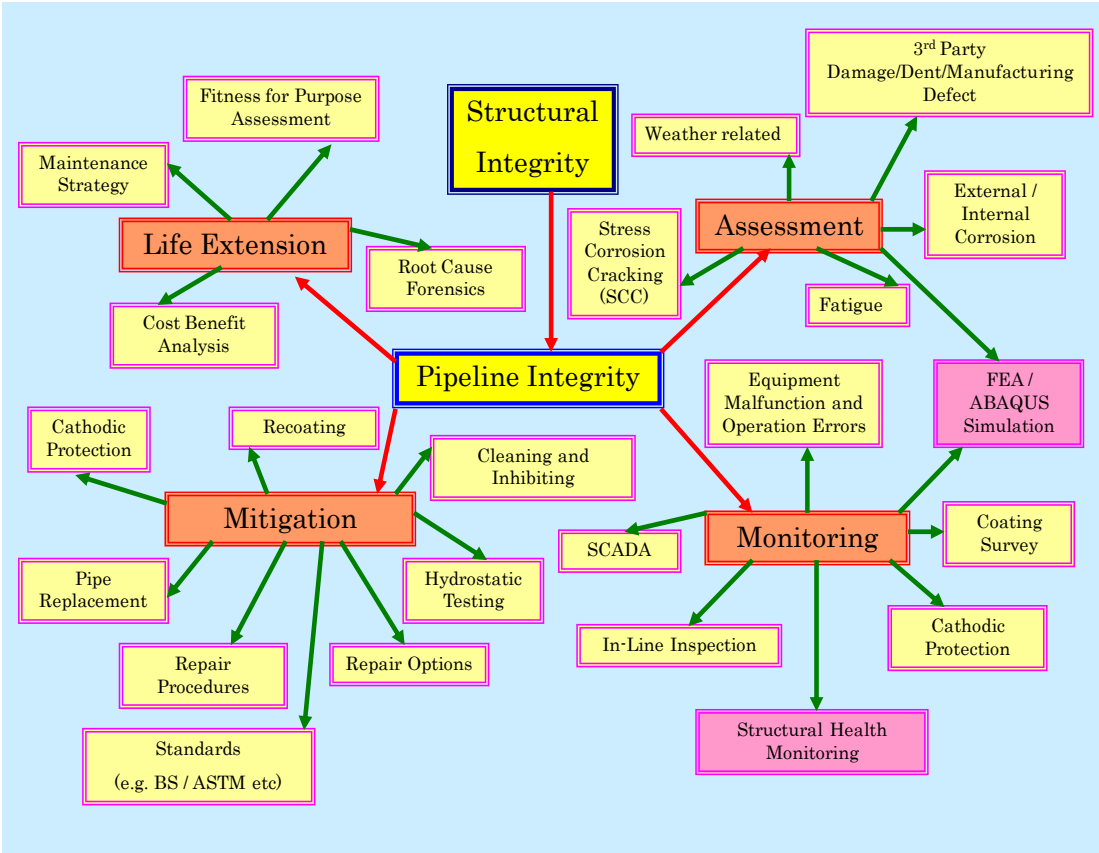
Figure 1.1: Summary of Pipeline Integrity Management programme

1.1   Objectives

Knowing this background, the objectives of this PhD study are shown below;

1. To analyse blunt defect (external corrosion) behaviour in a composite based pipeline repair system using a numerical finite element analysis (ABAQUS) and validate by experiment.

2. To prove the integrity of bonding between the base structure (pipeline) that contains defects and the reinforced composite wraps as a reliable solution in the elastic load transfers or distributions.

3. To develop a methodology for measuring the coefficient of thermal expansion of test materials (i.e. steel and composite).

These objectives were accomplished by designing and fabricating the simple and yet versatile pressure and temperature steel test rig. One of the test rig segments was introduced with an artificial arc-shaped defect on it that mimics real corrosion. Next, stress concentration and stress strain distribution studies were carried out using ABAQUS software and the strain distribution study was validated by the experimental work after the composite repair was carried out on the defect area.

In the strain measurement experimental work, rectangular strain gauges with 120 and 350 Ohms were bonded on a steel test rig and composite respectively and the data acquisition was carried out using the robust Compact Rio system together Labview software. Under the influence of the actual internal pressure loading, the numerical study of blunt defect (external corrosion) behaviour in the composite based repair was validated and the integrity of bonding between the base structure and composite repair was analysed and discussed.

Finally, by using a simple surface temperature detector or infrared laser thermometer, together with rectangular strain gauges and strain indicator, the coefficient of thermal expansion (CTE) of the steel specimen (i.e. part of the steel test rig) and the

Triaxial Woven Fibre (TWF) composite (repair material) were measured and further analysis was carried out.

1.2 Contributions of the Work

In pipeline repairs, there is no research that has been carried out so far in analysing the stress strain behaviour between the reinforced materials (i.e. steel) that contain arc-shaped defects and reinforcing material (i.e. composite) in the elastic working region. This study provides a methodology of the integrated Structural Health Monitoring (SHM) approach using numerical analysis (ABAQUS) and experiments that can provide insight into the optimisation of the composite repair thickness and length as a function of defect geometry. Using the conventional (analytical) method alone does not give a true picture of how well the stresses and strains behave when the above parameters (i.e. composite repair thickness, length and defect size) vary.

Although the simulation using ABAQUS can show better stress strain distributions in the composite repair, it is still inadequate because the composite repair is usually modelled at the macro-mechanics level whereby the material is presumed to be homogeneous and the effects of the constituent materials are detected only as averaged apparent properties of the composite (McGraw-Hill, 2003) and is anisotropic. According to Car et al. (2001), anisotropic material is one which exhibits properties with different values when measured in different directions. Often, there are some assumptions and errors involved. So no model so far can claim to produce exact behaviours of this stress strain distribution without a proper validation from the experiment. Therefore, this study proves that these objectives can be achieved if sensible procedures and guidelines are properly planned and established. Additionally, this integrated approach also demonstrates the easiest way to determine the coefficient of thermal expansion of the anisotropic composite without applying the standard laboratory procedures which are more expensive and complicated.

The methodology of this integrated approach can benefit pipeline manufacturers at large if it can be implemented during the design and operation stages of the composite repair that usually involve different material types (e.g. carbon fibre, glass fibre and others), dimensions etc. Through this, the integrity of bonding can be assessed in the most economic and effective way. Lastly, this integrated approach can also be considered as one of the potential structural health monitoring techniques that can be used on site because of its remarkable and convincing results that show good agreements between simulations and experiments. Figure 1.2 shows the methodology of this integrated pipeline repair.
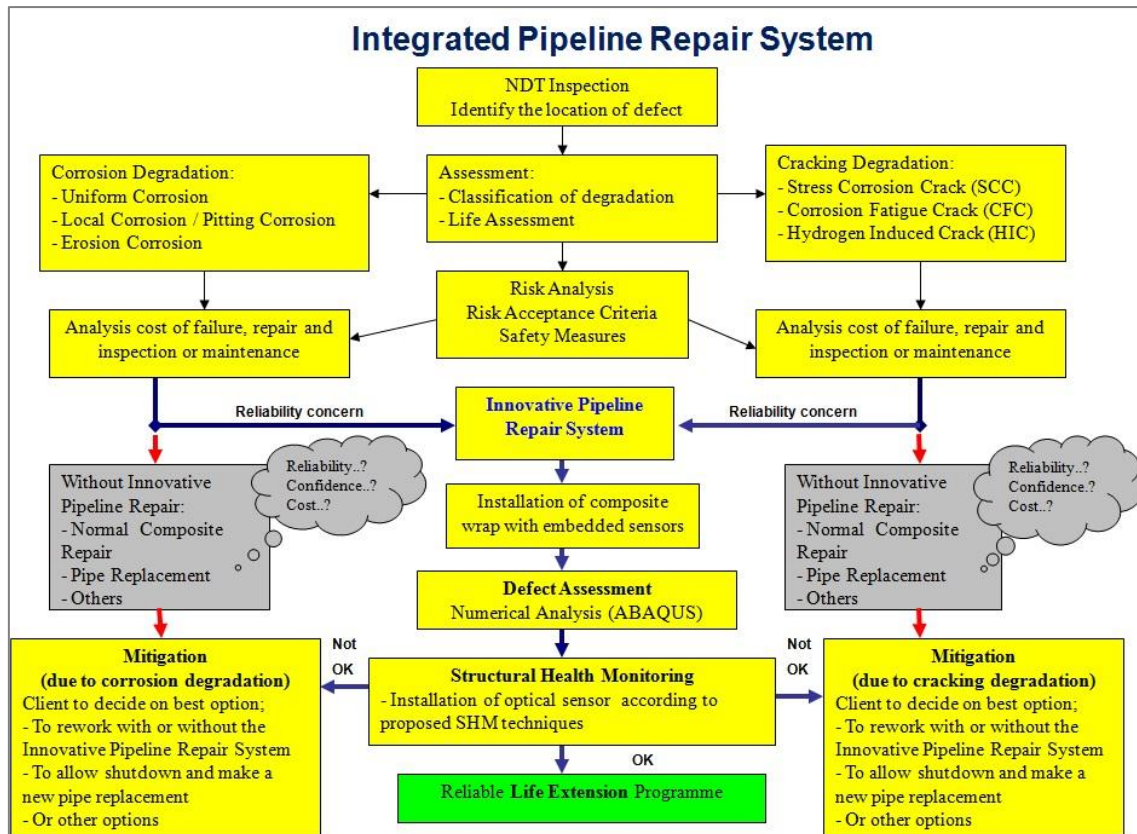
Figure 1.2: The Methodology of Integrated Pipeline Repair System

1.3   Summary and Layout of the Thesis

The following chapter provides a literature review on Structural Integrity (SI) in pipelines. The review provides some actions taken in achieving the stated objectives. The objectives and contributions of this thesis have been discussed in Chapter 1.

Chapter 2 discusses pipeline damages that have been inspected and monitored by many methods. This chapter highlights that the reliability of information has played a significant role in determining the intervals of inspection, and maintenance which includes composite repairs. Maintenance strategy and corrective and preventive actions are also explained. Some comparisons of Structural Health Monitoring (SHM) using Optical Fibre Sensors (OFSs) and electrical sensors are discussed. This chapter also discusses the literature on finite element analysis (FEA) and experimental approaches, and ends with answers for the question why SHM is really important in the composite repair.

Chapter 3 describes the numerical analyses that involve the influence of pressure on the FEA pipe model, stress concentration factor study, and simulation works on the composite repair. Chapter 3 is considered to be one of the most important chapters in this PhD study.

Chapter 4 describes the SHM technique used in stress strain analysis of composite based pipeline repair. This includes the methodology for the experiments, strain gauge application, analysis and validation of results. The gap of knowledge in the composite repair, especially during analysing the integrity of bonding between different materials, is addressed. All the project activities that are related to this study are further presented in the Appendices.

In Chapter 5, the thermo-mechanical behavior of the composite that was used in the experimental work is described. This includes the methodology for the temperature test, the coefficient of thermal expansion (CTE) results etc.

Chapter 6 contains the summary and future works of the PhD thesis. The thesis concludes with a List of References and Appendices. The detailed calculations of the test rig development are also included in the Appendices.

2 LITERATURE REVIEW ON STRUCTURAL INTEGRITY

2.1 Introduction

This chapter presents an overview of relevant research that has been carried out for the topics proposed in this study. Initially, the scenario of current pipeline problems and condition assessment, which includes inspection, monitoring and reliability of information, is presented. Next, maintenance strategy, and corrective and preventive actions in terms of pipeline repair are also presented. These include the current practice of composite repairs which refers to relevant standards as part of the maintenance strategy. Afterwards, an overview of structural health monitoring as a preventive solution is explored, and a brief discussion on Finite Element Analysis (FEA) and experiments as an integrated Structural Health Monitoring (SHM) approach to the composite based pipeline repair are presented. This chapter ends with a summary and conclusions.

2.2 Pipeline damage scenario

One of the most important problems facing pipeline engineers at the beginning of the 21st century is ensuring the reliability and safety of operating gas and oil pipelines. The large number of pipe ruptures in recent years has led to loss of human life, the destruction of dwellings and industrial facilities, and huge environmental losses (Kaminskii and Bastun, 1997). To meet safety and environmental regulations, and operate cost effectively, striking the right balance between operational costs versus performance and potential failures is the main challenge (www.dnvsoftware.com, 2006).

In the North Sea, as highlighted by Clausard (2006), many assets have been in operation more than 20 years and have almost reached the end of their design lives of 25-30 years. Kotrechko et al. (2002) in their study, also mention that the operating

period of the major part of the existing pipelines can be estimated as 20-30 years only. But, as oil prices increase, oil companies cannot afford to shut down production despite the threat of ageing problems (Alexander's Gas & Oil Connections, 2005). As a result, this long operating time leads not only to the appearance of macro defects but also affects the mechanical properties of pipelines, as addressed by Thodi et al. (2008), and changes to the material and/or geometric properties of these systems, including changes to the boundary conditions and system connectivity which are defined as damage by Farrar and Worden (2007), adversely affecting the system's performance.

According to statistics, every second failure has been caused by metal degradation (Lebedev et al., 2003); this is also agreed by Sosnovskii and Vorob'ev (2000) who, in their literature study, list a few main factors as being responsible for the deterioration of material properties and that threaten the integrity of the assets, thus becoming the inducing factors to failures. Normally, this phenomenon occurs during the operation itself and, inevitably, the mechanical properties undergo changes. The main factors are: mechanical loads, temperature and environment.

Fatigue is another factor that causes pipeline damage. According to Benham et al. (1996), it happens when a material is subjected to cyclic or fluctuating strains at nominal stresses that have maximum values less than the static yield strength of the material. The resulting stress may be below the ultimate tensile stress, or even the yield stress of the material, yet still cause catastrophic failure. They also mention that fatigue mechanism has influenced the stress concentration to play a major part in causing failure. Brennan (2008) explains that fatigue mechanism has two distinct phases: crack initiation which is based on strain life (e.g. low cycle pressure vessel) and stress life (e.g. high cycle gas turbine blade), and crack propagation. A good example of the crack initiation and propagation study has been carried out by Brennan et al. (2007). They have developed a technique termed controlled stitched cold working which applies different intensities of compressive residual stress at specific regions in a structure. This technique has considerably influenced the fatigue crack propagation by containing crack propagation in one primary direction (i.e. crack growth restricted in one direction); one

9

of the fracture surface photos is shown in Figure 2.1. One of their main objectives is to develop the concept of controlled failure design.

Figure 2.1: Surface fracture due to fatigue (Brennan et al., 2007)

The earlier experiment by Student et al. (1999) shows that the long-term action of the stress field and high temperature working environments can cause non-uniformity of the process fatigue crack growth or propagation. Based on European Framework IV project MONITOR, as presented by Fixter and Williamson (2006) in Figure 2.2, shows fatigue has contributed the highest defect percentage in metallic structures.
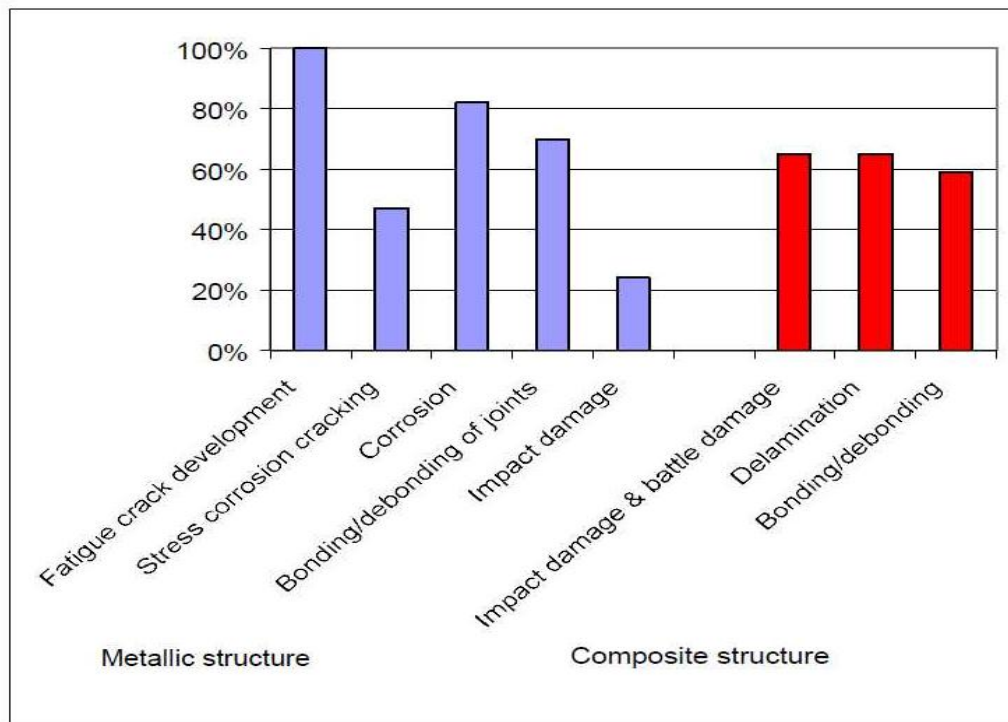
Figure 2.2: Reported interest in defect types (Fixter and Williamson, 2006)

Corrosion is defined as loss of material as a result of chemical reaction between a metal or metal alloy and its environment (Thodi et al., 2008). They point out the major corrosion mechanisms for pipeline installations include uniform corrosion, as shown in Figure 2.3, localised or pitting corrosion, and erosion corrosion, as referred to in their risk-based integrity assessment using the Bayes Theorem and actual inspection data.

Figure 2.3: Excessive corrosion occurs on the surface of refinery pipeline

(Thodi et al., 2008)

The results obtained by Sosnovskii and Vorob'ev (2000) also show some significant effects of corrosion on the general fatigue strength degradation of steel pipe. Prior to operation, they observed a higher strength in the inner pipe surface in comparison to the outer one but after the operation, the outer surface was determined to be stronger. After a long period of operation, the wall thickness of the pipe had decreased by 13% because of the erosion corrosion process. Besides fatigue and corrosion being the main causes for structural degradation, damage such as dents caused by third parties, pipeline operators or contractors (Brownlee and Alexander, 2007), vandalism (Bruno, 2008), wrinkles (Alexander, 2009; Kulkarni and Alexander, 2008) and creep (Benham et al., 1996) can also cause pipeline damage.

Figure 2.4: Dent damage caused by vandalism (Left) and failure due to dent (Right) (Bruno, 2008)

Figure 2.4 shows that as a result of dents, the contour of the pipe has been changed which leads to local areas of high strain (Bruno, 2008). When this damage occurs, the pipe may fail immediately or may continue to operate for some time before failing.

A good study on creep by Harada et al. (1999) can be referred to. They performed tests on reactor coolant system (RCS) piping failure, along with high temperature, tensile and creep rupture tests, including metallography, to investigate failure behaviour. Figure 2.5 shows photos of crack development due to creep damage. Intragranular (transgranular) cracks occur in the fractured tensile specimen at room temperature as referred to in photo (a). Other photos show that intergranular cracks predominately occur in the creep damaged specimen to rupture at (b) 600ºC in 87 hours; (c) 800ºC in 85 hours and; (d) 1150ºC in 94 hours.
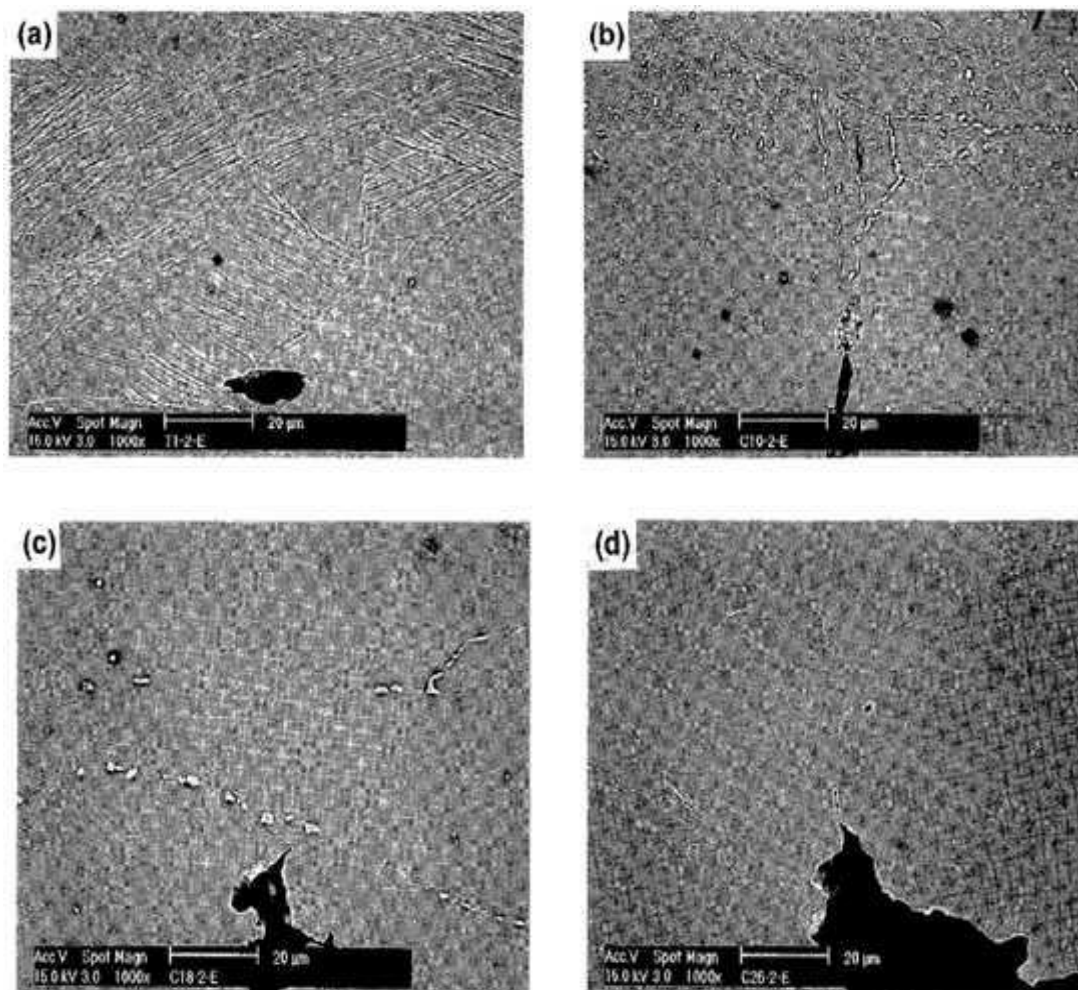
Figure 2.5: Back-scattered micrographs of the influence of time and precipitation in deformed gauge portions of specimens for hot extruded type 316 stainless steel piping (Harada et al., 1999)

2.3   Condition Assessment of Ageing Pipelines

Often, age-related deterioration such as fatigue cracking, corrosion, mechanical damage and others, as discussed above, can give rise to significant issues in terms of safety, health, environment and financial expenditures. Hence, it is of great importance to develop advanced technologies which can allow for the proper management and control of such age-related deterioration. Brennan et al. (2006) for example, have

presented current practices, recent advances and future trends on the condition assessment of ageing structures – namely ships. There is no reason why their report, which involves condition assessment with inspection, monitoring and reliability of information, cannot be applied to other structures including pipelines.

In the context of ageing pipelines, Wayman (2008) mentions that condition assessment involves the development of an understanding of the current pipeline performance under applied loads. Generally, this process provides a prediction of the remaining life of the pipeline based on leakage and structural failure criteria. Hence, the long-term maintenance requirement can be defined immediately and future investment requirement can be predicted.

PICA Corp (2011) provides direct condition assessment of pipelines through the use of in-line inspection (ILI) tools. According to them, direct condition assessment is the only way for asset managers to truly know if a pipeline can be repaired, rehabilitated or replaced, by the use of electromagnetic technology which does not require the sensors to be in contact with either the inside or outside of the pipe. Their condition assessment provides accurate measurements of remaining wall thickness, leaks etc.

2.3.1 Pipeline Inspection Technology

According to Palmer and King (2008), inspection is generally regarded as providing snapshots in time of the material condition and the hard factual data from which the condition of the pipeline can be deduced and remaining life estimated. The aim of the pipeline inspection technology that is being developed by many operators is to detect and quantify the damage which leads to failures in any structures as reported by ETD Ltd. (2003). According to Jaske et al. (2002), pipeline inspection typically reveals a number of anomalies in a pipeline system. Often, these anomalies are evaluated to determine if they are manufacturing defects, mechanical damage, cracking, or corrosion before the final determination is documented in the inspection report.

In the ferrous pipeline condition assessment, Wayman (2008) uses a range of available ultrasonic and magnetic inspection tools that can provide sizing and imaging of pipe wall deterioration including internal and external defects. Besides these two tools, acoustic transducer using the Lamb wave mode can also determine defects. However, it works through the interaction of Lamb waves with defects rather than a direct measurement on the wall thickness. According to Sinha (2005), the Microwave Droppler Interference technique has accomplished much the same as the acoustic technique but has advantages over the acoustic technique. One of the advantages is that the measurements are invariant with regard to the pressure or flow of in the gas inside the pipe.

According to Matelect Ltd. (2004), ACPD (Alternating Current Potential Drop) is used to measure crack depth and, in general, it is suitable for both high and low frequency fatigue studies where pulsed DCPD (Direct Current Potential Drop) is only suitable for low frequency work. Undoubtedly, Ultrasonic, X-Ray and Eddy Current techniques are three NDT methods that are most common in the assessment of the geometry and the detection and location of flaws in structures. The major aspect in using these methods is related to defect characterisation as mentioned by Habib and Nahas (1998).

Dover et al. (2001) introduce a new non-contacting stress measurement system. The ASCM (Alternating Current Stress Measurement) Stressprobe can be used to measure both static load, e.g. in subsea clamp, bolts, beams and pipes, and cyclic stress. They are the first to have investigated the use of ACSM as a stress monitoring system. Han et al. (2002) report that by using this ACSM, residual stress from the orthogonal magnetic field model can be calculated. They mention that the ACSM system developed from the TSC Inspection Systems provides a far more uniform magnetic field test specimen compared with that achieved by other researchers. Their model allows expansion of the applicability of ACSM to the prediction of readings under biaxial stress conditions. This shows that ACSM is capable of monitoring structural integrity against fatigue through residual stress measurement and its relaxation.

16

Energy Workforce Sdn Bhd (2011) claim that their ACFM (Alternating Current Field Measurement) unit has significant advantages over conventional magnetic and dye-penetrant techniques. ACFM provides surface and near surface examination without coating removal. It is at least five times faster than the above-mentioned techniques, providing accurate sizing of defect (i.e. length and depth) (Energy Workforce Sdn Bhd, 2011). However, conventional techniques are still used and acceptable in any engineering works because of their simplicity and for economic reasons. According to Brennan et al. (2006) a visual examination should determine the type of crack and assess whether it is likely to propagate. Magnetic particle and dye-penetrant tests provide approximate measurements of surface crack length but not crack depth.

2.3.1.1   Risk Based Inspection (RBI)

According to Emslie and Gibson (2010), industry today is embracing the Risk Based Inspection (RBI) approach with the key outcome of any RBI being a prioritised and focused inspection schedule. In other words, RBI is replacing the conventional time-based inspection method. Lloyds Register (2011) defines RBI as a method in which priorities are assigned to inspection based on a risk analysis and Brennan et al. (2006) define risk as the probability of occurrence of a hazard times its consequence.

Canaway (2011) highlights that RBI can imperatively reduce lifestyle cost by basing inspection on risk of incurring damage, rather than on arbitrary periods. The aim of RBI is to develop an inspection plan that is able to identify the potential deterioration mechanism and threats to the integrity of the equipment as well as to assess the consequences and risk failures. This ensures high risk items are correctly scrutinised and produces a safety focused and cost effective inspection scheme. Emslie and Gibson (2010) point out that RBI is now recognised as a key tool in meeting legislative requirements (i.e. HSE's best practice guidelines).

2.3.2 Pipeline Monitoring

Monitoring is often done on a more frequent basis than inspection, and it provides more global information as referred to by Palmer and King (2008). According to them, monitoring will only be used as an adjunct to inspection and for a specific function, and is often a requirement that is beyond the scope of the inspection techniques. ETD Ltd. (2003) highlight that monitoring shall allow the targeting of inspections to the most highly stressed areas.

Effective continuous pipeline monitoring is essential and has saved the day in many parts of the world. Mahgerefteh and Atti (2006) and Mahgerefteh and Abbasi (2007) have provided a selection of examples of lack of monitoring leading to these examples include the one of the most catastrophic types of accidents for example Piper Alpha tragedy on 6 July 1988 that killed 167 men with the total insured loss of about £1.7 Billion and the Belgium pipeline rupture incident on 30 July 2004 resulted in 24 deaths and 120 injuries. The incident of a natural gas explosion in Virginia on 14 September 2008 which destroyed a residential building and injured five people nearby is another example of what can happen if there is a lack of proper monitoring. According to Pipeline Monitoring Ltd. (2011), there are two types of effective pipeline monitoring system which can avoid the future accident due to lack of monitoring. The first type monitors the strain placed on the actual pipeline which is normally due to internal or thermodynamic stress. The second monitors the surrounding geologic medium externally, for example by measuring displacement in the rock or soil that encases the pipelines.

Pipeline Monitoring Ltd. (2011) also mentions that today there are many advanced methods of pipeline monitoring. TDR (Time Domain Reflectometry) which transmits a pulse of energy as a waveform and also measures reflections of this transmission, is able to calculate the distance to a disturbance within the pipeline. OTDR (Optical Time Domain Reflectometry) is more advanced than TDR and is very useful in monitoring ground motion along pipeline routes and therefore helps avert failure. Zostrich Geotechnical Ltd. (2001) also claims that no other technique currently

available provides real time detection of ground motion with associated warning and remediation potential as does TDR or OTDR.

Instead of using time domain, LIOS Technology Inc. (2010) has developed a distributed temperature monitoring system that comprises a range of real time fibre optic based linear temperature measuring devices. It measures the temperature profiles along optical fibres up to 30 km with a single ended, single mode fibre. The spatial resolution is achieved by OFDR (Optical Frequency Domain Reflectometry). With the advanced controller, the system can be operated from a remote location without a PC and transfer data via standard network protocols to PCs in control centres, SCADA or PLC systems.

Roctest Ltd (2011) highlights that the main concern for pipeline owners or operators at present is the possible leakages which can cause a severe impact on the environment and result in a shutdown for repair or replacement. Earthquakes, landslides, corrosion, wear, material flaws, or third party intrusion, are possible causes for leakages. Therefore, they have provided integrated monitoring solutions for pipelines not only to detect leakages but also to measure local and distributed temperature, soil stability and pipe corrosion. With this integrated pipeline monitoring, they have also developed a methodology to design and implement an optimal Structural Health Monitoring (SHM) system for any pipelines which will be discussed further in the next section.

Although the potential benefits of applying long-term continuous monitoring are well publicised, little attention has been paid to determining how well such systems perform their intended task. De Leeuw and Brennan (2009) present the Structural Integrity Monitoring Index (SIMdex) that can provide a measure of the performance of a particular monitoring system and is based on its ability to measure the actual damaging stresses within a component. SIMdex provides a quick and robust approach to assessing the performance of stress monitoring system under different conditions. Although parameters such as probability of detection (POD) and probability of sizing (POS) are available, De Leeuw and Brennan (2009) also mention that no such approach exists for stress or strain monitoring applications. Unlike the traditional statistical

approaches (i.e. POD and POS) which rely on a single measurement taken at a particular point in time, with structural integrity monitoring (SIM), the continuous collection of data over a longer period of time is possible. The assessment process takes into account the stage of the lifetime of the structure which is being monitored and the S-N curve for the welded steel plate joint for example, is expressed as Log (N) = 11.705 – 3Log(S) and is plotted on a log-log scale as illustrated in Figure 2.6.
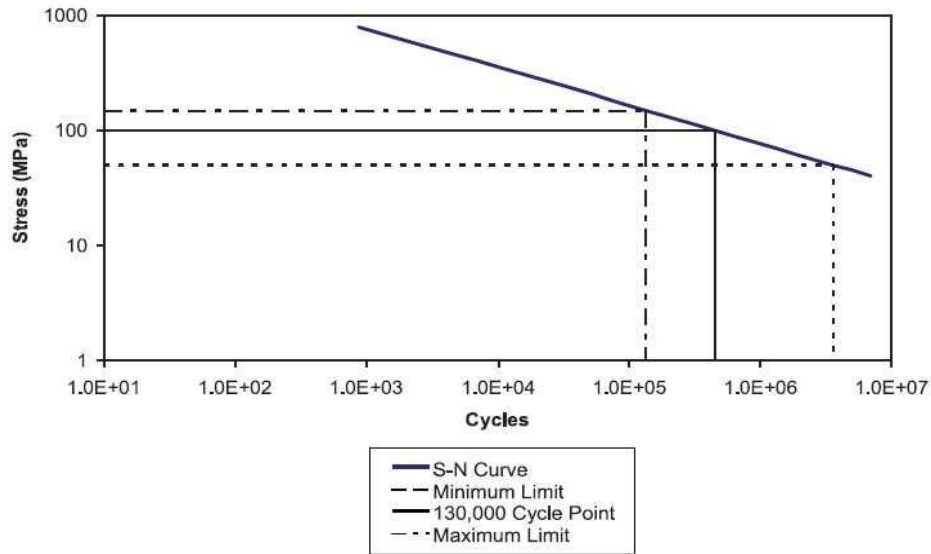
Figure 2.6: Stress life curve and SIMdex limit setting after 130 000 cycles on a log scale (De Leeuw and Brennan, 2009)

Brennan (2007) also presents several other case studies of stress monitoring in rail application and steel structures. According to him, a wireless and self-powered stress memory system is able to identify components which, by the nature of their history, are more likely to contain stress-related flaws. As explained earlier, the conventional POD and POS can only tell the existence, type, size of the flaw and location at any point in time but not give any indication of whether or not a flaw is likely to develop. Therefore, this type of memory system has the possibility to be explored further for pipeline structures and research works are required to prove the effectiveness of this system in continuous pipeline stress monitoring.

2.3.3 Reliability Analysis of Information

Hallen et al. (2003) explain how the use of probabilistic condition assessment to evaluate the integrity condition of corroding pipelines is beneficial to the operator or owner of pipelines because the uncertainties associated with in-line inspection (ILI) tools, pipeline geometry, corrosion growth rate and others can be modelled and considered over any chosen time period. By using the structural reliability methods, the probability of failures can be determined for the entire pipeline. The target probabilities which are established either from the historic failure rates (Greenwood, 2002) or from risk criteria (ERSG Ltd., 2009), will allow the operator to formulate cost-effective strategies for the future safe design and operation of the pipelines as agreed by Britto et al. (2010). By referring to reliability criteria and risk factors, Kharionovski (2006) has demonstrated his established express method which yields approximate expectations for the remaining gas pipeline service life-span.

In their approach to determine the actions that guarantee the safe operation and cost-effective maintenance of the corroded pipeline over its expected service life, Hallen et al. (2003) present how this comparison is carried out in order to assess the benefits of remedial actions such as conducting repairs, as illustrated in Figure 2.7. According to them, the time it takes the failure probability to exceed the target probability is assumed to be the remaining safe life of the pipeline and the time to the next inspection. Figure 2.8 shows the scheme used to investigate the relationship between composite repairs, maximum allowable operating pressure (MAOP), corrosion growth rate and remaining safe life of the assessed pipeline. From that figure, as the composite repairs increase, the corrosion rate will reduce and the remaining life will increase significantly. Figure 2.9 shows the relationship between composite repairs and re-inspection intervals. As the number of composite repair increases, the re-inspection interval will be longer.
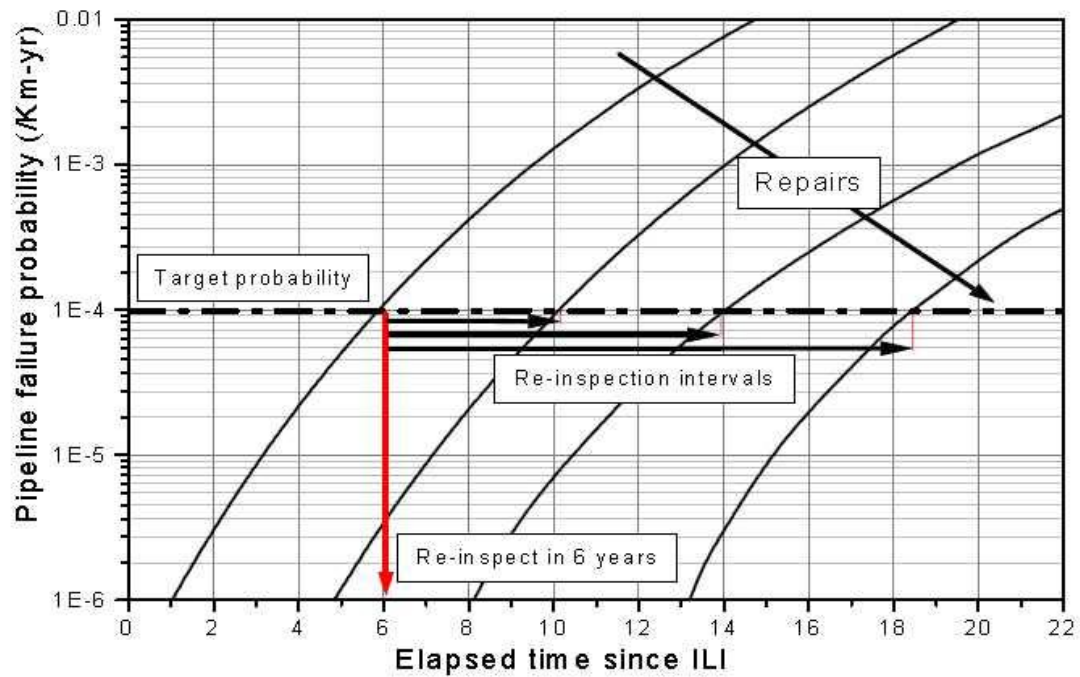
Figure 2.7: An example of integrity management from comparison of pipeline failure probability with target reliability levels - Benefits of conducting repairs (Hallen et al., 2003)
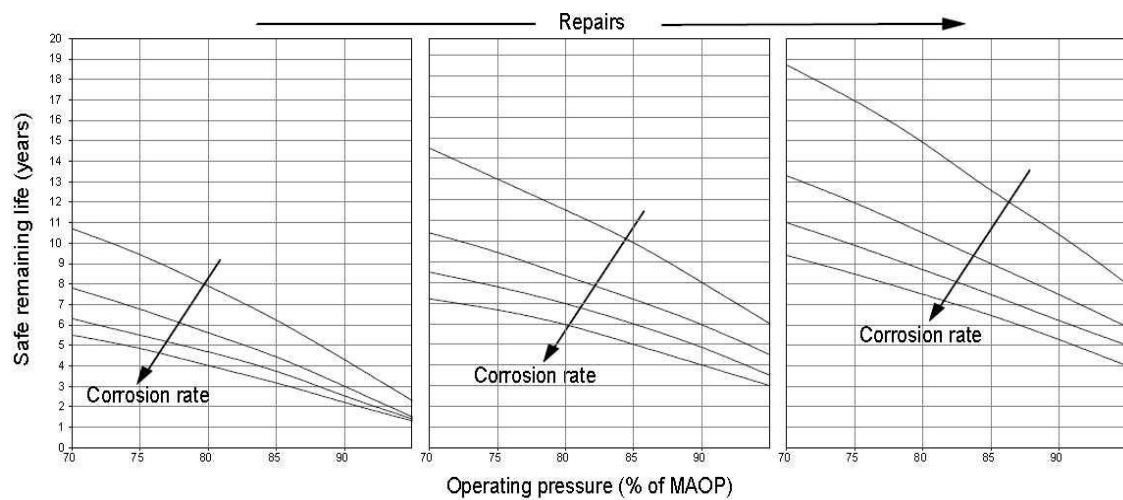
Figure 2.8: An example of integrity management from comparison of pipeline failure probability with target reliability levels - Relationship between repairs, corrosion rate, operating pressure and pipeline's safe remaining life (Hallen et al., 2003)

22
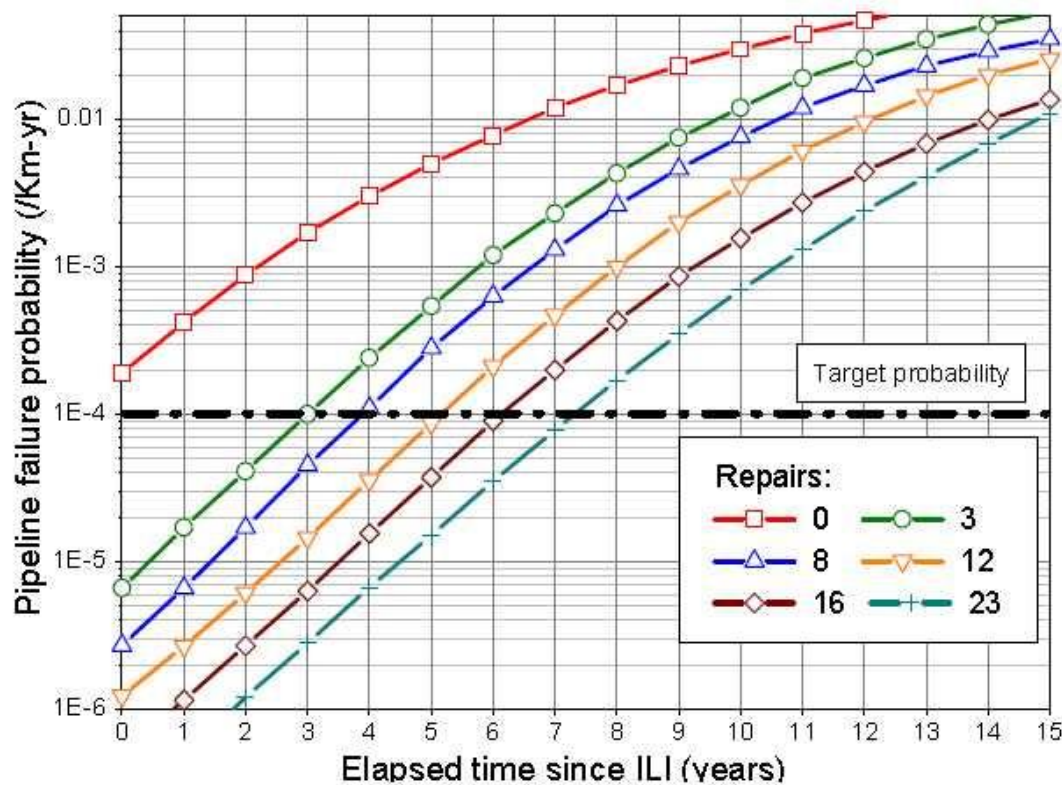
Figure 2.9: Pipeline failure probability with time. Effect of repairs on safe working life (time to next inspection) and re-inspection intervals (Hallen et al., 2003)

According to Wayman (2008), when the system containing large numbers of interdependent variables with associated uncertainties cannot be dealt with effectively in a wholly deterministic manner (Brennan et al., 2006) or direct inspection such as using a pig mounted system is not possible (Wayman, 2008), then probabilistic means or statistical models to predict the condition of length of pipeline based on selective external local inspection are required.

Therefore, the reliability of information literally depends on the pipeline damage database created, based on the result of pipeline inspection and monitoring. According to Greenwood (2002), the purpose of having a damage database or information is to:

- Estimate leak and pipeline rupture frequencies, based directly on historical failure rates data

23

- Provide the means to estimate failure rates for risk assessment for pipelines

- Provide a more realistic and rigorous approach to the design of pipelines

- Determine the effect of engineering changes (e.g. wall thickness of pipe)

In an effort to develop the damage database, as addressed by Greenwood (2002) above, Brennan et al. (2009) recommend reliability-based analysis procedures and uncertainty models should be further developed and refined, adopting a systematic approach. The reliability has to be estimated in a reliability-based decision format. More organisations are strongly encouraged to cooperate in obtaining reliable failure data and a proper format of data recording is also needed. Forsyth (1998) also has a similar opinion to Brennan et al. (2009) in terms of reliability of information. Without the cooperation of many organisations, the best reliability data that require a significant number of flawed or flaw-free components will be always expensive. Because of these limitations, NDE reliability is often estimated by using artificially generated flaws or even computer models.

Francis (2011) presents an evaluation of the likelihood of failure occurring rather than the evaluation of consequences. For this purpose, he uses structural reliability analysis (SRA) that comprises six elements: establishment of limit states, identification of failure modes, formation of limit state functions, uncertainties analysis, evaluation of failure probability and assessment of result. He demonstrates how this probabilistic reliability analysis approach can be used specifically for the purpose of inspection and maintenance scheduling. According to Simola et al. (2009), the intention of developing the probabilistic approach is to capture the main random behaviour and uncertainties based as much as possible on data that is obtained from service records and damage statistics.

Brennan et al. (2009) also agree with the above researchers that it is preferable to use a probabilistic model for presenting the degradation processes and that such a model should reflect various uncertainties and can be updated based on the latest information on structural conditions which becomes available during inspections.

24

2.3.3.1   NDT Reliability and POD curves

Georgiou (2006) defines NDT reliability as the probability of detecting a crack in a given size group under the inspection conditions and procedures specified. In the NDT reliability methods, there are two related probabilistic methods for analysing reliability data and producing POD curves as functions of the flaw size a. According to him, repeat inspections of the same flaw size or the same flaw type will not necessarily result in consistent hit or miss indications. Therefore, there is a spread of detection results for each flaw size and flaw type and this is precisely why detection capability is expressed in statistical terms as POD. The POD curves provide reference to results that have been obtained for particular flaws using specific NDT procedures.

There have been many researchers who put great effort into improving this reliability approach that involves POD and POS experimentally and numerically. Smith et al. (2004) present a new model-assisted POD which has more advantages over the empirical POD. With their development, a more accurate method can be provided to set the threshold since it is better able to sample noise and understand false calls and their influence on flaw detectability. They have validated their model by comparing the calculated empirical POD curve with the calculated model based POD using validated signal (i.e. transducer) and noise models (i.e. material and electronic noise), see Figure 2.10.
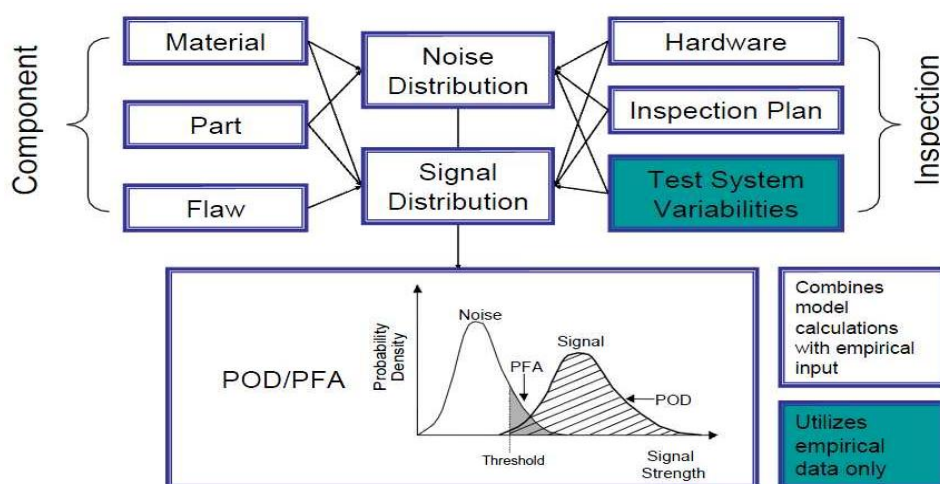
Figure 2.10: POD Modular Methodology (Smith et al., 2004)

Simola et al. (2009) present several project studies with the purpose of investigating reasonable and practical requirements that should be set for assumptions about the accuracy of how inspection reliability is quantified in terms of POD. Their pilot studies resulted in a set of recommendations related to the quantification of inspection qualification. In addition, if defect growth can be modelled further, it is possible to link inspection qualification results, risk reduction and inspection intervals.

According to Reboud et al. (2010), POD curves relate the detectability of a flaw to its size. For a specific inspection method, the POD expresses the probability that it is a flaw of a certain size that will be detected, assuming this flaw is actually present in the inspected component. Traditional POD curves are estimated from experimental data, the large amount of data required makes the determination of a reliable POD curve very expensive and time-consuming if there is a lack of support and contribution by the relevant organisations as addressed by Brennan et al. (2009) earlier. One of the solutions is using a simulation approach. Reboud et al. (2010) have used CIVA, a software for statistical tools, enabling POD computations to bring a cheaper and faster complement to POD studies. These simulation-based POD calculations have been recently introduced in the NDE community as reported by Jenson et al. (2009).

2.4 Maintenance Strategy

Maintenance strategy is one of the important sub-components of the life extension programme which is under the pipeline integrity system as referred to in Figure 1.2 in Chapter 1. There is the possibility of ending up with a catastrophic disaster caused by ageing and/or other factors if this strategy is not properly carried out by operators.

An example of damage or disaster due to ageing has been studied by Kotrechko et al. (2002). They conclude that from their low temperature testing results, the long-term operation does not affect the microscopic cleavage resistance (minimum brittle-fracture stress) of steel and has no influence on the strain-hardening exponent. But the

increase in the yield limit of steel caused by ageing is the main cause of the drop in its toughness after 30 years of operation. However, the risk of this damage due to lack of maintenance strategy should be proved by statistical model. Hence, Thodi et al. (2008) define risk as the product of probability of failure of an undesirable event and its likely consequences. The main steps in risk-based integrity modelling are the estimation of the probability of structural failure and its consequences. In their study, the maintenance plan or strategy has also been included in their consequence analysis (Thodi et al. (2008).

In order to make sure the maintenance strategy is successful, operators and protective system providers must work together. Gunalton et al. (2008) highlight that TOTAL is working closely with manufacturers to improve the characteristics of repair systems and to complete them by additional components if needed. The gap between the performance of the existing systems and TOTAL's requirements are evaluated.

One example of a very successful Life Extension programme is that of the Composite Hull Embedded Sensor System (CHESS) as highlighted by Todd et al. (2007). CHESS is used to measure global bending in ship hulls, local strain in selected areas and strain in the waterjet propulsion system. Fibre Bragg Grating (FBG) sensors are used and Finite Element Method (FEM) analysis is performed in their life extension programme.

In pipeline repair maintenance, there has been the established development of a high strength, lightweight, monitored reinforced thermoplastic pipe called a Smart Pipe that can be used for the rehabilitation of an existing pipeline, or as a stand alone replacement (Smart Pipe Company, 2008). Qinetic (2006) has also developed OptaSense distributed acoustic sensing that can detect threats before any damage occurs such as combating third party interference, condition monitoring, leak detection and pig monitoring etc. In order to address single critical integrity threats found at several locations of a pipeline system, Scrivner and Alexander (2008) have developed an Engineering-Based Integrity Management Program (EB-IMP). The uniqueness of this development is the integration of actual pipeline data coupled with analysis and testing

efforts tailored to suit engineering based on addressing specific threats to pipeline integrity.

Despite all these developments, there is a duty of operators to conduct periodic inspections and perform maintenance as appropriate. A long-term performance is directly related to how well the composite materials are protected and maintained. Failure to properly maintain these repair systems will result in sub-standard performance. Thus, Structural Health Monitoring (SHM) is one of the answers to the current reliability issue of composite-repaired ageing pipelines.

2.5   Corrective and Preventive Actions

Protecting pipelines from rapid crack propagation is a critical issue to avoid casualties and disaster. The mechanism of avoiding crack propagation in high pressure steel gas pipelines, so as to set up a second defence line against the rupture has to be sought. Hence, there have been many studies on this matter and one good example is a study carried out by You et al. (2003). They used a unique modified finite element (FE) code, PFRAC that was initially used to simulate the behaviour of steel rings as crack arrestors by O'Donoghue and Zhuang (1999), and with this proper FE simulation, together with experiment data (Drop Weight Tear Test), they managed to estimate the deceleration of fracture propagation in high strength and high toughness steel gas pipelines. Another study carried out by Ostsemin and Saidov (2004) shows that the evaluation of the crack resistance and mechanical properties of the pipe metal under static and dynamic loading enables to model the pipeline more closely.

In addition, a research project funded by the Australian Pipeline Industry Association confirms that after a pressure cycling equivalent of approximately 8,000 years of daily and maintenance-related pressure cycling, SCC cracks can safely survive in service for many pipe lifetimes, provided the corrosion environment is removed by recoating as shown in Figure 2.11 (Linton, 2008). However, the Office of Pipeline Safety (OPS), USA still considers SCC to be a safety risk to the pipeline and includes

the SCC assessment in their integrity management plans. Hence, In-line Inspection technology and a hydrostatic programme are the two main and most suitable approaches to identify SCC as reported by Wang et al. (2001).

Figure 2.11: Photos of (left) test set-up reinforcement sleeves applied over stress corrosion cracking, and (right) Opened stress corrosion crack (black region) which had extended with fatigue (Linton, 2008)

In the process of effectively assessing crack behaviour, BMT Fleet Technology (2005) developed engineering assessment expertise, tools and techniques mainly to provide support for equipment design and to evaluate the long-term structural integrity of welded and non-welded structures and facilities. The pipeline integrity assessment software "FlawCheck" offers a comprehensive assessment tool for crack-like flaws in metallic structures that incorporates stress intensity factor and net section stress solutions for various structures and flaw geometries. Dinovitzer et al. (2002) report that ASME B31.4 and B31.8 allow dents in pipelines up to 6% of their diameter. But leaks have been known to occur from dents with a depth even less than 3% of pipe diameter. They believe the depth of a dent is not the only factor affecting the operating life of the dented pipe segment. Thus, the issue of dent characterisation using a dent assessment model based on the FE method has been developed. Another practical assessment, as

suggested by Lee and Pyun (2002) is to implement the failure probability model that can effectively control the pipeline failure.

To prevent the potential damage caused by third party activities Wan et al. (2008) propose a novel automatic pipeline monitoring system based on classifying sounds. In their experiments, they have tested the effective sensing range of the sensor. Recognition resolution of the road cutter, which is considered to be one of the potential damages to the underground pipeline, is tested and analysed at different distances. It has shown that a road cutter at 41.9 m radius can be effectively recognised.

From the above overview of pipeline damage, some reliable corrective and preventive actions have been discussed. However, the composite repair system has also proved to be one of the effective and cost saving solutions in repairing damaged pipelines for over 20 years, as compared to the traditional repair solution which requires a shutdown in order to cut out the damaged section and replace it with a new section (Malcolm, 2009). Therefore, in the next section, the design and development, installation and operation of the composite repair system will be discussed. The importance of reliability issues will also be highlighted in the following sections since it is a key to the success of prolonging the life of ageing pipelines.

2.5.1 Composite Repair

Composite repairs have been utilised within the high pressure oil and gas transmission pipeline industry for permanent repair and reinforcement of sections of the pipe wall which have been weakened due to corrosion, third party interference or mechanical damage (Lesmana, 2010). The majority of this remedial work has involved the repair of onshore pipelines subject to corrosion. By using this system, pipeline damage, such as dents from gouges, corrosion etc., have been restored to or even given a higher strength than the parent material without expensive and time-consuming shutdowns. In other words, the life of the damaged pipelines has been extended for a couple more years depending on the request from the operators.

Manufacturers such as Walkers Technical Resources Ltd. (Frost, 2009) for example, have provided warranties of life extension of the repaired pipe to their clients based on their fibre glass composite Technowrap 2K Technologies. Figure 2.12 shows the relationship of the operating pressure and the repair thickness as the defect diameter increases. The thicker the repair thickness, the higher the operating pressure will be. Figure 2.13 shows the relationship of the operating pressure and the design life as the repair thickness increases. In order to make sure the design life of the composite repair is longer, the operating pressure has to be lower. Because of the reliability and flexibility of composite repair systems, several operators are now even using composite materials to repair their offshore pipeline and risers.
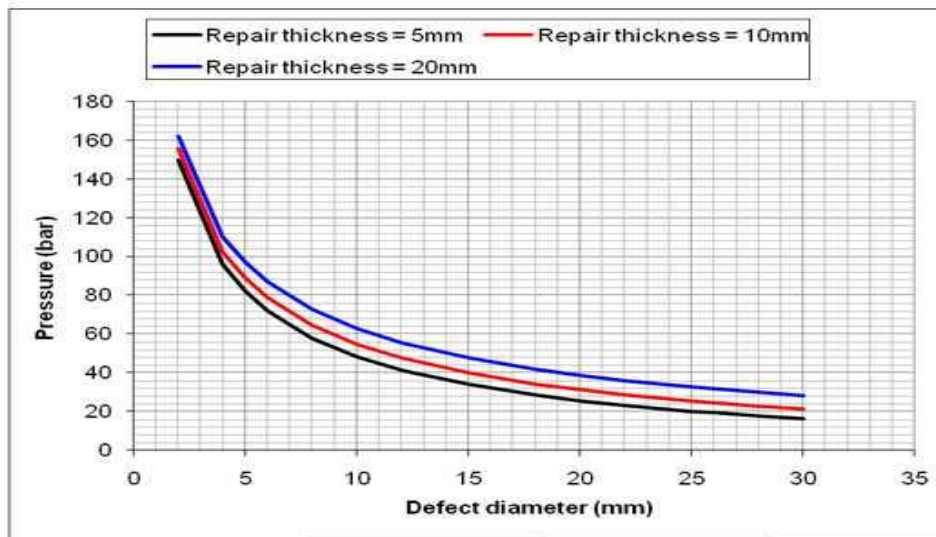
Figure 2.12: Design curves for Technowrap 2K (Frost, 2009)
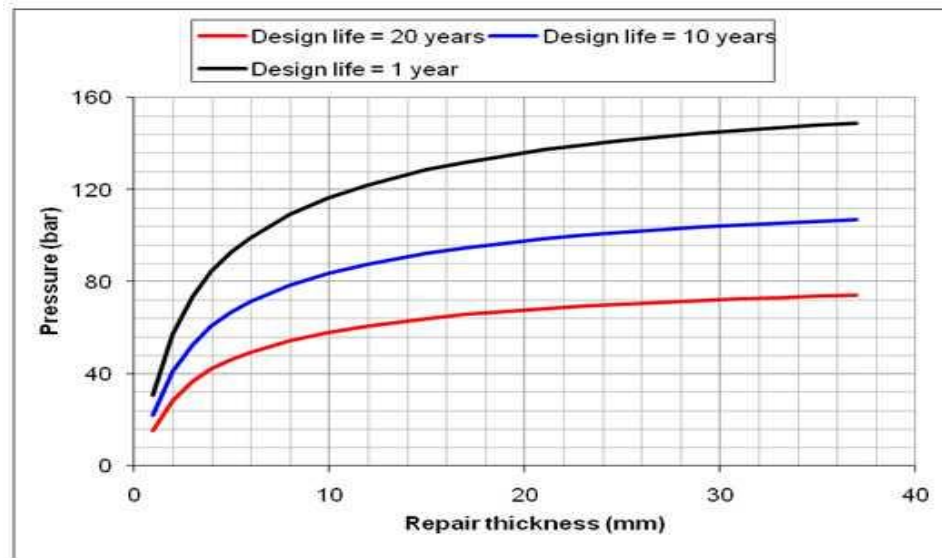
Figure 2.13: Design pressure as a function of repair thickness and fibre glass composite repair lifetime (Frost, 2009)

There are three main repair scenarios that should be seriously considered by the operators as reported by AEA Technology Consulting (2001) in their guidance document: pipe subject to external metal loss (caused by corrosion or mechanical damage), pipe subject to internal metal loss (caused by corrosion, erosion or erosion/corrosion), and piping components that are leaking. This subject area ensures that the composite technology has been designed with appropriate service conditions in mind, and most importantly, that the manufacturer has properly addressed and accounted for factors that can lead to inadequate performance and long-term degradation. It is the responsibility of the manufacturer to ensure that the design of their particular system meets minimum design and service requirements.

The design must provide an effective permanent repair alternative for corrosion, mechanical damage or other defects on high-pressure pipelines which includes: to repair blunt defects in pipes, arrest ductile fractures in high-pressure gas pipelines, reinforce dents or other mechanical defects in high-pressure pipelines, protect pipe at support location and repair defects in low pressure pipes, etc. There are many product designs at present such as Clock Spring®, the pioneer in the composite repair (Clock Spring

32

Company L.P, 2005); Aquawrap® provides a simple yet effective method (CorroDefense LLC, 2005); Diamond Wrap® system uses 100% epoxy and carbon composite system (Citadel Technologies, 2007); Denso petrolatum tapes, the product that can be used above or below ground and underwater (Denso North America, 2009); PermaWrap/WrapMaster, the only composite pipeline repair sleeve designed to be detected by Magnetic Flux Leakage (MFL) "Smart Pig" tools (WrapMaster, 2009); and, Technowrap2K®, the product that is validated to ISO/TS 24817 and ASME PCC-2-2006 with Lloyd's Register "Type Approval" and all repairs come with a lifetime guarantee in excess of up to 20 years (Walker Technical Resources, 2009).

By referring to Figure 1.1 (i.e. Pipeline Integrity System) in the earlier chapter, it can be seen that manufacturers' guidelines and standards are among the most important sub-components of the mitigation process. In providing a permanent repair alternative to welded sleeves, bolt on repair clamps and/or pipe replacement, this composite wrap system must meet the engineering design requirement. History has shown that even with the best designs, when technology is not properly used, the potential for sub-standard performance exists and sometimes with catastrophic results. For this reason, implementation guidelines are provided to ensure that the repair of a pipeline is done correctly. Hence, Enduro Pipeline Services (2009) emphasise that the correct identification of dented areas with metal loss or stress risers will enable operators to better maintain the integrity of pipeline systems. Likewise, correct identification of dented areas without metal loss or stress risers will prevent unnecessary excavations, allowing operators to allocate integrity management resources more effectively.

Besides the manufacturers' guidelines, many new codes and standards have been developed in providing recognised and accepted good engineering practice, and guiding the owner in the inspection, evaluation and repair of existing equipment (Becht IV and Sims, 2006). For example, codes and standards such as ANSI/ASME B31G that deal with the reference and standard for the corrosion pipeline in detail, have been widely utilised in the oil and gas industries as explained by Lee and Pyun (2002).

Recently, ASME (2010) has developed a document focused on the repair of pressure equipment, PCC-2-2006 Repair of Pressure Equipment and Piping Standard;

Article 4.1: Non-metallic composite repair systems for pipelines and pipeworks for High Risk Applications, which provides details on how composite materials are to be used to repair pipes (Ochoa and Alexander, 2007). According to Malcolm (2009), all aspects of composite repairs that include the prequalification of materials and repair system, the design of the repair, training and validation of applicators, are now governed not only by the above PCC-2 standard but also ISO/TS 24817 (composite repairs for pipework; qualification and design, installation, testing and inspection). He reports a repair is only compliant if the materials used have been tested in accordance with the above standards.

In order to ensure that the manufacturer or supplier complies with the above standards, ACORES (Association of Composite Repair Suppliers) which is a trade association has been established. All the accredited members of ACORES are independently audited at regular intervals and the audit process covers issues with regard to qualification, design, installer training and installation process (Frost, 2008).

2.6   Structural Health Monitoring (SHM)

2.6.1   Definitions

In ensuring the reliability of the composite repair in solving pipeline damage, the above maintenance strategy and adherence to the related standards are still inadequate to have a completely successful lifetime extension programme without a contribution from the Structural Health Monitoring (SHM) system. Before discussing the techniques and contributions of SHM in the pipeline repair, it is useful to really understand what SHM is all about in terms of its definition.

In this literature review, there have been several authors who define and explain SHM. Rao et al. (2006) for example, define SHM as the process of establishing some knowledge of the current physical condition of a structure. The essence of SHM technology is to develop autonomous built-in systems for the continuous real-time

monitoring, inspection, and damage detection of structures with minimum labour involvement with a high level of confidence and reliability.

According to Chung (2001), SHM refers to the monitoring of the integrity of a structure for the purpose of hazard mitigation, whether the hazard is due to live load, earthquake, ocean, waves, fatigue, heat, ageing and other factors. This process involves the observation of a system over time using periodically sampled dynamic response measurements from an array of sensors, the extraction of damage-sensitive features from these measurements, and the statistical analysis of these features to determine the current state of the system's health (Fixter and Williamson, 2006). In addition, Sohn (2007) emphasises that SHM has the ability to perform its intended function in the light of the inevitable ageing and degradation resulting from operational environments and Inaudi and Glisic (2006) describe it as one of the most powerful management tools that has become important in the civil engineering community. A typical health monitoring system is composed of a network of sensors that measure the parameters relevant to the state of the structure and its environment.

Herszberg et al. (2007) define SHM as the system that has the potential to continually monitor the health of a structure through strategically located sensors coupled with monitoring technology enabling remote interrogation of the sensors. This is endorsed by Wang et al. (2001a) but they remind us that a major challenge for the development of robust SHM system is all about the accurate interpretation of sensor measurement in terms of physical changes in structure. The summary of the concept of SHM is clearly presented by Herszberg et al. (2007) and is shown in Figure 2.14.
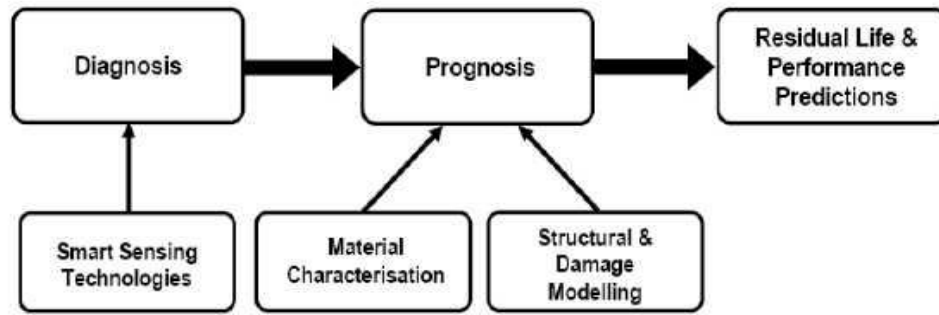
Figure 2.14: Integrated Structural Health Monitoring Approach

(Herszberg et al., 2007)

In the context of composite repair, the SHM definition should not be driven by the process of implementing a damage detection strategy as is done on aerospace, civil and mechanical engineering infrastructures. But it should be driven by the process of ensuring the reliability of the repair instead, where attempts are made to measure the inputs to and responses of a structure after damage has been repaired so that the regression analysis can be used to predict future damage or deterioration (often due to poor installation, materials etc.) in the structural condition. Coupled with the installation of sensors and numerical modelling, the remaining useful life of the system can then be assured. Therefore, the following literature review provides an insight into the selection of the most suitable and practical sensor to be used in the composite repair. The aims, implementations, limitations and benefits of SHM will also be addressed. However, the discussion is limited to sensing structural responses only and is confined to strain and temperature. Other elements of data acquisition and signal processing such as excitation methods and data transmission are not discussed in this chapter but will be explained in a later chapter.

2.6.2 Aims of Structural Health Monitoring (SHM)

The main aims of SHM are to maximise the life structure, reducing whole life cost by reducing the number of scheduled non-destructive examination (NDE) services, and providing additional safety measures as explained by Fixter and Williamson (2006). These aims are further discussed in their comprehensive report in a state of the art review on SHM which looks at the current status of optical fibre and electrical technologies with the main interest being on those sensors that are applied to composite structures. Sohn et al. (2003) also provide a comprehensive review of the technical literature on SHM with similar aims.

2.6.3 Optical Fibre Sensor (OFS)

Inaudi and Glisic (2005) discuss distributed fibre optic sensing as one of the most effective SHM techniques since it is able to measure temperatures and strain at thousands of points along a single fibre in the monitoring of large structures such as pipelines, oil wells etc. The sensing system is based on Brillouin and Raman Scattering works with three cable designs for high temperature sensing, strain sensing (called SMARTape) as shown in Figure 2.15, and combined strain and temperature monitoring (called SMARTProfile).
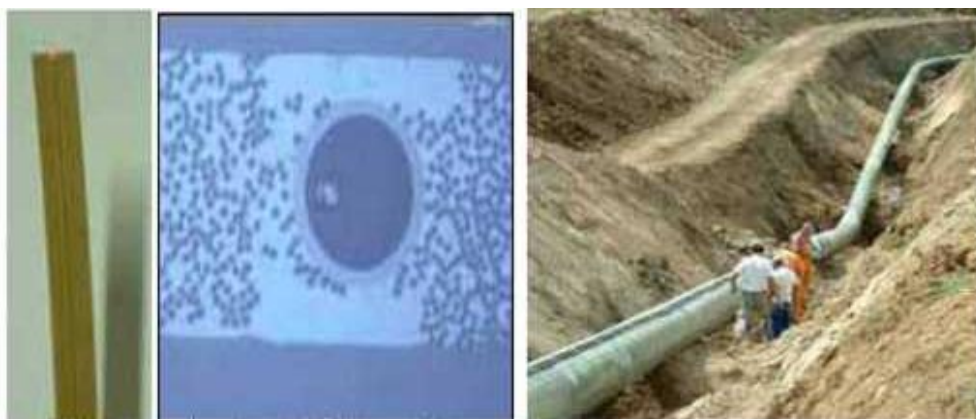
Figure 2.15: Graph of the sensing SMARTape (Left), SMARTape on the gas pipeline (Right) (Inaudi and Glisic, 2005)

The capability of using a single fibre has also been proved by Elvin and Leung (1997). With a single fibre optic sensor embedded within the composite structure that serves as a reference fibre, they were able to develop an SHM approach that can detect and characterise the delamination. They have concluded that the change in total extension of the fibre optic sensor within the composite structure gives accurate readings and with this type of sensor, they managed to achieve their objective.

In other researches, which have been done by many researchers, OFS performance remains acceptable compared to conventional strain gauge performance which deteriorates quite rapidly as a result of moisture as reported by Rizkalla et al. (2000). However, they admit that there is the necessity of measuring temperatures to account for the significant thermal effects because these effects on the measured strains are dominant. Tennyson and Mufti (2000) and Moerman et al. (2000) also recognise the importance of cancelling the effects of thermally induced strains in OFS especially Fibre Bragg Grating (FBG) sensors.

One of the methods used to overcome the thermal effect problem, as suggested by Inaudi and Glisic (2006) is to use the sensors of two bonded and two free single mode optical fibres embedded in a polyethylene thermoplastic profile. The bonded fibres are used for strain monitoring, while the free fibres are used for temperature measurement and to compensate for the temperature effects of the bonded fibres. This will guarantee that the optical fibre does not experience any strain that can be misinterpreted as a temperature change due to cross sensitivity between strain and temperature. With the ability to minimise the thermal effect, Foedinger et al. (2000) use embedded FBG sensor arrays that are embedded in the composite pressure vessel to measure the internal strain during curing and pressurisation.

Other researchers such as Furrow et al. (2000), use the extrinsic Fabry Perot Interferometer (EFPI) in measuring the displacement and monitoring strain in the composite bridge decks. Their investigation shows that the EFPI sensor is the only sensor sensitive to the axial strain components and relatively insensitive to temperature variations.
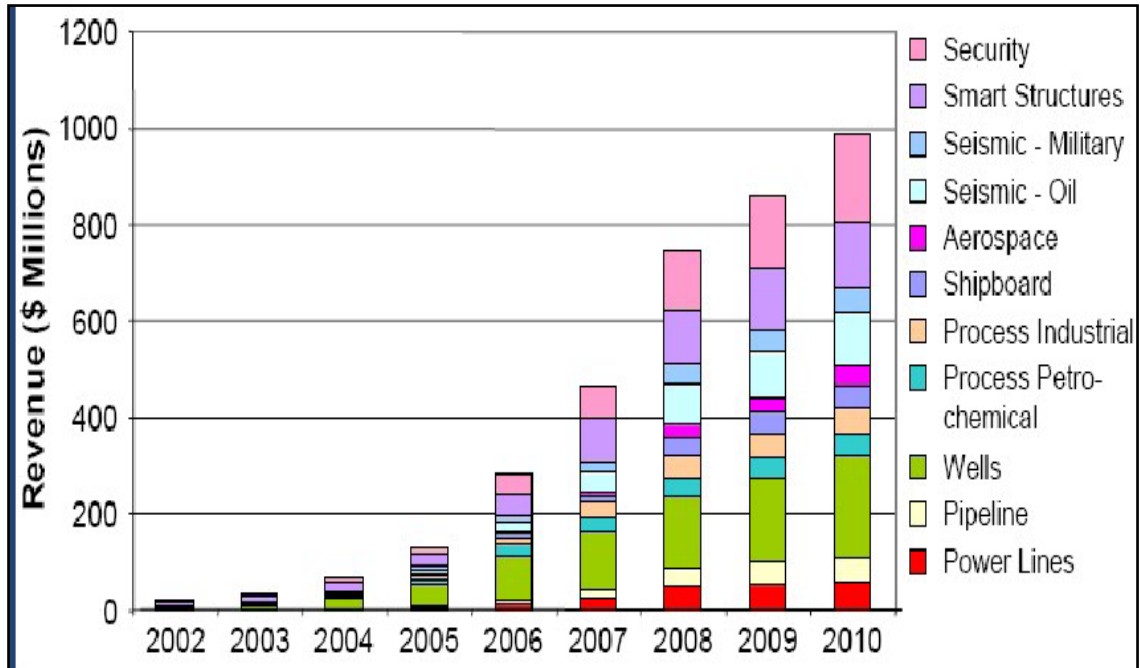
Figure 2.16: Application fields and market share forecast of distributed fibre optic sensors (Ecke, 2008)

OFSs have been used widely since they offer numerous advantages in terms of low inertia, high speed, immunity to electromagnetic interference, nonelectrical contact to the sensing region and are intrinsically safe. At least five modulation techniques have been identified: intensity, phase, frequency, colour and polarisation (Culshaw, 1984). Under various options of fibre optics, the distributed fibre optic is one OFS that has been widely accepted and used in the various fields (Ecke, 2008) as referred to in Figure 2.16.

A simple explanation on how the OFS works can be found in the literature study by Fixter and Williamson (2006). According to them, OFS and electrical strain gauges have their own advantages but the most important thing is how effective these sensors can perform in specific applications. Therefore, the following literature highlights the capability of electrical strain gauges in terms of versatility, accuracy, low cost and others in various SHM applications.

2.6.4 SHM using Electrical Strain Gauges

Vel and Batra (2001) use shear mode piezoelectric actuators in obtaining static cylindrical bending. The piezoelectric materials are capable of altering the structure's response through sensing, actuation and control, and by integrating surface bonded and embedded actuators into the structural system, desired localised strains may be induced by applying the appropriate voltage to the actuators. Wang et al. (2008) agree that piezoelectric materials can act both as actuators and sensors for detecting damage by using their active diagnostic technique.

A study carried out by Birchmeier et al. (2009) shows the capability of an Active Fibre Composite transducer to work effectively with the acoustic NDT method (i.e. Lamb waves). These Lamb waves (elastic guided waves) are able to propagate over long distances and are sensitive to even small defects such as crack, delamination and local changes in wall thickness. In other research works, Thien et al. (2007) use a piezoelectric macro-fibre composite (MFC) transducer for the development of a real time, low cost, SHM system for pipeline structures. This dual MFC transducer is experimentally employed to utilise both impedance methods and Lamb wave propagations. Self-sensing impedance methods are used to detect structural damage occurring at pipeline connection joints, while the Lamb wave propagation measurement identifies cracks and corrosion along the surface and through the thickness of the pipe structure. In fact, this impedance-based SHM monitoring, as investigated by Park and Inman (2007) under temperature varying conditions, is able to detect and distinguish incipient damage. The effect of the temperature is minimised by the empirically-based compensation technique where for other piezoelectric transducers, SHM is unable to be done.

In terms of strain measurement accuracy, Gregory et al. (1999) report that typical electrical strain gauges such as resistive type, piezoelectric, semiconductor and capacitance gauges are all suitable for very accurate strain measuring devices but have disadvantages such as small dynamic range, gauge factors of less than 5. However, there are many ways to overcome this limitation. Osmont et al. (2000) have used a passive technique using the High Frequency Root Mean Square value of the electrical signal

registered by the piezoelectric sensors in identifying the location of the damaging impact on a composite plate successfully.

In other limitations examples, Blanas et al. (1999) report that the embedded sensors may introduce disadvantages because of incompatibility with the organic host. In order to overcome this limitation, they use ferroelectric sheets and extensional plate waves to detect damage in the composite structures. Actually, this incompatibility issue had been identified earlier by Chen et al. (1997). They use the techniques of ferromagnetic particles into the Glass Fibre Reinforced Polymer (GFRP) composite matrix. The vibration signatures from the damage and undamaged specimens have been recorded successfully by a Laser Doppler Vibrometer.

In the development of achieving low cost electrical strain gauges, Satpathi et al. (1999) have used PolyVinylidene Fluoride (PVDF) as strain gauges. The authors conclude PVDF has several advantages over other piezoelectric materials, including cost. It also shows excellent strain sensitivity at room temperature and is easy for temperature compensation since PVDF strain sensitivity is a linear function of temperature. Their study is motivated by SHM projects that are sometimes limited by the high cost of sensors and associated signal conditioning as with Optical Fibre Optics (OFSs).

In terms of the comparisons of performance between OFSs and electrical strain gauges, Rao et al. (2006) have carried out a very good comparative study with the main aim of demonstrating the feasibility of using Fibre Bragg Grating (FBG) with a Rectangular Strain Gauge (RSG) in an experiment on the composite wing of a mini automated vehicle. The results show that FBG sensors are as good as RSGs in the strain measurement. One of the advantages of FBG over a RSG is its durability and suitability to be used for SHM for large structures.

In other applications of SHM sensors, besides OFSs and electrical strain gauges, Chung (2001) reports that electrical resistance measurement, which has received relatively little attention in terms of structural health monitoring, has its own advantages. Since it does not involve any embedment or attachment, it does not suffer

41

from the problems described earlier for embedded or attached sensors. In his study, he has found that the electrical resistance method is only particularly effective for detecting small and subtle defects in composite materials and in joints.

Based on the above literature, SHM can be summarised as the acquisition of information to enable the diagnosis and prognosis of structural integrity and the ultimate objective is to continuously monitor and assess the status of the integrity of a structure or its components with a high level of confidence and reliability. Each of the techniques has its own advantages and disadvantages. Therefore, selection of the right sensors to be used for the right application will ensure the success of the SHM. Having described the full definitions and concepts of SHM, FEA and experiments that have been used as an integrated approach to the diagnosis and prognosis of the composite based pipeline repair will be discussed in the following sections.

2.7   Introduction to Finite Element Analysis (FEA)

FEA (also known as the method) has been successfully used for many years in the analysis of complex structures (Walz et al., 1968) and historically, it was first developed in the 1940s by Alexander Hrennikoff and Richard Courant. During this period it was called the finite-element method. In 1965 the first finite-element software was created by NASA and it was called NASTRAN. At present, there are many types of structural analysis software on the market. Some of these brands include: ALGOR, ANSYS, ABAQUS and MARC (Knoxville, 2009).

The Finite Element is a numerical technique for finding approximate solutions for partial differential equations (PDEs) as well as for integral equations. The solution approach is based either on eliminating the differential equation completely (steady state problems), or rendering the PDE into an approximating system of ordinary differential equations, which are then numerically integrated using standard techniques such as Euler's method, Runge-Kutta, etc. (Gilbert and Fix, 1973). The major sources of error resulting from the use of finite element methods are round-off error and

discretization error. Round-off error is the error associated with the accuracy with which numbers are manipulated in a computer and discretization error is the error that is associated with using discrete variables to represent a problem where the state variables are continuous (Walz et al., 1968). In order to overcome this problem, a study of the convergence of the numerical results as the number of elements increase, has to be carried out.

The most effective method, as suggested by the University of Alberta, (2002) is to conduct a convergence test, beginning with a mesh discretization and then recording the solution. The problem with a finer mesh (i.e. more elements) should be repeated and the result compared with the previous test. If the results are similar, then the first mesh is probably good enough for that particular loading, geometry and constraint. An example of a good convergence study was carried out by Longest and Vinchurkar (2007). They established the effects of mesh generation techniques and grid convergence on velocity fields and particle deposition patterns in bifurcating respiratory models, which included structured hexahedral, unstructured tetrahedral, flow adaptive tetrahedral and hybrid grids. From their observations based on a Grid Convergence Index, generating structured meshes based on hexahedral elements requires significant time and effort; however, these meshes are associated with high quality solutions.

Beden et al. (2008) point out that an FEA technique that has been used for modelling and simulation is able to produce more accurate fatigue life predictions for pipe elbows. They demonstrate how Tet10 ABAQUS element mesh predicts higher maximum principle stresses than the Tet4 mesh of the same size, but with a greater number of elements, nodes and degree of freedom. However, they have not compared with other element types such as hexahedral which would produce better results. DeVries et al. (2009) demonstrate their developed IA-FEMesh as a user friendly toolkit for generating FE models in orthopaedic (biomedical) research. IA-FEMesh enables geometrically accurate hexahedral meshes to take less time than traditional methods such as PATRAN which have proved to be time-consuming and laborious. Their study of IA-FEMesh is capable of generating anatomically accurate hexahedral meshes of the human phalanx in less time than the traditionally used commercial mesh generator.

According to Bahai (2001) calculation of the stress concentration factor (SCF) is an essential initial step in the fatigue life estimation of a threaded connection using a particular finite element (ABAQUS) sub-modelling technique. The data obtained can form the basis for obtaining parametric equations describing SCFs in terms of drill string thread geometric parameters. Hence thread design optimisations based on minimum axial and bending SCFs can be established.

Rinehart (2003) used the finite element method by using ABAQUS Viewer to study the effects of localised geometric imperfections that cause the dent stress concentration behaviour of pressurised cylindrical shells. Khazhinskii (2005) agrees that more accurate estimates of stress concentration are obtained by the finite element method or experimentally by strain measurement (Xue et al., 2005; Alexander, 2008a). However, Xue et al. (2005) used different software for the finite element method using ANSYS in their study of cylindrical shell intersection stress concentration and flexibility factor before the structure experiences plastic behaviour. They determine limit load and burst pressure when an elastic – plastic analysis method is employed.

Kosai et al. (1999) also mention that a numerical procedure is able to help them predict the crack trajectories in full-scale fuselage rupture tests. All numerical results agree well with their measured counterparts regardless of size. By using this ABAQUS software, Kim et al. (2007) manage to present plastic limit loads and approximate J estimates for axial through-wall cracked pipe bends under internal pressure and in-plane bending successfully. In order to avoid problems associated with incompressibility, they use reduced integration elements (i.e. element type C3D20R within ABAQUS).

Shin (1986) makes a comparison study, based on the elastic stress distributions in single and double edge notched geometries in a finite plate, that have been estimated from Creager and Paris (1967), and Neuber's expressions. He demonstrates the stress concentration factor expressed by Creager and Paris as $K_t = 1 + 2 F \sqrt{\frac{a}{\rho}}$ and Neuber as $K_t = F(1 + 2 \sqrt{\frac{a}{\rho}})$ which are very close to the FEM result just ahead of the notch. The error increases with distance from the notch root. Shin (1986) concludes that both the Creager and Paris expressions are more accurate for the notch root of sharper

notches and Neuber's is better for the blunter notches. However, these predictions are not applicable for the external notched pipe which is subjected to internal pressure and, therefore, other expressions are needed.

Other example of finite element application is the use of a Non Destructive Examination (NDE) field, especially in the detection of gas pipe wall thickness based on Electromagnetic Flux Leakage as presented by Zhang and Yan (2007). Their numerical calculation of the FEA, using ANSYS, provides a good solution in revealing the relation between the wall thickness and the magnetic flux density at the same position in a magnetic leakage field. Parvin and Wu (2008) demonstrate that the finite element analysis is able to show that Carbon Fibre Reinforced Polymer (CFRP) wrapping is effective in retrofitting the existing beam-column joints. The wrap ply angle stacking sequence of -45°/ +45°/ -45°/ +45° appears to offer prevention against the brittle shear failure of the joint under combined axial and cyclic loads.

2.7.1 Stress Concentration Factor (SCF) and Stress Intensity Factor (SIF) Measurement in Pipeline

The stress concentration factor (SCF), $K_t = \dfrac{\sigma_{max}}{\sigma_{nom}}$ can be used for fatigue assessment of pipelines whenever they are subjected to variations of internal pressure. For a fatigue assessment to be carried out, a rather detailed analytical expression for stress concentration factors in pipes that are derived for a number of design cases based on classical shell theory has been presented by Lotsberg (2008). In another study carried out by Radaj and Zhang (1996), they point out that with the presence of a stress concentration notch in pipelines, the initiation of a surface crack is often provoked. Carpinteri et al. (2004) numerically demonstrate that the SCF parameter is very important especially in presence of cracks since it heavily affects the SIF results. Therefore, Radaj and Zhang (1996) emphasise that local notch stress concentration is the basis for the assessment of the fatigue strength and life of structural components.

45

Generally, most of the numerical research that has been conducted to determine the stress intensity factors (Raju and Newman, 1986; Bergman, 1995; Carpinteri and Brighenti, 1998) are on plates, not pipes. For that reason, a good study carried out by Wallbrink et al. (2005) shows a feasible method for dealing with the major problems associated with the analysis of partly circumferential cracks in pipes. They demonstrate a new method where the conformal transform has been used to relate the position of a point in a flat plate to a point in a pipe using FEA and an analytical solution for a semi elliptical flaw in a flat plate, as provided by Vijayakumar and Atluri (1981). For a simple flat plate solution, as shown by the schematic representation in Figure 2.17, Gauss points have been used to extract stresses from the pipe and relate them to a point in the flat plate. Comparisons with solutions presented by Bergman (1995) and Raju and Newman (1986) show a good agreement as the solution is within 5% for cases where a uniform load is applied to the external crack.
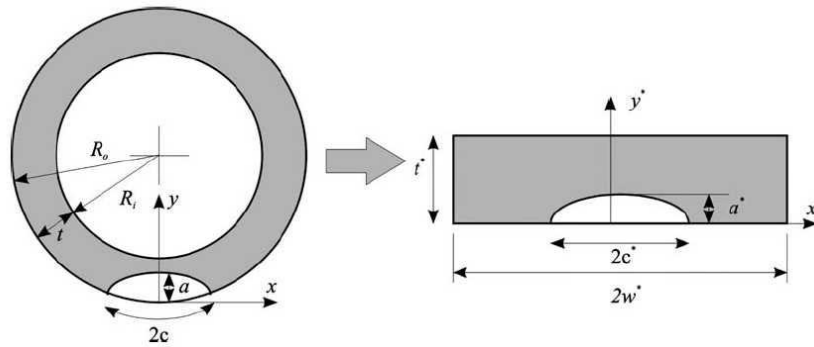
Figure 2.17: Conversion from a circumferential crack to a semi-elliptical crack (Wallbrink et al., 2005)

Besides stress intensity factor, several studies have also been carried out to determine the stress concentration factors using finite element methods such as on the cylindrical shell intersection (Xue et al., 2005), pressurized cylindrical shell with dents (Rinehart, 2003; Alexander and Worth, 2006; Khazhinskii, 2005), u-notch pipe (De Carvalho, 2005), and circular shape notch pipe (Kim and Son, 2004). Often, the local wall thinning in pipelines due to corrosion provides stress concentrations initially and a

maximum local stress at discontinuity could be many times greater than the nominal stress of the pipe. To evaluate the corrosion damage in the region of local wall thinning, an SCF is needed as a function of defect geometry, pipe geometry and loading, as reported by Kim and Son (2004). Hence, the values of the elastic stress concentration factor for pipes with local wall thinning, subject to internal pressure and global bending, using 3D elastic FEA (ABAQUS) have been established. The defect has been modelled as a circular shape in both axial and circumferential directions inside the pipe.

De Carvalho (2005) also demonstrates in the same way as Kim and Son (2004) but with a radial u-notch inside the pipe instead. However, they all refer to maximum hoop stress at the notch root being determined by the finite element method. For the nominal hoop stress, De Carvalho (2005) refers to it as being calculated at the same point in the thickness and the expression which describes hoop stress acting in a perfectly cylindrical region as;

$$\sigma_{nom} = P. \frac{R_i^2}{R_o^2 - R_i^2}\left[1 + \frac{R_o^2}{r^2}\right] \qquad \text{(Equation 2.1)}$$

Where P is the internal pressure, R_i, R_o and r are the inside, outside and a given radius. The schematic representation of the model is shown in Figure 2.18.
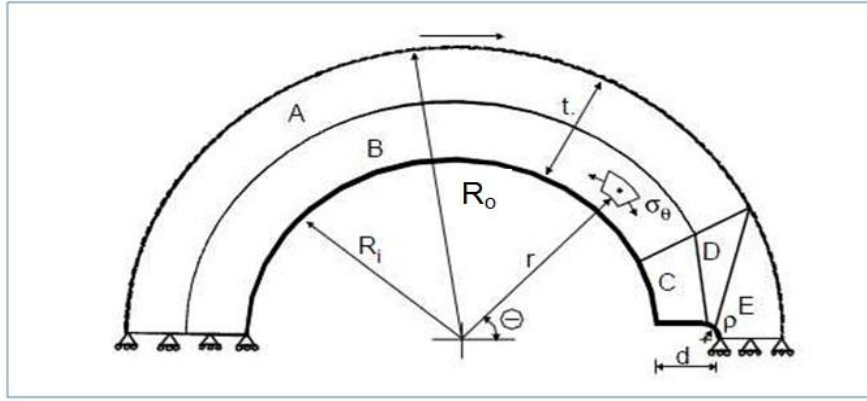
Figure 2.18: Mesh and geometry. Θ is the angle associated with the hoop stress, *t* is wall thickness, *d* is notch depth and *ρ* is notch radius (De Carvalho, 2005)

Kim and Son (2004) on the other hand, mention that the nominal hoop stress can be taken as the mid-thickness stress as expressed in Equation 2.2; the schematic illustration of the model is shown in Figure 2.19. They point out that all four parameters, R_m/t, Θ/π, d/t and l/t, affect values of Kt significantly:

$$\sigma_{nom} = \frac{P.R_i{}^2}{R_o{}^2 - R_i{}^2}\left[1 + (\frac{R_o}{R_m})^2\right] \qquad \text{(Equation 2.2)}$$
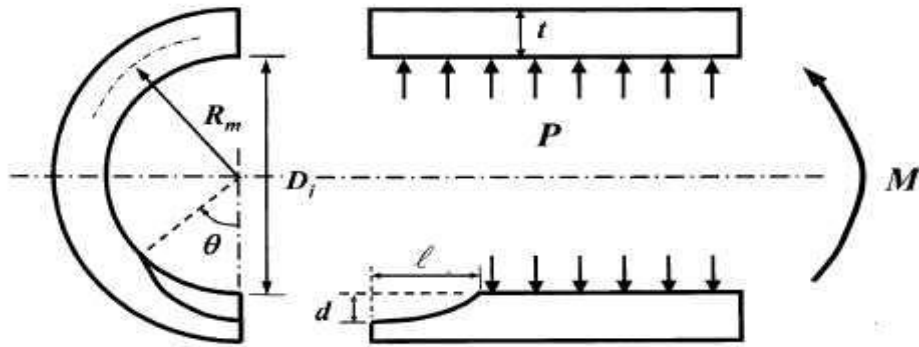
Figure 2.19: A pipe with local wall thinning, subject to internal pressure *P* and bending *M*. *R_m* Mid thickness radius, Θ is the angle associated with the hoop stress, *t* is the thickness, *D_i* is the internal diameter, *d* is the notch depth and *l* is the notch length (Kim and Son, 2004)

48

De Carvalho (2005) concludes that the stress concentration is proportional to the thickness of the pipe and depth of the notch. The increase in both pipe thickness and notch depth will increase the stress concentration factor accordingly. This relationship is also agreed by Kim and Son (2004). However, their studies can only relate to the wall thinning due to internal corrosion or erosion. There is a need for further numerical studies on the wall thinning due to external corrosion. Therefore, the current numerical study carried out by Murad and Brennan (2010) on the circumferential external arc-shaped notch outside the pipeline has notably contributed to the process development of repairing pipelines using composite and the future development of fatigue assessment of the current ageing pipelines.

2.8   Experimental Approach

Using an analysis-only approach does not provide pipeline operators with a complete methodology to assess the integrity of their pipeline systems. Experimental evaluation methods, including testing, are required to provide the pipeline industry with a robust integrity solution using composite materials (Alexander, 2008b; 2009a). Traditional methods for the evaluation of the composite repair system often rely on classical mechanics derived from strength of materials and compatibility relations. There are limitations with these traditional methods, specifically in quantifying the level of reinforcement provided by the repair as reported by Alexander (2008a).

As a way to measure the load transfer from steel substrate into composite, strain gauges are effectively used in the experimental evaluation. Since biaxial stress states occur very commonly in pipelines, the right strain gauges to be used would be rosettes. However, understanding in the selection and application of rosettes is critical to their successful use in the experimental stress strain analysis. Measurements Group (2000) reminds us that the tee rosette should be used only when the principal strain directions are known in advance from other considerations and extraneous stress (e.g. bending, axial stress etc.) is not present, since these will always affect the directions of the principal axes. Other irregularities such as notch, holes etc. can also locally alter the

principal directions. Thus, Measurements Group (2000) suggests that when the directions of the principal strains are unknown, a rectangular or delta rosette is always required and the rosette can be installed without regard to orientation.

With respect to the above guidelines, Khan and Hsiao (1984) have used strain gauge rosettes to measure stress concentration in the intersection region of straight cylinder shells. Three element rosettes have been used in the immediate vicinity of the intersection region where appreciable values of shear stresses are expected. Two element rosettes or tee rosettes are used at locations which are not in the immediate vicinity of the intersection because before that they measure the magnitude of shear stresses which are small even around the intersection region.

In the process of investigating the feasibility of extending onshore composite repair techniques to offshore risers by developing integrated analytical and experimental methods, Alexander (2007a) installed tee strain rosettes on the flat bottomed notch steel pipe as well as on the outside of the repair. Under different series of tests, such as pressure test, pressure-tension test and pressure-tension bending test, Alexander (2007a) claims that the gauges which have provided the greatest information, relative to the performance of the repair, are those located in the centre of the corrosion groove beneath the repair. Those gauges also indicate the level of reinforcement provided by the composite material in terms of load being transferred from the steel to the composite material. However, the results are still sceptical because, according to Measurements Group (2000), for this type of application the rectangular strain gauge (RSG) rosette is more suitable than the tee rosette.

In a current research study on a new bonding integrity of a composite repair system using the experimental approach, Murad et al. (2011) have made a preliminary study, firstly in terms of choosing the right type of strain gauges before carrying out the experiment. Based on the above and other literature, RSG rosettes have been chosen since the experimental pipe specimen contains some irregularities such as notch and welded joints. This method has shown the ability to evaluate the actual level of load transfer despite being in the elastic region and will be discussed further in the following chapters. Actually, other techniques such as the photo elastic method can provide an

accurate simulation of loading especially in the study of stress concentration, as explained by Bahai and Esat (1994). However, this method is expensive and time-consuming and can only be justified for validation purposes or when strain gauging is impractical to be installed, for example in the study of complex stress distribution in threaded connectors.

There are also a few important parameters that need to be highlighted in this experimental approach section. Firstly, the repair system that is used in this experiment is fully qualified to the relevant standards governing the use of composite repairs, ISO/TS 24817 and ASME PCC-2 (Frost, 2010a). Secondly, a package of knowledge skill and competency in installing strain gauges, and acquiring data using the Compact Rio system/Labview software is considered to be one of the main ingredients to produce more accurate and sensible data. With reliable experimental data, the numerical result using ABAQUS can be validated accordingly and a completely integrated SHM approach can be implemented successfully.

2.9   Why is SHM important in the composite repair?

Lesmana (2010) reports there are two application techniques that are available for the repair of pipelines using composite:

1) Wet wrap application (wet applied cloth)

2) Full cure application

Wet wrap application: A flexible cloth, woven from E-glass (e.g. based on the product of Technowrap from Walker Technical Resources Ltd) or carbon (e.g. Black Diamond from Citadel Technologies) is impregnated with resin on the repair site. The fibre provides the strength needed in the repair and the resin provides the bonding matrix to hold the repair in place.

Full cure application: This eliminates the variables of the wet wrap process. The fully cured composite (e.g. Clock Spring) is taken to the repair location and secured to the pipe with adhesive. A high compressive strength filler material fills the defects and voids beneath the composite sleeve in order to ensure a proper load transfer as shown in Figure 2.20.

Lesmana (2010) claims that with the full cure application, the unidirectional glass strands which are carefully positioned and aligned, and held within the factory applied cured resin matrix, have better performance than the wet wrap application where the ratio of resin to glass, degree of resin saturation, alignment of the glass and consistency of tension in the repair are difficult to control. In fact, the woven cloth can allow moisture to penetrate into the composite and weaken the repair. Hence, the effectiveness and long-term performance are unpredictable. It is likely there have been many unreported cases where this wet wrap repair has caused huge losses to operators worldwide.

Figure 2.20: Photos of repaired pipeline using composite wraps based on Clock Spring (CLOCK SPRING Company L.P., 2005)

52

Based on the above facts, the operators and manufacturers that have been using wet wrap applications for years as their preferred method of composite repairs should consider implementing this new bonding integrity reliability, using the integrated SHM approach as part of their life extension programme.

2.10 Summary and Conclusions

This chapter has provided a literature review of various damage scenarios, especially within the pipeline industry. Inspection and monitoring have been discussed and differences between these two have been explained. Reliability analysis of information, which includes probabilistic condition assessment and others, is important in guaranteeing safe operation and cost-effective maintenance.

Composite repair, as one of the best corrective and preventive solutions, has been reviewed and it is understood that the SHM contribution is very important in ensuring the reliability of this approach in tackling the issue of pipeline damage in this day and age. According to Herszberg et al. (2007) damage diagnosis which possesses a certain degree of universality in terms of its application, and structural health prognosis are highly specific to the target structure and necessitate the creation of high fidelity numerical models. The combined diagnostic and prognostic capabilities through SHM can minimise uncertainties associated with composite structures and lead to significantly more optimised designs with quantifiable increases in structural reliability.

Preliminary understanding of local notch stress concentration factors (SCFs), especially on wall thinning due to corrosion, is very important before any corrective and preventive action such as composite repair can be carried out. SCF, which is the basis on which the assessment of fatigue strength and the structural component's life can be further studied in the most efficient and cost-effective ways using finite element analysis (FEA) is discussed in this chapter. SCFs using FEA will be further discussed in depth in Chapter 3 and the experimental work that is used to validate the numerical

results will be discussed in Chapter 4. In fact the FEA and experiments are used as SHM approaches in this PhD study that involves composite pipeline repair.

In this chapter also, it is understood that generally electrical strain gauges have some limitations compared to OFSs, yet they have been used in this research work (i.e. rectangular strain gauge rosettes). The main reasons are because of their low cost, their ability to measure accurate strain readings within a small predetermined area (i.e. within the defect region), and can also be easily embedded in the composite repair without any problem. However, some proper guidance from the manufacturer's standards and technical documents is needed, and a proper adherence to the code and practice of strain gauges is required in order to obtain accurate and reliable results.

In the study of pipeline composite repair, good bonding integrity should be considered as a yardstick to ensure that the repair meets the standard design and installation requirement. With this scientific yardstick, the operator can have higher confidence levels and full satisfaction based on their selection of cost-effective repair methods. However, to the best of the author's knowledge, there is no evidence of a bonding integrity study on the composite-based pipeline repair. This inadequacy or lack of information on the specific issues of a reliable bonding integrity, as shown in Figure 2.21, and also regarded as a gap in knowledge, has motivated this research work. Detailed studies of this bonding integrity refer to the FEA and the methodology employed in this thesis, and these are presented in Chapter 3.
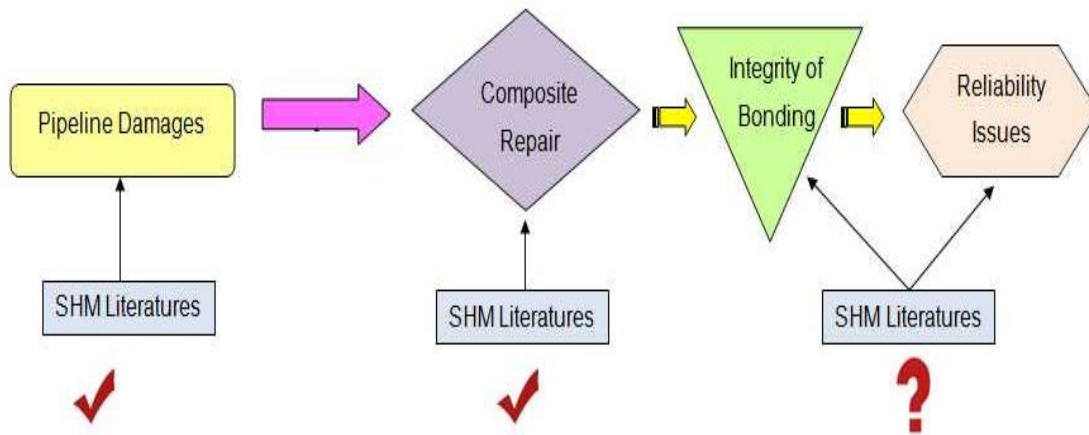
Figure 2.21: The current scenario of research study in the composite repair

3   FINITE ELEMENT ANALYSIS (FEA) IN THE COMPOSITE BASED PIPELINE REPAIR

3.1   Introduction

The previous chapter has discussed several open literature related to FEA, especially the studies of stress concentration factors. In this chapter, several simulation works that include the study of blunt defect behaviour in a thin walled cylinder, the development of the composite repair modelling, and stress and strain analyses of composite repairs, are presented. The main aim of this chapter is to show that FEA does not only provide a good tool in the study of stress and strain concentration of the damaged pipeline due to corrosion, but most importantly, how the composite repair is proved to be a reliable corrective and preventive solution in the pipeline industry. This aim can be achieved by referring to the following objectives.

3.2   Objectives

There are several finite element works that have been done for this PhD study but the main objectives of this chapter are;

1. To analyse the influence of pressure on the finite element (FE) pipe model and assess the blunt defect behaviours of the model.
2. To analyse the stress concentration factors in the notched pipeline and then compare it with the composite repair pipeline.
3. To analyse the influence of a composite repair on a pipe model that contains various sizes of arc-shaped notch defects and to establish a Pipeline Repair Index (PRI).

3.3 Model and Other Parameters Selection

A carbon steel pipe model with the nominal thickness of 8.2 mm that has a circumferential arc-shaped notch defect with 3.5 mm deep and 40 mm long is shown in Figure 3.1. This type of defect has a constant radius of curvature and is therefore a section from a circle. This model represents the pipe that contains the external defect due to corrosion and the shape has an impact on the stress concentration factor. The main reason why the arc-shaped notch was made circumferential rather than localized is because the experimental work that validates this numerical model requires the installation of several rectangular strain gauges along the notch root so that the objectives of this study can be achieved.
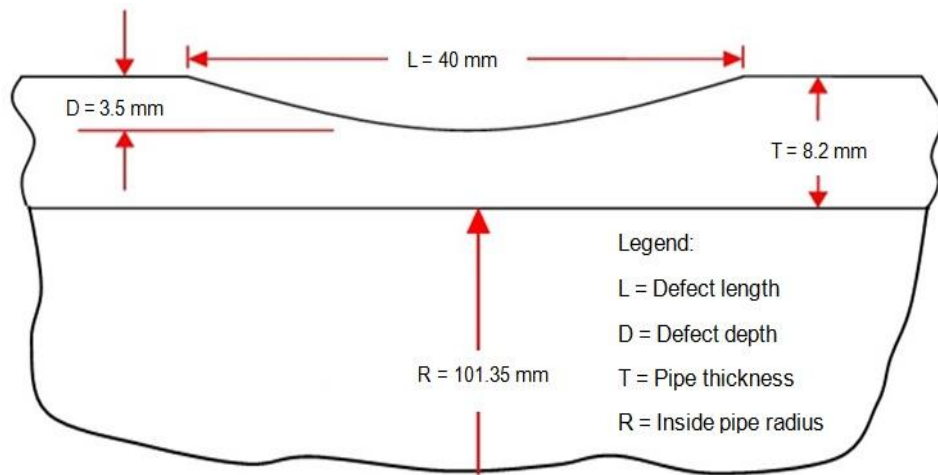
Figure 3.1: Schematic diagram of the circumferential arc-shaped notch defect

In normal engineering practice, symmetry considerations with boundary conditions dictate that a half section of the specimen was fully utilised in this study so that the computing time could be reduced. In fact, De Carvalho (2005) reminds us that incorrect boundary conditions and meshing clearly yield incorrect results. After considering all these factors, the above FE pipe model is represented in the 3D ABAQUS model as shown in Figure 3.2 *(Note: This model was used as the actual model in the Study)*.
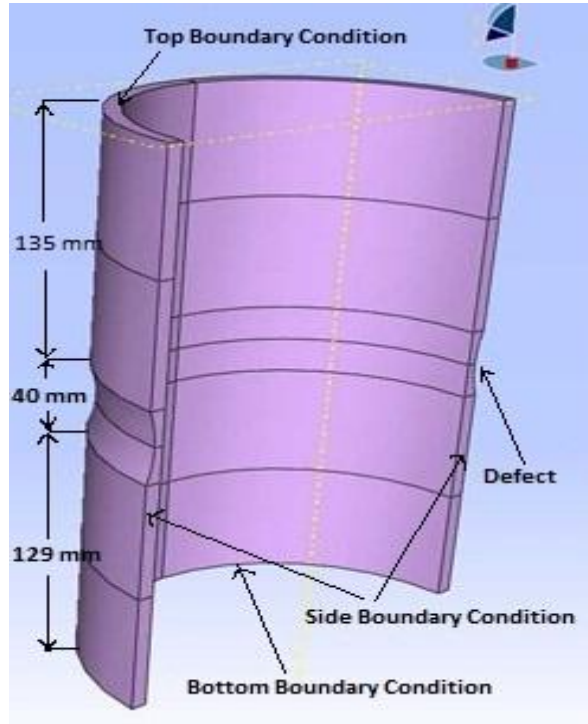
Figure 3.2: Schematic diagram of the half pipe model with boundary conditions

3.4 Fundamentals of Modelling in Finite Element Analysis

Some fundamentals of finite element analysis (FEA) and ABAQUS/CAE are briefly discussed in this section. There are a few important areas during the initial stage of carrying out an FEA. The first criterion in FEA or ABAQUS is to know the basic element type before proceeding to other steps and the second one is to know the mesh controls that are involved with meshing techniques and algorithms.

3.4.1 Element type selection

- The **Line** tab allows the user to choose an applicable element type and assign it to one-dimensional mesh elements in the region.

- The **Quad** and **Tri** tabs allow the user to choose an applicable element type and assign it to two-dimensional mesh elements in the region.
- The **Hex**, **Wedge**, and **Tet** tabs allow the user to assign three-dimensional element types to the three dimensional mesh elements in the region.

For a typical 3D pipeline and the study of stress concentration, the hexahedral (Hex) element type is often recommended. According to Qian et al. (2010), the Hex element type has superior performance in FEA in terms of increased accuracy, smaller element numbers and improved reliability. The examples of element shapes are illustrated in Figure 3.3.
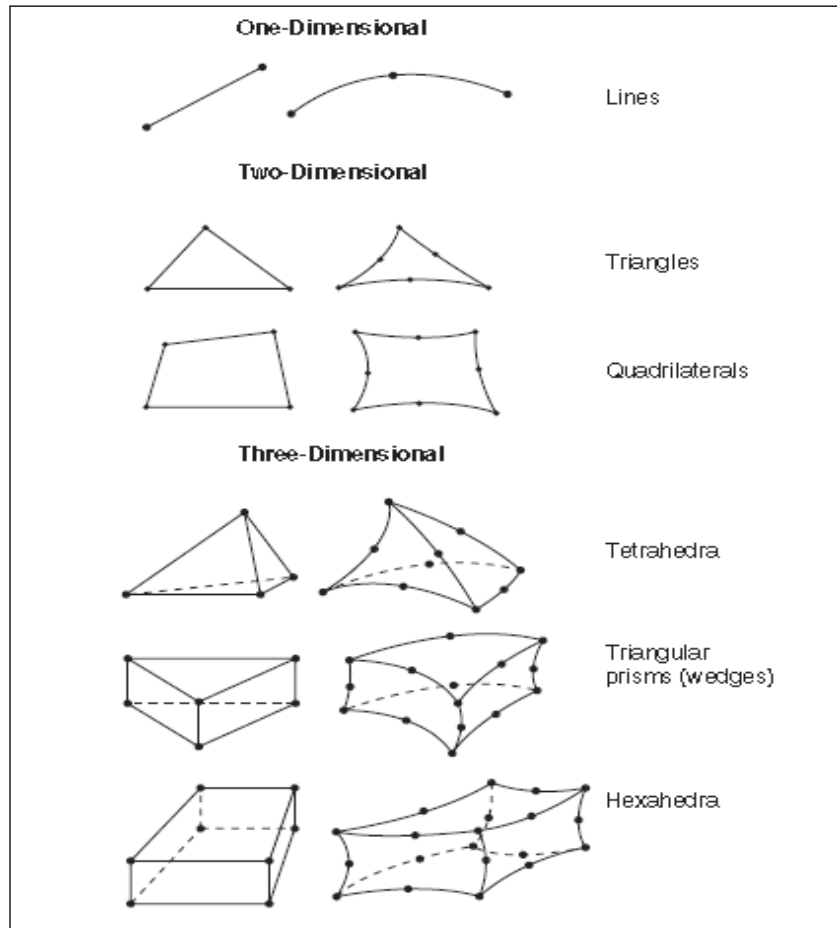
Figure 3.3: Element shapes (Abaqus Inc and DS, 2007a)

In this modelling work (i.e. composite-based repaired pipeline) that involved three different types of material, namely steel, epoxy compound and composite, a standard linear hexahedral with reduced integration elements was used, as shown in Figure 3.4 after considering various factors including suiting the CPU time and memory consumption. Based on the literature provided by Kim and Son (2004), the reduced integration elements may avoid problems associated with incompressibility. Although Gaussian quadratures have been extensively used for the numerical integration of functions where exact integration is not possible, as reported by Mousavi et al. (2010), Simpson's rule was used in this study. This rule is actually another member of a family of formulae for numerical integration besides the trapezoidal rule, and in general has a faster convergence than the trapezoidal rule for functions, though not in all specific cases as mentioned by Uribe and Neugebauer (2002).
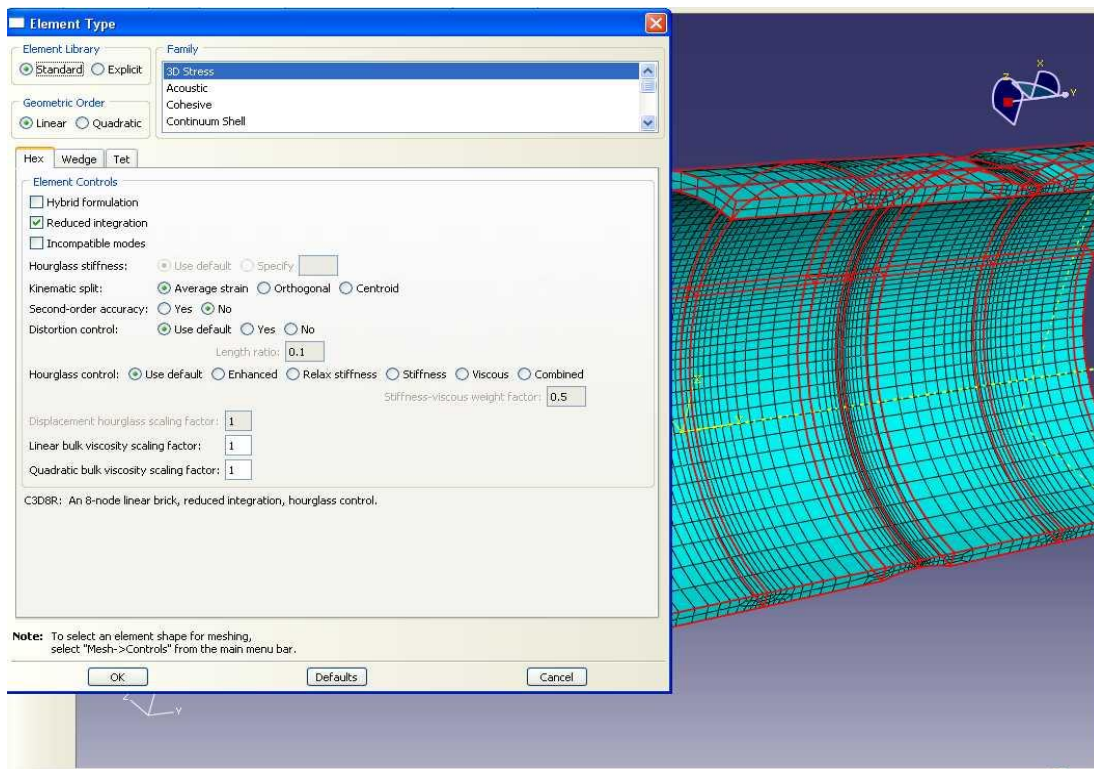
Figure 3.4: The selection of the parameters (i.e. element type) in the composite based pipeline repair

Several attempts have been made to produce very fine elements with quadratic types of geometric order elements but these often resulted in failures. One of the main reasons for this was due to insufficient memory. With limited numbers of elements (i.e. maximum limit of only 15,000 elements) provided by the current software, the total number of element that can be effectively generated should be less than 11,000 (or 75% of the maximum limit) after taking into account the efficiency of the current system. Therefore, the total number of elements generated in this study was only 10,256; where 6,880 elements were generated for steel solids, 880 for epoxy compound and 2,496 for composite material.

However, some improving steps were carried out such as using partition, seeding and bias ratio so that neither the quality of the element type nor the mesh refinement were adversely affected. With the basic and default selection of parameters provided by ABAQUS 6.7.1, the results fulfilled the objectives of this study after the final model had been validated experimentally. In addition, since this model has a simple geometry configuration and was carried out in the static condition as well as the elastic region, the selection of the parameters such as element types, mesh refinement and others were not so crucial. However, it is important to be highlighted here that the numerical result will be very much more accurate with very few anticipated errors if improvements, as suggested by several researchers in the following sections can be made in the future.

3.4.2 Mesh refinement

Generally, the mesh module provides a set of tools that allows us to refine a mesh (ABAQUS Inc and DS, 2007). To generate a successful result for a 3D pipeline model with stress concentration, the partition toolset was used to divide geometric regions into smaller regions in this modelling work. The resulting partitions introduced new edges that could seed and therefore combined partitioning and seeding to gain additional control over the mesh generation process (ABAQUS Inc and DS, 2007).

This partition toolset also helps us divide independent part instances into several regions so that ABAQUS CAE can mesh using primarily the hexahedral element. Seeding and bias ratio also help us reduce the size of elements in the area of interest and indirectly reduce the total number of elements. Figure 3.5 shows the roles of partitioning, seeding and bias ratio in this mesh refinement work. It also indicates the local (at notch root) and the remote stress points (away from the defect) respectively.
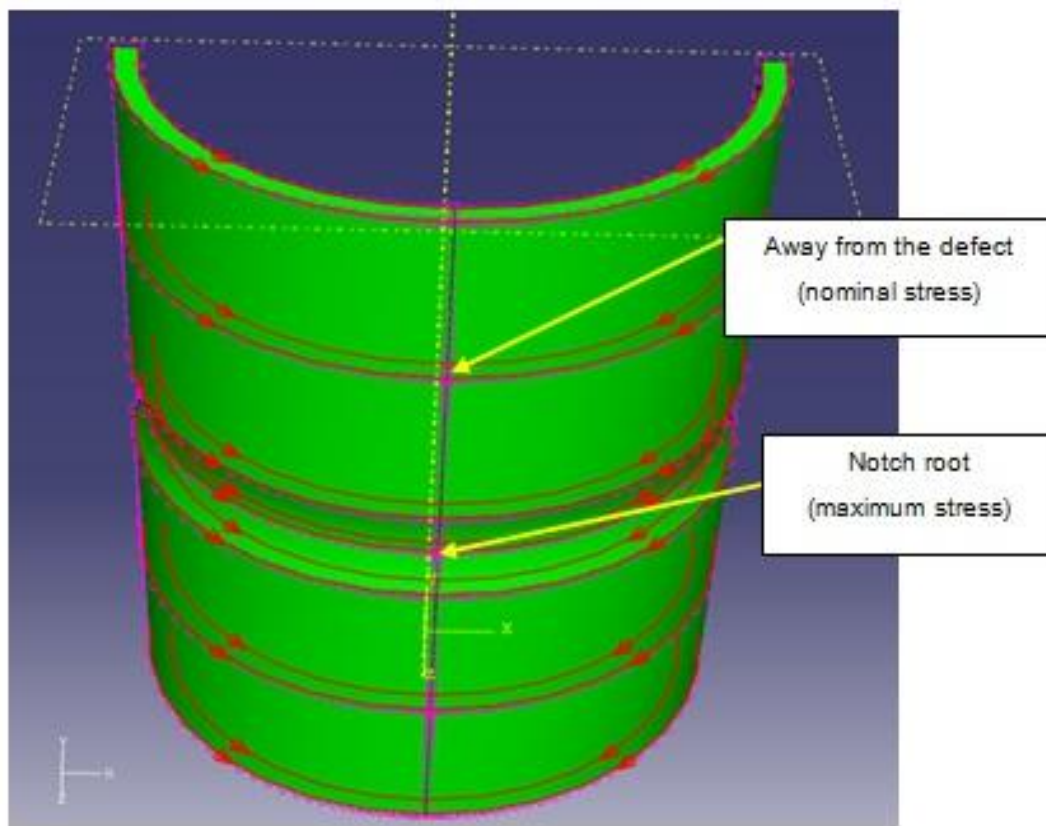
Figure 3.5: Partitioning, local mesh seed and bias ratio that allow us to refine the mesh in the area of a stress concentration

In terms of meshing technique, most meshing in ABAQUS CAE is completed in a "top-down" fashion. This means that the mesh is created to conform exactly to the geometry of a region and works down to the element and node positions. By default,

ABAQUS CAE generates meshes with first-order line, quadrilateral, or hexahedral elements throughout. Top-down meshes generated by ABAQUS CAE conform to the geometry of the part they discretize. The "bottom-up" meshing technique, in place of the automated top-down meshing technique, is also able to generate a hexahedral mesh. However, bottom-up meshing is a manual, incremental meshing process that builds up a 3D mesh from 2D entities and an incremental meshing process that allows us to build a hexahedral mesh. In fact, bottom-up meshing relaxes the constraint that ties the mesh to the geometry so that a mesh can be built up which ignores some geometric features (ABAQUS Inc and DS, 2007).

Although the bottom-up technique allows us to create a mesh using only hexahedral elements as compared to top-down meshing techniques that require extensive partitioning or the use of tetrahedral elements to complete the mesh, for the development of this half pipe model, another technique was found to be more suitable and easier. Due to some difficulties found with the bottom-up tool in this ABAQUS version 6.7.1, a sweeping based technique, referred to by Staten et al. (2010a) as among the most widely used hexahedral meshing algorithms in industry today, has been adopted in this modelling – see Figure 3.6. According to them, this technique is most suitable to decompose and sweep solids of low to medium complexity. However, sweeping applies only to topology swept volumes or solids which can be decomposed into 2.5 partitions. In other words, sweeping methods place strict requirements on the model topology. If the solid model is too complex, this technique is not suitable because it can cause algorithm failures or may produce poor element quality.
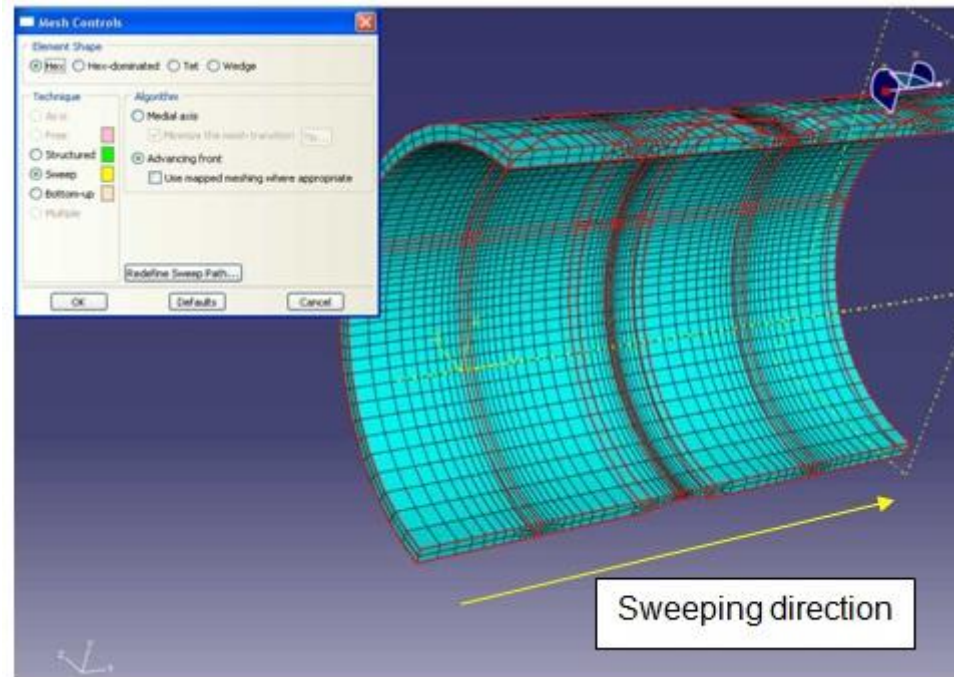
Figure 3.6: Mesh control using Sweeping Techniques and Algorithms

3.4.3   Types of Algorithms

In FEA, there are many types of algorithms that can be used based on the complexity of the model configurations. In a commercial ABAQUS software, for example, Advancing Front algorithms have proved to be ideal for triangular, quadrilateral and even tetrahedral meshes because of the connectivity of these simple element shapes. If the medial axis algorithm was used for example in a 2D modelling, a free mesh generated with quadrilateral-dominated elements will be similar to a free mesh generated with all quadrilateral elements and without transition minimisation. ABAQUS CAE normally inserts a few isolated triangles in an effort to match the mesh seeds more closely. Therefore, a mesh with quadrilateral-dominated elements sometimes can be generated faster than a mesh with all quadrilateral elements (ABAQUS Inc and DS, 2007).

Another class of algorithms are overlay grid, octree or inside-out methods that follow a top-down approach by placing elements on the inside of the volume first,

without defining a boundary surface mesh. Despite these methods placing high quality elements on the interior of the volume, the shaping nodes to fit the boundary tend to decrease quality along the boundary. Hence Staten et al. (2010a) have introduced a new concept, known as unconstrained plastering, in order to produce a reliable hexahedral meshing algorithm. With this approach, they relax the constraint while still maintaining the desirable characteristic of advancing front meshes and it is then free to define the topology of its boundary mesh as a consequence of the interior meshing process.

Besides Staten et al. (2010a), Qian et al. (2010) have also introduced the improved meshes that have good Jacobians and are smooth on the boundaries. The issue of the stair-casing effect at the boundaries due to the direct conversion of voxel data to 3D brick element (hexahedral) has motivated their research to choose an octree-based isocontouring algorithm to construct hexahedral meshes. This improved algorithm works with arbitrarily complicated geometry and topology. Although their approaches produce better meshing, in this PhD study no improvement has been carried out except to use the default Advancing Front algorithm as provided by ABAQUS 6.7.1. Figure 3.7 shows that despite there being some distortions in the hexahedral elements, the Advancing Front algorithm was able to generate hexahedral elements at the boundary of the region and continue to generate them as it moved systematically through the thickness of the solid model. In other words, this hexahedral meshing was able to maintain a connectivity of 8 nodes, 12 edges and 6 faces per element.
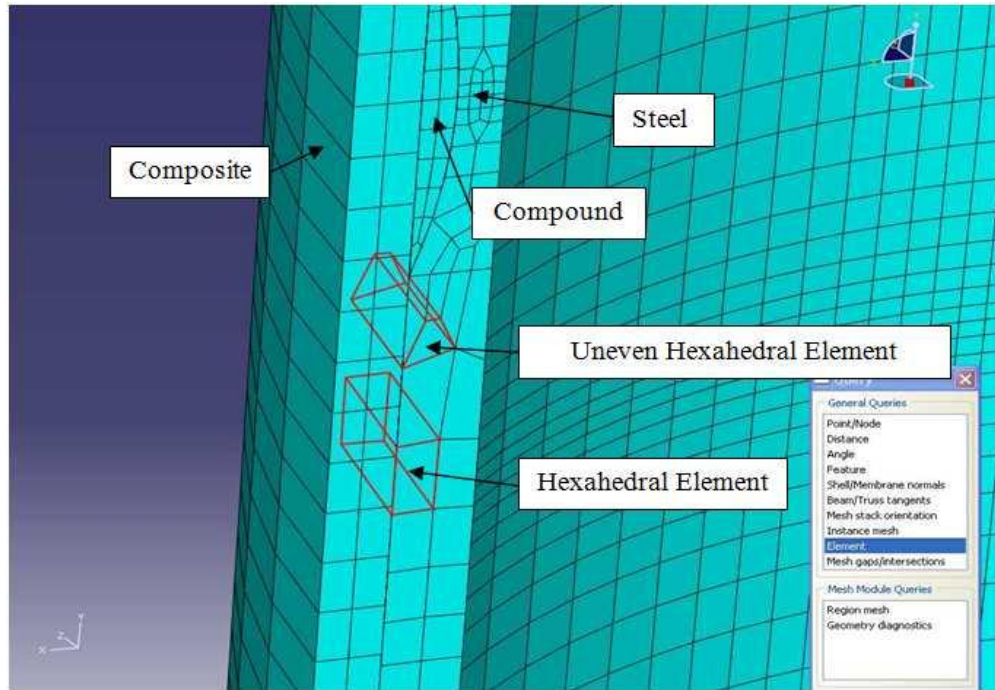
Figure 3.7: Schematic representation of the cross-sectional view along x plane of the composite repair model

Another improvement of the meshing that can be considered in a future study can be referred to from Fries and Belytschko's (2010) approaches. In finite element modelling, they point out that the resulting solutions typically involve discontinuities (e.g. cracks), singularities, high gradients (e.g. notches) and other non-smooth properties. For the approximation of non-smooth solutions, normally commercial software such as ABAQUS CAE uses polynomial approximation spaces and relies on meshes that conform to discontinuities, singularities and high gradients. To treat this, remeshing is required.

Fries and Belytschko (2010) have also examined the similarities of the partition of unity method, generalised finite element method and the extended finite element method (XFEM). They place more emphasis on the XFEM methods for discontinuities (e.g. cracks) and high stress gradients (e.g. notches). For typical high stress gradients, the classical FEM requires an appropriate refinement of the mesh. This refinement can lead to a large increase in computational effort. In ABAQUS for example, mesh

refinement is often not a fully automatic procedure and user-controlled adjustments are required in order to generate better meshing, and it relies on the approximation properties of (mapped) polynomials. Therefore, Fries and Belytschko (2010) point out that an alternative to remeshing is to enrich the approximation space of the FEM so that these non-smooth solution properties are accounted for correctly, and independent of the mesh, and this is the path chosen in the XFEM. As a result, simple fixed meshes can be used throughout the simulation so that mesh construction and maintenance are reduced to a minimum and to enrich a polynomial approximation space such that non-smooth solutions can be modelled independent of the mesh.

Alternatively to the technique of Fries and Belytschko (2010), Compere et al. (2010) propose improved mesh adaption using local mesh modifications. They understand that the remeshing technique normally removes the existing mesh and replaces it with an adapted one. However, they identify two problems with the current remeshing technique:

1) It introduces a lot of numerical diffusion in the mesh-to-mesh interpolation procedure

2) It is difficult to be applied when the computation is done in parallel.

Therefore, in order to satisfy a prescribed mesh field size and maximise mesh quality, they have developed the open source Mesh Adaptation Library (Madlib) that describes a new code repositioning algorithm which combines a standard global node repositioning with local mesh modifications. Although this technique can improve the efficiency of the CPU time and memory consumption, these Madlib tools and algorithms are only suitable for adapting the tetrahedral meshes.

3.4.4   Artificial constraints

In the composite-based pipeline repair modelling, the composite wraps and the solid pipeline that are subjected to biaxial loading are inappropriate for 2D

discretization. Therefore, in this study, they were modelled by 3D elements instead. The Triaxial Woven Fibre (TWF) composites were meshed with continuum shell elements (SC8R). These elements enabled capturing 3D geometry and consequently improved accuracy in contact problems. Pipe and repair compounds were modelled by solid C3D8 elements. As both continuum shell and solid elements have only a translational degree of freedom, coupling at the interface of the face layer and core elements was achieved by sharing the same interface nodes, thereby eliminating the need for kinematic constraints.

According to Smojver and Ivancevic, (2010), in order to correctly transfer rotational degrees of freedom at the interface of 3D and conventional shell elements, appropriate coupling constraints need to be provided at the interface of different element types. This kinematic coupling constraint was achieved by tie surface-based constraints which were imposed on the nodes at the joint line of the continuum shells and solid elements. The methods that describe the above explanations are illustrated in Figures 3.8, 3.9, and 3.10. Without these artificial constraints such as tie and rigid body constraints, results cannot be generated successfully (ABAQUS Inc and DS, 2007).
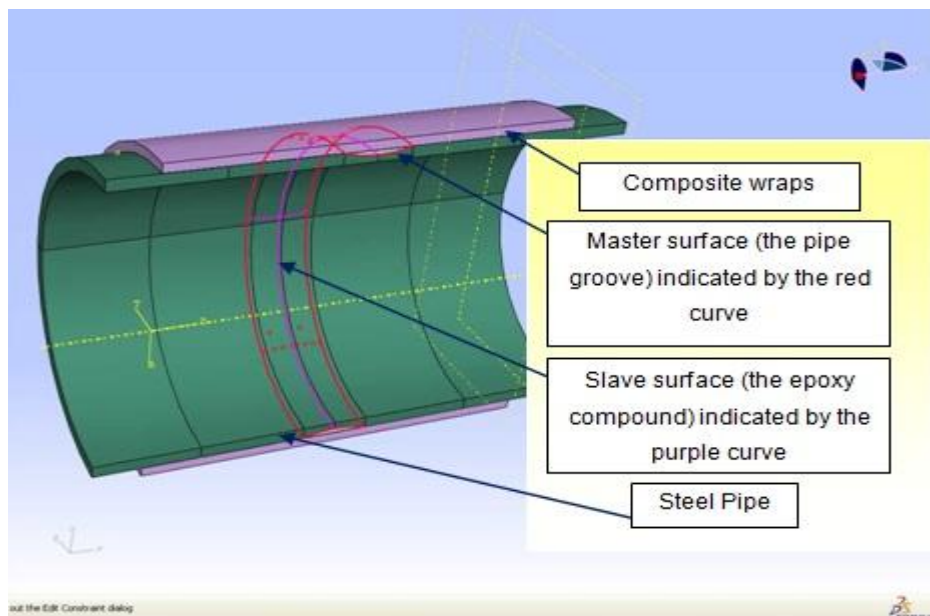
Figure 3.8: The first tie constraint between pipe and epoxy compound

Master surface (the composite wraps) indicated by the red curves and lines

Slave surface (the pipe surface beneath the composite wraps) indicated by the purple curves and lines
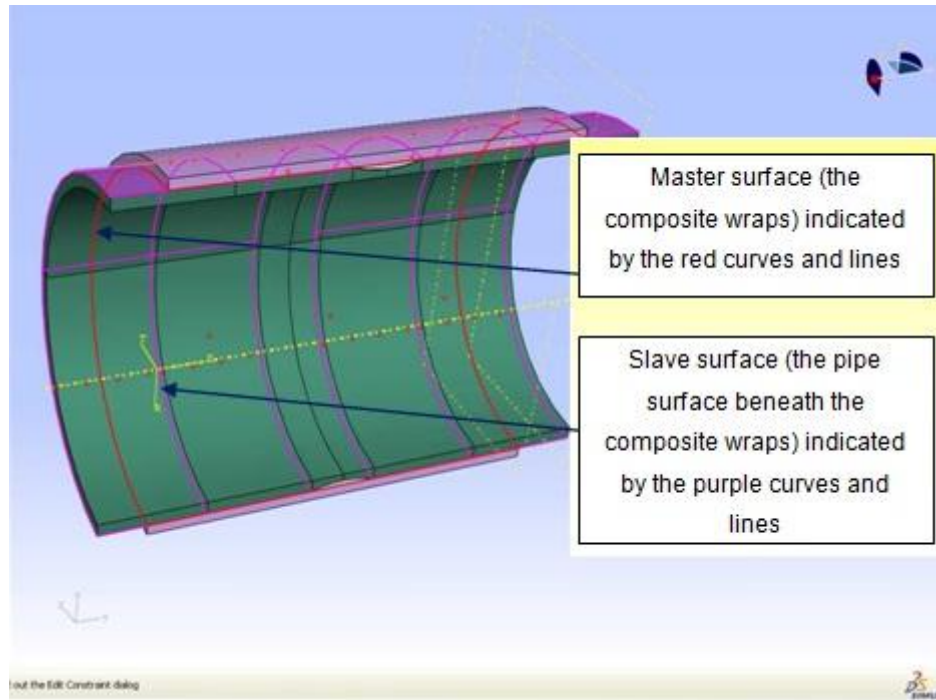
Figure 3.9: The second tie constraint between composite and pipe

Master surface (the composite wraps) indicated by the red curves and lines

Slave surface (the epoxy compound surface) indicated by the purple curves and lines
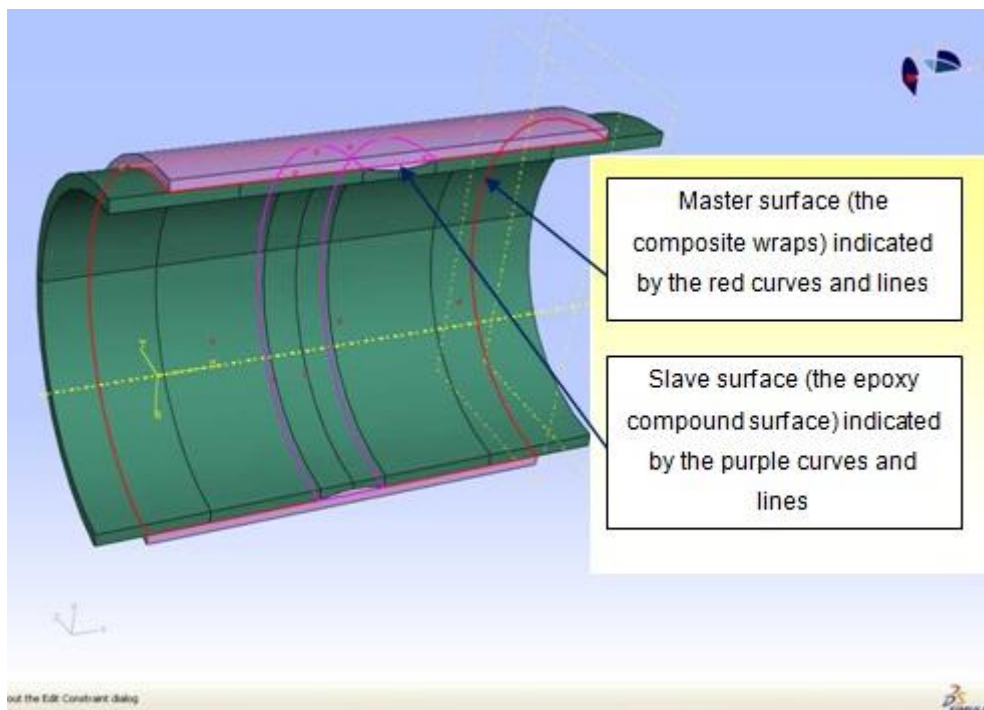
Figure 3.10: The third tie constraint between composite and epoxy compound

68

According to Staten et al. (2010b), there is another method for handling non-conforming interfaces that involves the above artificial constraints. In their study, they proposed using the new technique or method that involves new algorithms where the non conforming hexahedral-to-hexahedral interfaces can be converted into conforming interfaces by using mesh matching. This technique is able to locally modify the topology of the hexahedral elements. It provides inter-element continuity in the finite element shape functions ensuring a smooth and continuous solution over the interface. Their main goal was not to replace the artificial constraints in the solver but to reduce the amount of time required to create conforming hexahedral finite element meshes on complex assembly models.

However, in this PhD study, only default artificial constraints were used. Apparently, tie constraints are able to fuse together two regions even though the meshes created on the surfaces of the regions may be dissimilar; the rigid body constraint managed to constrain the motion of regions of the assembly to the motion of a reference point. The relative positions of the regions that were part of the rigid body remained constant throughout the analysis (ABAQUS Inc and DS, 2007).

Element types, including eight-node hexahedrons, led to more reliable FEA solutions. There are many reasons why the eight-node hexahedral elements produce more accurate results than other elements (e.g. four-node tetrahedrons). In fact, they captured the singularities of the model at much less cost since they consumed much less computer time and memory than the processing of higher order polynomials (p) or making element sizes smaller (h) or both. In order to eliminate shear, volume locking and enhance model flexibility, reduced integration was employed as suggested by Kim and Son (2004).

This PhD study contains two types of modelling. The first model was developed without composite repair and the second with the repair. In order to meet the objectives of this numerical study, the second model was identical to the first model and therefore the specifications of the hexahedral elements remain constant throughout the study.

In this Study, the linear eight node hexahedral elements (p = 1) with reduced integration (C3D8R) were used. For the pipe with a 40 mm arc-shaped notch (N40 model), 4,452 up to 14,504 elements and 19,722 nodes were used and resulted in the smallest element size (h) = 0.996 mm, as shown in Figure 3.11. Although tetrahedral elements are linear, they were not used in this FEA model. According to Kim and Son (2004) tetrahedral elements can have more discretization errors since they have a constant strain.
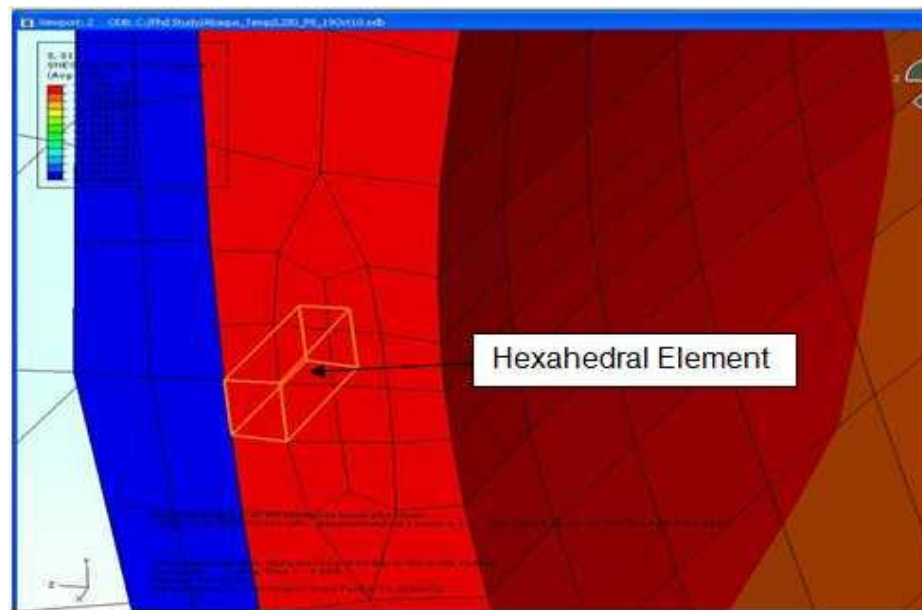
Figure 3.11: An example of a perfect hexahedral element

3.5   The influence of pressure on the FEA pipe model

The aim of this section is to study the influence of the internal pressure on the model shown in Figure 3.2. This study assumes the pipe is perfectly straight and there is no effect of bending moments normally induced by misalignment.

3.5.1 Pressure test on the converged model

This section discusses the convergence study that had been carried out on the numerical model, based on a constant pressure of 10 bar, and the results are summarised in Table 3.1. The convergence of stress and strain values at the notch root was achieved when the number of elements had reached 14,504.

Table 3.1: The convergence study at the notch root - constant pressure of 10 bar

No of Elements	Hoop Stress (σ_x) - MPa	Axial Stress (σ_y) - MPa	Hoop Strain (ε_x) x 10^{-5}	Axial Strain (ε_y) x 10^{-5}
1,620	20.756	11.580	8.270	2.560
4,170	20.183	11.367	8.035	2.550
8,840	20.241	11.552	8.028	2.623
12,558	20.261	11.635	8.027	2.652
14,504	20.257	11.638	8.026	2.654

After identifying the number of elements through the linear study, the pressure of 10 bar increments was applied on the inside surface of the model up to 50 bar. Results are summarized in Table 3.2 and plotted in Figures 3.12 and 3.13.

71

Table 3.2: Increasing Pressure on the Converged Model

Pressure (bar)	Hoop Stress (σ_x) – MPa	Axial Stress (σ_y) – MPa	Hoop Strain (ε_x) x 10^{-4}	Axial Strain (ε_y) x 10^{-4}
10	20.247	11.658	0.7996	0.265
20	40.494	23.315	1.600	0.531
30	60.741	34.973	2.400	0.796
40	80.980	46.631	3.200	1.060
50	101.235	58.288	3.998	1.327
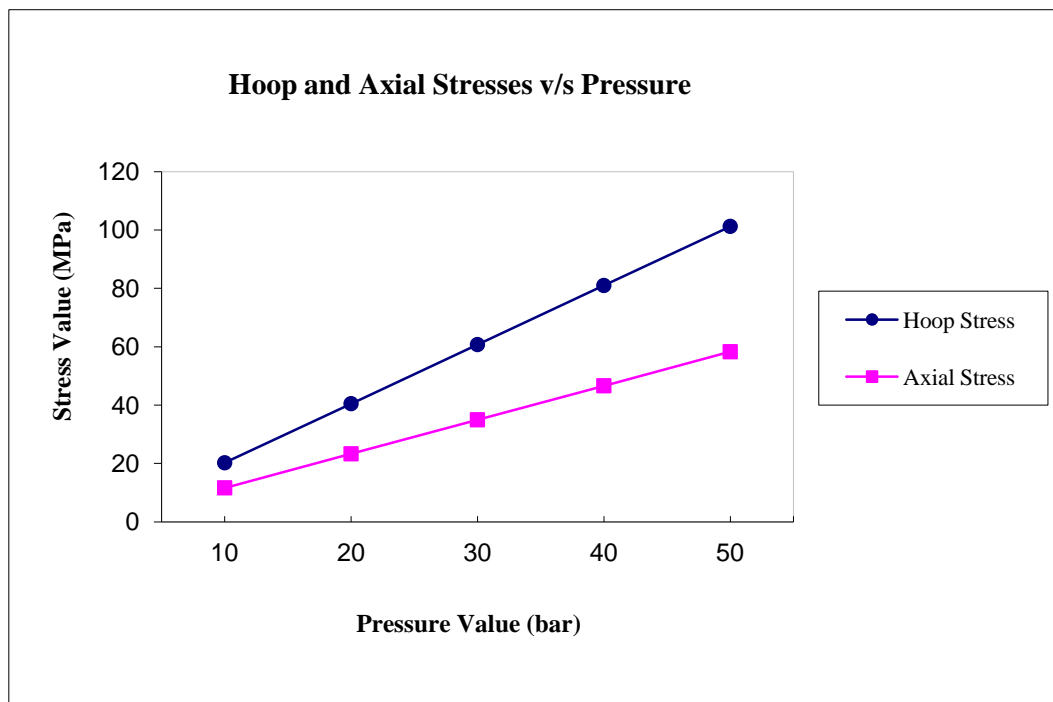
Figure 3.11: Stresses at the Notch Root versus Pressure

Figure 3.12 shows that the hoop and axial stresses increase linearly with the pressure increment. This confirms that the simulation tests were performed in the true elastic working region. Also, the percentage difference of hoop and axial stresses at

each pressure value remains constant at 42.4% as the pressure increases from 10 to 50 bar. The consistency of this reading was achieved because this simulation test was performed on the converged model.

Figure 3.13 also shows that the hoop and axial strains increase linearly with the pressure increment. Likewise, the percentage difference of hoop and axial strain at each pressure value remains constant but slightly higher at 66.8% as the pressure increases from 10 to 50 bar. Again, this plot proves that the simulation tests were performed in the true elastic working region using the converged model.
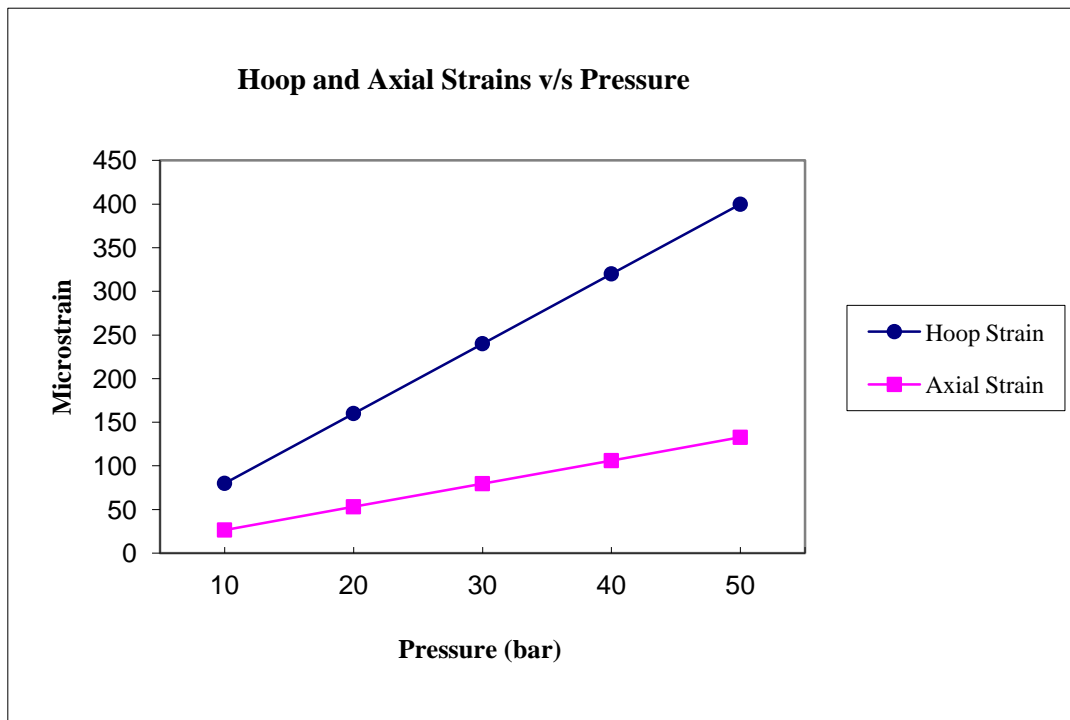
Figure 3.13: Strains at the Notch Root versus Pressure

3.6 To determine other factors' influences on the Numerical Model

3.6.1 Introduction

In this section, it is important to show that the developed numerical model that has been discussed in the previous section is the right and suitable model to be used in the next stress and strain distribution studies. There are two methods of validating this model. The first is to compare the numerical hoop and axial stress values of the chosen model with several other models and validate them analytically. Details of this method are going to be discussed further in this section. The second method is to compare this chosen numerical model against the actual pipe specimen which has similar physical and mechanical properties, dimension and geometry. This will be further explained and discussed in a later chapter (i.e. experimental work). In this stress comparison study, which involves several models, what must be clearly addressed is that the defect and nominal pipe thicknesses of each model remain constant and follow the actual test rig specifications.

3.6.2 Comparison of Results

As mentioned in the earlier section, in order to justify the preselected model (in this case Model 3) as the right and most suitable model, the numerical results of hoop stress (S11) and axial stress (S22) of each model from ABAQUS were obtained and compared against the results of the manual calculation (analytical method). A simple shell theory was applied in this manual calculation as shown below;

For Hoop stress, σ_h (S11), it was referred to as Hoop Strain, ε_h (Kaminski, 2005) and multiplied by Young's Modulus as shown below;

$$\varepsilon_h = \frac{PD}{4tE}(2 - v) \qquad \text{(Equation 3.1)}$$

and,
$$\sigma_h = E. \; \varepsilon_h \qquad \text{(Equation 3.2)}$$

74

Axial Stress, σ_a (S22) was referred to as Axial Strain, ε_a (Kaminski, 2005) and multiplied by Young's Modulus;

$$\varepsilon_a = \frac{PD}{4tE}(1 - 2v) \qquad \text{(Equation 3.3)}$$

and,
$$\sigma_a = E.\,\varepsilon_a \qquad \text{(Equation 3.4)}$$

Where;

ε_h is Hoop strain

ε_a is Axial strain

P is operating pressure, MPa

D is Outer diameter of Pipe API 5L Grade B

E is Young's Modulus

v is Poisson ratio of steel

t is the thickness of the pipe

Table 3.3 summarises the manually calculated (analytical) and numerical hoop (S11) and axial (S22) stresses for all models involved that have the same diameter. All the stress values of each model were measured in the centre of the pipe (i.e. for the pipe without a defect) and for the models with a defect in them, their stress values were obtained from the notch root of the defect. However, for Model 6, two measurements were taken. One was at the notch root (i.e. maximum value) and the second was away from the defect (i.e. nominal value).

Table 3.3: Stress study among 6 different models (Pressure at 50 bar)

Model	Descriptions	Dimension	Hoop Stress S11 (MPa)		Axial Stress S22 (MPa)	
			From Equation 3.2	From FEA	From Equation 3.4	From FEA
1	Symmetrical Short Pipe without defect (reading taken in the centre of the specimen)	L = 304 mm *L is the length of specimen*	56.92	57.87	13.39	17.49
2	Symmetrical Long Pipe without defect (reading taken in the centre of the specimen)	L = 608 mm *L is the length of specimen*	56.92	51.84	13.39	16.2
3	Short Pipe with defect of 40 mm (reading taken in the centre of the pipe) *Note: This is the actual model used in the PhD study*	L = 304 mm *L is the length of specimen*	99.48	100.14	23.41	53.84
4	Symmetrical Short Pipe with defect of 40 mm (reading taken in the centre of the pipe)	L = 304 mm *L is the length of specimen*	99.48	100.18	23.41	55.50
5	Symmetrical Long Pipe with defect of 40 mm (reading taken in the centre of the pipe)	L = 608 mm *L is the length of specimen*	99.48	105.42	23.41	63.80
6	Full Pipe model with 40mm defect i) at the notch root ii) away from the defect	L = 888 mm *L is the length of specimen including flanges*	99.48 56.92	99.47 57.99	23.41 13.39	45.43 13.89

Figure 3.14 shows a graph of analytical (Equation) and numerical (FEA) stresses against models that have different geometries and dimensions. The comparison study on Model 3 (chosen model) with other models, in terms of numerical stress values, is very important because it has to prove that this chosen model is not influenced by other factors such as geometry, dimension etc.
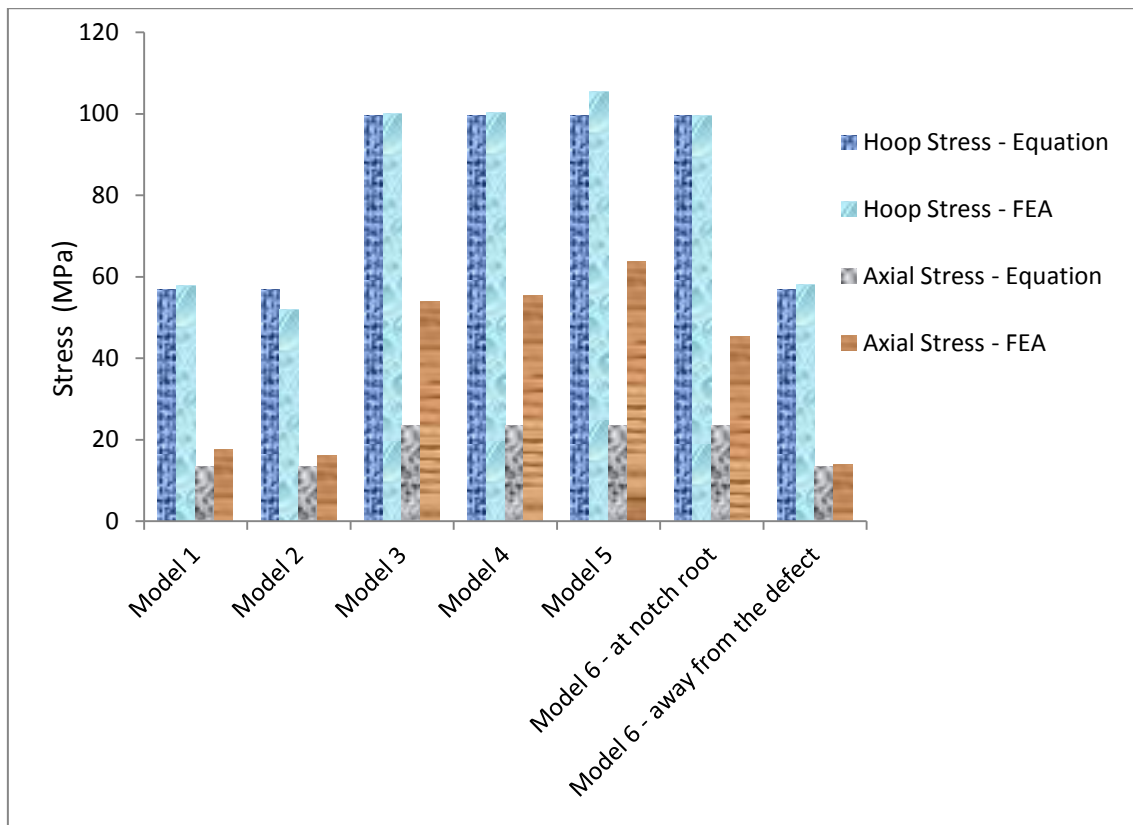
Figure 3.14: Results of six different models

From Table 3.3 and Figure 3.14, Model 1 which represents a symmetrical short pipe without defect, shows almost good agreements with Model 2 (a symmetrical long pipe without defect) with the difference (error) of only 10% for numerical hoop stress and 7% for numerical axial stress. This justifies that in this simulation work, it is not necessary to design a very long pipe in order to obtain a better result.

The above graph also shows that Model 3 has almost similar results to Model 4 with a very small difference (error) of 0.03% for hoop stress and 2.99% for axial stress. This means that a slight difference of length between the notch root to the top and bottom edges of Model 3 (slightly asymmetric) does not make any difference at all to the symmetrical model (i.e. Model 4). Hence, Model 3 that represents the numerical and experimental model can also be assumed to be symmetrical in this study.

Model 5 also shows that when there is a notch on the long pipe model, the axial stress value that was measured in the notch root of the pipe has a slightly higher value than the shorter pipe models (i.e. Models 3 and 4), but it is not too obvious, with a difference (error) of only 13%. However, the hoop stress of Model 5 shows a better agreement with Model 3 or 4 with a small difference (error) of less than 5%. Therefore, the dimension factor has no significant influence on the model that contains a defect.

The effects of boundary conditions in the pipe models can be further discussed using Model 6. Since this a full pipe model and represents the actual complete test specimen dimension, no boundary condition was introduced on the pipe model. The differences (errors) of hoop and axial stresses between Models 6 and 3 are 0.67% and 15.6% respectively. This proved that dimension and boundary condition factors do not influence the stress reading despite the difference of the axial stress being slightly on the higher side.

Finally, the above comparison study on the numerical results of different models was validated analytically. From the graph, most of the hoop stresses of all the six models show a good agreement with manually calculated results with a maximum error of only 8.9% which mostly occurred in Model 2. However, the axial stress is less apparent in Models 3, 4, 5 and 6 and they fail to show the true values. The main reason for this is because the manual calculation is based on the simple shell theory that assumed the defect was a flat notch rather than arc-shaped. A more complex mathematical approach is required in the future to determine the axial stress on the arc-shaped defect. In this comparison study also, it shows that finite element is right because it was able to take into consideration the complexity of the defect profile into its calculations. On the other hand, the axial stress value that was measured away from

78

the notch defect is found to be in a good agreement with the manually calculated value with a difference (error) of only 3.6%.

3.6.3 Concluding Remarks

In order to produce a good and reliable model, it is not necessary to develop a long model (e.g. Model 5) or a complete geometry (e.g. Model 6) which, of course, is more expensive and time-consuming. As mentioned earlier, manually calculated stress values are equally important to validate analytically all the numerical models, especially for Model 3.

Equations 3.2 and 3.4 were found to be adequate in validating the hoop stress for the model with and without defects. For the validation of axial stress, these equations were found to be acceptable for the model without defect only. For the model with the defect (e.g. Model 3), a more complex mathematical expression is required and this can be done in future work.

Hence, it can be concluded the Finite Element (numerical analysis) was able to take into account the biaxial effects due to the presence of discontinuities such as notches. The objective – to prove that Model 3 is the right and suitable model to be used – in the stress and strain distribution study was achieved and justified.

3.7 The simulation of blunt defect behaviour in a thin walled cylinder (FE Pipe Model)

3.7.1 Introduction

The flaw type considered here is a blunt flaw (notch) due to local wall thinning caused by erosion or corrosion. The presence of a notch in a structural system is not a common occurrence only in engineering; any geometric discontinuity can initiate a surface crack due to the stress concentration effects, and the methodology for strength

and fatigue life assessments of notched components is well known, as addressed by Kim and Son (2004).

It is important to understand this notch effect in terms of stress concentration factors (SCFs). SCFs are normally obtained analytically from elastic theory, computationally from Finite Element Analyses (FEAs), and experimentally using methods such as photoelasticity or strain gauges (Pilkey, 1997). In fact, the stress concentration effects of V-shaped, U-shaped and hyperbolic notches in a long thin tensile plate were studied by using experimental methods, Neuber's theory, singular integral method (Tian et al., 1997); Peterson's design curves (Peterson, 1953) also provides some useful values of stress concentration factors for pipes but they are limited to typical 2D geometries.

Yang et al. (2008) highlight the stress concentration locations such as notch is being critical in determining crack initiation and growth and hence the life of the structures. Often cracks initiate and propagate from the location of high stress concentration. Thus, by conducting a 3D FEA, the elastic stress concentration factor for a pressurised pipe with a circumferentially arc-shaped notch on the external surface was determined in this study as a precursor to further FEA analysis of the stress strain distribution in the composite-based pipeline repair. Knowing the loading, the stress concentration factor can be obtained in the 3D pipeline repair as a function of defect geometry and Poisson's ratio, as explained by Murad and Brennan (2010) .

3.7.2 Geometry of Notches in FE Pipe Model

Referring back to the previous researchers, such as De Carvalho (2005) and Kim and Son (2004), none of them models the defect on the external surface. Their stress concentration factors are more related to wall thinning due to erosion rather than external corrosion. Hence, this study presents the stress concentration factor measured on the outside of the pipe.

One of the contributions of this study is the use of finite element method to determine nominal and maximum stresses for stress concentration factor values. Earlier researchers used the empirical formula to identify the nominal stress and only the maximum stress at the notch root is determined by the finite element method. The present work uses ABAQUS to determine both nominal and maximum stresses and no empirical formula is generated.

In this study, the geometry presents an interesting biaxial situation changing in significance with notch length and depth. The FEA model, once validated, will allow the study of the biaxial SCFs so that an optimum repair scenario can be investigated. The notch length is denoted L, nominal thickness t, and defect depth d. The nominal thickness t is 8.2 mm and defect depth d is 3.5 mm and these remain constant throughout the whole process (during the course of the study). Five FE models of various arc-shaped notches are shown in Figure 3.15. The shortest arc-shaped notch has the length of 7 mm and is denoted by N7 followed by N40 (Notch length = 40 mm), N60 (Notch length = 60 mm), N90 (Notch length = 90 mm) and N100 (Notch length = 100 mm).
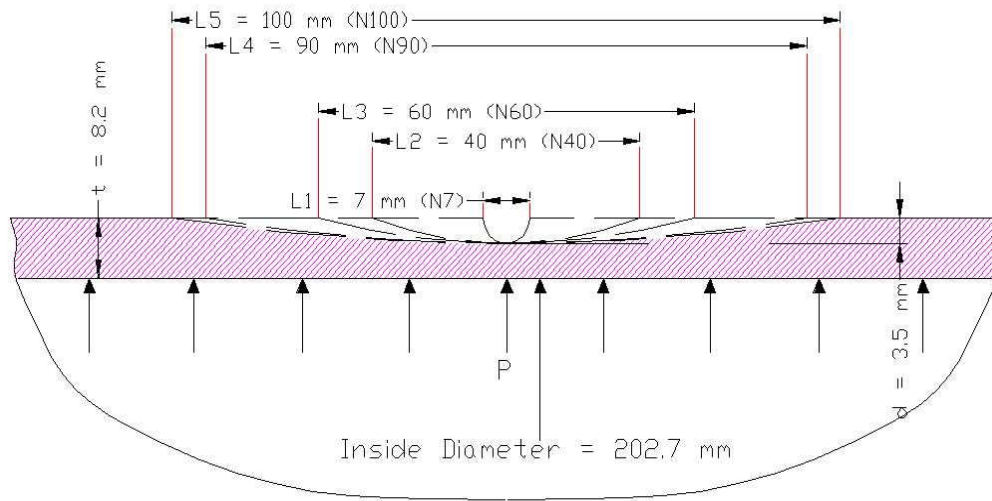
Figure 3.15: Detailed dimensions of different arc-shaped notch sizes

81

3.7.3 Internal Pressure

For a pipe under internal pressure, the hoop stress, σ_h, and the axial stress, σ_a are the two major stress components that are always considered. In this FE model, the maximum hoop and axial stresses were taken at the notch root and nominal hoop and axial stresses were taken at the point away from the defect (refer to Figure 3.5) which gives the stress concentration factor, K_t, by

$$K_t^h = \frac{\sigma_{max}^h}{\sigma_{nom}^h} \quad \text{(Equation 3.5)} \quad \text{and} \quad K_t^a = \frac{\sigma_{max}^a}{\sigma_{nom}^a} \quad \text{(Equation 3.6)}$$

The problem of SCF for circumferentially notched pipe has been examined by several authors (Carpinteri et al., 2004), yet a study on an arc-shaped notch in a pipe has not been carried out so far. The outer radius of the external notch is difficult to obtain because of the nature of its geometry and this makes comparison against other types of notches (e.g. those given by Pilkey (1997)) impractical. Prior to making experimental measurements, confidence can be attributed to the current FEA by considering the results of the parametric variations and using engineering experience and judgment.

Convergence tests were carried out on all notch geometries, as represented in Table 3.4 and Figures 3.16 and 3.17. These show that all the convergence results of stress concentration factors are based on both hoop and axial stresses as the number of elements increases and the size of the elements becomes smaller.

Table 3.4: Convergence tests on various sizes of notch; Test Pressure at 50 bar

No of Elements	σ_{max}^h	σ_{nom}^h	K_t^h	σ_{max}^a	σ_{nom}^a	K_t^a
Relative Notch, L/t = 0.85 (N7); Arc-shaped (semi-circle) Notch						
4576	90.86	62.61	1.45	55.45	15.44	3.59
5120	90.94	61.36	1.48	55.65	15.37	3.62
11872	90.86	61.23	1.48	55.47	15.51	3.57
14000	90.82	61.25	1.48	55.33	15.63	3.54
Relative Notch, L/t = 4.88 (N40); Arc-shaped Notch						
4454	98.04	66.86	1.61	48.69	17.80	2.73
6800	98.94	60.99	1.62	49.94	17.69	2.82
11664	100.73	61.01	1.65	56.21	17.95	3.13
14504	100.74	60.90	1.66	56.18	17.73	3.17
Relative Notch, L/t = 7.32 (N60); Arc-shaped Notch						
3840	104.98	61.76	1.70	50.05	19.46	2.57
7200	105.04	61.82	1.70	48.91	19.32	2.53
11520	105.07	61.59	1.71	48.54	19.86	2.44
14190	105.08	61.75	1.70	48.31	19.77	2.44
Relative Notch, L/t = 10.98 (N90); Arc-shaped Notch						
3840	107.88	61.49	1.75	42.89	22.53	1.90
7200	107.31	61.47	1.75	41.34	22.36	1.85
11520	107.17	61.21	1.75	40.91	22.33	1.83
14448	107.14	61.15	1.75	40.78	22.35	1.83
Relative Notch, L/t = 12.20 (N100); Arc-shaped Notch						
3936	108.17	61.17	1.77	40.79	23.65	1.72
7200	107.29	61.08	1.76	39.22	23.43	1.67
11520	107.10	60.81	1.76	38.80	23.40	1.66
14448	107.10	60.75	1.76	38.68	23.42	1.65

As referred to Figure 3.16, Notch N100 has the highest hoop stress concentration, K_t^h (i.e. 1.76) and N7 has the lowest hoop stress concentration of 1.48.
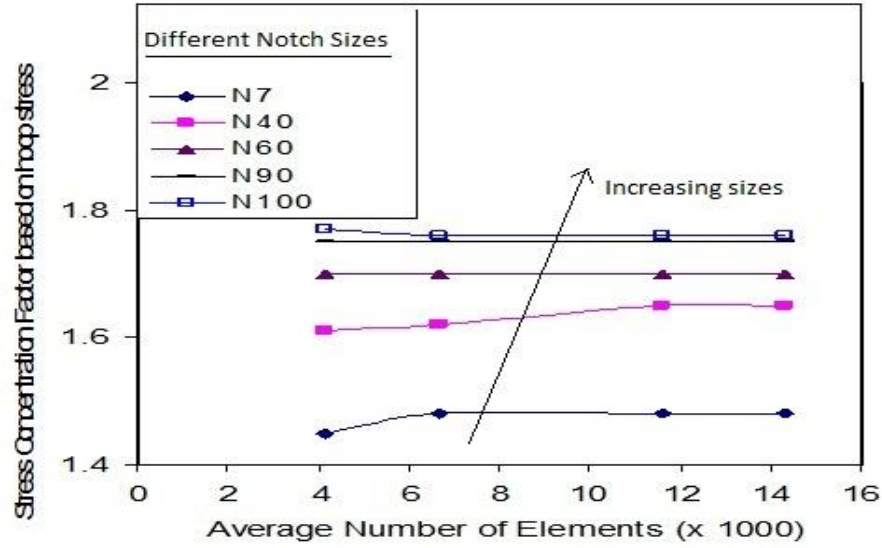
Figure 3.16: Convergence test for SCF: Notched pipe under hoop stress

Figure 3.17 shows that Notch N7 has the highest axial stress concentration, K_t^a (i.e. 3.54) and N100 has the lowest axial stress concentration of 1.65.
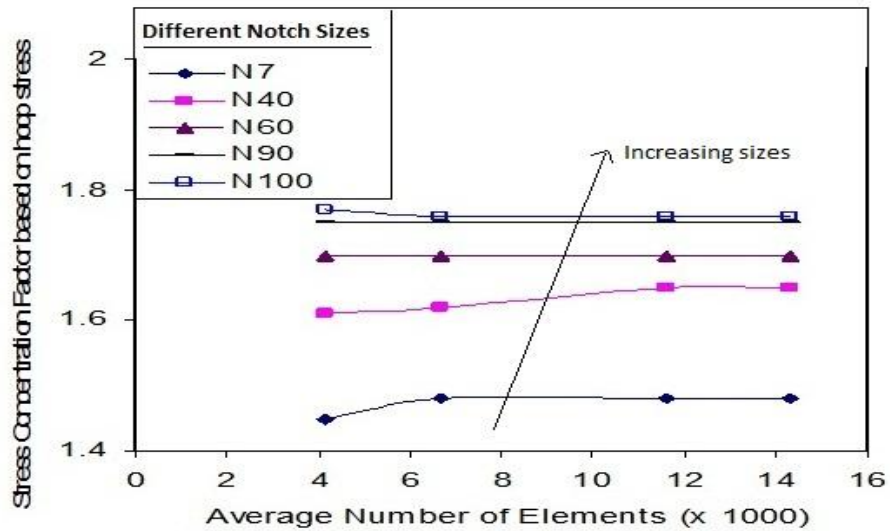
Figure 3.17: Convergence test for SCF: Notched pipe under axial stress

84

Figures 3.16 and 3.17 show that the longer the arc defect length, the higher the hoop stress concentration, K_t^h will be. This proportional relationship is also agreed by De Carvalho (2005) if the test is under internal pressure only. He demonstrates that the relationship is inversely proportional when the stress concentration is subjected to bending. Table 3.5 summarises the results of the hoop and axial stress concentrations of various notches as the Poisson's ratio increases.

Table 3.5: Poisson's ratio influence on hoop stress concentration of various notches; Pressure at 50 bar

Notch size	N7	N40	N60	N90	N100
K_t^h		Stress Concentration Factor (SCF)			
0.26	1.42	1.62	1.68	1.74	1.75
0.30	1.48	1.65	1.70	1.75	1.76
0.34	1.55	1.70	1.73	1.76	1.77
K_t^a					
0.26	3.65	3.29	2.51	1.83	1.64
0.30	3.54	3.17	2.44	1.83	1.65
0.34	3.46	3.07	2.39	1.82	1.66
0.38	3.39	2.99	2.35	1.81	1.66

Based on Table 3.5, Figures 3.18 and 3.19 illustrate that Notch N100 has the highest hoop stress concentration K_t^h and the lowest axial stress concentration K_t^a, as the Poisson's ratio increases. Due to the increased biaxial effect, all notches show a converging increment in SCF values based on hoop stress. It can also be observed that

for notch N100, the SCF based on both stresses remains constant as the Poisson's ratio increases. Therefore, it can be concluded that the Poisson's ratio has a lesser influence on stress concentration factors if the arc-shaped notch is lengthened.
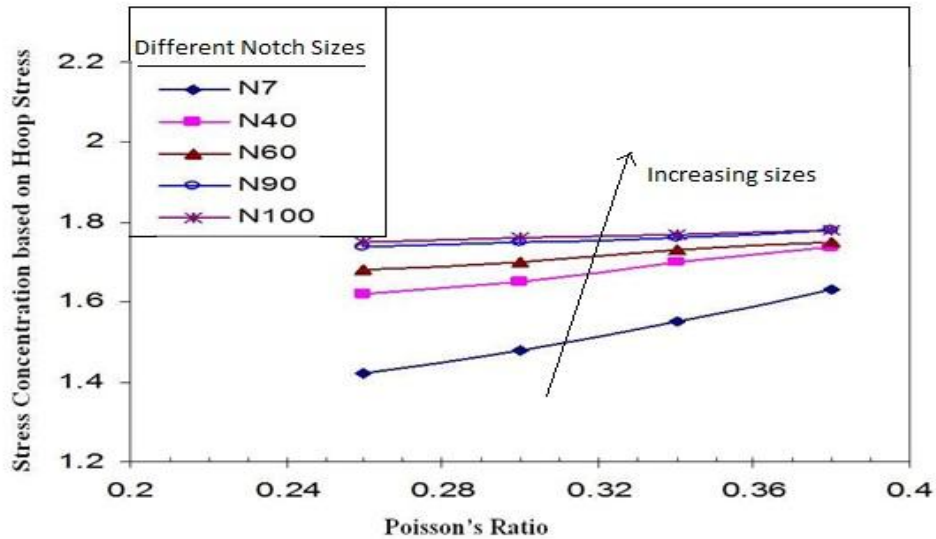
Figure 3.18: Hoop stress concentration against Poisson's ratio
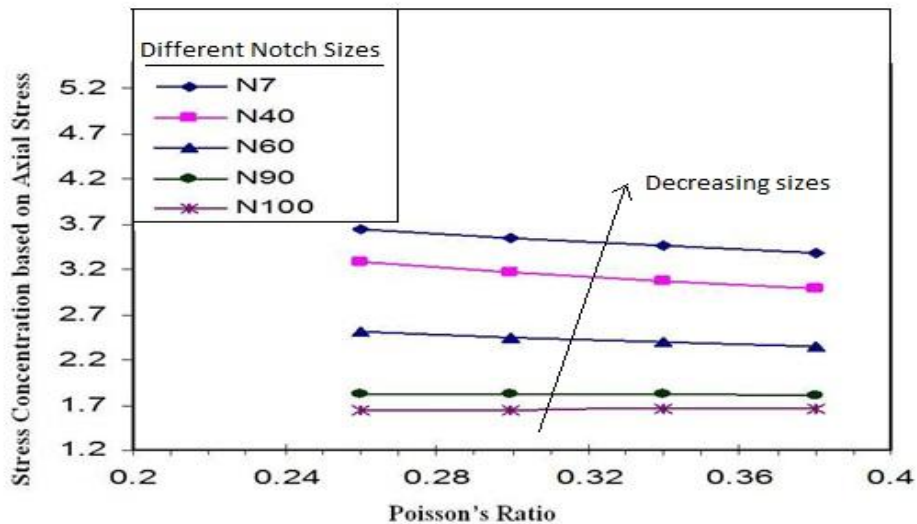
Figure 3.19: Axial stress concentration against Poisson's ratio

86

Figure 3.20 shows that as the relative notch increases, K_t^h increases and K_t^a decreases. From this plot, we can conclude that it is a likelihood that the hoop and axial stress concentrations will have the same value as the relative notch length (i.e. the length of defect divided by the thickness) increases.
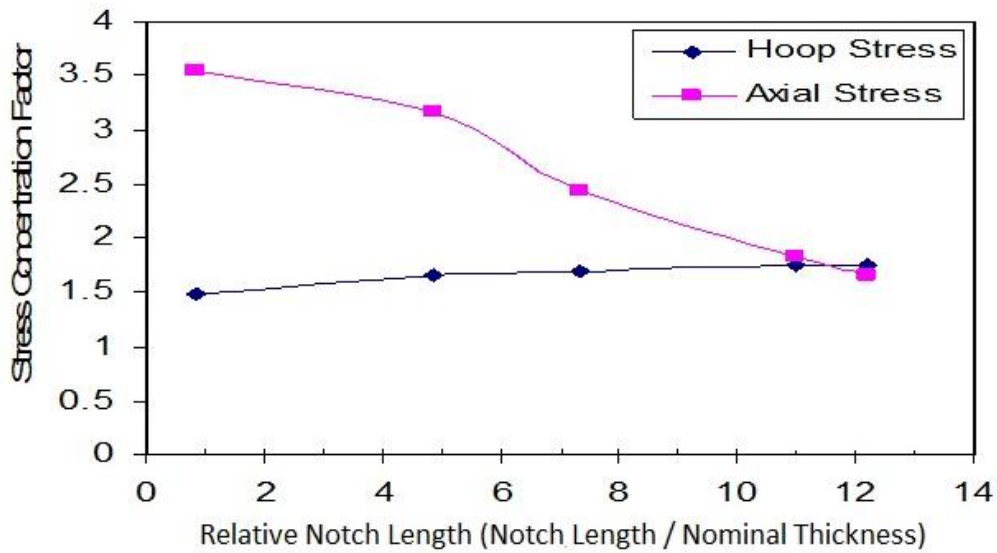
Figure 3.20: Stress concentration factor against relative notch length

Table 3.6: Loading influence on stress concentrations

Pressure	K_t^h		K_t^a	
	N7	N40	N7	N40
(bar)				
0	1.48	1.66	3.54	3.17
20	1.48	1.66	3.54	3.17
30	1.48	1.66	3.54	3.17
40	1.48	1.66	3.54	3.17
50	1.48	1.66	3.54	3.17

In the earlier section, the relationship between elastic loading and the hoop and axial stresses have been discussed. Again, in this section the elastic loading is analysed but this time to see the influence of the elastic loading on the stress concentration values instead. Hence, Table 3.6 summarises the results of the stress concentration of two notches – 7 mm notch (N7) and 40 mm notch (N40) – as the elastic loading increases from 10 up to 50 bar.
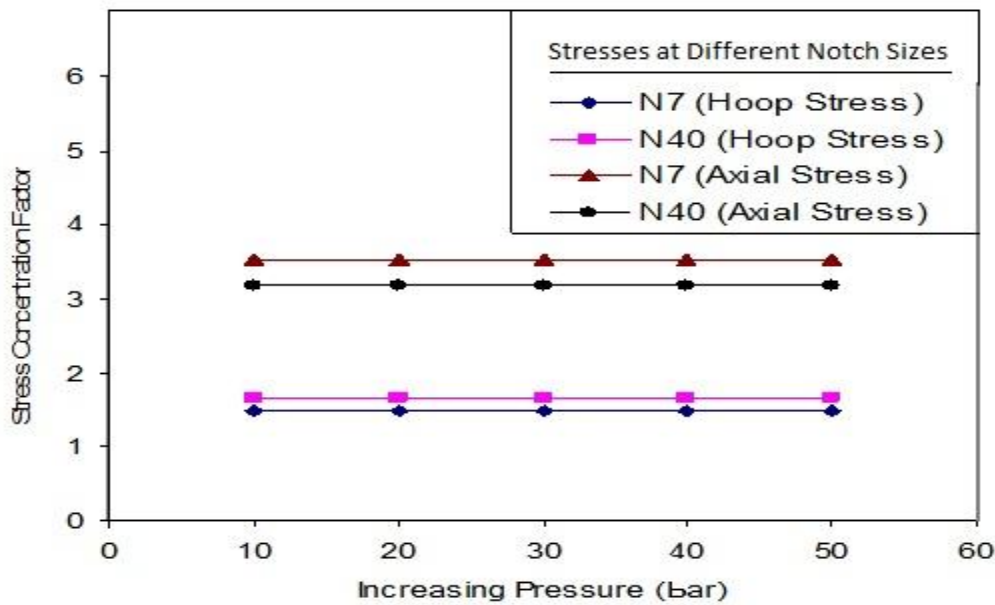
Figure 3.21: Effects of increasing pressure to SCF

Based on the results shown in Table 3.6, Figure 3.21 illustrates that hoop stress concentration is directly proportional to the length of the arc-shaped defect and axial stress concentration is inversely proportional to the length of the arc-shaped defect. In this plot also, it is shown that the increasing pressure in the elastic working region has no influence on the increment of SCF values for any type of FE model.

3.7.4   Concluding Remarks

A biaxial notch situation has been studied in an internally pressurised pipe as a precursor to a repair method study. Without published results for a comparison, results have been examined to consider whether or not the FEA model is acting sensibly. As predicted, the relationship between hoop and axial stress concentration factors varies with notch geometry and Poisson's ratio has less influence on the stress concentration for the longer defect. The later work will be to validate the models against strain gauge results and then to apply a composite wrap repair technique.

3.8   The development of the composite repair modelling

3.8.1   Introduction

In oil and gas applications, pipes containing flaws and cracks detected during inspection are sized and assessed using fracture mechanics techniques (Kim and Son, 2004). In order to assess whether or not a flaw is critical, the structural integrity engineer needs to understand the ability of the structure to resist further and the critical amount of damage that the structure can sustain before remedial action is required (Brennan and Leeuw, 2008). If repair is required, then composite materials may be used to contain the flaw or mitigate against other mechanical damage in pipelines (Alexander, 2008a).

3.8.2   The theory of Homogenisation in the Triaxial Woven Fabric (TWF) composite

Composite materials consist of continuous and discontinuous fibres embedded in a matrix. Such a composite is heterogeneous and the properties vary from point to point. Usually on a scale that is large with respect to the fibre diameter, the fibre and matrix properties may be averaged and the material may be treated as homogeneous.

According to Coenen et al. (2010), this assumption is commonly employed in macro-mechanical analyses of composites. Then, the material is considered to be quasi-homogeneous which implies that the properties are taken to be the same at every point. These properties are not the same as the properties of either the fibre or the matrix, but are a combination of the properties of the constituents. This homogenisation theory also allows for obtaining a variation of field variables associated with different problems of physics and mechanics in heterogeneous media when the scale ratio, i.e. the ratio between the fine and coarse scale, tends to be zero (Tootkaboni and Brady, 2010).

3.8.3 The study of predicted elastic constant in the TWF composite repair modelling

The main problem for the FE approach lies in the requirement of accurate models for all the significant aspects of the forming process. The mechanical behaviour of fabrics is complex due to intricate interactions of the yarns and fibres. It is a multi-scale problem as reported by Hamila and Boisse (2009). According to Verhoosel et al. (2010), the restricted interest in micro-scale behaviour offers the possibility for multi-scale analyses in which only part of the micro-scale complexity is carried over to the macro-scale. Hence, in a multi-scale analysis, information is exchanged between different scale lengths by means of the homogenisation technique that has been discussed in the earlier section and the use of 'rules of mixture' that will be discussed later. However, Hamila and Boisse (2009) point out that macroscopic behaviour is also very much dependent on the interaction of yarns at the meso-scale (scale of the woven unit cell) and at the micro-scale (level of the fibres consisting of yarns). Despite much work in the field, there is no widely accepted model that accurately describes all the main aspects of this anisotropic continuum in composite woven reinforcement mechanical behaviour.

Hamila and Boisse (2009) also give several reasons for that in their literature. Firstly, the identification of homogenised material parameters change when the fabric is subjected to the large strains due to forming and consequently the directions of the

yarns change and lateral contact between the yarns occurs. Secondly there are large slidings between fibres and continuity. Thirdly, the stress notion used in continuum mechanics is also questionable because a stress vector is an elementary load on an elementary surface that, in the case of fibrous material, is not well defined.

In order to improve the homogenisation methods that are generally referred to as unit cell methods, Verhoosel et al. (2010) suggest using a suitable technique that is called computational homogenisation where it describes the macroscopic constitutive behaviour using a finite element model (or other discretization technique) on the micro-scale, rather than via analytic constitutive laws. Verhoosel et al. (2010) demonstrate this technique as being capable of effectively capturing non-linear micro-scale behaviour such as debonding, cracks etc. in macro-scale analyses.

However, in this study which involves only the integrity of bonding, the repaired model was developed based on the macro-scale rather than on the micro-scale level of the composite material. There are several reasons for this. The first is because the objectives of the study are more towards predicting the overall composite behaviour rather than predicting the behaviour of one single fibre tow, resin pocket or the response of the fibre-matrix interface (Littell, 2008). The second reason is that structured and layered thin sheets (composites) are used in the pipeline repair simulation.

According to Coenen et al. (2010), the size of the fine scale details in these heterogeneous, thin sheets is typically much smaller compared to the dimensions of the whole structure, thus making direct numerical analyses very expensive even using modern computer power. Therefore, it is preferable to model these shells on the macro-scale as a homogeneous continuum with effective properties obtained through, for example, homogenisation procedures.

The third reason is because the micro-structured material behaviour may be arbitrarily complex and include a physical and/or geometrical evolution of the microstructure (e.g. phase transitions, decohesion, delamination, inter- or intra-granular fracture etc). Since this study is not involved with the defect, the macroscopic material behaviour is the only concern. As a result, no through thickness integration is needed in

91

the shell, as the micro-scale representative volume element (RVE) analysis immediately provides the resultant quantities integrated through the thickness. With only a single RVE computation that involves the stiffness matrix being required for each plane (integration) point of the macro shell, a significant gain in computational efficiency can be provided.

Based on the above discussions, undoubtedly, the rule of mixtures can be used in approximating estimations of composite material properties such as modulus of elasticity, Poisson's ratio and shear modulus. However, these properties only include the main tows that constitute the overall dominant composite composition such as glass fibre and epoxy matrix. The very small amount of Kevlar fibre that was used in the actual composite repair was assumed to be negligible and not taken into the composite repair modelling although the overall properties may change slightly. However, the actual overall properties of the composite may also slightly change. According to Barucci et al. (2000), any addition of other fibres to the composite may lead to a significant increase in strength, stiffness and dimensional stability.

From the simple law of mixture relationships:

Young's modulus along the fibre direction E_1:

$$E_l = E_m V_m + E_r V_f \qquad \text{(Equation 3.7)}$$

Where;
V_m = Volume fraction matrix
V_f = Volume fraction of fibre
E_m = Young's modulus of matrix
E_f = Young's modulus of fibre

Major Poisson's ratio ν_{12}:
$$\nu_{12} = \nu_m V_m + \nu_f V_f \qquad \text{(Equation 3.8)}$$

For predicting E_2 and G_{12}, a number of different models have been suggested, each having some modifications to the simple law of mixtures formula, given by equations below (Daniel and Ishai, 2006).

Young's modulus transverse to the fibre direction E_2:

$$\frac{1}{E2} = \frac{Vm}{Em} + \frac{Vf}{Ef}$$ (Equation 3.9)

And

Axial Shear modulus of the composite G_{12}:

$$\frac{1}{G12} = \frac{Vm}{Gm} + \frac{Vf}{Gf}$$ (Equation 3.10)

The last elastic constant G23 is obtained by solving the following quadratic equation (Kueh and Pellegrino, 2007).

$$\left(\frac{G_{23}}{G_m}\right)^2 A + \left(\frac{G_{23}}{G_m}\right) B + C = 0$$ (Equation 3.11)

Where;

$$
\begin{aligned}
A = {} & 3V_f(1-V_f)^2 \left(\frac{G_{12f}}{G_m}-1\right)\left(\frac{G_{12f}}{G_m}+\zeta_f\right) \\
& + \left[\left(\frac{G_{12f}}{G_m}\right)\zeta_m + \zeta_m\zeta_f - \left(\left(\frac{G_{12f}}{G_m}\right)\zeta_m-\zeta_f\right)(V_f)^3\right] \\
& \times \left[\zeta_m V_f\left(\frac{G_{12f}}{G_m}-1\right)-\left(\left(\frac{G_{12f}}{G_m}\right)\zeta_m+1\right)\right]
\end{aligned}
$$

$$
\begin{aligned}
B = {} & -6V_f(1-V_f)^2\left(\frac{G_{12f}}{G_m}-1\right)\left(\frac{G_{12f}}{G_m}+\zeta_f\right) \\
& + \left[\left(\frac{G_{12f}}{G_m}\right)\zeta_m + \left(\frac{G_{12f}}{G_m}-1\right)V_f+1\right] \\
& \times \left[(\zeta_m-1)\left(\frac{G_{12f}}{G_m}+\zeta_f\right)-2(V_f)^3\left(\left(\frac{G_{12f}}{G_m}\right)\zeta_m-\zeta_f\right)\right] \\
& +(\zeta_m+1)V_f\left(\frac{G_{12f}}{G_m}-1\right)\left[\frac{G_{12f}}{G_m}+\zeta_f+\left(\left(\frac{G_{12f}}{G_m}\right)\zeta_m-\zeta_f\right)(V_f)^3\right]
\end{aligned}
$$

$$
\begin{aligned}
C = {} & 3V_f(1-V_f)^2\left(\frac{G_{12f}}{G_m}-1\right)\left(\frac{G_{12f}}{G_m}+\zeta_f\right) \\
& + \left[\left(\frac{G_{12f}}{G_m}\right)\zeta_m + \left(\frac{G_{12f}}{G_m}-1\right)V_f+1\right] \\
& \times \left[\frac{G_{12f}}{G_m}+\zeta_f+\left(\left(\frac{G_{12f}}{G_m}\right)\zeta_m-\zeta_f\right)(V_f)^3\right]
\end{aligned}
$$

93

and;

$$\zeta_m = 3 - 4\nu_m$$
$$\zeta_f = 3 - 4\nu_{12f}$$

Before applying the above elastic constants formulae, the volume fraction of fibre and matrix shall be determined first and according to ASTM International (2009a). *Note: The Rules of Mixture (Equations 3.7 till 3.11) were not used in this thesis since all the elastic constants were based on predicted values and they will be discussed further in the following section.*

The fibre volume fraction is calculated as;

$$V_f = \frac{\rho_m W_f}{\rho_f W_m + \rho_m W_f}$$ (Equation 3.12)

Where;

V_f = *volume fraction of fibres*

W_f = *weight of fibres*

W_m = *weight of matrix*

ρ_f = *density of fibres*

ρ_m = *density of matrix*

For the Density of the fibre;

$\rho_c = M_i/(A \times h \times 1000)$ (Equation 3.13)

Where:

Mi = *mass of the specimen, g;*

A = *area of the specimen, m^2; and*

h = *thickness of the specimen, mm.*

For the Weight percent of the fibre;

$W_r = (A_r \times N \times 0.1)/ (\rho_c \times h)$ (Equation 3.14)

94

Where:

A_r = *weight of one sheet of reinforcement / unit area, g/m^2*

N = *number of sheets in the test specimen.*

For the Reinforcement Content, Volume Percent;

$$V_r = (A_r \times N \times 0.1)(\rho_c \times h) \qquad \text{(Equation 3.15)}$$

For the Matrix Content, Weight Percent;

$$W_m = 100 - (A_r \times N \times 0.1)/(\rho_c \times h) \qquad \text{(Equation 3.16)}$$

and

For the Matrix Content, Volume Percent;

$$V_m = W_m \times \rho_c / \rho_m \qquad \text{(Equation 3.17)}$$

The earlier five elastic constants equations (i.e. Equations 3.7 till 3.11) are required in the study of the macro-mechanics of lamina, whereby the material is presumed to be homogeneous and the effects of the constituent materials are detected only as averaged apparent properties of the composite (McGraw-Hill, 2003).

In other words, given the material properties of the fibres, and the matrix and volume fraction of fibres, those equations will estimate the equivalent material properties of the composite lamina in the principal directions (Efunda, 2011).

There are a few assumptions in the macro-mechanics of laminated composites:

- The matrix is homogeneous, isotropic, and linearly elastic.
- The fibre is homogeneous, isotropic, linearly elastic, continuous, regularly spaced, and perfectly aligned.
- The lamina (single layer) is macroscopically homogeneous, macroscopically orthotropic, linearly elastic, initially stress-free, void-free, and perfectly bonded.

- The laminate is composed of two or more perfectly bonded lamina to act as an integrated structural element.

The study of the macro-mechanics of laminated composites is also referred to as the classical lamination theory. This theory is almost identical to the classical plate theory except that the material properties (stress strain relations) are different. There are four cornerstones of the lamination theory which are kinematic, constitutive, force resultant and equilibrium equations (Efunda, 2011). Only the constitutive relation is relevant to this PhD study since all the elastic constants (Equations 3.7 till 3.11) are derived from this theory and this constitutive lamination theory is discussed below.

3.8.3.1 Constitutive Lamination Theory

The constitutive lamination equation is expressed in the matrix form as shown below;

$$
\left\{ \begin{array}{c} \varepsilon_x \\ \varepsilon_y \\ \gamma_{xy} \end{array} \right\}_k = [T]_k^T [S]_k [T]_k = \begin{bmatrix} \bar{S}_{11} & \bar{S}_{12} & \bar{S}_{16} \\ & \bar{S}_{22} & \bar{S}_{26} \\ sym. & & \bar{S}_{66} \end{bmatrix}_k \left\{ \begin{array}{c} \sigma_x \\ \sigma_y \\ \sigma_{xy} \end{array} \right\}_k
$$

Or

$$
\left\{ \begin{array}{c} \sigma_x \\ \sigma_y \\ \sigma_{xy} \end{array} \right\}_k = [T]_k^{-1} [C]_k [T]_k^{-T} = \begin{bmatrix} \bar{C}_{11} & \bar{C}_{12} & \bar{C}_{16} \\ & \bar{C}_{22} & \bar{C}_{26} \\ sym. & & \bar{C}_{66} \end{bmatrix}_k \left\{ \begin{array}{c} \varepsilon_x \\ \varepsilon_y \\ \gamma_{xy} \end{array} \right\}_k
$$

(Equation 3.18)

Where;

The Stiffness matrix is traditionally represented by the symbol **C**, while **S** is reserved for the Compliance matrix. The subscript k indicates the kth layer counting from the top of the laminate.

Since this Classical Lamination Theory is only valid for thin lamina (Efunda, 2011), there are a few basic assumptions to be addressed:

- Based on the Kirchhoff Hypothesis, normals should remain straight (no bending), unstretch (keeping the same length) and normal (always making a right angle to the neutral plane).

- Based on the Perfect Bonding, the bonding itself is infinitesimally small (there is no flaw or gap between layers), non-shear-deformable (no lamina can slip relative to another) and the strength of bonding is as strong as it needs to be (the laminate acts as a single lamina with special integrated properties).

In this study, all the elastic constants of the composite, for example Young's (E) and shear (G) modulus and Poisson's ratio (G), are only based on predictions referring to other researchers' references or reliable sources of information. Since the main interest of this PhD is just to study how the overall composite behaves rather than the specific fibre tow behaviour, there was no specific mechanical test carried out for the composite repair study. In fact, these composite repair simulations that used the predicted elastic constant inputs would be then validated experimentally using strain gauge rosettes at the macro-mechanics level later.

However, this interesting work to determine the tow properties of the composite repair lamina at the micro-mechanic level should be carried out by other researchers in the future and perhaps better results can be produced. Hence, the predicted elastic constant values that represent the generic composite lamina properties, as referred to in Table 3.7, were used in the development of composite repair modelling. Since there were three complete sets of data, the next step was to compare numerically if there was

any significant difference among them. This comparison had to be carried out before one of them could be selected as a final set of elastic constant values which could be used in the stress and strain distribution study later.

Table 3.7: Predicted mechanical properties (SWComposites/Eng-Tips Forums, 2010) and (Performance Composites Ltd, 2009)

Properties	Unit	Predicted Values for the Composite Lamina		
		Simulation 1	Simulation 2	Simulation 3
Longitudinal Modulus, E_1	GPa	39	20	24.9
Transverse Modulus, E_2	GPa	8.6	12	24.9
In Plane Poisson's Ratio, v		0.28	0.28	0.28
In Plane Shear Modulus, G_{12} / G_{13}	GPa	3.8	20	5.9
Transverse Shear Modulus, G_{23}	GPa	2.56	10	4

The first set of the predicted elastic constant inputs was called Simulation 1 because they were meant for the first simulation work using the composite repair modelling. After the result of Simulation 1 had been obtained, the simulation was repeated using a second set of elastic constant inputs from Table 3.7 and then followed by the third set of elastic constant inputs (Simulation 3) accordingly. The results of these simulation works were plotted and are shown in Figure 3.22.

This figure shows the final result of simulations using predicted elastic constant values of the glass epoxy composite lamina. The maximum error of these three

simulations for the hoop strain at defect is only 1.6% and 0.4% for the nominal hoop strain. However, for axial strains at defect and nominal areas, Simulation 1 shows a higher strain value compared to others. Simulation 3 shows a very small nominal axial strain of only 1.7 microstrain which is almost negligible. Among these three simulations, Simulation 1 which refers to the first set of predicted elastic constant values was selected for the study of stress and strain distribution that will be discussed further in the next sections and chapter.

Figure 3.22: Using predicted elastic constant values in composite repair simulation (with 8 layers of repairs)

3.9 Numerical Stress Analysis of Composite Repair

There are two main objectives in this section. The first is to use the stress concentration factor (SCF) of non repaired pipe and compare it with the composite

repaired pipe, as shown in Figure 3.23. Details of the exact point that was used in the calculations of SCF will be presented and the importance of the composite repair to the stress concentration factor will be discussed. The second objective, relating to the comparison of two different materials namely glass fibre and carbon fibre composites, will be discussed later. Different parameters such as length and thickness of repair are compared against the variable notch sizes.
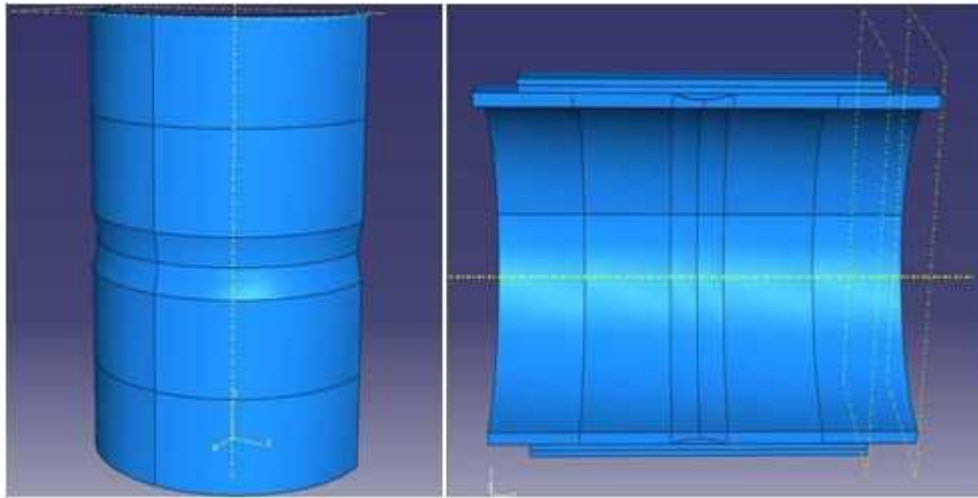
Figure 3.23: Pipe model without repair (Left) and with composite repair (Right)

3.9.1 Stress concentration comparison of the pipe with and without the repair

In this section, the SCF is studied between the pipe model with and without the repair. The reference of the SCF of the pipe model without repair is available and has already been discussed in the earlier section. The maximum hoop and nominal stresses are referred to at element 5094 (i.e. at the notch root) and element 2141 (i.e. away from the defect) as shown in Figure 3.24. Figure 3.25 shows axial stresses.
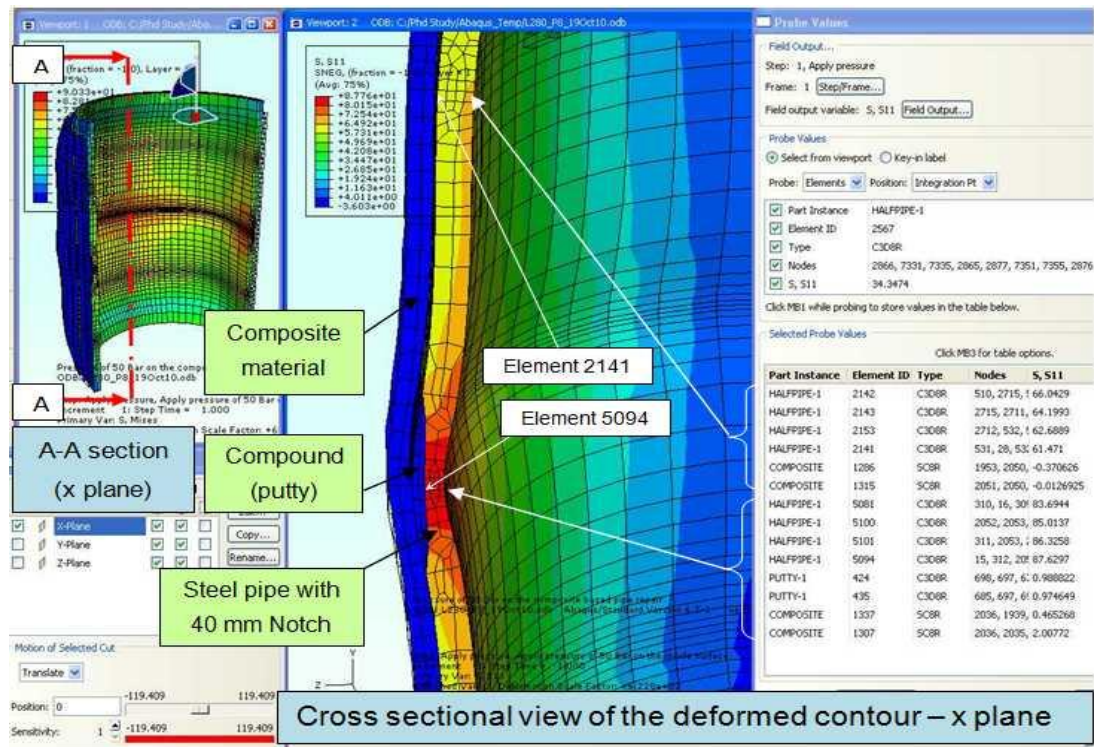
Figure 3.24: Finding the hoop stress concentration value (K_t^h) in the repaired steel pipeline (i.e. at elements 5094 and 2141)

Figure 3.24 shows a simple method to measure the maximum values of not only the hoop stress and but also strain at the notch root and away from the defect (nominal area) before further study on stress concentration factor with composite repair can be carried out in this section and strain concentration factor studies in the later section. Basically, when the pressurised Model 3, as discussed in the earlier sections, was repaired by the epoxy compound and composite wraps, apparently the points where the maximum readings of stress and strain at the notch root or nominal area were measured have been hidden beneath the repair. Therefore, the cut section tool, available in ABAQUS 6.7.1, which is the only way to gain access to those two points was used. The model was cut through the A-A section (x plane), as shown in Figure 3.24, in order to measure the relevant readings. In fact by following this method, other studies can be carried out such as measuring the size of element etc.

101

The same method was repeated to measure the maximum value of axial stress and strain, as illustrated in Figure 3.25. The same elements – 5094 at the notch root and element 2141 at the point away from the defect – were referred to throughout the course of this study.
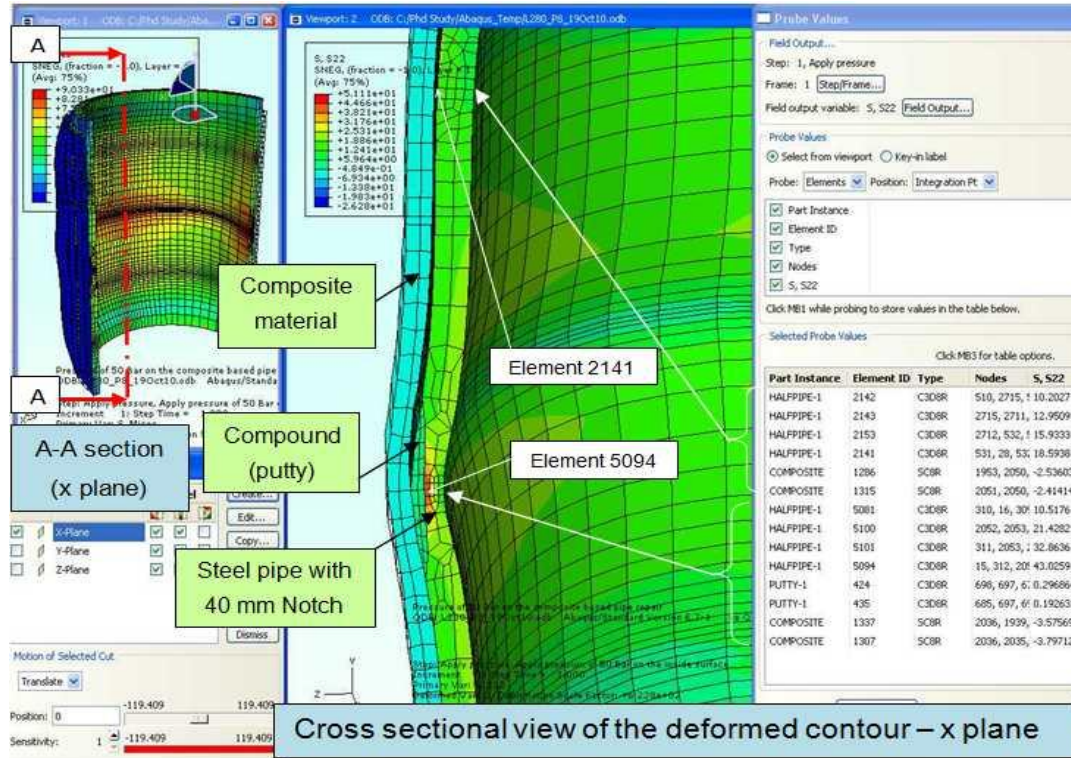
Figure 3.25: Finding the Axial stress concentration value (K_t^a) in the repaired steel pipeline (i.e. at elements 5094 and 2141)

The maximum hoop and axial stresses at the notch root and nominal hoop and axial stresses at the point away from the defect were tabulated and are given in Table 3.8. The stress concentration factor was determined at variable lengths of the composite repair. In this study, the thickness of repair was only eight layers and the length of the arc-shaped notch remained constant at 40 mm.

Table 3.8: The effect of repair length to stress concentration

Length (mm)	$\sigma_{\max}^{h}$	σ_{nom}^{h}	K_t^{h}	$\sigma_{\max}^{a}$	σ_{nom}^{a}	K_t^{a}
			(MPa)			
Thickness of repair = 6.56 mm (8 layers) ; Length of Arc-shaped Notch = 40 mm;						
280	87.16	60.64	1.44	40.69	17.80	2.29
240	86.54	60.06	1.44	39.15	16.77	2.33
160	85.93	60.11	1.43	38.29	16.64	2.30
120	88.87	61.19	1.45	41.60	17.71	2.34

By referring to Figure 3.26, apparently the increase of the repair length does not have any influence on reducing the SCF values. The plot shows that the average axial stress concentration, K_t^{a} is 2.32 and it is higher than the average of the hoop stress concentration, K_t^{h} which is only 1.44. By comparing with Figure 3.20 (i.e. stress concentration study on the non repaired pipe model), the axial SCF, K_t^{a} is 3.17 and hoop SCF, K_t^{h} is 1.66. We can also see that after the pipe model with 40 mm arc-shaped defect has been repaired with eight layers of glass fibre reinforced polymer, a significant reduction of stress concentration of 26.81% has been achieved in the axial direction and 13.25% in the hoop direction.
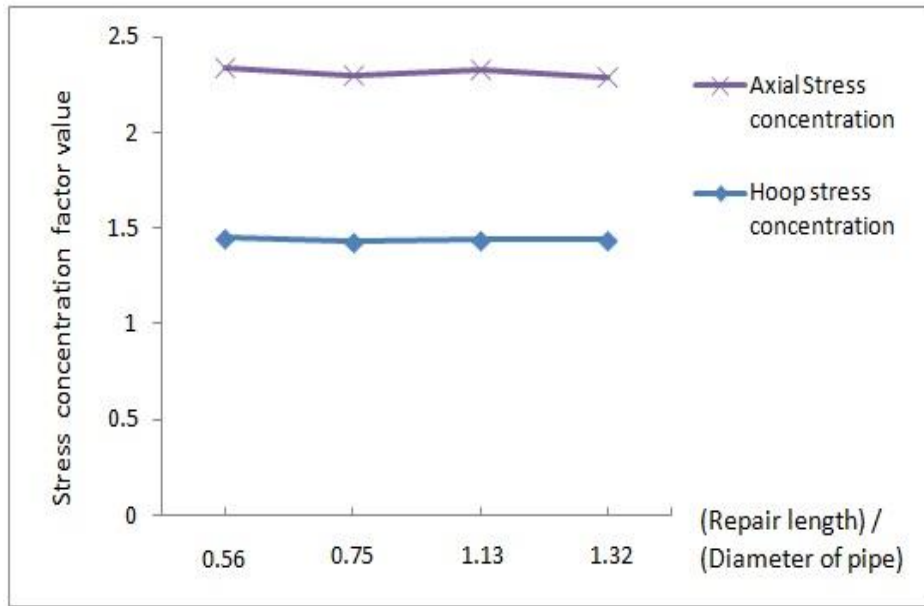
Figure 3.26: The effect of the ratio of repair length to diameter of pipe on stress concentration factor (with eight layers of wrapping)

Table 3.9: The effect of repair thickness on stress concentration

Layers	σ_{max}^{h}	σ_{nom}^{h}	K_t^h	σ_{max}^{a}	σ_{nom}^{a}	K_t^a
			(MPa)			
Length of repair = 280 mm ; Length of Arc-shaped Notch = 40 mm;						
4	88.94	61.92	1.44	42.19	18.80	2.24
8	87.16	60.64	1.44	40.69	17.80	2.29
12	85.50	59.47	1.44	39.23	17.28	2.27
18	83.57	57.44	1.45	36.41	16.54	2.20

Table 3.9 summarises the maximum hoop and axial stresses at the notch root and nominal hoop and axial stresses at the point away from the defect. This time, the stress concentration factor was determined at variable thicknesses of repair starting from

four up to 18 layers. In this study, the length of repair was 280 mm and the length of arc-shaped notch remained constant at 40 mm.
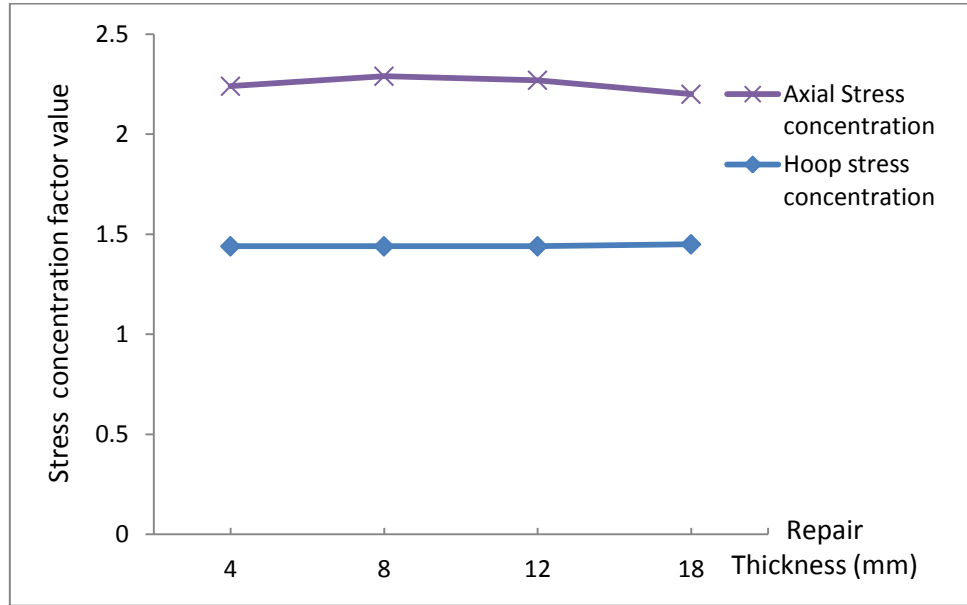
Figure 3.27: The effect of thickness of repair on the stress concentration factor

From Figure 3.27, it can be seen that the increase of repair thickness does not have any influence on reducing the SCF values. The plot shows that the average axial stress concentration, K_t^a is 2.25 and it is higher than the average of the hoop stress concentration, K_t^h which is only 1.44. By comparing with Figure 3.20 (i.e. stress concentration study on the non repaired pipe model), the axial SCF, K_t^a is 3.17 and hoop SCF, K_t^h is 1.66. We can also see that after the pipe model with 40 mm arc-shaped defect has been repaired with the length of 280 mm of the glass fibre reinforced polymer, a significant reduction of stress concentration of 29.02% has been achieved in the axial direction and 13.25% in the hoop direction.

In another comparison study of SCF with and without composite repair, Table 3.10 summarises the resultant SCF using carbon fibre reinforced polymer at the variable

width of defect. Other parameter, such as the length of repair and number of layers and material type remained constant in this study.

Table 3.10: Comparison of stress concentration with and without repair; Length of repair = 280 mm; Number of layers = 18; Composite = CFRP

Length of Notch (L)	7 mm		40 mm		60 mm		90 mm		100 mm	
Stress	σ_{max}	σ_{nom}	σ_{max}	σ_{nom}	σ_{max}	σ_{nom}	σ_{max}	σ_{nom}	σ_{max}	σ_{nom}
Hoop stress (MPa)	74.64	59.02	82.37	59.48	86.24	57.89	91.13	58.39	92.32	57.23
Stress Concentration K_t^h	1.26		1.38		1.49		1.56		1.61	
Axial stress (MPa)	42.84	15.68	35.89	16.70	30.00	16.05	26.82	17.27	26.59	17.6
Stress Concentration K_t^a	2.73		2.14		1.86		1.55		1.51	
Stress Concentration K_t^h (Without repair)	1.48		1.66		1.70		1.75		1.76	
Stress Concentration K_t^a (Without repair)	3.54		3.17		2.44		1.83		1.65	

Figure 3.28 shows that as the length of defect increases, the axial SCFs with and without repair decrease dramatically and settle down at an SCF value between 1.51 and 1.65. From the plot, we can see the hoop stress concentration factors with and without repair increase slightly from 1.26 and 1.48 up to 1.61 and 1.76 respectively. Obviously,

hoop and axial stress concentration factors with a composite repair are lower than without a composite repair and they also show a uniform pattern before and after the repair. This figure concludes that the use of a predicted elastic constant in the development of a composite repair has produced a sensible result and the later works that involve stress strain distribution will, therefore, be carried out with greater confidence.
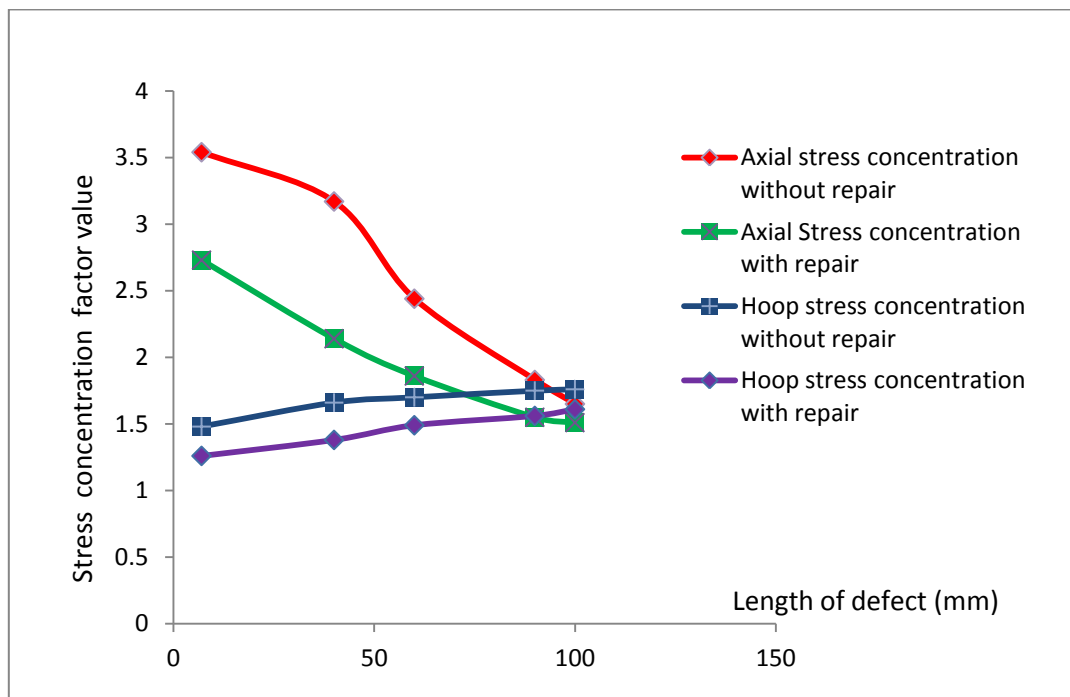
Figure 3.28: The effect of defect length to stress concentration factor

From Figure 3.29, we can see the trend of the percentage of SCF reduction (SCFR %), which is defined as the difference between the SCF before and after repair divided by the stress concentration before the repair multiplied by 100, increases as the length of the defect increases but after 40 mm, SCFR % decreases. This phenomenon shows that the SCF is not only influenced by the length of the defect but also the biaxial effects.

Since this graph shows that a composite repair has the highest reduction in hoop and axial stress concentration factor values (i.e. 16.9% and 32.5%) at the defect length of 40 mm, it can be concluded that the numerical and experimental models which have similar specifications should receive optimum benefits from this composite repair compared to other notch sizes.
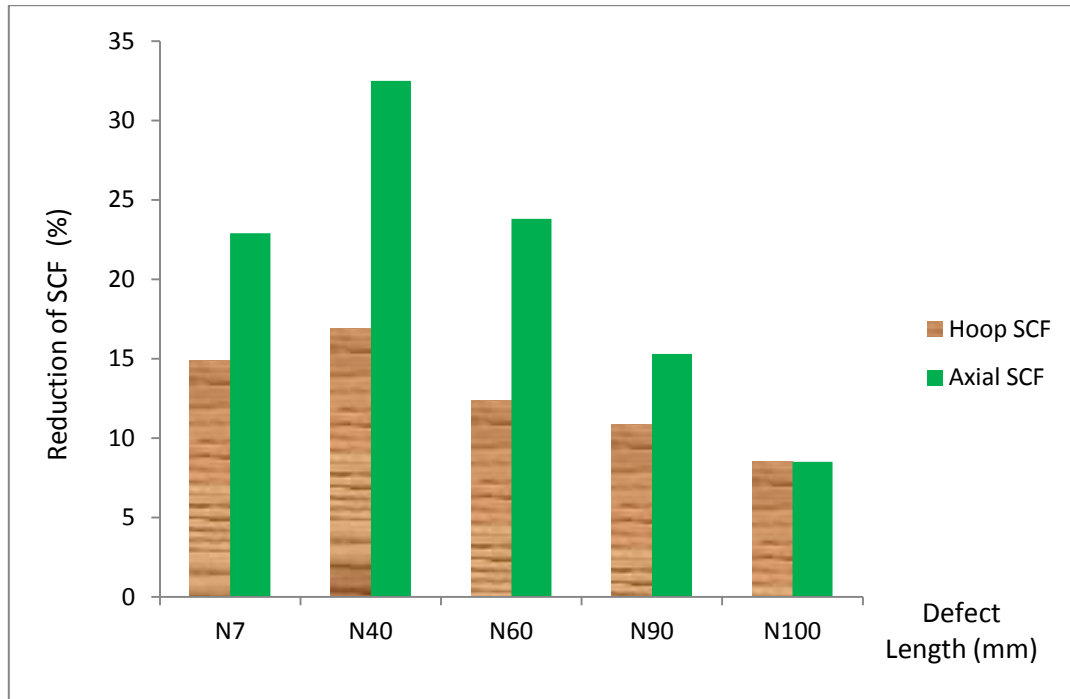
Figure 3.29: Reduction of SCF (%) versus Defect Length

3.9.1.1 Numerical Stress Results

The elastic constant values, as discussed in the earlier section, are summarised in Table 3.11 and were used in the simulation works. Table 3.12 summarises the hoop stress values with respect to variable ratio of length of repair to notch length, number of plies and composite material.

Table 3.11: Predicted Elastic Constant Values

Descriptions	E_1 (MPa)	E_2 (MPa)	v_{12}	G_{12} (MPa)	G_{13} (MPa)	G_{23} (MPa)
Carbon Epoxy	156000	7230	0.337	4120	4120	3350
Glass Epoxy	39000	8600	0.28	3800	3800	2560

Table 3.12: Hoop Stress v/s L/W Ratio (defect length, W= 40 mm) and Predicted Elastic Constant Values

Length of Repair (L)		50 mm	80 mm	120 mm	160 mm	200 mm	240 mm	280 mm	290 mm
Length of Notch (W)					40 mm				
L/W ratio		1.25	2	3	4	5	6	7	7.25
Material	Ply				Hoop Stress (MPa)				
Carbon Epoxy	4 Plies	91.11	89.22	88.8	91.68	90.88	89.81	88.94	90.16
Carbon Epoxy	8 Plies	89.66	86.71	86.15	85.93	85.92	86.54	87.17	87.54
Carbon Epoxy	12 Plies	86.53	84.44	83	83.44	83.59	84.45	85.5	85.85
Carbon Epoxy	18 Plies	85.07	82.47	80.97	80.64	81.88	82.37	83.57	83.61
Glass Epoxy	4 Plies	92.99	92.87	92.57	93.94	93.66	92.97	92.45	93.84
Glass Epoxy	8 Plies	90.46	89.68	88.94	88.87	88.94	88.88	89.34	89.93
Glass Epoxy	12 Plies	87.61	86.62	85.32	85.74	85.96	86.57	86.95	87.49
Glass Epoxy	18 Plies	86.31	83.66	82.63	82.34	83.55	84.18	85.1	85.26
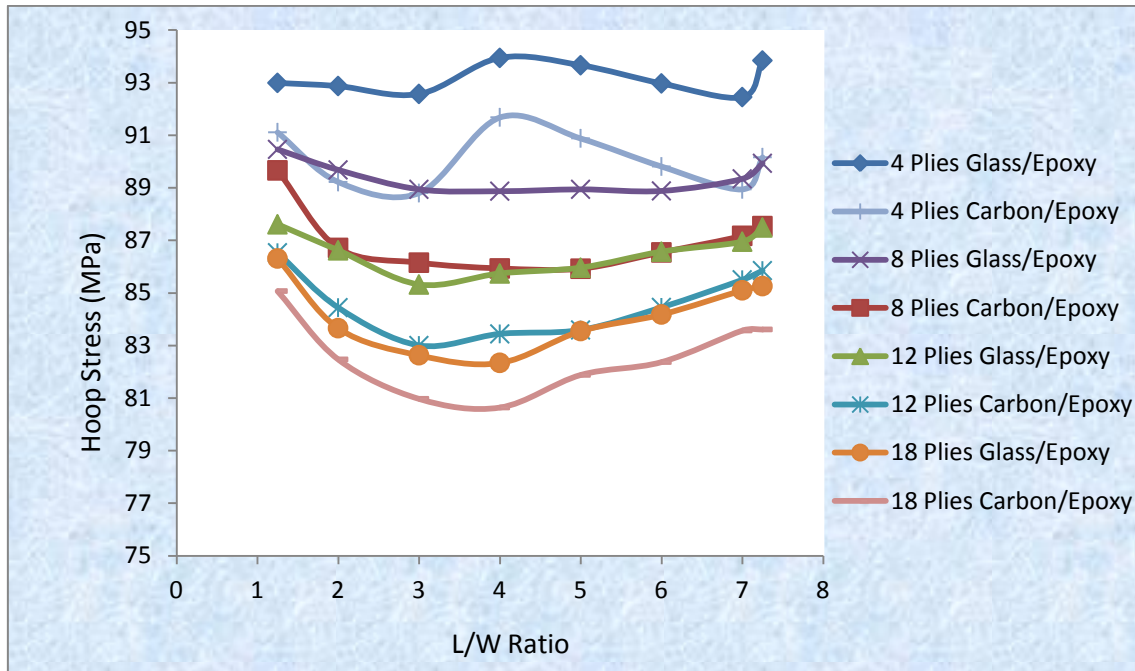
Figure 3.30: Hoop Stress versus L/W Ratio (2 different materials)

From Figure 3.30, as the length of composite repair and ply thickness increase, the hoop stress that is measured in the centre of the notch root of the steel pipe model decreases until the minimum value is reached at 80.64 MPa (i.e. referring to carbon epoxy with 18 plies). Most of the repaired pipes with variable plies have reached their minimum stresses as the composite repair length is around 160 mm except for carbon epoxy with four plies where, at this length, the maximum hoop stress occurs. However, a further increase in length of the composite repair of each variable ply, gradually increases the hoop stress. Hence, from the graph, the optimum length of repair for the defect width of 40 mm is 160 mm.

Table 3.13 summarises the axial stress results against the ratio of repair length to notch length. Likewise, the phenomenon of the hoop stress distribution, as shown in Figure 3.30, occurs in the axial stress distribution but at a smaller magnitude, as referred to in Figure 3.31. The minimum axial stress that has been recorded for 18 plies of carbon epoxy composite at a length of 160 mm is 34.75 MPa.

Table 3.13: Axial Stress v/s L/W ratio (defect length, W= 40 mm)

Length of Repair (L)		50 mm	80 mm	120 mm	160 mm	200 mm	240 mm	280 mm	290 mm
Length of Notch (W)						40 mm			
L/W ratio		1.25	2	3	4	5	6	7	7.25
Material	Ply					Axial Stress (MPa)			
Carbon Epoxy	4 Plies	41.39	39.78	39.98	42.9	42.3	42.04	42.19	46.38
Carbon Epoxy	8 Plies	41.32	38.56	38	38.29	38.38	39.15	41.23	43.59
Carbon Epoxy	12 Plies	37.96	37.74	35.83	36.68	36.71	37.49	39.23	42.02
Carbon Epoxy	18 Plies	37.11	37.31	35.45	34.75	36.25	35.9	36.41	38.07
Glass Epoxy	4 Plies	44.2	44.56	44.65	45.82	45.67	45.42	45.26	49.88
Glass Epoxy	8 Plies	42.35	42	41.39	41.61	41.78	42.69	43.34	46.44
Glass Epoxy	12 Plies	39.6	40.16	38.78	39.53	39.68	40.59	41.83	45.32
Glass Epoxy	18 Plies	39.27	38.93	37.77	37.23	38.63	39.03	40.33	42.78
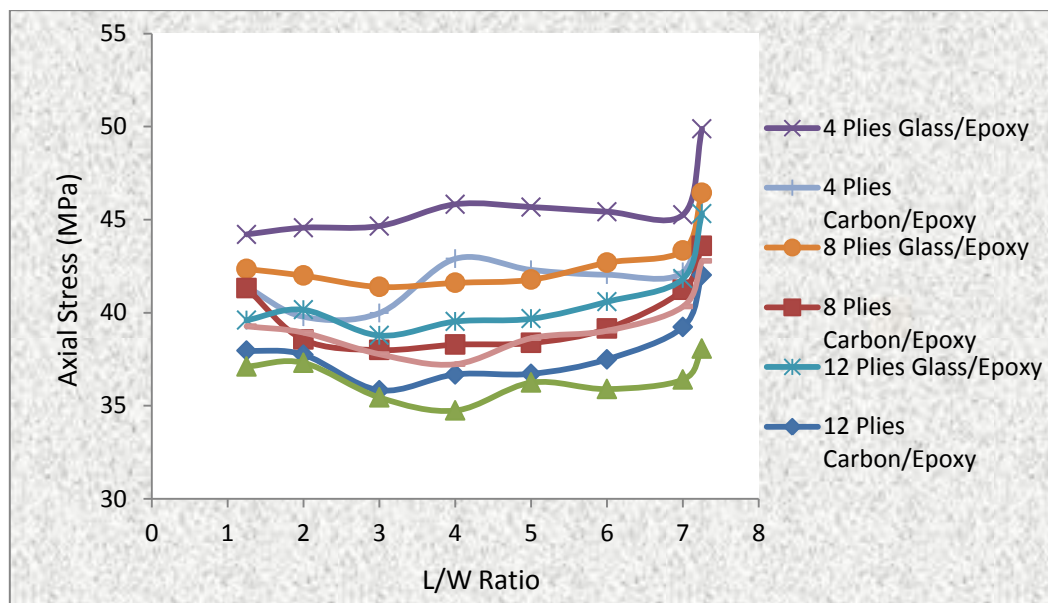
Figure 3.2: Axial Stress versus L/W Ratio (2 different materials)

Tables 3.14 and 3.15 summarise the hoop and axial stress values with respect to variable ratio of thickness of repair to repair length, notch length and composite material.

Table 3.14: Hoop Stress v/s P/L Ratio (Length of composite, L= 240 mm)

Thickness of Repair (P) /mm		0.83	1.66	3.32	4.98	6.64	8.3	9.96	11.62	13.28	14.94
Length of Repair (L) /mm						240					
P/L Ratio		0.0034	0.0069	0.014	0.02	0.028	0.035	0.042	0.048	0.055	0.062
Material	Notch					Hoop Stress (MPa)					
Carbon Epoxy	7 mm	80.68	78.49	77.2	77.28	77.26	77.06	76.42	76.31	74.84	74.64
Carbon Epoxy	40 mm	94.88	92.04	89.02	87.16	86.02	85.11	84.32	83.78	82.86	82.27
Carbon Epoxy	100 mm	103.65	102.28	100.49	99.08	97.94	96.9	95.9	94.93	93.4	92.32
Glass Epoxy	7 mm	84.63	82.57	80.45	79.4	78.85	78.56	78.27	78.01	76.35	76.35
Glass Epoxy	40 mm	97.11	95.23	92.69	90.45	88.88	87.6	86.55	85.8	84.83	84.18
Glass Epoxy	100 mm	104.91	103.79	102.08	100.65	99.43	98.31	97.27	96.25	95.12	94.06

Table 3.15: Axial Stress v/s P/L Ratio (Length of composite, L= 240 mm)

Thickness of Repair (P) /mm		0.83	1.66	3.32	4.98	6.64	8.3	9.96	11.62	13.28	14.94
Length of Repair (L) /mm						240					
P/L Ratio		0.0034	0.0069	0.014	0.02	0.028	0.035	0.042	0.048	0.055	0.062
Material	Notch					Axial Stress (MPa)					
Carbon Epoxy	7 mm	50.25	48.75	47.59	46.69	47.11	48.7	46.09	46.38	42.92	42.84
Carbon Epoxy	40 mm	45.87	44.61	41.85	40.27	39.22	38.39	37.72	37.42	36.47	35.98
Carbon Epoxy	100 mm	32.53	31.37	30.08	29.4	28.63	27.93	27.27	26.66	27.03	26.59
Glass Epoxy	7 mm	60.28	56.75	53.7	52.55	52.16	52.13	51.03	51.12	47.18	47.18
Glass Epoxy	40 mm	49.9	48.05	45.88	43.94	42.69	41.75	41.04	40.57	39.8	39.03
Glass Epoxy	100 mm	33.69	32.76	31.66	31.26	30.64	30.12	29.62	29.16	29.21	28.82
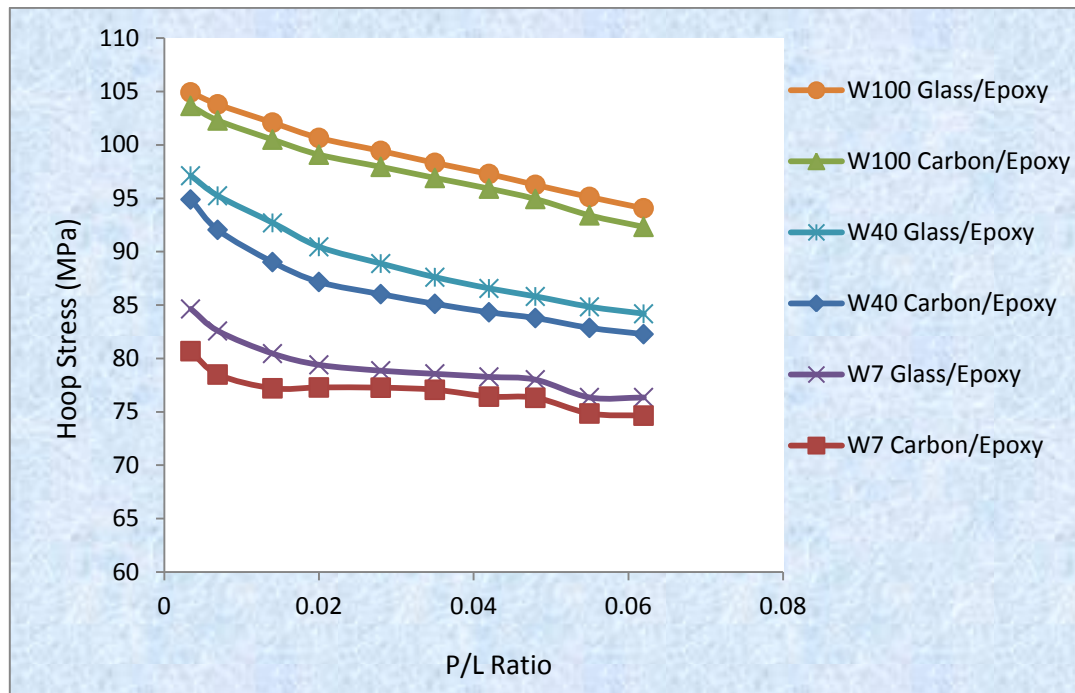
Figure 3.3: Hoop Stress versus P/L Ratio (2 different materials)

Figure 3.32 shows hoop and axial stresses as a function of composite repair thickness to repair length ratio and also notch length. The hoop stress decreases steadily as thickness increases and length of defect decreases. Likewise, Figure 3.33 shows the same pattern. However, as the axial stress decreases, the thickness increases but the length of defect also increases. There are some fluctuations in axial stress readings as shown by Glass and Carbon epoxies at the length defect of 7 mm. This is because of biaxial effects. From these figures, it can be concluded that hoop stress is directly proportional to the length of the defect and inversely proportional to the thickness of the repair. Axial stress is inversely proportional to both the defect length and repair thickness.
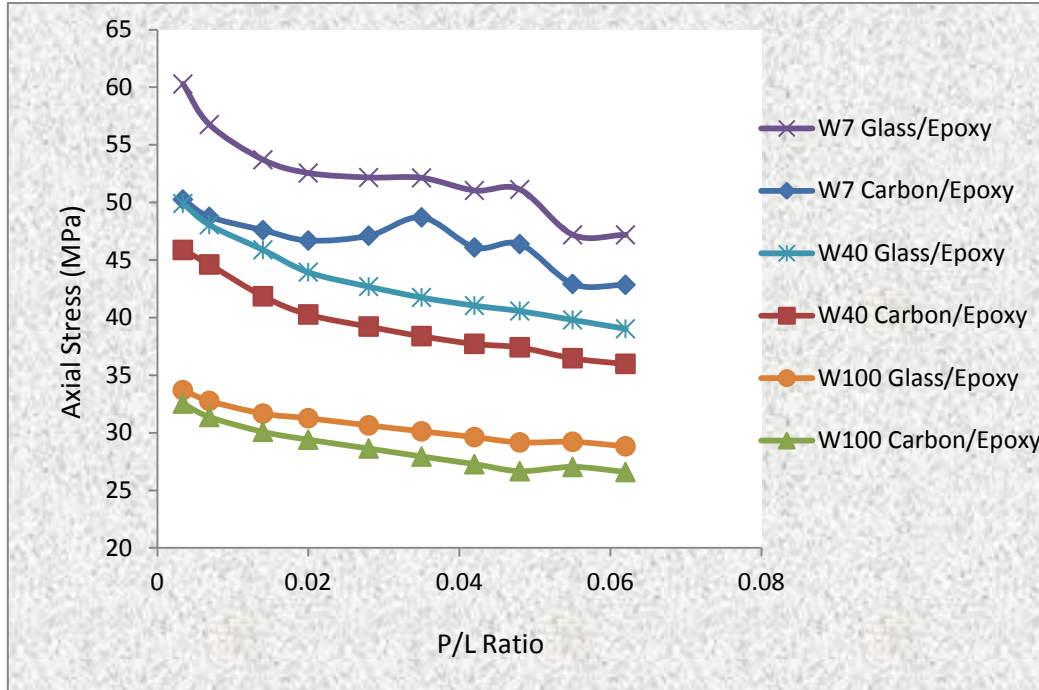
Figure 3.4: Axial Stress versus P/L Ratio (two different materials)

In order to show how effective the stress loading has been when transferred from the steel substrate into the composite materials (i.e. Carbon or Glass epoxy composites), the graphical interpretation of the results is based on the ratio of hoop or axial notch with repair to the hoop or axial stress without repair, which is defined as the Pipeline Repair Index (PRI) against the ratio of length to thickness.

There are a few reasons why PRI is important in this PhD study. At present, the minimum standard width of the woven fibres which is 300 mm (12 inches) has been used by many manufacturers in wet applications (Frost, 2008) for years. For a normal application, such as the overhead straight pipeline that is subjected to internal pressure only, it is not necessary to use a very wide fibre cloth wrapping which of course in a long term implication, may unnecessarily waste the expensive adhesive and fibres if the defect is very small. Hence, there is a room for design optimisation in terms of using the right amount of composite in any straight pipeline repair in the future. So far, there is no open literature or reference that discusses this matter or has provided any specific equation.

114

However, Frost (2008) and Alexander (2007b) refer to the below calculation (ASME, 2010) for the axial extent of the repair that ensures that the repair is sufficiently long to transfer the load carried by the pipe substrate into the repair laminate. The axial extent of the repair, L_{axial} (mm), (i.e. from the edge of the defect to the end of the repair) is determined by;

$$L_{axial} = 2.5\sqrt{D\,t_{orig}} \qquad \text{(Equation 3.19)}$$

where t_{orig} = original pipeline wall thickness (mm)

D = pipeline diameter (mm)

For internal pressure only, the axial length of the repair is given by;

$$L = 2.L_{over} + L_{defect} \qquad \text{(Equation 3.20)}$$

According to pipeline ASME PCC-2 standard (ASME, 2010), the edges of the composite wraps should be tapered if the repair thickness is governed by an axial load. A minimum taper of 5:1 (horizontal/vertical) is recommended. Hence the total axial length of the repair is given by;

$$L = 2.L_{over} + L_{defect} + 2.L_{taper} \qquad \text{(Equation 3.21)}$$

Since the repair thickness in this PhD study is governed by the hoop load only (i.e. no tension or bending, only internal pressure), the taper length in Equation 3.21 can be ignored and Equation 3.20 applied instead. The results are summarised in Tables 3.16 and 3.17. In these results, carbon fibre has shown a better result than glass fibre composite in terms of stress load transfer and Figures 3.34 and 3.35 further discuss in detail the behaviour of the stress distribution.

Table 3.16: Ratio of Hoop Stress Notch with Repair to Hoop Stress Notch without repair (σHNR/σHNWR) v/s L/P Ratio (Ply Thickness, P= 14.94 mm @ 18 Plies)

Carbon Epoxy Material	Hoop Stress with repair (σ_{HNR} - MPa)							
Notch 7 mm	75.43	73.14	73.84	73.71	73.76	74.64	76.37	76.78
Notch 40 mm	85.07	82.47	80.97	80.64	81.88	82.37	83.57	83.61
Notch 100 mm	98.41	94.22	92.53	92.34	92.54	93.19	94.45	94.5

Glass Epoxy Material	Hoop Stress with repair (σ_{HNR} - MPa)							
Notch 7 mm	76.28	73.6	74.8	74.35	74.35	76.35	77.45	78.05
Notch 40 mm	86.31	83.66	82.63	82.34	83.55	84.18	85.1	85.26
Notch 100 mm	98.31	94.92	94.26	94.24	94.43	94.45	95.88	95.92

For Carbon and Glass Epoxy Materials	Hoop Stress without Repair (σ_{HNWR} – MPa)
Notch 7 mm	90.82
Notch 40 mm	100.74
Notch 100 mm	107.1

Length of repair (L) / mm	50	80	120	160	200	240	280	290
Thickness of Ply (P) / mm	14.94							
L/P Ratio	3.35	5.35	8.03	10.71	13.39	16.06	18.74	19.41
Material / Notch	$\sigma_{HNR}/\sigma_{HNWR}$							
Carbon Epoxy								
Notch 7mm	0.8305	0.8053	0.8130	0.8116	0.8121	0.8218	0.8408	0.8454
Notch 40 mm	0.8444	0.8186	0.8037	0.8004	0.8127	0.8176	0.8295	0.8299
Notch100 mm	0.9188	0.8797	0.8639	0.8621	0.8640	0.8701	0.8818	0.8823
Glass Epoxy								
Notch 7mm	0.8399	0.8103	0.8236	0.8186	0.8186	0.8406	0.8527	0.8593
Notch 40 mm	0.8567	0.8304	0.8202	0.8173	0.8293	0.8356	0.8447	0.8463
Notch100 mm	0.9179	0.8862	0.8801	0.8799	0.8816	0.8818	0.8952	0.8956

Table 3.17: Ratio of Axial Stress Notch with Repair to Axial Notch without repair ($\sigma_{ANR}/\sigma_{ANWR}$) v/s L/P Ratio (Ply Thickness, P= 14.94 mm @ 18 Plies)

Carbon Epoxy Material	Axial Stress with repair (σ_{ANR} - MPa)							
Notch 7 mm	44.17	41	43.22	41.85	41.85	42.85	44.8	47.15
Notch 40 mm	37.11	37.31	35.45	34.75	36.25	35.9	36.41	38.07
Notch 100 mm	32.26	31.5	29.9	29.33	29.14	28.97	29.54	30.86

Glass Epoxy Material	Axial Stress with repair (σ_{ANR} - MPa)							
Notch 7 mm	46.62	42.7	45.94	43.75	43.21	47.18	49.56	52.89
Notch 40 mm	39.27	38.93	37.77	37.23	38.63	39.03	40.33	42.78
Notch 100 mm	32.24	31.93	31.22	31.04	31.03	28.88	32.49	34.25

For Carbon and Glass Epoxy Materials	Axial Stress without Repair (σ_{ANWR} – MPa)
Notch 7 mm	55.33
Notch 40 mm	56.18
Notch 100 mm	38.68

Length of repair (L) / mm	50	80	120	160	200	240	280	290
Thickness of Ply (P) / mm	14.94							
L/P Ratio	3.35	5.35	8.03	10.71	13.39	16.06	18.74	19.41
Material Notch	$\sigma_{ANR}/\sigma_{ANWR}$							
Carbon/Epoxy								
Notch 7mm	0.7983	0.7410	0.7811	0.7563	0.7563	0.7744	0.8096	0.8521
Notch 40 mm	0.6605	0.6641	0.6310	0.6185	0.6452	0.6390	0.6480	0.6776
Notch100 mm	0.8340	0.8143	0.7730	0.7582	0.7533	0.7489	0.7637	0.7978
Glass Epoxy								
Notch 7mm	0.8425	0.7717	0.8302	0.7907	0.7809	0.8527	0.8957	0.9559
Notch 40 mm	0.6990	0.6929	0.6723	0.6626	0.6876	0.6947	0.7178	0.7614
Notch100 mm	0.8335	0.8254	0.8071	0.8024	0.8022	0.7574	0.8399	0.8854
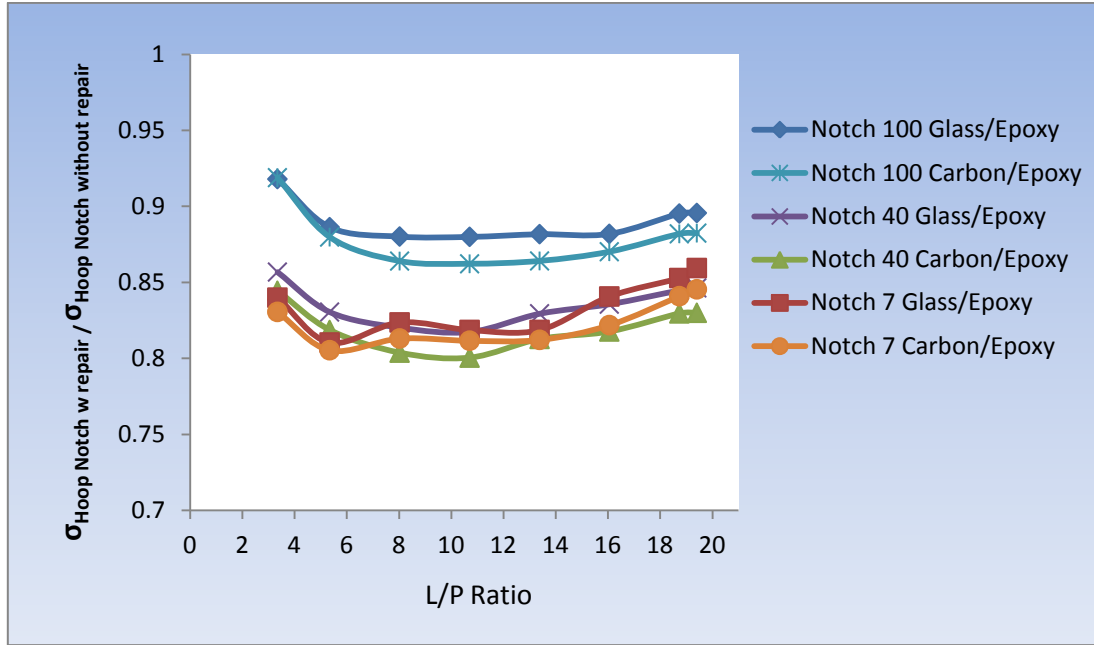
Figure 3.5: Ratio of Hoop Stress Notch with Repair to Hoop Stress Notch   without Repair ($\sigma_{HNR}/\sigma_{HNWR}$) v/s L/P Ratio

From the analysis of the Pipeline Repair Index (PRI) of three different defect lengths (i.e. 7 mm, 40 mm and 100 mm) as illustrated in Figures 3.34 and 3.35, the composite repair at the defect length of 40 mm (Notch 40) shows the best result in terms of having the lowest PRI if compared with Notches 7 and 100. In fact the plot of Notch 40 also shows the most consistent PRI pattern of carbon and glass composites as the L/P ratio increases.

For Notch 40 Carbon Epoxy, at L/P = 10.71 or at a repair length of 160 mm, the hoop PRI which is approximately equal to 0.8 or 19.96% stress load has been transferred in the hoop direction and the axial PRI which is approximately equal to 0.62 or 38.15% of stress load has been transferred in the axial direction. Likewise, for Notch 40 Glass Epoxy, the maximum load transfer also occurs at the repair length of 160 mm. However, its PRI is slightly lower than for Carbon Epoxy, for example 18.27% of stress load is transferred in the hoop and 33.74% in the axial directions. From Equation 3.20, the recommended length of the repair for a defect length of 40 mm is 188 mm if subjected to internal pressure only. However, if the repair thickness is governed by an

axial load (e.g. buried pipelines that are subjected to soil movement), the total repair axial length would be 337.4 mm instead, as referred to in Equation 3.21. Since the repair thickness in this PhD study is only governed by the hoop load (i.e. internal pressure only), the analytical repair axial length refers to 188 mm only. Therefore, from this study, it can be concluded that about 12% of material saving can be achieved if the numerical repair length can be considered in the manufacturers' design optimisation in the future.
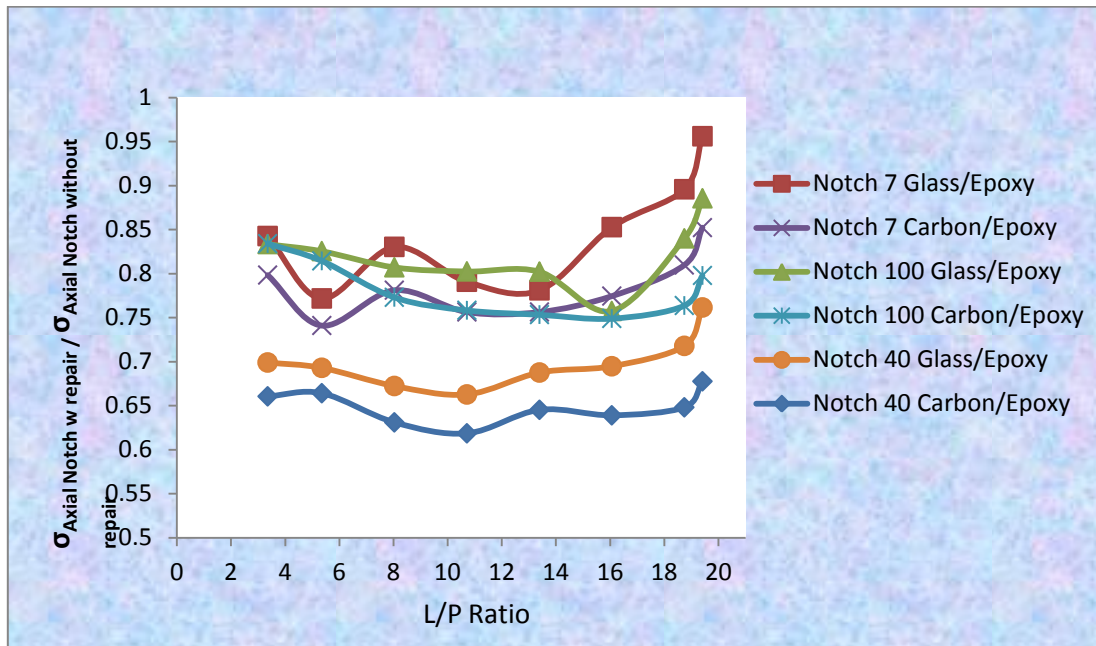
Figure 3.6: Ratio of Axial Stress Notch with repair to Axial Stress Notch without repair ($\sigma_{ANR}/\sigma_{ANWR}$) v/s L/P Ratio

For the second notch length (Notch 7), the results of Notch 7 Carbon Epoxy show that 19.5% of stress load has been transferred in the hoop direction and 26% in the axial direction and both occur at L/P = 5.35 or at a repair axial length of 80 mm as illustrated in Figures 3.34 and 3.35. Likewise, the maximum load transfer of Notch 7 Glass Epoxy also occurs at L/P = 5.35 but with the higher PRI; for example, 18.97% of the stress load transfers in the hoop direction and 22.83% of the axial stress load

transfers in the axial direction. Again, referring to Equation 3.20, the recommended analytical repair axial length is 155 mm. If we compare the numerical repair length against the analytical repair length, a repair saving of 48% can be achieved through this design optimisation.

The longest notch (i.e. Notch 100 Carbon/Epoxy) shows the maximum load transfer in hoop and axial directions occurs at different L/P ratios. The hoop stress load transfer of 13.8% occurs at L/P = 10.71 or a repair length of 160 mm and the axial stress load transfer of 25.11% occurs at L/P = 16.06 or at a repair length of 240 mm. Likewise, the maximum load transfer occurs at L/P = 10.71 for N100 Glass Epoxy with 12.01% in the hoop direction and 24.26% of axial stress load transfer occurs at L/P = 16.06 or a repair length at 240 mm. From the ASME PCC-2 guidelines, the analytical axial repair length is 248 mm only. Hence, a repair saving of only 3% can be achieved in the axial direction.

3.9.1.2   Concluding Remarks

Analysis of the above results, shows that PRI has the ability to provide a good and helpful tool to the manufacturer in benchmarking the efficiency of their composite repair in the stress distribution study as well as in the design optimisation of composite repairs in the future. From the previous comparison of results between the numerical PRI and the analytical method (i.e. ASME PCC-2), the optimum length of composite repair, especially for the defect length of 40 mm in this study, is 160 mm as compared to the recommended length by ASME (2010) which is 188 mm. About 20% of stress loading has been transferred in the hoop direction and around 35 ~ 38% in the axial direction. Carbon fibres have given better results than glass fibres throughout the simulation tests.

This study also shows that the smaller the notch length, the higher the material saving will be. Nevertheless, in this the PhD experimental work, only Glass Epoxy composite was used. The length of the defect and the length of repair were fixed at 40 mm and 280 mm. The number of plies was limited, i.e. up to eight plies only.

3.10 Numerical Strain Analysis of Composite Repair

In this section, there are two objectives to be discussed. The first is the continuity of the modelling study from the previous section, but this time with more emphasis on hoop and axial strains. The second objective is to study the significance of a composite repair on the strain concentration factor.

3.10.1 Strain study on the chosen models prior to composite repair

Table 3.18: The hoop and axial strain results at notch root
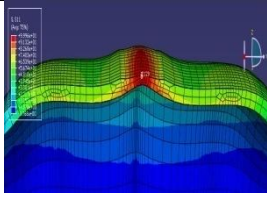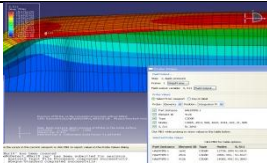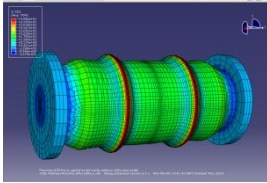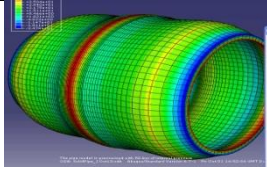
Diagram	Descriptions (Different Type)	E11 (με)- Hoop strain		E22 (με)- Axial strain	
		Analytical	FEA	Analytical	FEA
	Short Pipe with defect of 40 mm (Half Pipe Model – Actual Model in this PhD Study)	460	402.35	108	114.4
	Symmetrical long pipe with defect of 40 mm (Half Pipe Model)	460	412.69	108	153.87
	Full Pipe Model with 40mm defect	460	412.17	108	76.77
	Full Pipe Model with 40 mm defect without flanges	460	405.93	108	99.086

Table 3.18 shows the hoop strain values of the finite element from different types of model that were measured at the notch root are slightly lower than those of the manual (analytical) calculation. This is because the simple shell theory does not take into account the complexity of the geometry of the defect. The behaviour of the axial strain at the defect and nominal areas will be further discussed in the Validation of Results section in the next chapter.

In this strain analysis modelling also, it is not necessary to have a complete model that represents the actual test specimen (i.e. a complete pipe with flanges). By using boundary conditions, the model can be simplified which can reduce time and cost of the simulation works. Again, a short pipe with a defect of 40 mm (i.e. half pipe model) is shown to be the most suitable and acceptable model in this simulation work.

3.10.2 Strain study on the composite repair
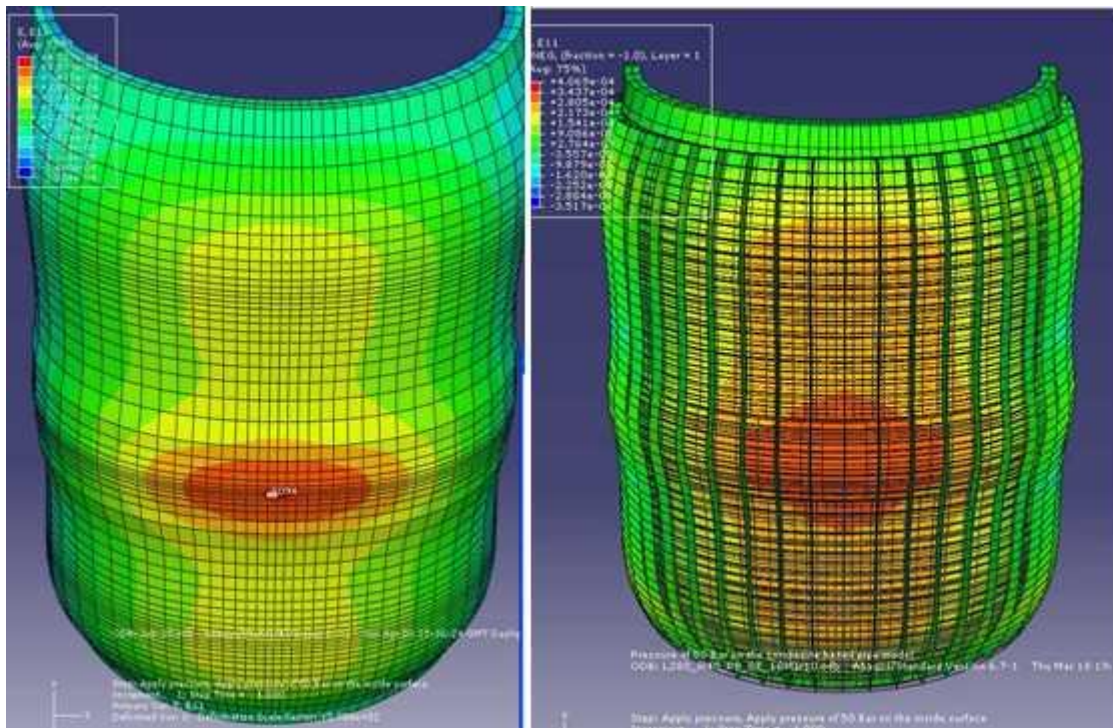
Figure 3.7: Strain distribution on the notched pipe without repair (Left) and with repair (Right)

Figure 3.36 shows the contours before and after the composite repair. Before the repair, a higher strain contour is concentrated in the centre of pipe (i.e. the notch) but after the composite wrapping, the strain loading has been better distributed over the surface of the pipe model. This means that the maximum strain value at the notch root has been imperatively reduced due to composite repair.

Table 3.19: Comparison of numerical strain concentration factor with and without repair; Repair length = 280 mm; Number of layers = 18; Composite = CFRP

Length of Notch	7 mm	40 mm	60 mm	90 mm	100 mm
Maximum hoop strain without repair	319.0	399.7	434.3	463.2	461.5
Nominal hoop strain without repair	263.2	265.2	263.2	261.6	259.0
Hoop SCF without repair	1.21	1.51	1.65	1.87	1.78
Nominal hoop strain with repair	293.3	345.0	370.7	399.9	404.6
Nominal strain with repair	260.8	260.0	255.7	253.3	251.5
Hoop SCF with repair	1.12	1.32	1.45	1.58	1.61

Table 3.19 summarises the hoop strain concentration factor of various notch lengths at constant repair length and thickness but with the same composite material. In this section, only hoop strains were analysed. Axial strains were not analysed because they are much less apparent, hence the results are not tabulated here. According to Martineau and Romero (1996), this is attributed to mass and pressure loading differences between the numerical model and the experimental system.

By referring to the hoop strain concentration factor (with and without repair) from Table 3.19 and the hoop stress concentration factor (with and without repair) from Table 3.10, as discussed in the earlier section, the results of improvement in stress and strain concentration factors in the hoop direction are presented in Figure 3.37. The trend of both stress concentration factors (SCFs) increases as the notch length increases but after N40, the trend decreases dramatically. Again, this is due to the biaxial effect experienced by the pipe model. N40 shows the SCF reduction for both hoop stress

123

(12.58%) and strain (16.9%) concentration factors respectively. At N60 and N90, both hoop stress and strain concentration factors are almost the same with a difference of only 1.86% and 1.2% respectively. At N100, hoop strain concentration has a greater reduction, i.e. of about 11%, than the hoop stress concentration factor. N7 shows the hoop stress concentration factor is 50% higher than the hoop strain concentration factor.
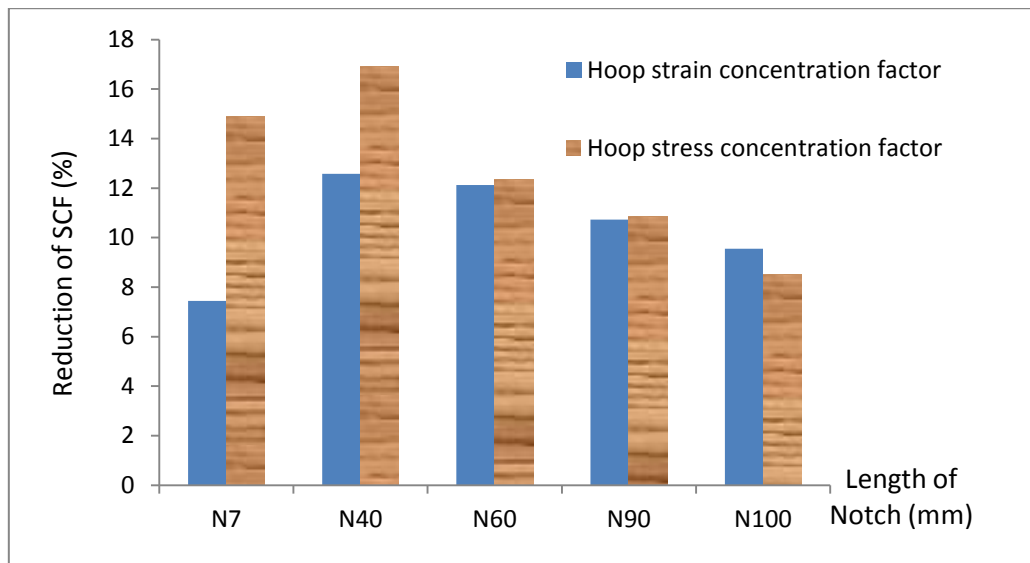
Figure 3.37: Reduction after the repair in hoop stress and strain concentration factors

Figure 3.38 shows several line curves of stress and strain concentration factors with and without repair. Since strain concentration factor $K\varepsilon$ and stress concentration factor $K\sigma$ are widely used in estimating the fatigue life of a notched body, it is important to relate these two factors together. Polak (1983) reports that if stresses and strains obey Hooke's law, both factors are equal to the theoretical stress concentration factor K_t and this relationship is expressed as;

$$K\sigma \, K\varepsilon = K_t^2 \qquad \text{(Equation 3.22)}$$
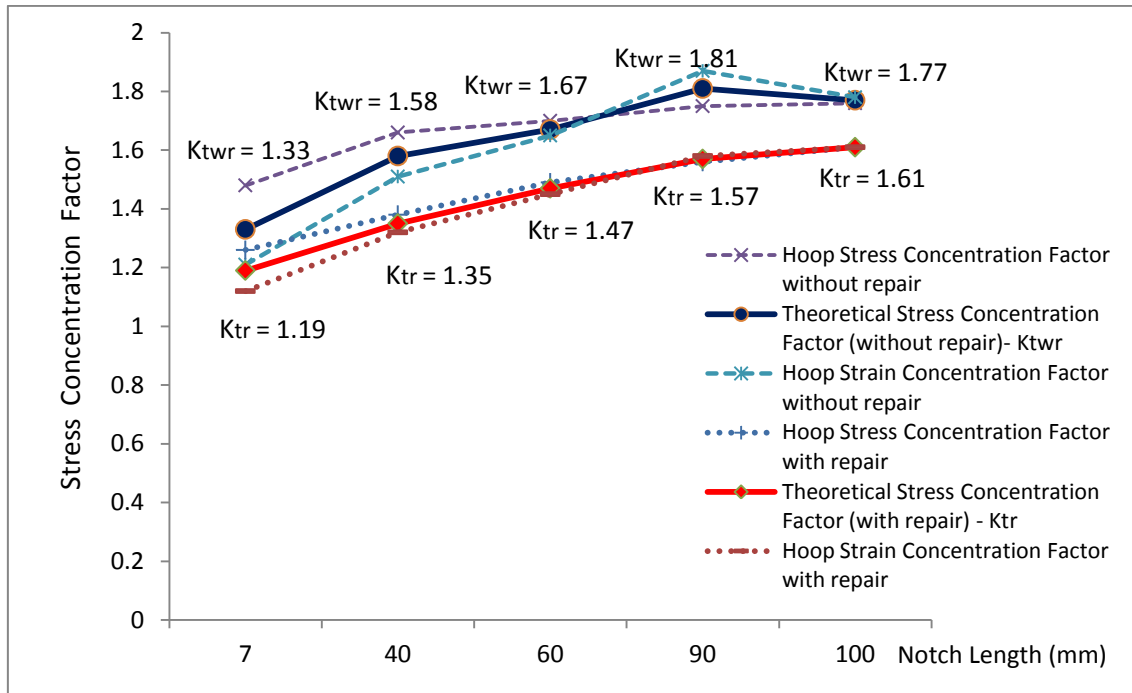
Figure 3.8: Theoretical Stress Concentration Factors (with and without repair)

If the theoretical concentration factor with repair (Ktr) for a particular notch is known, for example for N40, Ktr is equal to 1.35, and a hoop or axial strain concentration factor is obtained experimentally, then the hoop or axial stress concentration can be determined easily. From Figure 3.38 also, it can be seen that hoop stress and strain concentration factors without repair are not really uniform or close to each other if compared to hoop stress and strain concentration factors with repair that are closer to each other as the notch length increases and they steadily converge at notch length equals 100 mm.

3.11 Summary and Conclusions

The convergence study is important to be carried out on the FE model before any other studies, such as the influence of pressure, stress concentration factors and others, can be carried out. It is necessary and beneficial to make a comparison study on

several models that have variable geometry and dimensions before the final model can be chosen. In the comparison study it is understood that dimensions, such as length, and complete geometry model are not the main factors that influence the accuracy of the results. Hence, the half and short pipe model (i.e. Model 3) that requires a fewer number of elements was acceptable and chosen for this study.

Since the nature of this study involves the integrity of bonding between reinforced material (i.e. steel) and reinforcing material (i.e. composite), the composite repair model was developed based on a macro-scale level only. The theory of homogenisation was applied and rules of mixture were used in this development. Several sets of predicted elastic constant values were analysed numerically as a precursor to the stress and strain distribution study. The numerical results have shown a good consistency of stress and strain concentration factors before and after the composite repair as the defect length increases.

In this numerical stress analysis study, both hoop and axial stresses are inversely proportional to the composite repair thickness. However, the defect length has a proportional relationship with hoop stress but an inversely proportional relationship with axial stress. Interestingly, in the stress and strain concentration study, these concentration factors do not depend on the repair length and thickness but on defect length and the biaxial effects on structural response instead. In fact, based on the earlier study (i.e. stress concentration on the unrepaired pipe model), the hoop stress concentration is directly proportional to the length of the arc-shaped defect and the axial stress concentration is inversely proportional to the length of the arc-shaped defect.

In the stress analysis of composite repair, Notch 40 has shown the highest reduction in hoop and axial stress concentration values (i.e. 16.9% and 32.5% respectively) compared to other notches. In another study, PRI has been presented as one of the potential aid tools for benchmarking the efficiency and design optimisation in composite repairs, for example the optimum composite repair for a 40 mm defect is 160 mm instead of 188 mm as recommended by ASME.

In fact, for Notch 40 with 18 plies of composite repair, at the optimum repair length of 160 mm, PRI shows that a 19.96% stress load has been transferred in the hoop direction and 38.15% of stress load has been transferred in the axial direction if the material is Carbon Epoxy. For Glass Epoxy, 18.27% of stress load has been transferred in the hoop direction and 33.74% in the axial direction. Commercially, the manufacturer would benefit if they decided to perform this PRI first, i.e. before the actual pipeline repair work is carried out. Therefore, this PRI gives greater confidence not only to manufacturers but also to operators or pipeline owners. Regardless of the geometry and size of the defect, this PRI will be able to provide insights into the verification of manual calculations.

The study on the theoretical stress concentration with and without composite repair at this end of this chapter concludes that there is the possibility of expanding the theoretical stress concentration factors in a more diversified way in the future which may involve various types of notch (e.g. U or V shaped defects) at different lengths and defect depths. Hence, this theoretical concentration factor with and without repair, based on the finite element method, can provide a good source of information or a database which later would help manufacturers in their design and operation of composite repairs.

4 STRUCTURAL HEALTH MONITORING APPROACH IN STRESS STRAIN ANALYSIS OF COMPOSITE BASED PIPELINE REPAIR

4.1 Introduction

As discussed in Chapter 3, the first approach in understanding the relationship between the stress strain concentrations and distributions of the pipe that contains a blunt defect is to examine it numerically using finite element analysis (FEA). The behaviour of the blunt defect before and after the composite repair was studied thoroughly and it was understood that more complex mathematical equations would need to be established if the blunt defect behaviour had to be studied analytically. Chapter 3 concludes that this numerical approach has proved that the integrity of bonding between the reinforced material (i.e. steel substrate) and reinforcing material (i.e. composite) can be analysed efficiently in terms of stress and strain distributions.

However, the most important issue that has to be addressed in this chapter is how these numerical results that have been discussed in the earlier chapter are validated. It is known that the finite element (FE) is a numerical technique that finds only approximate solutions of partial differential equations (PDEs) as well as of integral equations. Inevitably, they are subject to round-off error and discretization error, as explained in Chapter 2. Although these errors can be reduced by the convergence study, the reliability of data is yet to be proved analytically or experimentally. Therefore, the most convincing way to tackle this issue was to carry out relevant experiments, not only for the purpose of validation but also to overcome any possible deficiencies in the FE method. In fact, reliable experimental data cannot be sensibly obtained if a proper methodology is not carried out first, especially in the pipeline-based composite repair.

In this chapter, the temperature and pressure test rig that was able to provide a practical platform in the acquisition of strain data is presented. This second approach, which was based on a laboratory experiment, has provided an insight into the possibility of performing structural health monitoring on actual site conditions in the future. Before

this second approach (i.e. the experiment) is discussed in depth, it is important to highlight some fundamentals of strain measurement using electrical strain gauges and how the data were acquired by using one of the versatile and robust systems (i.e. the National Instrument CompactRio data acquisition system). These will be explained in the following section.

4.2   Data acquisition of Composite-based Pipeline Repair

4.2.1   Introduction

In this data acquisition of the composite-based pipeline repair, several sensors and instruments involved. Basically, the strain gauges, sometimes called electrical conversion elements or converters, were used as the main sensors because they were able to translate small changes in dimension into an equivalent change of resistance as explained by Weymouth et al. (1979) and the Georgia Institute of Technology (2010). In other words, these sensors were able to convert the physical parameters into an electrical signal. Details of these strain gauges will be discussed further in the next section.

For more reliable strain gauge measurements, proper selections of signal conditioning are equally important and required in this Study. Often, these strain gauge signal conditioners include amplifiers to boost the sensor signal level so that the measurement resolution (that has been converted from analogue to digital values) can be increased and signal-to-noise ratios can be improved (National Instruments Measurement, 2001). NI CompactRio which is a reconfigurable embedded control and acquisition system was one of the main and important instruments used in this Study. This rugged hardware includes I/O modules, reconfigurable field-programmable gate array (FPGA) chassis and real-time controller, and is programmed with Labview graphical software as referred to by National Instruments Measurement (2011).

In this Study, the NI 9148 controller with eight slots and C-series modules NI 9237 were used. Since C-series modules work on Half and Full bridge circuits only, additional accessories such as NI 9944 (for 120 Ohm) and NI 9945 (for 350 Ohm) were added so that the theory of the Wheatstone Quarter-Bridge Circuit, as illustrated in Figure 4.1, could be carried out in this Study. Knowing the voltage applied across the bridge (excitation), the voltage output and gauge factor, then the strain value can be obtained as shown in Equation 4.1.
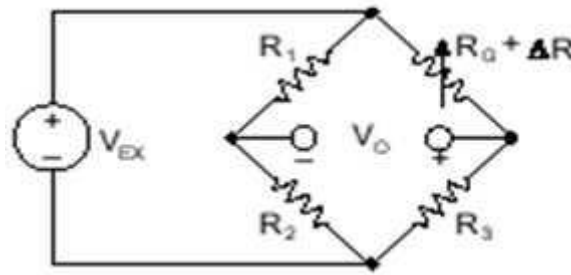
Figure 4.1: Quarter-Bridge Circuit (National Instruments Measurement, 2001)

$$\frac{V_o}{V_{EX}} = -\frac{GF.\varepsilon}{4}\left[\frac{1}{1+GF.\frac{\varepsilon}{2}}\right] \qquad \text{(Equation 4.1)}$$

Where,

V_{EX} = Voltage applied across the bridge

V_o = The output voltage of the bridge,

GF = Gauge Factor

ε = Strain

4.2.2 Strain Gauge Selection and Criteria

In preparing for the strain gauge installation, the first step in this experimental work was the selection of an appropriate gauge for the task. This is because optimising the gauge performance for specified environmental and operating conditions will contribute to the ease of installation and minimise the total cost of the gauge installation as referred to by Vishay Micro Measurements (2005).

A rectangular strain gauge rosette, which is defined as an arrangement of two or more closely positioned gauge grids, separately oriented to measure the normal strains along different directions in the underlying surface of the test part, was selected for this Study. The main reason for selecting this type of gauge is because it is designed to perform a very practical and important function in experimental stress analysis (Measurement Group, 2000). In fact, there was some uncertainty about the principal directions, since the pipe specimen has geometric irregularities such as an arc-shaped defect and welding joint. Therefore, rectangular strain gauges were preferable and these rosettes could be installed without regard to orientation.

It is recommended by Vishay Micro Measurements (2005) that the gauge length should be no greater than 0.1 times the radius of a hole, fillet, or notch, or the corresponding dimension of any other stress raiser at which the strain measurement is to be made. Hence, in this experimental work, the 3 mm instead of 6 mm gauge length with the Constantan A-Alloy type was selected to measure strains at the 40 mm wide arc-shaped notch located on the pipe specimen. Strain gauges of less than 3 mm gauge length are not favourable because they tend to exhibit degraded performance in terms of maximum allowable elongation, stability under static strain and endurance under alternating cyclic strain.

However, the active grid length of the strain gauge for the Triaxial Woven Fabric composite (i.e. that was used in this composite repair study) was 6 mm. This is because ASTM International (2009b) recommends that the gauge length and width should, at a minimum, be equal to the stitch spacing and stitch pitch respectively or

equal or larger than the unit cell or the smallest section of the textile architecture. An example of a unit cell is shown in Figure 4.2.
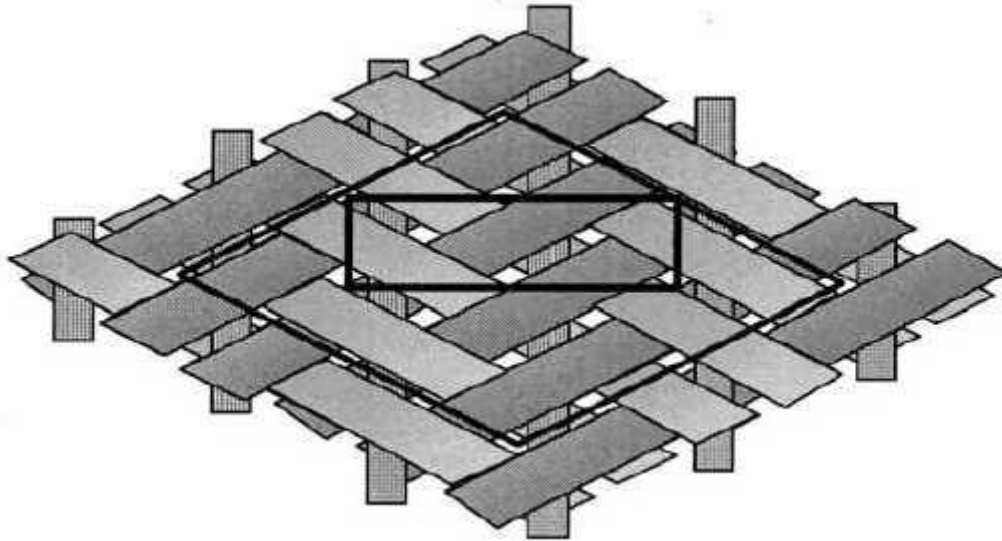
Figure 4.2: An example of the unit cell in the Triaxial Woven Fabric Composite (ASTM International, 2009b)

4.2.3   Calculation of Principal Strains using a Rectangular Strain Gauge Rosette

The equation for calculating principal strains from rectangular strain gauge rosette measurements is derived from strain transformation relationship which is referred to in many Mechanics of Solids text books (Pilkey, 1997). In this study, only a few procedures that were followed in calculating the principal strains are discussed.

- First, the correction of the raw strain readings for the loads transverse to the principal axis of the individual element is presented.

- Then, a summary of the calculations used to compute principal strains directly from the corrected strain gauge data is established.

- Finally, a method used to calculate the principal strains from the corrected values using Principal Strain and Mohr's Circle are discussed.

4.2.3.1 Correcting Strain Gauge Data

Under biaxial stress (pressure loading), three strain values based on a rectangular strain gauge rosette were recorded at each load increment. These raw strain or uncorrected strain readings were designated as ε'_a , ε'_b and ε'_c. According to Weymouth et al. (1979) in this rosette analysis, there is a chance that the design has resulted in considerable misalignment between the gauge measuring axes and the principal strain axes. In other words, an error occurs as the loops in the strain gauge grids are stretched transversely to the primary direction of the gauge, as shown in Figure 4.3 and explained by Bucinell (2001). Therefore, appropriate corrections should be done on transverse sensitivity or the ratio of the gauge response perpendicular to the grid axis and gauge response parallel to the grid axis (i.e. GF (transverse)/GF (longitudinal)).
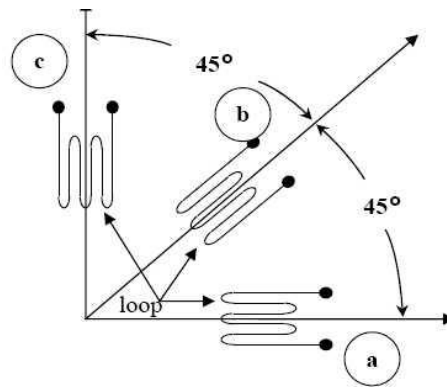
Figure 4.3: Orientation of the rectangular strain gauge rosette (Bucinell, 2001)

4.2.3.2 Calculations used to compute principal strains

Below are the corrected strain equations for a rectangular rosette.

$$\varepsilon_a = \frac{\varepsilon'_a.(1-\nu_o.K_a) - K_a.\varepsilon'_c.(1-\nu_o.K_c)}{1-K_a.K_c} \qquad \text{(Equation 4.2)}$$

$$\varepsilon_b = \frac{\varepsilon'_b.(1-\nu_o.K_b)}{1-K_b} - \frac{K_b.\left[\varepsilon'_a.(1-\nu_o.K_a).(1-K_c) + \varepsilon'_c.(1-\nu_o.K_c).(1-K_a)\right]}{(1-K_a.K_c).(1-K_b)} \qquad \text{(Equation 4.3)}$$

$$\varepsilon_c = \frac{\varepsilon'_c.(1-\nu_o.K_c) - K_c.\varepsilon'_a.(1-\nu_o.K_a)}{1-K_a.K_c} \qquad \text{(Equation 4.4)}$$

Where, ε_a , ε_b and ε_c are the corrected strains; ν_o is Poisson's ratio for material used in calibration by the strain gauge manufacturer (typically 0.285); and K_a, K_b, K_c are the transverse sensitivity coefficients for the gauges (refer to manufacturer's data sheet) (Bucinell, 2001).

4.2.3.3 Direct Calculation of Principal Strains from Corrected Strains

These three equations were used to calculate the two principal strains from the corrected strains;

$$\varepsilon_1 = \frac{1}{2}.(\varepsilon_a + \varepsilon_c) + \frac{1}{2}.\sqrt{(\varepsilon_a - \varepsilon_c)^2 + (2.\varepsilon_b - \varepsilon_a - \varepsilon_c)^2} \qquad \text{(Equation 4.5)}$$

$$\varepsilon_2 = \frac{1}{2}.(\varepsilon_a + \varepsilon_c) - \frac{1}{2}.\sqrt{(\varepsilon_a - \varepsilon_c)^2 + (2.\varepsilon_b - \varepsilon_a - \varepsilon_c)^2} \qquad \text{(Equation 4.6)}$$

$$\tan 2\phi = \frac{2.\varepsilon_b - \varepsilon_a - \varepsilon_c}{\varepsilon_a - \varepsilon_c} \qquad \text{(Equation 4.7)}$$

Where, ε_1 and ε_2 are the maximum and minimum principal strains and $\emptyset$ is the principal angle.

As mentioned in the earlier section, if the material is linear, isotropic in mechanical properties and homogeneous in its component structure, then the principal stresses can be computed directly from the corrected strains as follows (Bucinell, 2001):

$$\sigma_1 = E.\left[\frac{(\varepsilon_a + \varepsilon_c)}{2.(1-v)} + \frac{1}{2.(1+v)}.\sqrt{(\varepsilon_a - \varepsilon_c)^2 + (2.\varepsilon_b - \varepsilon_a - \varepsilon_c)^2}\right] \qquad \text{(Equation 4.8)}$$

$$\sigma_2 = E.\left[\frac{(\varepsilon_a + \varepsilon_c)}{2.(1-v)} - \frac{1}{2.(1+v)}.\sqrt{(\varepsilon_a - \varepsilon_c)^2 + (2.\varepsilon_b - \varepsilon_a - \varepsilon_c)^2}\right] \qquad \text{(Equation 4.9)}$$

Where, E is the modulus of Elasticity and v is Poisson's ratio for structural material.

4.3 The design of composite repair

Before the installation of the composite repair on the test rig was carried out, the design of the repair was verified first in accordance with the established Repair of Pressure Equipment and Piping of ASME's codes and standards, as suggested by Alexander (2009b). In this case, the design of the repair laminate was based on PCC-2 – Article 4.1 (Non-metallic composite repair systems for pipelines and pipework: High risk applications) and specifically referred to the Type A design case where the component has no leak, and requires a structural reinforcement only (ASME, 2010).

By following strictly these ASME codes and standards, the adequate performance of the repair throughout the whole service lifetime of the pipeline can be generated, and according to Frassine (1997) this can be achieved if the pre-compression stresses exerted by the composite wraps do not decay below a certain value before the end of the determined period. In Equation 4.10 which was used in this repair, it is

assumed that the underlying substrate does not yield and it is used for the hoop stresses due to internal pressure only.

$$t_{min} = \frac{D}{2S} \cdot \left[\frac{E_s}{E_c}\right] \cdot (P - P_s)$$ (Equation 4.10)

Where,

External pipe diameter with circumferential defect, D = 0.2121 m

Specified Minimum Yield Strength, S = 241 N/m^2

Tensile Modulus for steel pipe, E_s = 209 GPa

Tensile Modulus for composite laminate, E_c = 25 GPa

Internal design pressure, P = 9.05 MPa

Maximum allowable operating pressure (MAOP), P_s = 7.68 MPa

From the calculation, the minimum thickness (t_{min}) required for the composite repair is 5.04 mm and the installed composite repair with eight layers has a thickness of 6.56 mm. This means this repair design is safe to be used in the experimental work.

4.4 Methodology of Experiment

In any study of the integrity of oil and gas pipeline repair, it is wise to design and fabricate a test rig on site which mimics the actual pipeline, especially in terms of specifications and operating pressures. Normally, a common diameter of oil and gas pipeline is eight inches as reported by the Department of Resources (2010) and one of the examples, is the Mereenie crude oil pipeline project in South Australia. With this size, the maximum operating pressure is around 90 bar. Likewise, with a similar pipe size, the County of Santa Barbara (2009) reports that the normal operating pressure

should be between 20 and 28 bar and the maximum allowable pressure should not be more than 95 bar.

Based on the above operating pressures and size, the simulation of a pipe model and an experimental test rig for this PhD study were carried out. The experimental test rig was fabricated from API 5L Grade B carbon steel with an eight inch nominal pipe size (NPS). By referring to the results of detailed calculation for pressure vessel and development of the test rig in **Appendix 1**, the maximum operating pressure was 90.8 bar. ASME B31.4 and 31.8 standards were followed in this development in terms of design, construction, testing, welding and other quality related factors as referred to by Michalopoulos and Babka (2000).

Since one of the objectives of this study was to analyse the integrity of bonding between the damaged pipeline, due to corrosion, and the composite repair, artificial arc-shaped notches were introduced on the outside of the test rig specimens with a groove defect of 40 mm length and 3.5 mm depth. Because of this defect, the maximum operating pressure in this experiment was reduced to 50 bar only, after taking into consideration the safety factor of the pipeline. The metal loss defects were actually machine simulated (by turning machine) or created by the actual corrosion that occurred during the normal operating life of the straight pipeline segments. Other researchers such as Freire et al. (October 2006) and Alexander (2007b) also present artificial metal loss defects but they use different types of defects and methodology. This damaged pipeline was later repaired with eight layers of composite wrap and each ply has a thickness of 0.83 mm.

Initially, this study had several technical and commercial constraints during the early stages and that is why some of the parameters were finally changed and simplified, as illustrated in Figures 4.4 and 4.5. This study involves blunt defects due to corrosion damage only. For through-wall corrosion damage, references can be made to other literature, for example work carried out by Da Costa Mattos et al. (2009) and others.
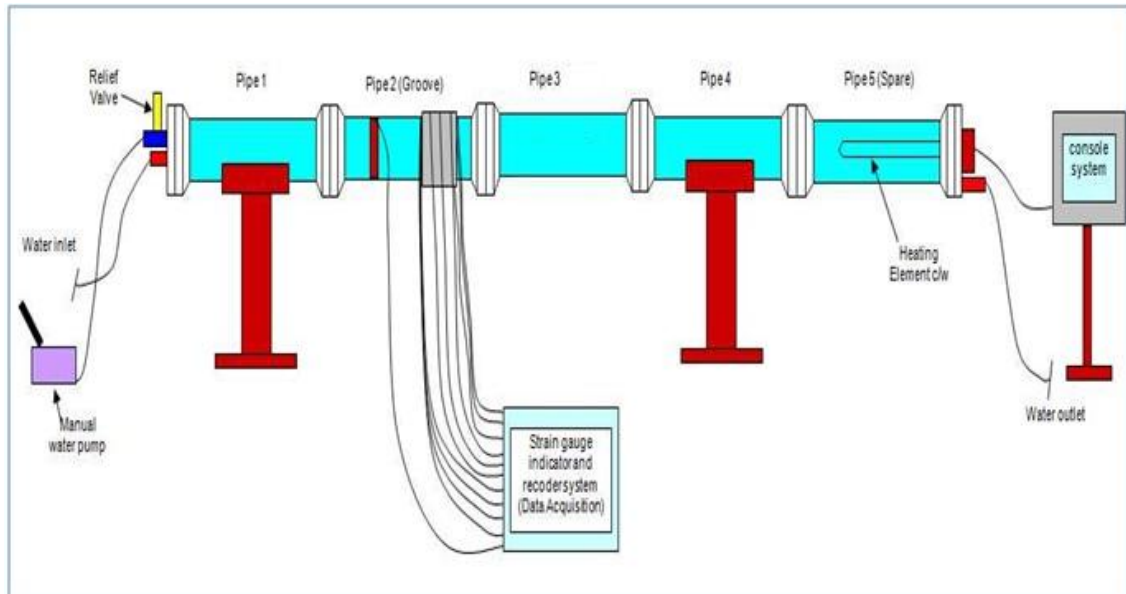
Figure 4.4: Schematic diagram of final conceptual design of the pressure and temperature test rig
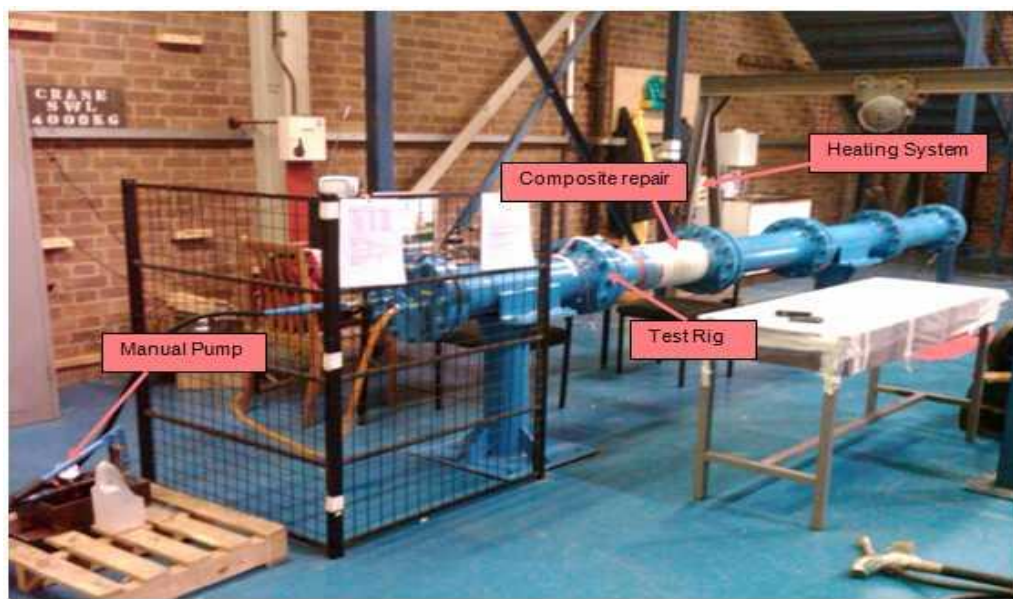
Figure 4.5: The actual pressure and temperature test rig

Figures 4.4 and 4.5 show the total length of the whole test rig is about 4.15 m and is comprised five independent pipe segments. Each of these segments includes the

welded weld neck flange at both ends and has a total length of 0.83 m. The overall height of the test rig was designed up 0.92 m after taking ergonomics into consideration and the whole length of this versatile structure is supported by two simple, yet rigid, supports. Each side of the test rig structure was closed by a blind flange and several parts were welded or joined to it. For example, the front side (head) of this test rig was equipped with a safety feature, namely a pressure relief valve. The incoming cold water from the water tap that flowed via PVC hose was controlled by the steel ball valve at the water inlet and the water pressure in the test rig was increased by a manual (hand) water pump.

In this experiment, a heavy duty polymer hose with a withstand capacity up to 69 bar (1000 psi) was used and a check valve was connected between the inlet at the blind flange and this polymer hose. This check valve ensured the water flowed in a one way direction only so there was no chance of any backflow of pressurised water from the test rig. There was another steel ball valve joined to the highest side of the plane surface of the blind flange and this valve functioned as a "control gate valve". Therefore, the test rig will never be fully filled up with water because by the time it reaches the control gate valve, it will be drained out and this always ensures there is a space inside this liquid-closed piping system (pressure vessel). This safety guideline refers to pipeline design and construction (Mohitpour et al., 2003) and is considered to be one of the safety measures taken during the course of this PhD experimental work. The pressure in this piping system was monitored by the pressure gauge installed at one of the inlets at the front side of this test rig. These installations are illustrated in Figure 4.6.
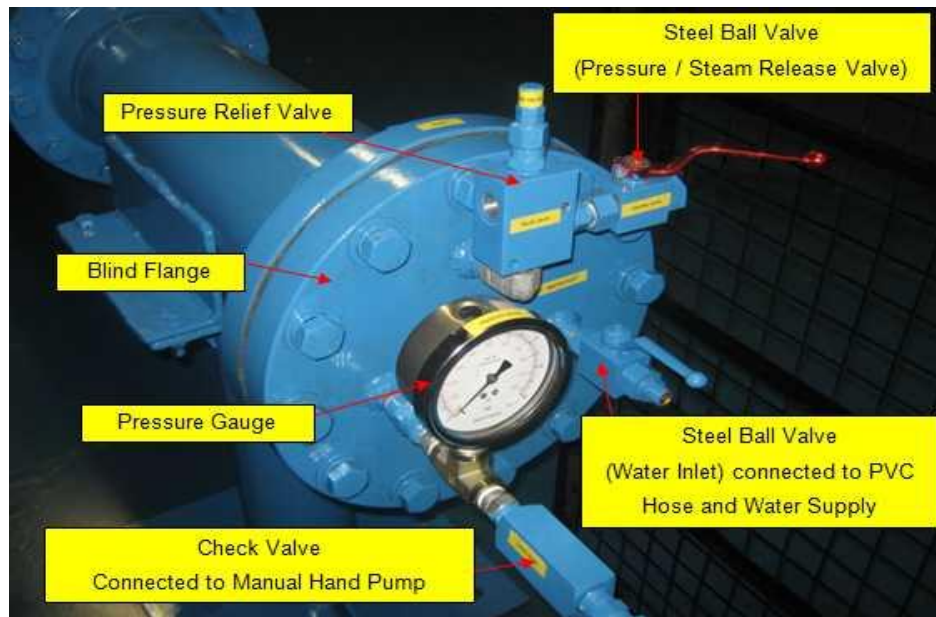
Figure 4.6: Instruments that are installed at the front side of the Test Rig

The rear side of the test rig had the access for the outgoing water (i.e. water outlet) and heating element system. The steel ball valve which was welded to the plane surface of the blind flange prevented water from flowing out from the test rig. Again, the outgoing water (discharged water) flowed via an ordinary low pressure PVC hose to the nearest drain. The heating element system in this experiment worked on a 3-phase power supply and the sensor that was installed next to the heating elements monitored the water temperature inside the piping system as illustrated in Figure 4.7. The cut in and off temperatures were controlled by Programmable Logic Controller (PLC) that was built into this console system and was located near to the test rig.

Since this test rig was not designed for gaseous application, a maximum working temperature of 60°C was set and once the heated water reached that set temperature, the console system would trip the supply until the temperature dropped below the set temperature. Then within a few milliseconds, the heater was re-energised and the process would continue and maintain the water temperature at a constant 60°C. In order to prevent any potential leakages or short-circuits, all the connections were fully insulated and the connecting cables from the console system to the heating element in the test rig was fully protected using PVC conduits.
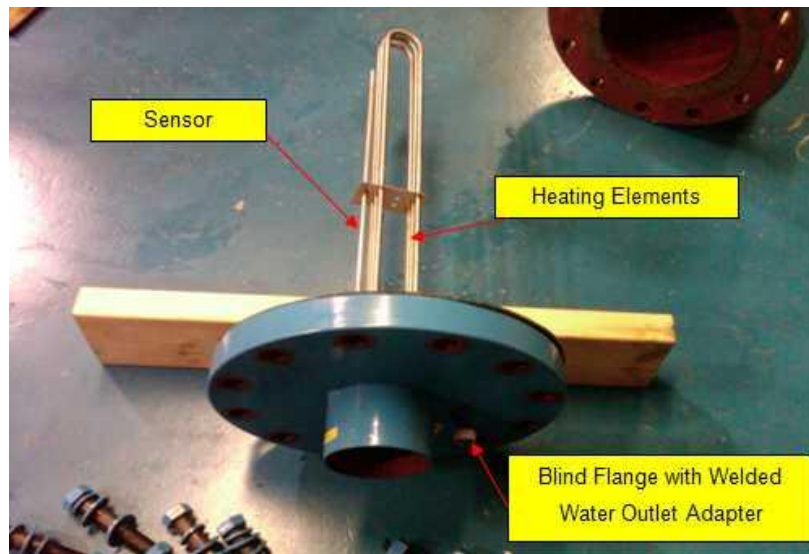
Figure 4.7: Sensor and heating element welded on to the 3-phase insulated socket at the rear side of test rig blind flange

From earlier figures (i.e. Figures 4.4 and 4.5), we can see that there are five pipe segments but only Pipe No. 2 which is called the pipe specimen was studied in this experimental work. This pipe specimen has artificial defects in it, as discussed earlier, and the composite repair will be discussed further in the following section. There were several strain gauges installed on those specific areas and the lead-wires from the sensors were connected to NI 9944/45 accessories, as illustrated in Figure 4.8. Pipe No, 3 which has also been introduced but with another type of artificial crack (i.e. cracks) was not studied in this Study but will be carried out in future works. The remaining pipe segments function as supporting pipes only.

Figure 4.8: Accessories NI9944/45 used in quarter bridge measurement (Left) and C Modules attached to CRio Housing / Controller (Right)

The overall data acquisition concept in this PhD study is summarised in Figure 4.9. Details of the conversion of sensor signals to digital numeric values is represented by the block diagram as illustrated in Figure 4.10. In this figure, we can see that the four C-series Modules NI 9237 provide only 12 channels for strain measurements for a particular test. In other words, only four rectangular strain gauge rosettes were connected to the circuit during each test. Other sensors remained disconnected. The main reason for this is because of the limited number of modules available for this Study. Otherwise, this block diagram should have shown a complete connection of channels (i.e. 30 channels) instead. Therefore, repetitions of the same test were carried out with the remaining sensors during the course of this Study. The digital results were then displayed in the form of an amplitude and waveform chart.
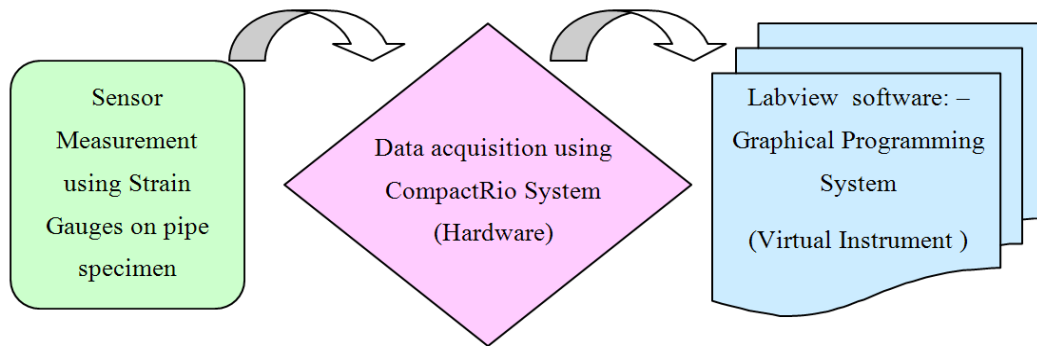
Figure 4.9: A summary of data acquisition in Study
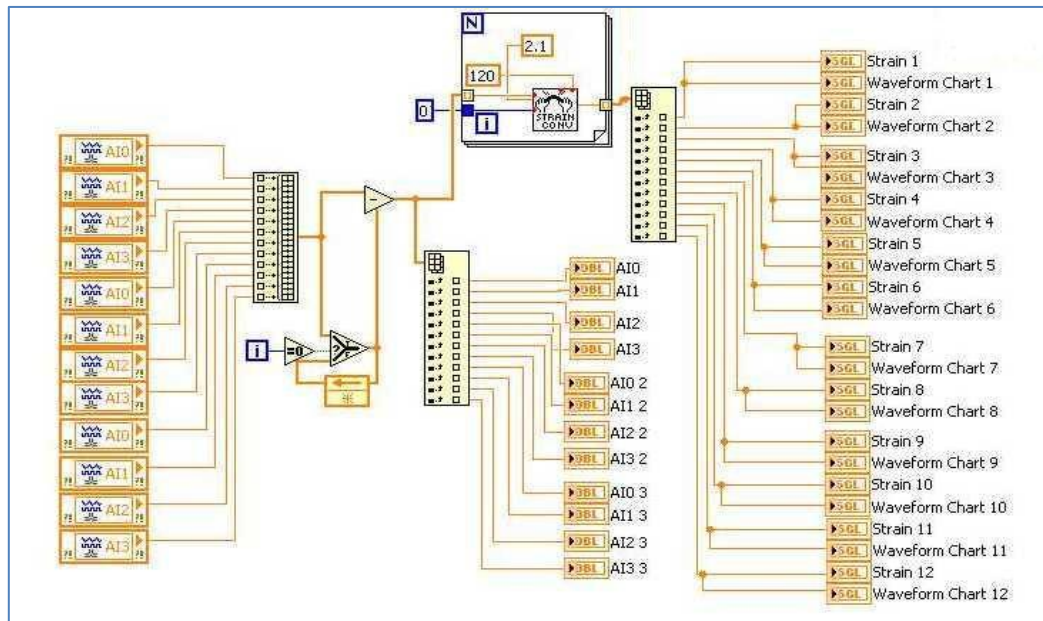
Figure 4.10: Block diagram of data acquisition using National Instruments CompactRio (NI CompactRio) system

4.4.1 Composite installation

Basically, the epoxy matrix was formulated by mixing a two-part standard wet-out system using an epoxy resin-to-hardener ratio of 5:1. Epoxy resin (Epichlorhydrin)

is called Part A and the hardener that consists of Triethylenetetramine, Isopropylidene and Diethylenetriamine chemicals is called Part B. After applying an epoxy-based primer to the repair area, the woven glass fibre fabrics with 300 mm (Width) x 500 mm (Length) dimensions were wrapped by hand around the pipe up to eight plies, as shown in Figure 4.11. Details of the composite wrap process are referred to **Appendix 2**.

Figure 4.11: The installation of the final layer of glass epoxy composite

There were two tests involved in this experiment. Test 1 was a pressure test where pressure varied at room temperature (e.g. 25ºC) and the results are discussed in this chapter. Test 2 was a temperature test where the temperature varied at a constant pressure of 0 - 2 bar. This test will be discussed in Chapter 5.

In Test 1, there were two stages of experiment. The first stage was the pressure test with no composite repair and the second stage was with the repair. In terms of the procedures in Test 1, basically, the pressure was raised in 10 bar increments and held constant for about 10 seconds, then increased again to 50 bar (maximum) and readings were taken in 10 bar increments. The pressure was released and the readings were taken in 10 bar decrements. Finally, graphs were plotted in terms of strain versus pressure.

One of the objectives of doing this was to validate the numerical stress concentration results. The same procedures were repeated in the second stage of Test 1 but this time the main objective was to observe how well the strains and stresses in the composite follow the strains and stresses in the pipe due to internal pressure loading. Hence, it would provide some insights into load transfer between steel and composite and the stress transfer through the epoxy matrix. A detailed description of the strain measurement methodology will be explained in the following section.

4.4.2 Detailed descriptions of strain measurement

Figures 4.12 and 4.13 show there were three locations of strain measurement (i.e. at base, middle and top or outer layer of the composite repair). Points 1a, b and c were referred to the points on the steel pipe (i.e. base). At point 1a (i.e. at the notch root), there were three strain gauges installed along the circumferential notch root as shown in Figure 4.14. Points 2a and b were referred to the 4th layer of the composite lamina (half of the composite thickness – middle layer) and Point 3a and b were referred to the outer layer (8th layer – top layer) of the composite. The measuring distance of strain gauge from the point away from the defect (nominal thickness) to the defect area on each layer was about 80 ~ 90 mm.
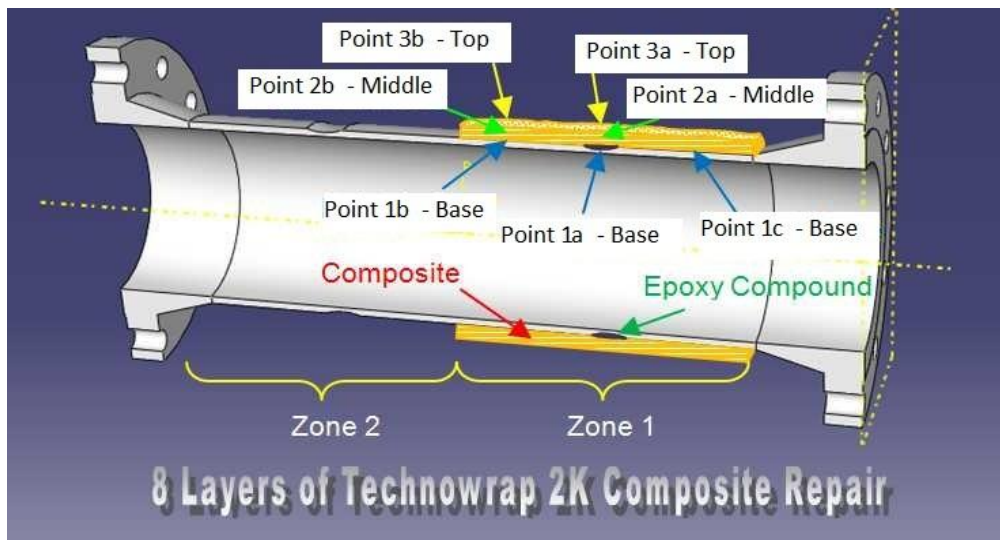
Figure 4.82: A schematic representation of the measuring point locations
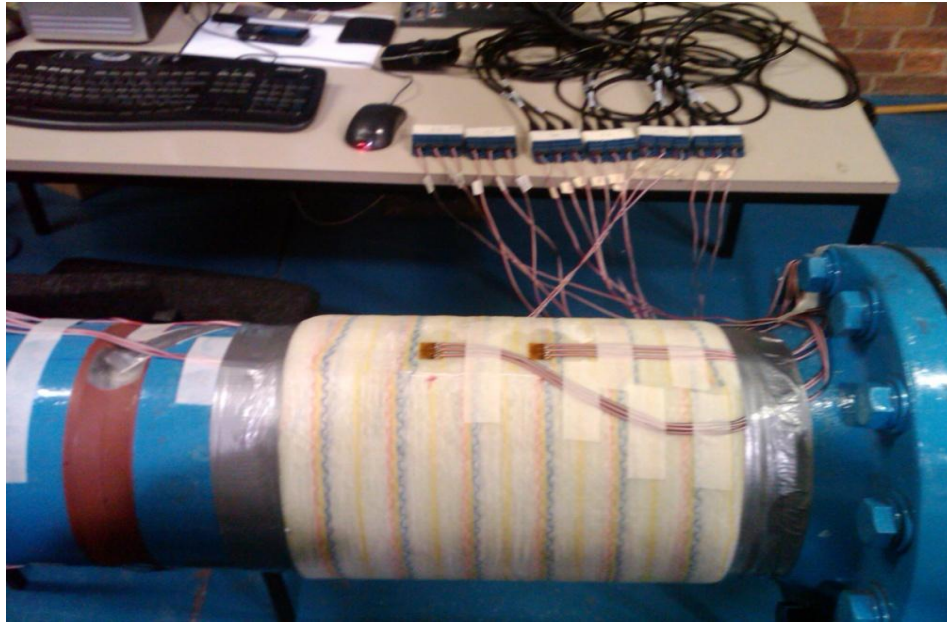
Figure 4.93: The actual installation of strain gauges on the steel, embedded and on the outer layer of composite repair

In order to obtain accurate and reliable experimental data, often the scope and capability of the most suitable sensors in experimental work should be studied properly first, as reported by Murad (2009). After a proper study had been carried out by Murad and Brennan, (2010), there were three sets of Rectangular Strain Gauge Rosettes type CEA-06-120CZ-120 with 120 Ohms (nine sensors or channels) installed on three different points, as shown in Figures 4.12 and 4.13. However, to compare the measurement readings, two more sets from the same rosettes but with different orientations of element direction were installed on each side of Point 1a at 45° apart. Hence, there were three different locations and positions of measuring strain along the notch root in Zone 1. Additionally, another similar set of rectangular rosettes was bonded at the same point (i.e. Point 1a or base layer) but on the second groove of the pipe specimen (test spool) in Zone 2, as shown in Figures 4.14 and 4.15.
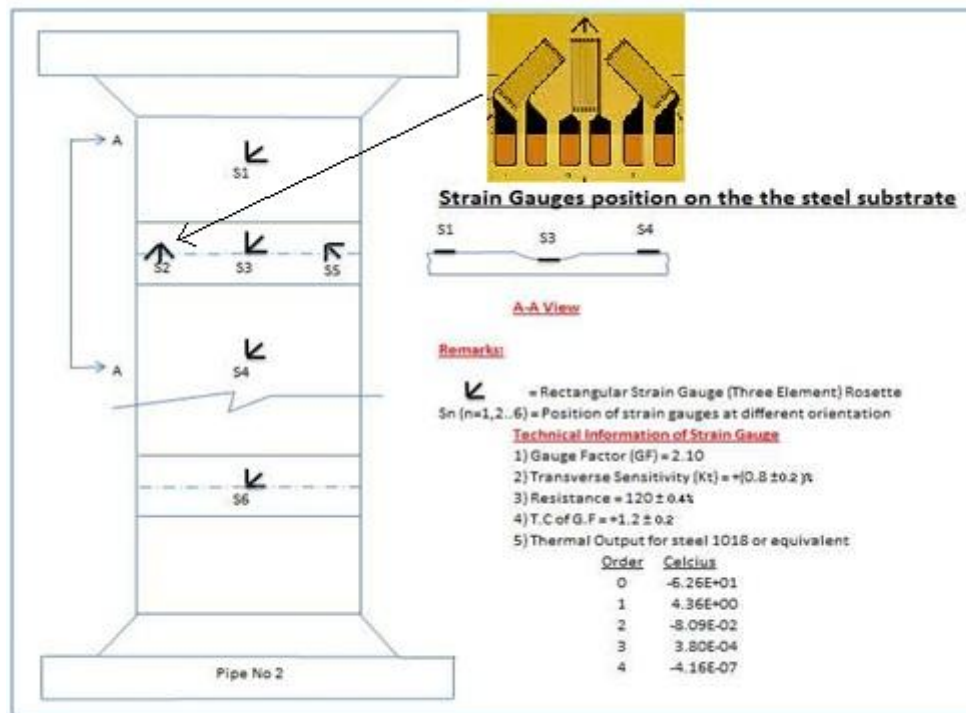
Figure 4.14: A schematic diagram of strain gauge positions

The errors of reading between these two positions of different zones were determined and used as a main cross-reference throughout the course of the experiment. So, at Points 1a, b and c, 18 channels or six rectangular rosette sensors were used. The study of load transfer in the base structure through certain layers of the composite wrap (50% of the overall composite wrap thickness) was carried out at points 2a and b.

In these experimental works, the areas of measurement were still referring to the previous point positions and similarly with the same through thickness planes. Only two Rectangular Strain Gauge Rosettes type CEA-06-250UR-350 were installed at Points 2a and b as shown in Figure 4.15 and the strain gauge installation process is described in **Appendix 3**. But this time, a resistance of 350 Ohm was used instead of 120 Ohm. This type of resistance was suitable in the composite application, as recommended by Vishay Micro Measurements (2005). According to Pople (1992), 350 Ohm grid resistance has several advantages over 120 Ohm in terms of higher bridge voltages and output signal obtainable and also fewer effects of lead resistance.

147
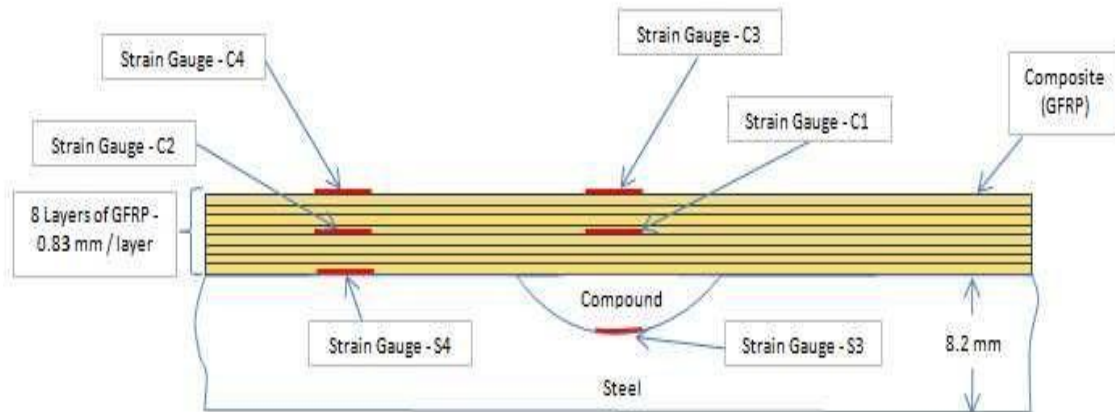
Figure 4.105: An illustration of gauge positions in the composite repair system

Finally, the study of stress and strain distributions on the final or completed layer of the composite wrap (e.g. eight layers) was carried out at Points 3a and b, which had the same specifications as Points 2a and b, as shown in Figure 4.15. The phenomenon of load transfer in the base structure throughout layers of composite wrap was further analysed based on the numerical and experimental readings taken from the earlier works. The total number of channels for the data acquisition using CompactRio system were 30 or 10 rectangular strain gauge rosettes.

4.5 Pressure Test

4.5.1 Results

This experiment has six sets of strain results at different locations with the maximum internal pressure of 50 bar (5 MPa). Only results at the S3 location are discussed in this section because its methodology is similar to others.

Table 4.1 summarises the results at the S3 location and the graph is shown in Figure 4.16. The overall results are illustrated and discussed in the following section.

Table 4.1: Strain gauge readings at S3 location

	Pressure (bar)				
Strain	10	20	30	40	50
Hoop strain (Load up)	81.6	174.2	267.5	351.3	432.4
Axial strain (Load up)	55.6	111.2	166.3	232.2	279.8
Hoop strain (Load down)	92.44	184.2	269.8	355.1	441.6
Axial strain (Load down)	62.52	121	167.8	235.3	286.6
Average Hoop Strain	87.02	179.2	268.6	353.2	437
Average Axial Strain	59.06	116.1	167	233.8	283.2
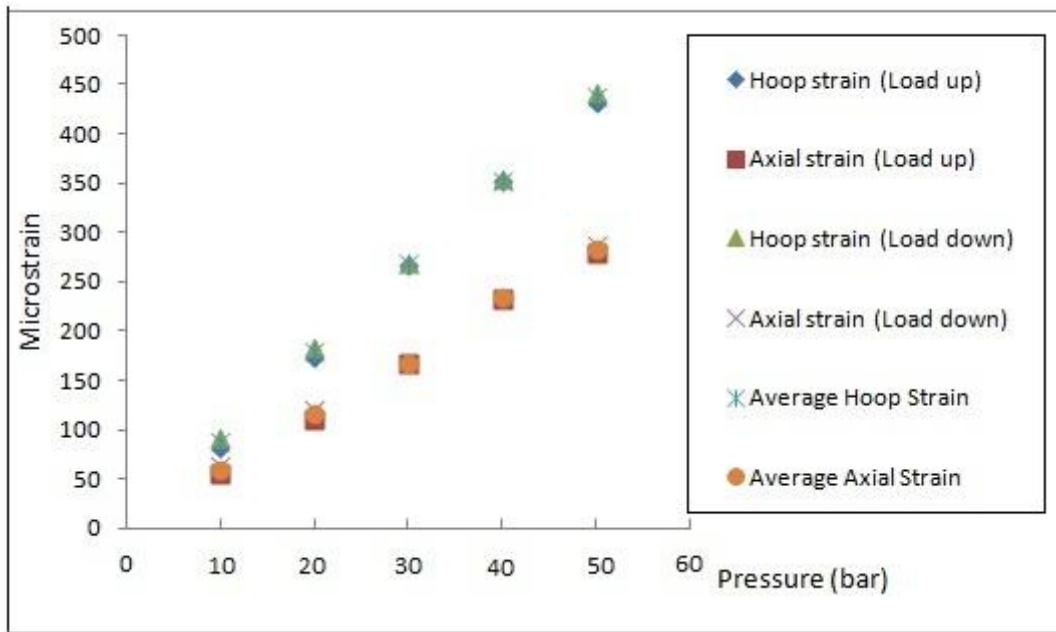
Figure 4.16: Strain (microstrain) versus pressure at S3 location

By referring Table 4.1, the pressure was raised in 10 bar increments up to 50 bar. For each step, time was allowed to settle and stabilise during loading up and down pressure. Figure 4.16 shows the gradients of the linear (average hoop and axial strains) curves of S3 show that at 50 bar, the corrected hoop strain is 8.8164E+01 x 50/10 =

149

440.82 microstrain and for the axial strain is 5.7153E+01 x 50/10 = 285.77 microstrain. The same method is applied to other locations. The overall results are tabulated in Table 4.2.

Figures 4.17 and 4.18 again show the strain results against pressure at the S3 location tested in a linear elastic region but this time with different layers of composite repair. From these two graphs, it can be seen that the increase of composite layer has reduced the strain value at the defect area (i.e. S3) and the percentage reduction is much higher in the axial direction.
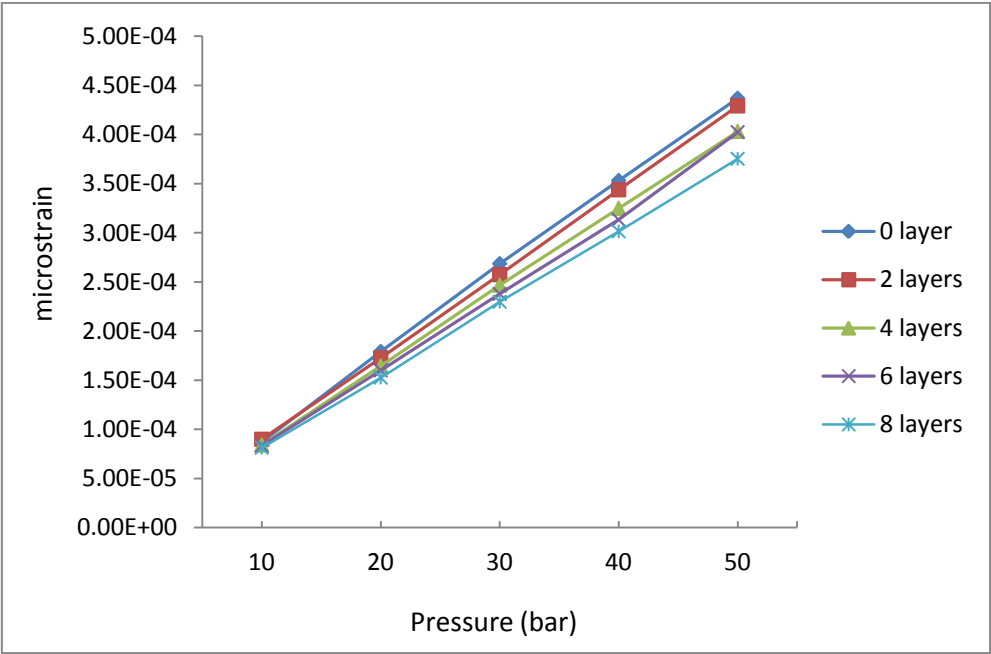
Figure 4.117: Hoop strain versus increasing pressure at S3 location
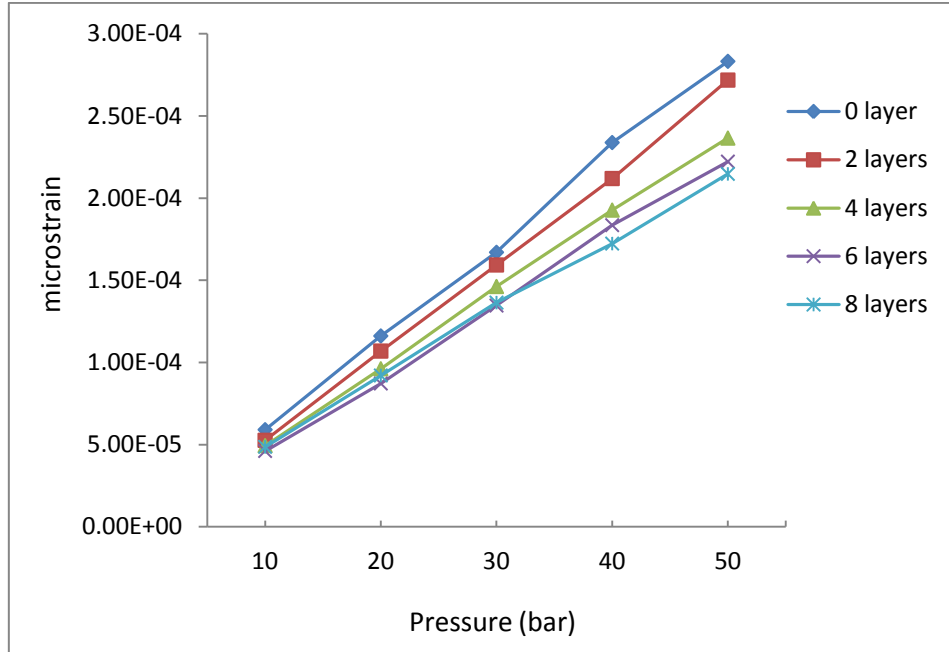
Figure 4.18: Axial strain versus increasing pressure at S3 location

4.5.2 Analysis of Experimental Result

Table 4.2 and Figure 4.19 show the strain distribution phenomenon of six sets of strain gauges that were installed at different locations and orientations. The hoop and axial strains at the nominal areas (i.e. S1 and S4) show a good agreement before, during and after the repair (i.e. eight layers). These results confirm that the methods for installing the sensors and composite are in accordance with standard practice. Although these are at the defect free areas, a hoop load transfer did occur from the steel into the final layer of composite at about 8.54% at S1 and 8.3% at S4 respectively.

Table 4.2: Strain gauge readings at all locations

Location and	Strain Values (Microstrain)				
Type of Strain	0 layer	2 Layers	4 Layers	6 Layers	8 Layers
S1-Hoop Strain	276.42	257.53	266	260.8	252.8
S1-Axial Strain	86	80	79.45	83.37	78.46
S2 - Hoop Strain	401.14	407.17	400.48	383.07	380.12
S2 - Axial Strain	363.41	335.29	310.88	305.58	287.65
S3-Hoop Strain	440.82	429.87	406.28	398.42	378.04
S3-Axial Strain	285.77	268.26	239.43	224.47	218.62
S4 - Hoop Strain	278.28	276.08	274.43	266.76	255.16
S4 - Axial Strain	68.38	72.3	67.82	70.8	66.13
S5 - Hoop Strain	479.77	396.87	380.71	368.72	356.86
S5 - Axial Strain	301.86	326.47	297.14	301.02	284.8
S6 - Hoop Strain	427.03	476	476.3	476.3	477.64
S6 - Axial Strain	334.7	301.18	302.52	302.52	280.02
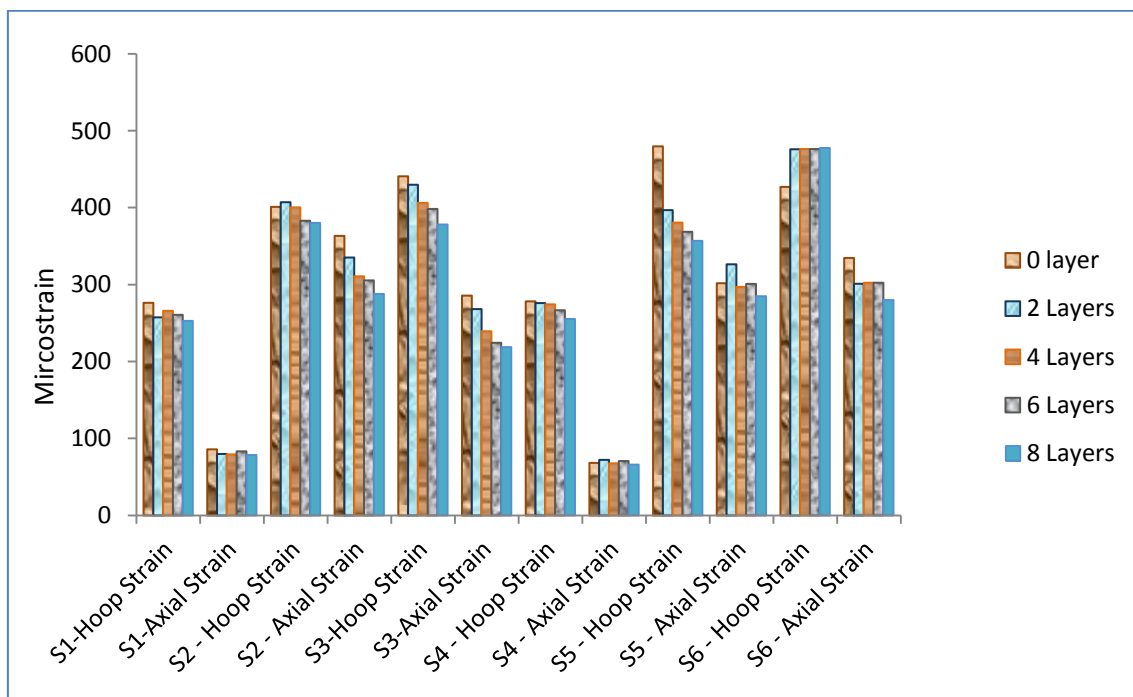
Figure 4.19: The load transfer behaviour at different positions on the steel (testing pressure at 50 bar)

However, the axial load transfer is slightly different. At S1 which is close to the stress riser (i.e. welding joint flange), the axial strain at the zero layer (i.e. 86 microstrain) is higher than at S4 (i.e. 68.38 microstrain) which is away from the notch defect and welding joint. This shows that the axial strain at S1 is not only the function of internal pressure but also the discontinuity or geometry of the structure. The axial load transfer from the non-repaired (i.e. zero layer) to fully repaired (i.e. eight layers) is more effective at S1 where the improvement of load transfer is 8.7% higher than at S4 which is only 3.29%. Finally, the difference in the axial strain readings at S1 and S4 after eight layers has been reduced from 20.49% to 15.71%.

Strain distributions at defect locations such as at S2, S3 and S5 shows a significant load transfer from 0 to 8 layers of the composite repair and this is further discussed at the end of this section. A strain distribution can also be seen at location S6, where location and orientation of the rectangular strain gauge are similar to S3 except that at this location no repair has been done. At the zero layer, the strain readings at S3 and S6 are very close to each other with an error of 3.12% only. The reason for this is mainly attributed to machining error at the defect shape and depth of both locations.

Interestingly, when the adjacent location (i.e. S3) is wrapped with two layers of composite, the hoop strain reading at S6 tends to increase instead of remaining constant. When the number of layers is increased from two to eight layers, the hoop strain readings remain steady and almost constant but higher than the reading at the zero layer. This shows that one side (i.e. S3) is under compression due to the effect of the composite repair and at the other end is under tension (i.e. S6) due to the unrepaired defect surface. However, the axial strain finally decreases when S3 has been fully repaired with 8 layers of composite. This shows that the effect of the composite repair not only reduces the axial strain values at the repaired area but also the adjacent (non-repaired) area as well.

Table 4.3: The experimental strain results at defect and nominal areas in the composite repair

Location / Type of Strain	0 layer	2 Layers	4 Layers	6 Layers	8 Layers	Percentage of Reduction (%)
S3-Hoop Strain	440.82	429.87	406.28	398.42	378.04	14.25
S3-Axial Strain	285.77	268.26	239.43	224.47	218.62	23.5
S4-Hoop Strain	278.28	276.08	274.43	266.76	255.16	8.3
S4-Axial Strain	68.38	72.3	67.82	70.8	66.13	3.29

Table 4.3 and Figure 4.20 show some significant amounts of load transfer at the defect and nominal areas after the completion of 8 layers of composite. The percentage of reduction that represents the amount of load transfer is defined as the difference between the strain before (without repair) and after repair (with 8 layers of composite material) divided by the strain before the repair multiplied by 100. At S3, about 14.25% load is transferred in the hoop (i.e. percentage of reduction) and 23.5% in axial directions; only 8.3% and 3.29% of hoop and axial load transfers occur at S4. This shows that the composite takes more load at the defect area than at the nominal area.
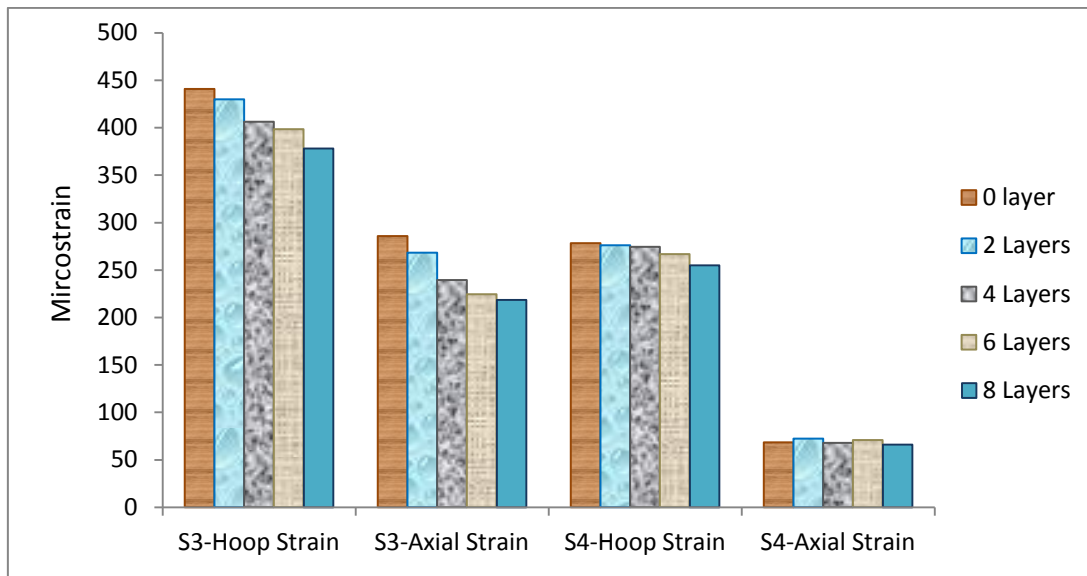
Figure 4.12: The load transfer behaviour from reinforced material (steel) into the reinforcing material (composite) as the thickness of composite increases

In this experiment, the technique of installing the strain gauge is of paramount importance. There are three significant locations of strain gauges, as shown in Figure 4.21. This shows that the orientation of each element of the rectangular strain gauge rosette plays a significant role in determining the more accurate and steady measurement. S3 in Figure 4.22 shows the most steady reduction of strain readings compared to S2 and S5, although all of them were installed along the circumferentially arc-shaped defect, as shown in Figure 4.21.
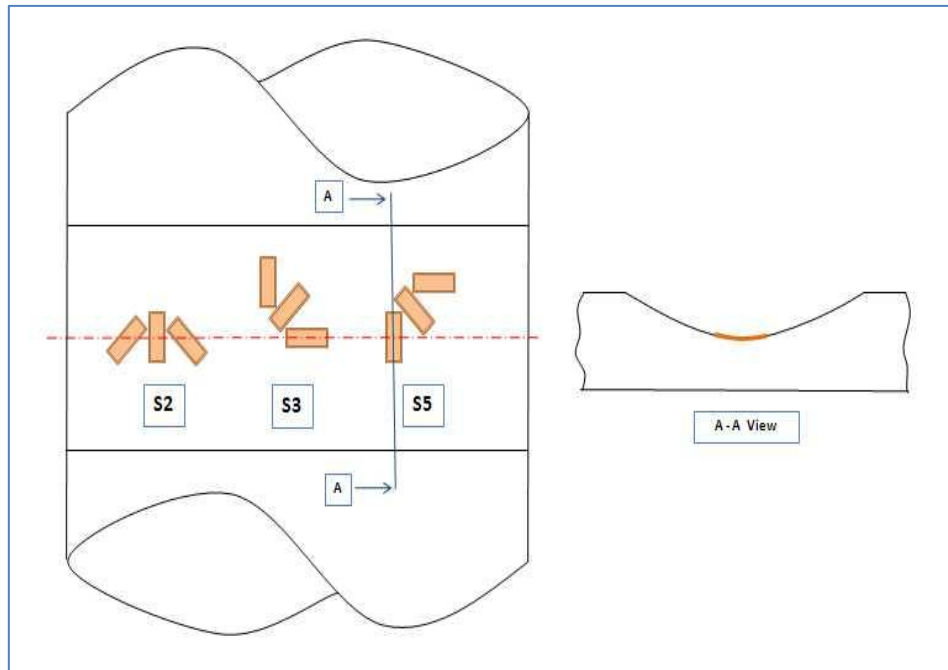
Figure 4.21: Schematic representation of layout of strain gauge installation on the specimen (Murad et al., 2011)
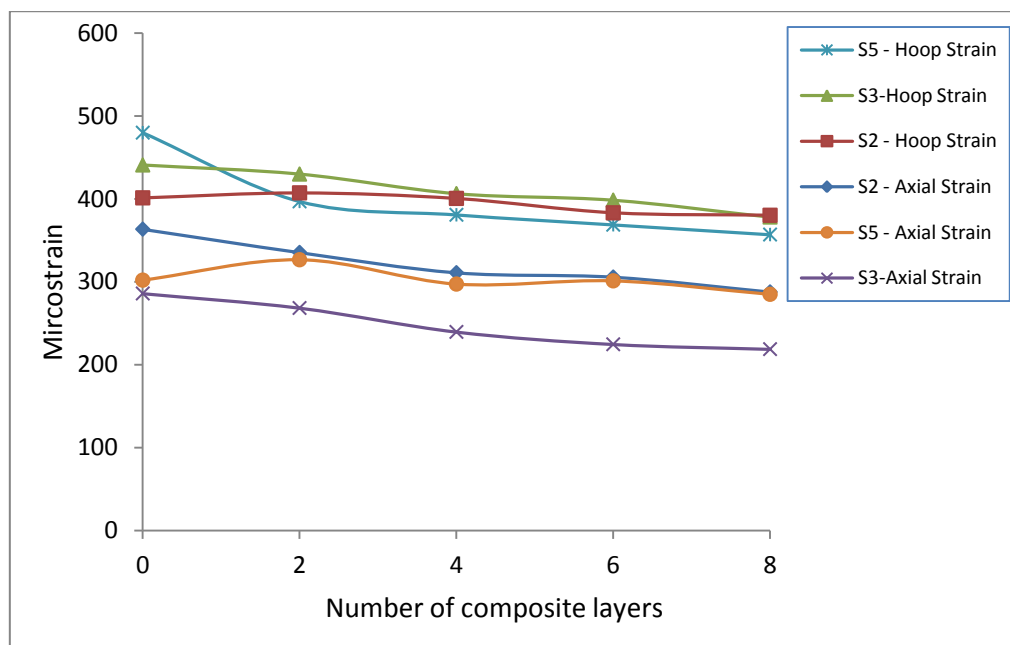
Figure 4.22: Different load transfer phenomenon due to biaxial effects

Since the defect is not a flat notch, the orientation of the strain gauge really does matter. Due to the uncontrolled biaxial effects at the defect area, the right technique of sensor installation is essential. Hence, to measure a typical arc-shaped defect like this, the installation technique should be similar to that of S3 and this orientation technique will be adopted in future works.

The results from this study also disagree with some results obtained by Alexander (2007b), particularly on the actual behaviour of strains due to internal pressure based on the glass epoxy composite repair (in the elastic working region). During that time, he failed to see the load transfer before yielding. He managed to see the contribution of the glass epoxy composite but only after the repaired material yielded.

However, there was a clearly a contrast in the behaviour of the carbon composite repair, as shown in his experimental result where the load transfer had occurred even in the earliest stage (i.e. elastic working region) until rupture. Therefore, this clearly shows that in strain measurements which use precise electrical strain gauges, a full understanding in terms of the fundamentals of strain gauge application is definitely required in order to obtain sensible and reliable results.

The effects of the quadruple layers of composite in the load transfer can be seen in Figure 4.23. At S3 (i.e. the sensor bonded on the steel defect and beneath the composite), the increment of composite layers from four to eight layers shows an improvement of 6.81% for hoop and 8.69% for axial. This is because, according to Francini and Alexander (2006), the stiffness (E.t) which refers to Modulus of Elasticity (E) and thickness (t) of the composite materials, plays a significant role in determining the strain level at which the load transfer takes place. In addition, at C1 (i.e. embedded sensors between eight layers at the defect area) a higher value of percentage of 21% and 33.98% for hoop and axial respectively is shown.
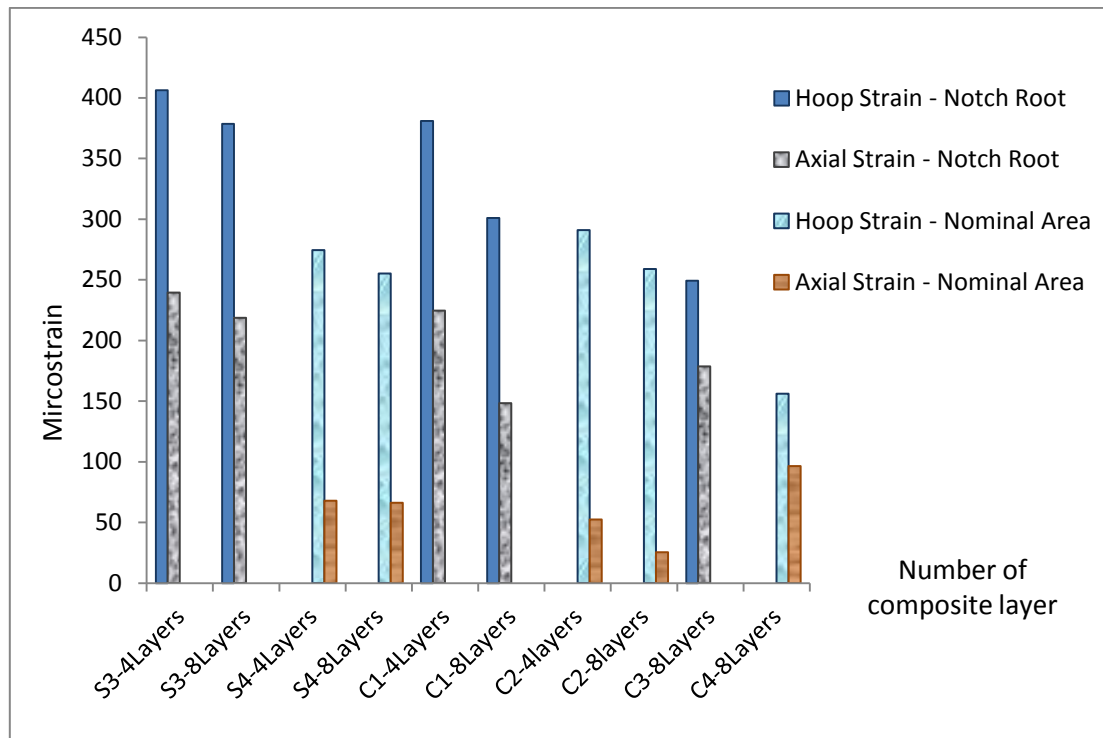
Figure 4.23: The strain load transfer behaviour between steel and composite

This clearly shows that besides stiffness, the matrix (i.e. epoxy resin) also plays a significant role in transferring the load between layers of composite. It takes much of the loading transverse to the fibre direction as referred to by Littell (2008). Azzi and Tsai (1965) suggest that further studies on the resin in this anisotropic composite are required on the micro-mechanics level, as they understand it is not always true that the composite material can carry the load only in the direction of the fibres. However, in this study the compatibility of both phases is only performed at the macro-mechanics level.

At S4 (i.e. the sensors that were bonded on the nominal steel and beneath the composite) an improvement of 7.02% for hoop and 2.49% for axial is shown. But C2 (i.e. embedded sensors between eight layers at the nominal area) shows 11.02% for hoop and 51.58% for axial. This clearly shows that the contribution of the composite is much less in terms of axial load transfer from steel to composite at the nominal area.

Again, the epoxy resin plays a significant role in effectively transferring the load between the layers of composite.

Figure 4.23 also shows that the hoop strain measured at C3 (i.e. on the 8th or outer layer of the composite repair at the defect area) is 249.4 microstrain and is lower than at S4 (i.e. nominal area before the composite repair) which is 278.28 microstrain. Hence, the minimum repair thickness and number of laminas which were calculated, based on the assumption that the repaired pipe will have the same strength or be better than the original pipe, as mentioned by Rosas et al. (2007), are actually true.

4.6 Validation of Results

4.6.1 Comparison of manual calculation, numerical and experimental results without composite repair

In order to validate the numerical strain results using ABAQUS and manual calculation, the experimental results are required.

Simple shell theory formulas were used to calculate the strains in the undamaged pipe section. For Longitudinal Strain (Kaminski, 2005)

$$\varepsilon_L = \frac{\sigma_L}{E} - \frac{v\sigma_h}{E} - \frac{v\sigma_r}{E} = \frac{PD}{4tE}(1 - 2v) \qquad \text{(Equation 4.11)}$$

For Hoop Strain (Kaminski, 2005)

$$\varepsilon_h = \frac{\sigma_h}{E} - \frac{v\sigma_L}{E} = \frac{PD}{4tE}(2 - v) \qquad \text{(Equation 4.12)}$$

For general tensile stress (Kaminski, 2005)

$$\sigma = E.\varepsilon \qquad \text{(Equation 4.13)}$$

Where:

Internal pressure, P = 50 bar (5 MPa)

Outer diameter of pipe, D = 219.1 mm (for 8" Nominal Pipe Size)

Length of pipe specimen (Pipe no 2), L = 608 mm (excluding welded flanges)

Nominal thickness, t = 8.18 mm (0.322 in)

Defect thickness, t_d = 4.68 mm (43% less than the nominal thickness)

Young Modulus, E = 209 x 10^9N/mm^2 (steel)

Poisson ratio, ν = 0.3 (steel)

At the defect area, the manually calculated hoop strain, shown in Table 4.4 and Figure 4.24, is much higher than that of ABAQUS and most of the experimental hoop strains. This is because, as explained in the earlier chapter, the simple shell theory does not take into account the shape factor of the defect surface. Also from Figure 4.24, the numerical hoop strain (ABAQUS) is relatively lower than others. The experimental hoop and axial strain results show a good agreement among themselves. Likewise, the experimental hoop and axial stresses also behave in the same way.

However, all the experimental axial strains are much higher than the manual calculation and ABAQUS. These experimental axial strain results actually show the true strain behaviour at the defect area as compared to manual calculations that depend only on the simple shell theory rather than complex analytical expressions. ABAQUS has mass and pressure loading differences that will be explained further in the next section. Nevertheless, S3 shows a better agreement with the manual calculation and ABAQUS compared to other measurement locations. The reason for this has been discussed in earlier sections.

Table 4.4: Study at the defect area (arc-shaped notch defect)

Strain	Manual calculation (S3)	ABAQUS (S3)	Experimental Result			
			S2	S3	S5	S6
Hoop Strain (microstrain)	476	402	401.14	440.82	479.77	427.03
Axial Strain (microstrain)	112	114.4	363.41	285.77	301.86	334.7
Hoop Stress (MPa)	99.5	100.14	83.84	92.13	100.27	89.25
Axial Stress (MPa)	23.41	53.84	75.95	59.73	63.09	69.95
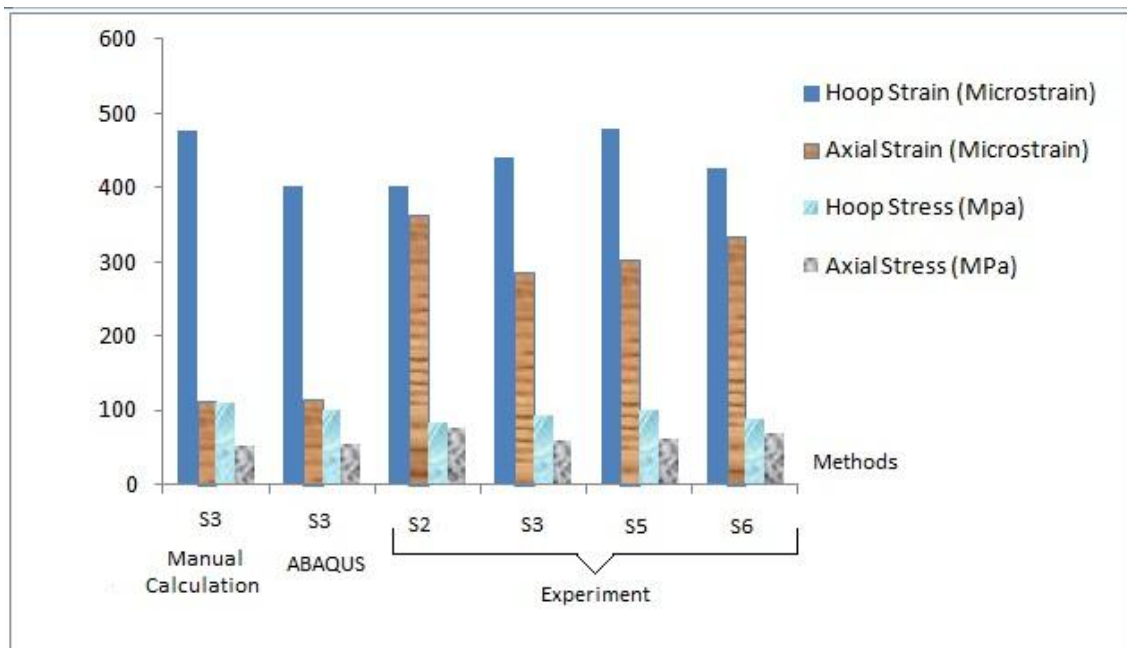
Figure 4.24: Comparison of stress strain results using three different approaches

At the nominal area (away from the defect) as referred to in Table 4.5 and Figure 4.25, all three methods (i.e. manual calculation, ABAQUS and experiment) almost

show a good agreement in hoop strain, hoop stress and axial stress. However, the axial strain shows some differences. Axial strain at S1 is higher than S4 because it is located close to the weld joint, as discussed in the earlier sections. The reason why the axial strain of ABAQUS is very low and least apparent than the others again will be discussed in the following section. However, the experimental axial strain at S4 shows a very good agreement with the manual calculation. This proves that under a normal structure that is free from any discontinuity or defect, a simple shell theory is acceptable and shows a sensible result.

Table 4.5: Study at the nominal area (away from the defect)

	Manual calculation	ABAQUS	Experimental Result	
			S1 (close to weld joint)	S4
Hoop Strain (Microstrain)	272	265.81	276.42	278.28
Axial Strain (Microstrain)	64	2.2	86	68.38
Hoop Stress (MPa)	56.85	60.62	57.77	58.16
Axial Stress (MPa)	13.38	18.91	17.97	14.29
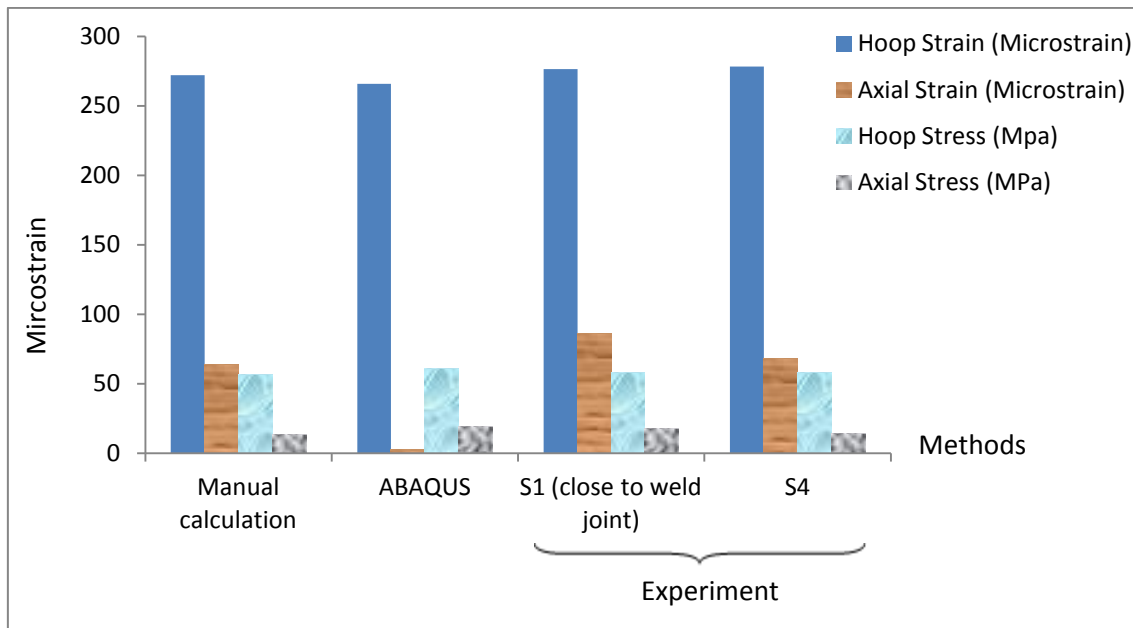
Figure 4.25: Comparison of stress strain results of three different approaches at the nominal area

4.6.2 Comparison of results between ABAQUS (simulation) and experiment with the composite repair

From Table 4.6 and Figure 4.26, both numerical and experimental hoop strains show a good agreement at the defect and nominal areas. However, the axial strain correlation, as discussed earlier, is much less apparent. This is attributed to mass and pressure loading differences between the numerical model and the experimental system as explained by Martineau and Romero (1996).

Table 4.6: Comparison of load transfer between simulation and experiment

Location / Type of Strain	0 Layers	8 Layers	Percentage of Reduction (%)
S2-Hoop Strain (Experiment)	401.14	380.12	5.24
S3-Hoop Strain (Experiment)	440.82	378.04	14.24
S5-Hoop Strain (Experiment)	479.77	356.86	25.62
*Defect Hoop Strain (Simulation)	402	365.87	8.99
S2-Axial Strain (Experiment)	363.41	287.65	20.85
S3-Axial Strain (Experiment)	285.77	218.62	23.50
S5-Axial Strain (Experiment)	301.86	284.8	5.65
*Defect Axial Strain (Simulation)	114.4	95.36	16.64
S4 - Hoop Strain (Experiment)	278.28	255.16	8.31
*Nominal Hoop Strain (Simulation)	265.81	267.34	-0.58
S4 - Axial Strain (Experiment)	68.38	66.13	3.29
*Nominal Axial Strain (Simulation)	2.2	5.99	-172.27

Nevertheless, these achieved results which are based on the test rig arrangement, have already met the objectives of this PhD study. In earlier discussions, the test rig that mimics the actual pipeline on site focuses on a straight pipe which relates to offshore or onshore pipelines rather than other shapes and it refers to above the ground pipelines only. In other research carried out by Lukacs et al. (2010), they conclude that in any experimental work (i.e. laboratory-based) which involves straight pipes, researchers are more concerned with hoop strain rather than axial strain. This is because of the nature of the test set-up itself which requires the pipe to have a closed system at both ends. Unlike the underground or buried pipelines which are subjected to soil movement, the axial strain is more important than hoop strain and the test set-up should be arranged in a different form.
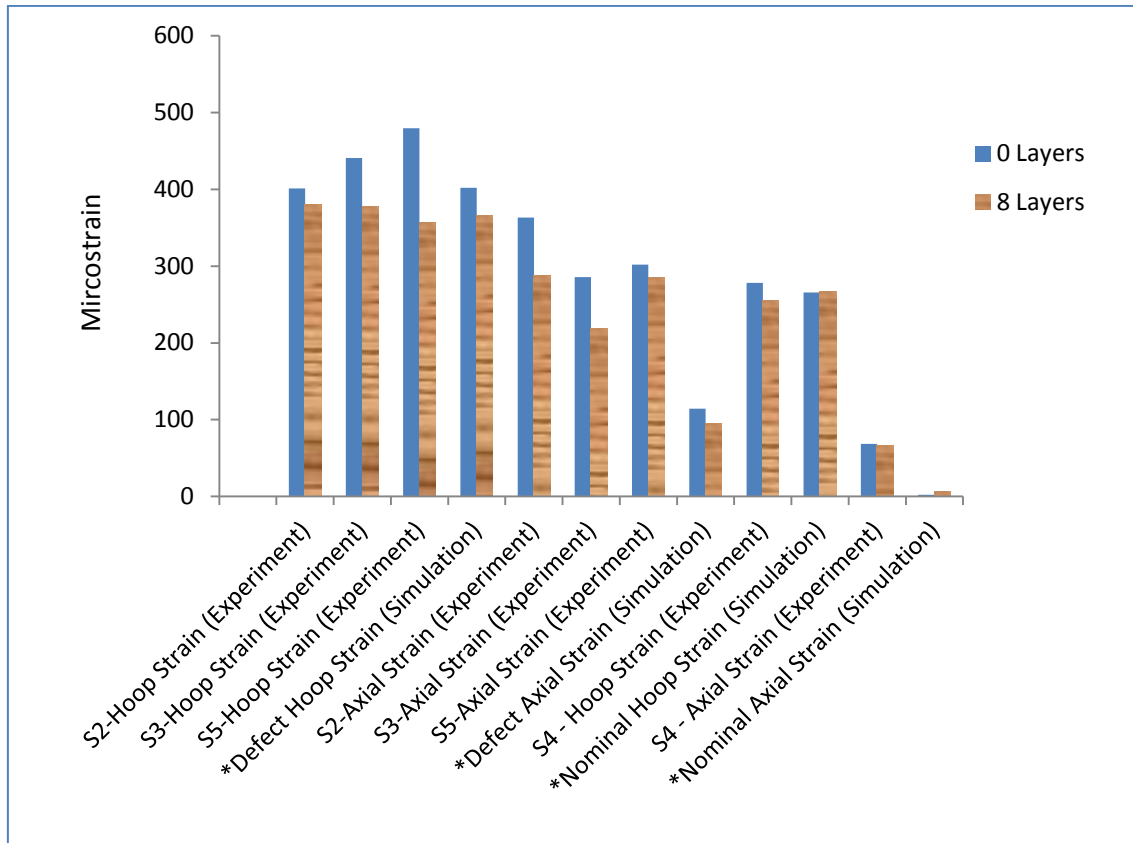
Figure 4.26: Strain distribution of experiment and simulation

Figure 4.26 also shows that the experimental hoop and axial strains measured at different locations along the circumferentially arc-shaped notch show slightly different results. This is because the strain gauge elements were installed at different orientations. The orientation of the strain gauge or sensor at the S3 location has produced better strain readings and this technique will be adopted in future strain gauge installations on any biaxially loaded pipe. This is agreed by Freire et al. (August 2006) who also highlight the importance of the experimental technique using sensors. According to them, the laboratory test is crucial because it gathers benchmark experimental results that will be used to verify analytical or numerical stress calculation procedures.

4.7   Summary and Conclusions

The right technique of installing the rectangular strain gauge rosettes on the right location on the pipe specimen and the practical methodology used in this experiment are both very important in order to obtain better and sensible strain results in the study of stress and strain distribution in the composite-based pipeline repair. In addition, the use of the NI CRio system in the data acquisition leads to more precise and easier strain measurements. Hence, these experimental results were not only able to show the good integrity of bonding between the reinforced material (i.e. steel) and reinforcing material (i.e. composite) but also the strain distribution between layers in the composite material.

As mentioned earlier, the experimental results do not only validate the numerical results but also become an important reference should there be any deficiency in the FEA. For example, the numerical axial strain result was much less apparent in this study but experimental axial strains were presented as more sensible results. However, numerical results have shown to be more valid and sensible in the hoop strain rather than the axial strain analysis. Additionally, they are also valid in the hoop and axial stresses analysis as referred to in the previous Numerical Model Stress Analysis - Pipeline Repair Index in Chapter 3. All these numerical results were validated analytically and experimentally. Several significant findings of the Chapter 4 can be concluded as:

- The epoxy matrix plays a significant role in transferring the load from the reinforced steel into the reinforcing composite. The highest hoop load transfer between the composite layers occurs at the defect area but for the axial load transfer, it occurs at the nominal area.
- The error of 4.17% between the numerical and experimental hoop strains at the defect area could have been further improved had the accurate elastic constant values been obtained. However, this small error confirms that the predicted elastic constant values used in the lamina type composite material in the modelling was correct and acceptable.

- After the defect has been repaired with eight layers of Technowrap Fibre Glass composite, the following percentage of strain reduction in steel have been achieved:

14.25% in hoop strain and 23.5% in axial strain (experimental results)

12.01% in hoop stress and 20.30% in axial stress (numerical results as referred to in Chapter 3)

- The results have proved that the study of integrity of bonding between steel substrate and composite is feasible, even in the true elastic region, and it is not true to claim that yielding is the only demarcation point at which the load transfer can take place from the reinforced material (steel) into the reinforcing material (composite).

5 THERMO-MECHANICAL BEHAVIOUR OF THE TRIAXIAL WOVEN FABRIC (TWF) COMPOSITE IN PIPELINE REPAIR

5.1 Introduction

The previous chapters have discussed a complete methodology to assess the integrity of the pipeline system especially in quantifying the level of the reinforcement provided the repair in the elastic working region. However, the integrity of bonding between the reinforced material (i.e. steel) and reinforcing material (i.e. composite) is not only subjected to pressure only but also temperature (heating).

In this chapter, the heating that influences the thermal expansion of these two materials was studied. According to Palmer and Paisley (2000), the difference in thermal expansion coefficient between the composite (repair) and the steel may have a detrimental effect on the composite to pipe (shell) bond and will certainly introduce significant changes to the internal stresses of the composite on heating. Avram (2001) demonstrates that the CTE mismatch between the composite patch and repaired structure plays an important role in the success of the repair. The closer the CTE's match, the greater the repair life because of less residual thermal stresses in the repair. Fouladi et al. (2010) in their study also agree that the difference in CTE of the patch material and the aluminium fuselage plays an important role in patching effectiveness.

In the composite-based pipeline repair industry for example, if the CTE of the composite based pipeline repair is known, then operators will be in a better position to evaluate how well their composite repairs behave in terms of linear and circumferential expansions under different working temperatures. According to Gedeon (2001), the temperature range of the produced oil and gas under extreme conditions can be expected to be a maximum of 110°C. Therefore the design of the pipeline system should be based on 120°C. Any safe design should be able to include this eventuality in the

consideration for the selection of material and maintenance. Therefore, this preventive measure will ensure both the reliability and durability of the composite repair as planned.

5.2 Objectives

The main objectives of this chapter are;

1. To study the internal thermal strain behaviour across the through thickness of the composite repair, and the stresses resulted from this expansion along with their effect on the SCF.

2. To determine and predict shear strain and shear angle values in the composite repair due to heating effect using a new approach.

3. To develop a simple and cost effective method in measuring the CTE measurement and prove as one of the acceptable CTE measurement techniques.

5.3 Techniques to Measure the Coefficient of Thermal Expansion (CTE)

To determine the CTE, two physical quantities (displacement and temperature) must be measured on a sample that is undergoing a thermal cycle (ASM International, 2002). There are several thermal analysis techniques in which the property of a sample is measured while the sample is subjected to a controlled temperature programme, for example Thermogravimetry (TG), Differential Scanning Calorimetry (DSC), Thermomechanical Analysis (TMA) and Dynamic Mechanical Analysis (DMA) (Chawla, 1998) and Dilatometer. All these techniques have different approaches. For example, if the Dilatometer is used, the difference in expansion between a rod made from the test material and a matching length of quartz or vitreous silica is compared

(McElroy et al., 1988; Vishay Micro Measurements, 2007) and this measurement has to be carried out in a laboratory environment. Weese et al. (2005) in their CTE investigation, used the TMA technique and their samples were uniaxially compressed at 10,000 psi and analysed over a dynamic temperature range of -20°C to 70°C using DSC. So, with all these techniques, precision strain measurements in a variable thermal environment can be achieved. However, the cost of running this experiment in this type of environment is high and is limited to a small test specimen only. In order to measure the thermal expansion on the actual structure (e.g. the overwrapped composite material on the pipeline) on site at a very low cost, another approach has been studied.

In this study, an experimental approach using a strain gauge sensor and surface temperature detector (i.e. an Amprobe) or digital Infrared laser thermometer with a temperature measurement precision of ±2°C were used. The idea to use the strain gauge in this approach was driven by the evolution of the CTE data. It all starts with the strain (Pederson, 2008). Having taken a proper measurement of strain data with the right derivation, the slope or gradient-based method may provide an alternative method to the above laboratory-based techniques.   Therefore, one of the objectives of this test was to find out whether or not the experimental approach used in determining the CTE of the actual structure is an acceptable method.

This can be done through the comparison of the experimental results with the known CTE values of the test materials, which in this case are the steel pipeline test rig and Triaxial Woven Fabric (TWF) composite repair material overwrapped on the test rig. From the analysis of results that will be discussed later, this approach which relies on rectangular strain gauge rosettes and surface temperature detector (Amprobe) was able to provide an alternative method that can easily measure the thermal expansion of a test material. Apart from its simplicity and economic cost, it has the distinct advantage of requiring no specialised instrument beyond those normally found in a stress analysis laboratory.

5.4 Methodology of Thermal Expansion Experiments

In this thermal expansion experiment, the new technique used two well-matched rectangular strain gauge rosettes in which the Self-Temperature-Compensation (S-T-C) number 06 and the resistance of 350 Ohm were first bonded to the reference composite material, referred to as Experiment 1; the second gauge to the test composite material (i.e. the test rig) is referred to as Experiment 2. However, both have the same mechanical properties and thickness. The objective of Experiment 1 was to determine the thermal output of the strain gauge bonded on to the stress-free specimen and Experiment 2 was to determine the CTE of the composite repair material on the stress constrained specimen. In Experiment 2, it also included determination of the CTE of the steel pipe test rig. The experimental result was later compared to the known CTE value of the TWF composite and steel pipe. The objective was to study how these two materials behaved in terms of thermal expansion and also to prove that this approach was acceptable in determining the CTE in any engineering material.

In Experiment 1, the TWF cloth used as a reference material was cut into 20 x 20 cm square and then impregnated with the matrix epoxy; the process of preparing this composite was similar to the process of preparing the test material except that this final cured reference material was on a flat surface rather than a circumferential shape and is referred to as the test material. The approach to determine the CTE and the thermal output in the anisotropic TWF composite materials using rectangular strain gauges was referred to procedural guidelines provided by Vishay Micro Measurements (2007) and their technique seems to be a more practical approach than the above laboratory methods, based on simplicity and cost. However, not all the procedures in the guidelines were complied with because they used two stress-free condition materials; one is treated as the reference material in which the CTE is known already and the second is called a specimen material where the CTE is going to be determined. Their technique is further discussed in the following section.

In this approach, the nature of this experimental test material involved several other constraints such as different dimensions, geometry, environments etc. and several assumptions were made. For example, the previous verification has been made

171

assuming a uniform specimen temperature under conditions of thermal equilibrium in the laboratory test chamber. So, these two experiments were conducted on different days and in different places. Since the strain gauge method as recommended by Vishay Micro Measurement imposes no special restriction on the nature or design of the chamber, the home oven, considered to be the most economical way, was used as part of the testing chamber in this experiment. The limitations that led towards errors in this experiment were addressed and some proposed solutions for improvements are discussed at the end of this section. Another assumption made was that the coefficients of thermal expansion of both steel and composite did not vary significantly over the range of temperatures in which they were designed to be used (Tippler and Mosca, 2007). So, the values of the coefficient of expansion were based on constant and average.

There were some preventive measurements taken in order to reduce the side effects of heating on the lead-wires in Experiment 1. A heat resistant ceramic tray and lead-wire insulation were used, as shown in Figure 5.1. A digital thermometer was used to measure the temperature of the specimen and surrounding area in the oven and also functioned as the temperature reference to the surface heat detector (Amprobe) – these are shown in Figure 5.2. The same strain indicator that was used in Experiment 1 was also used in Experiment 2, as shown in Figure 5.3. Figure 5.4 shows the area where the temperature readings were taken on the composite and steel, and the average readings of strain data were analysed and are further discussed in the following section.
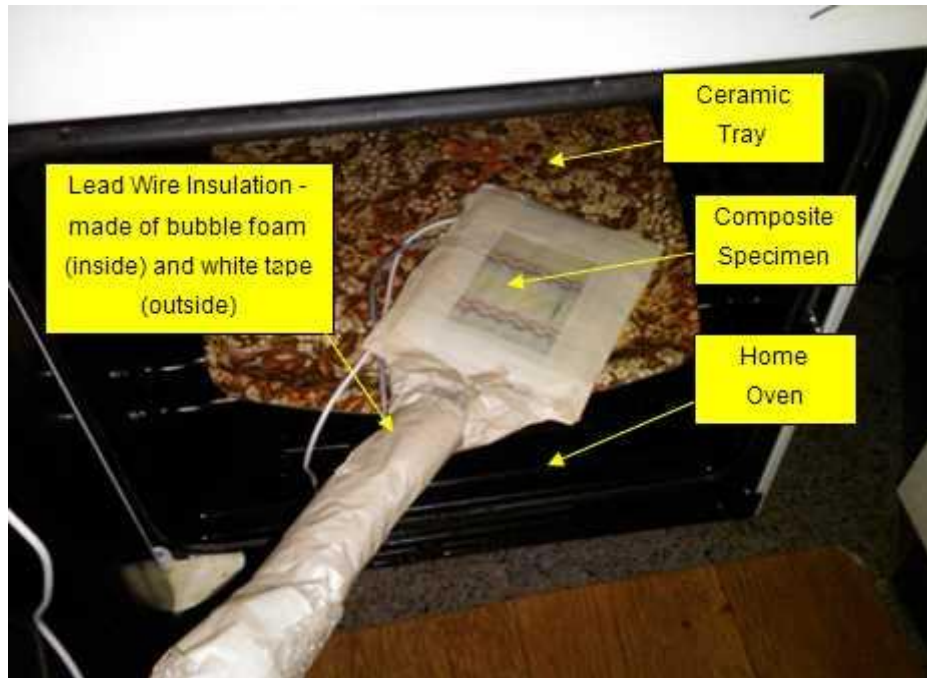
Figure 5.1: Some preventive measurements were taken to reduce the heating side effect on the lead-wires (Experiment 1)
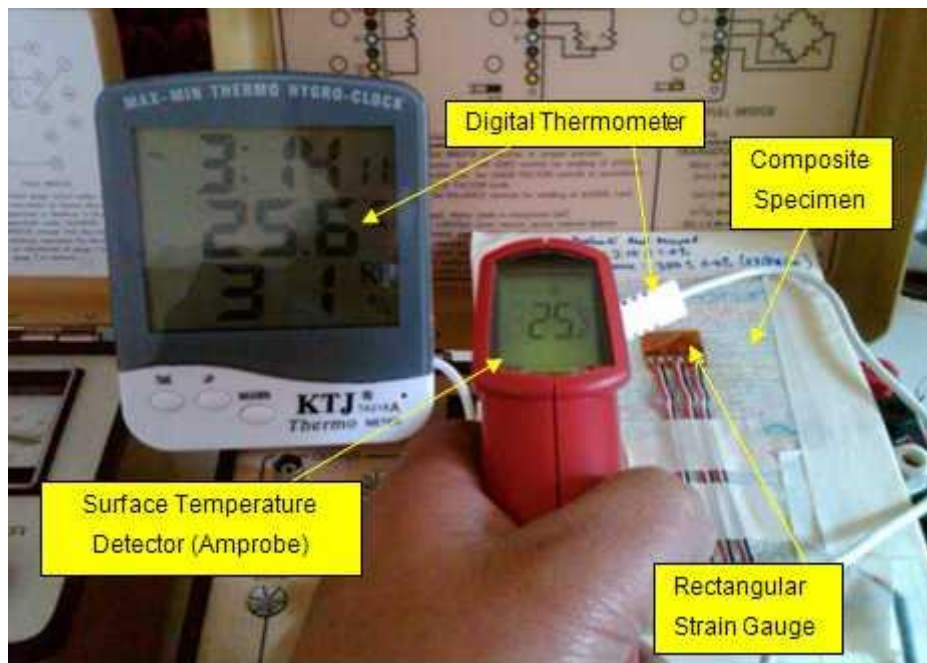
Figure 5.2: Instruments that were used in the thermal output experiment (Experiment 1)

Figure 5.3: Strain Indicator used in data acquisition of thermal expansion in steel and composite – Experiment 2

Figure 5.4: The average temperature readings were taken near to Point C4 (Left) and at the notch root of steel pipe test rig using surface temperature detector (Right) – Experiment 2

5.4.1   The Fundamentals of the Thermal Output Measurement

Vishay Micro Measurements (2007) report that under stress-free conditions, the differential output between the two gauges on the different specimens, at any common temperature, was equal to the differential unit expansion (in/in, or *m/m*) and the following equation was derived;

$$\alpha_S - \alpha_R = \frac{(\varepsilon_{T/O(G/S)} - \varepsilon_{T/O(G/R)})}{\Delta T} \qquad \text{(Equation 5.1)}$$

Where,

$\varepsilon_{T/O(G/S)}$ = Thermal output for grid alloy (G) on specimen material (S)

$\varepsilon_{T/O(G/R)}$ = Thermal output for grid alloy (G) on reference material (R)

ΔT = Temperature change from arbitrary initial reference temperature

$\alpha_S - \alpha_R$ = The difference between the unknown expansion coefficient α_S and a standard reference material with known expansion coefficient α_R

A typical thermal output, formerly referred to as "temperature-induced apparent strain" characteristics, for a Vishay Micro-Measurement A-Alloy gauge (self-temperature-compensated Constantan grid), bonded to 1018 steel is represented by the solid curve in Figure 5.5 and has the Self-Temperature-Compensation (S-T-C) number of 06 (Vishay Micro Measurements, 2007). This S-T-C number is identified to most closely match the thermal expansion coefficient of the test material and in this case this gauge will be suitable for use with steels. Therefore, when the strain gauge with an S-T-C number of 06 is bonded to any other steel structure, then only some mathematical corrections have to be carried out when the test material experiences temperature changes, and no reference material is required.

However, in this composite experiment, the reference material was required because composite was not available in the series of the Constantan alloy. The

mathematical correction was not applicable but the rotation of the thermal output curve, as shown in Figure 5.9, was done after carrying out the thermal output experiment.
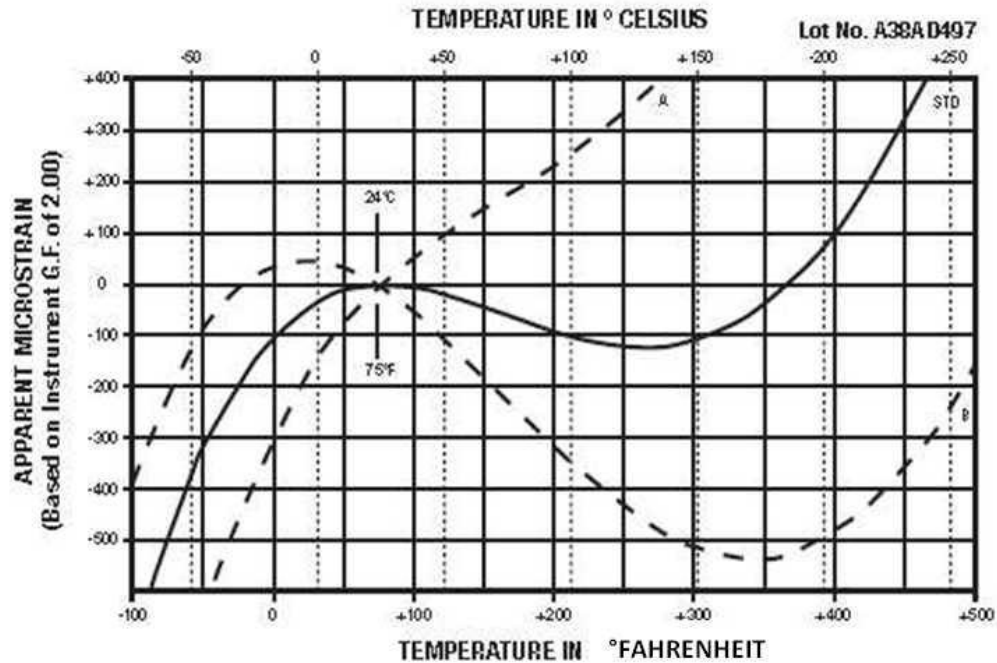
Figure 5.5: Rotation of the thermal output from a strain gauge when installed on materials with different thermal expansion coefficients (Vishay Micro Measurements, 2007)

According to Vishay Micro Measurements (2007), when the selected S-T-C number is lower than the thermal expansion coefficient (CTE) of the testing material, then a solid line curve, as shown in Figure 5.5, is rotated counter-clockwise to a broken line curve (A curve). When the testing material has a higher CTE, then the B-curve is expected. Therefore, at any given temperature on any material, the apparent strain on the material can be obtained by referring to the newly rotated curve.

5.5   Analysis of Results

5.5.1   The test result of Experiment 1 (Thermal output)

Since the rectangular strain gauge rosette (three elements) was used in this experiment, the thermal strain reading for each element was taken three times on a different day. Each test was performed up to 30 minutes and the second element of the rectangular strain gauge rosettes that was installed perpendicular to the fibre direction showed the highest thermal strain value compared to the other two elements. Apparently, all the thermal strains from each of these elements show exponential increments, as shown in Figure 5.6, and they all tend to remain constant after 10 minutes as the temperature was held constant at 60°C.
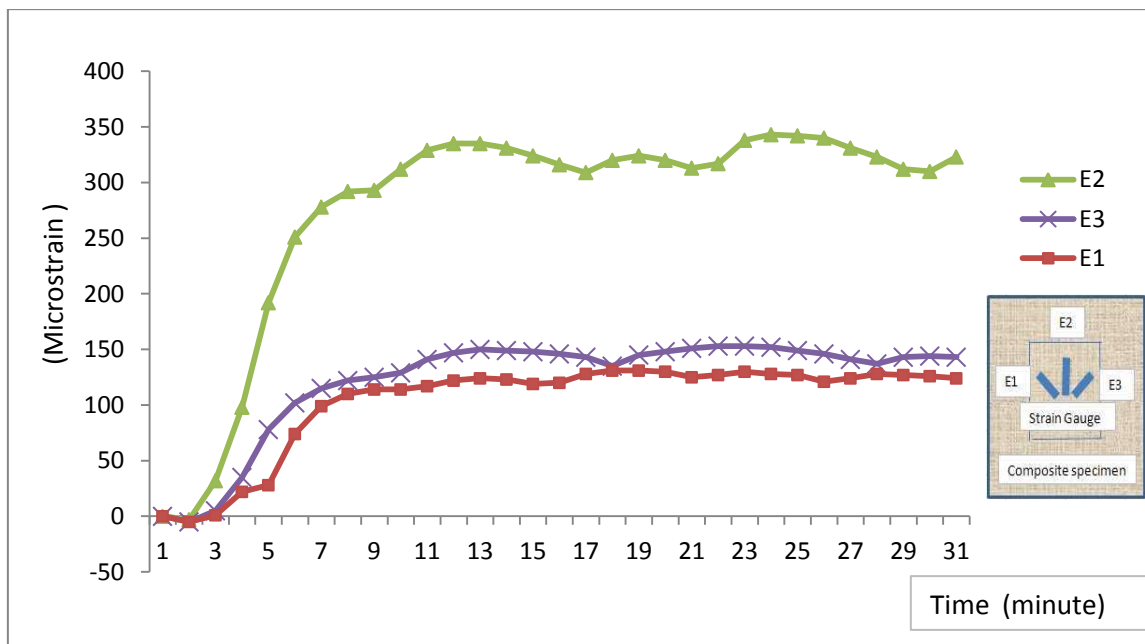
Figure 5.6: Self Temperature Compensation (S-T-C) graph of the individual element within 30 minutes

However, only a small time range (approximately around four minutes) was chosen in this analysis because the composite had already reached the expected

temperature value of 40°C as illustrated in Figure 5.7. The final transverse and longitudinal thermal outputs graph is shown in Figure 5.8. Since the thermal output shows the higher values in the transverse direction, the upper curve was chosen in this experiment. This curve was then plotted on the Vishay Micro Measurement graph as shown in Figure 5.5 earlier. This new curve, defined as C in Figure 5.9, shows a good agreement with the earlier rules where the solid line curve rotates anti-clockwise if the thermal expansion coefficient of the test material (i.e. composite) is higher than the sensor material (i.e. A – Alloy).
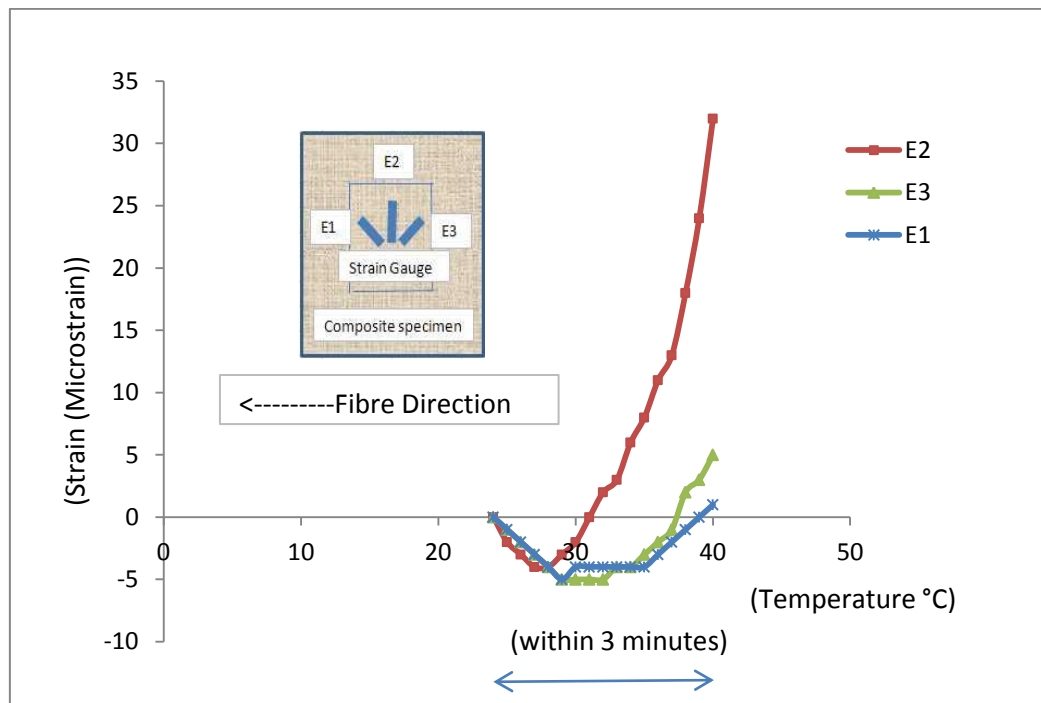
Figure 5.7: The behaviour of the thermal strain during the first three minutes

The graph shows:

$y = 2.1903\text{E-}11x^4 + 3.5110\text{E-}09x^3 - 2.4545\text{E-}07x^2 + 3.5658\text{E-}06x$ (Temperature °C)

$y = -1.9668\text{E-}10x^4 + 1.9040\text{E-}08x^3 - 6.4040\text{E-}07x^2 + 7.1243\text{E-}06x$
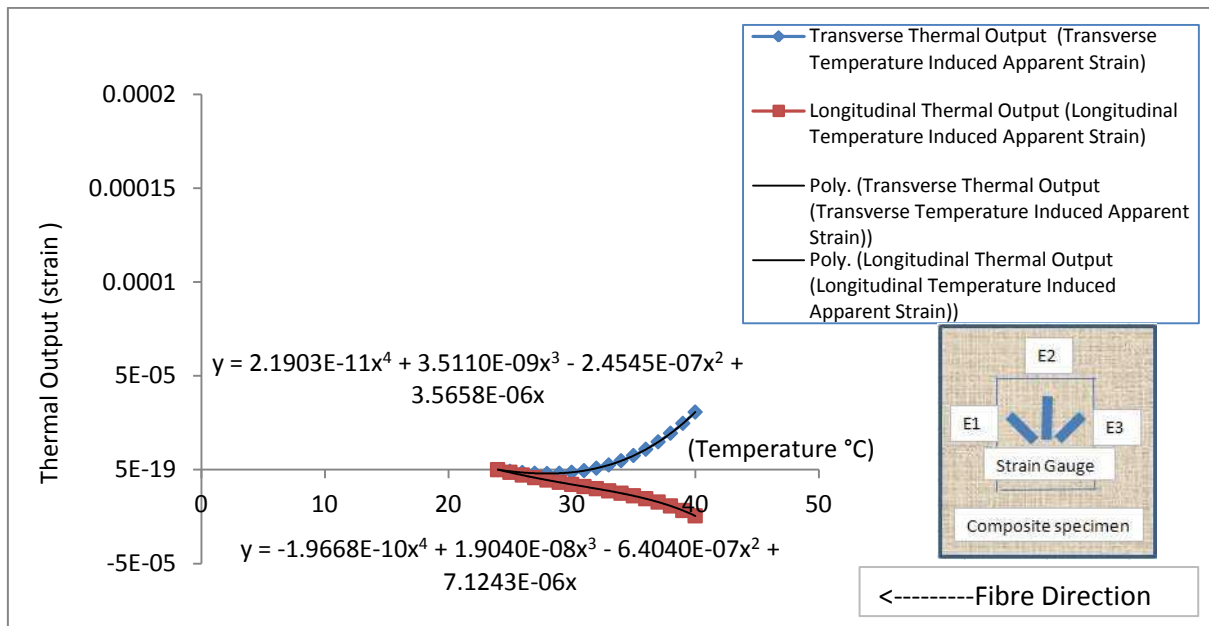
Figure 5.8: Corrected Self-Temperature-Compensation (S-T-C) graph of rosette gauge bonded on the eight-layer composite test specimen
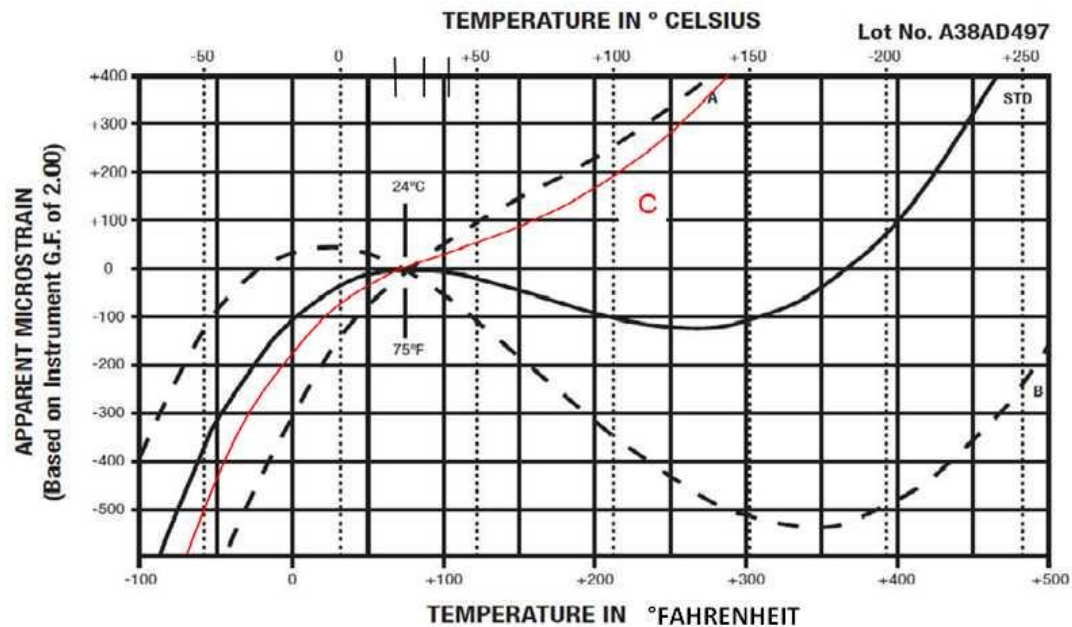
Figure 5.9: Expected thermal output curve of TWF composite defined as C Curve (Vishay Micro Measurements, 2007)

5.5.2 The test result of Experiment 2 (Thermal expansion)

This test was performed after the completion of Experiment 1. The same schematic representation of the measuring points, as shown in Figure 5.10, used during the pressure test is referred to. The orientation of each element of the rectangular strain gauge is shown in Figure 5.11.
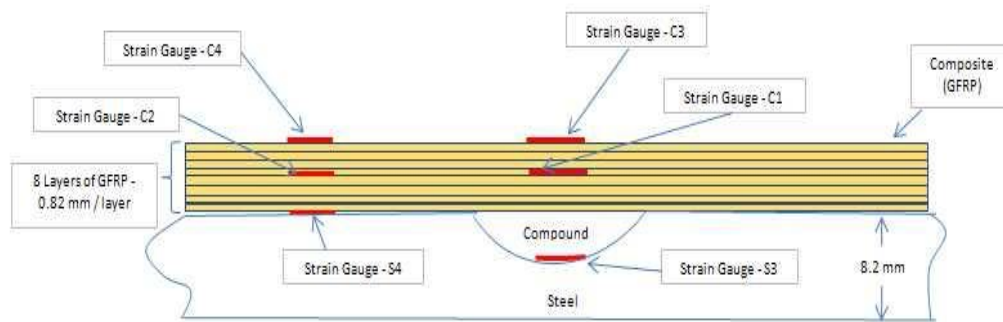
Figure 5.10: Schematic representation of the measuring points in composite and on steel
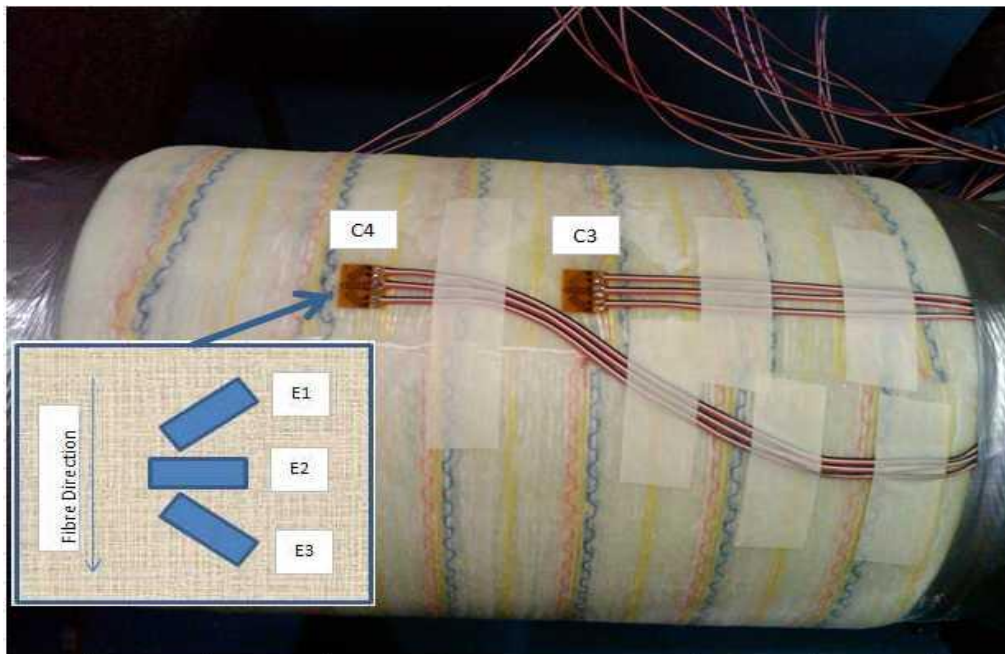
Figure 5.11: The position of the rectangular strain gauge perpendicular to the fibre direction
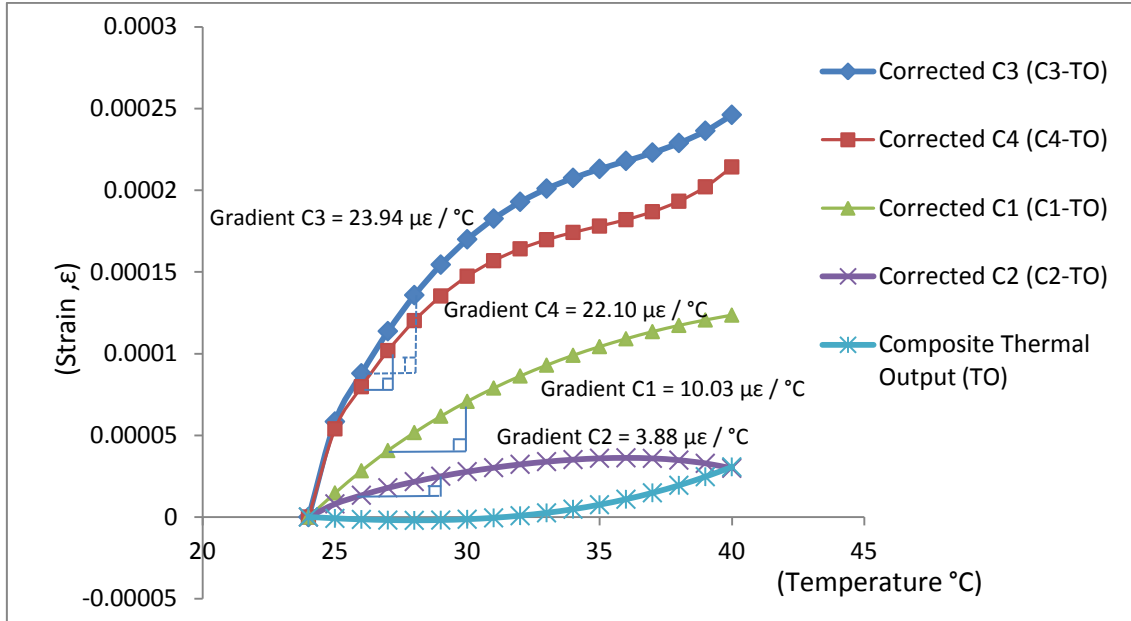
Figure 5.12: Coefficient of Thermal Expansion (CTE) of composite at different points

The relative thermal expansion ΔL/L of a glass fibre composite as a function of temperature T is shown in Figure 5.12. These five curves start at room temperature (24°C) and stop at 40°C only after taking into consideration the safety of the maximum resistance of the strain gauge adhesives to heating. Next they were corrected by being subtracted from the thermal output of composite obtained in the earlier section.

Theoretically, the thermal expansion of any engineering material should be linear and the slope of the curve or CTE ($\frac{\Delta Thermal\ strain}{\Delta°C}$) should be constant if using the same material. However, from Figure 5.12, all the curves do not show perfect linear expansions. This was due to some anticipated errors which occurred during the measurements. Since the test was carried out in an open space, the temperature was not fully controllable and subject to temperature fluctuations.

There are several reasons why gradients C1 and C2 are lower than C3 and C4; First, the thermal strain was measured at a different strain rate. Due to the limitations of the surface temperature detector, the actual temperature inside the composite layer was

unreachable. Therefore, the temperature increments for C1 and C2 were referred at points C3 and C4 only. The second reason was due to the thickness.

According to Apicella et al. (1994) the relative rates of heat generation and heat transfer determine the values of the temperature and therefore, the reaction advancement, resin viscosity and material mechanical response through the thickness of the composite may not be the same. The last reason may be because of the inconsistency of the average matrix volume fraction where the underneath layers of the composite repair were more resin rich than the outermost layer. According to Kueh et al. (2005), this resin rich phenomenon had contributed to unpredictable behaviour in the stiffness and CTE in their study. Therefore, a proper matrix volume fraction has to be measured correctly since the matrix CTE determines a great degree of the operational temperature limit for the composite (NASA, 1996) and the overall CTE values (Ito et al., 1999; You, 2004).

However, this approach has a better reading of CTE when the surface temperature detector is used to measure the outer layer of composite repair. The linear slope of C3 between the temperature ranges of 25 to 30°C shows a good agreement with the C4 slope. This similar CTE ($\frac{\Delta Thermal\ strain}{\Delta°C}$) shows that the simple surface temperature detector (Amprobe) was able to provide a better and simpler measurement. The experimental CTE of these two points were 23.94 x 10^{-6} /°C and 22.10 x 10^{-6} /°C respectively and both almost matched the known CTE of the TWF composite which was around 24 ~ 25 x 10^{-6}/°C, as provided by the manufacturer (Frost, 2010b).
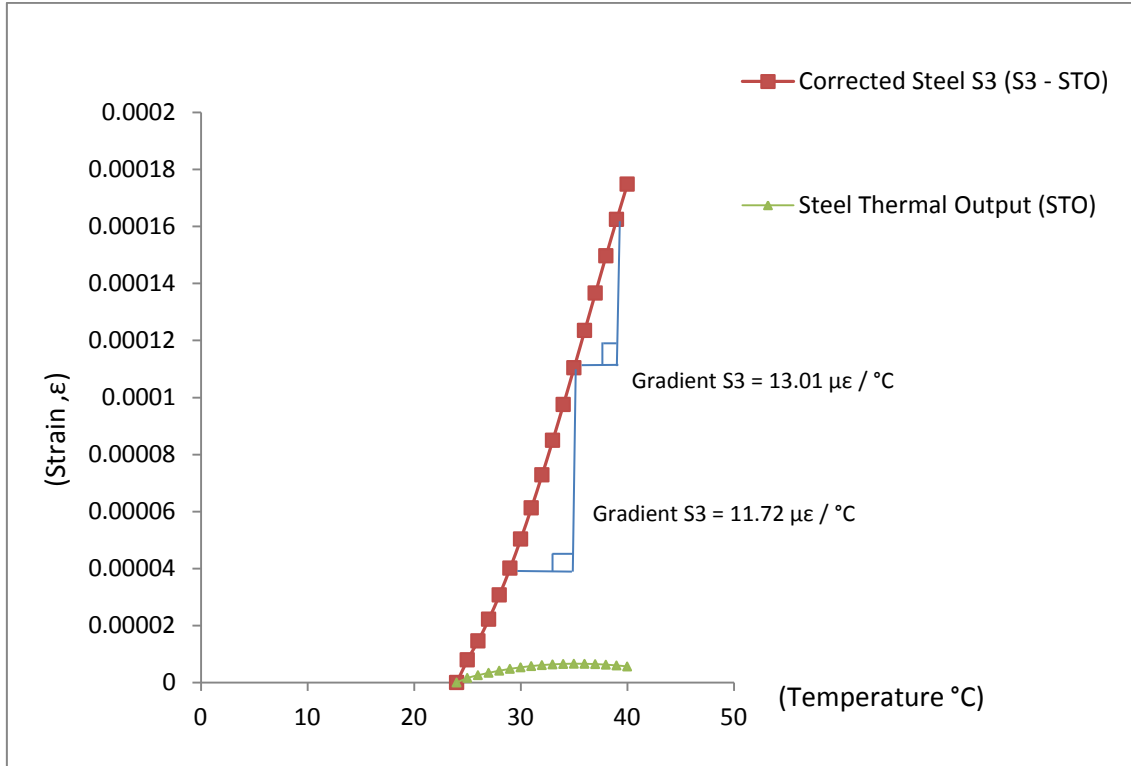
Figure 5.13: Coefficient of Thermal Expansion (CTE) of steel at different points

The steel thermal output curve, as shown in Figure 5.13, was produced by substituting the temperature values of 24°C up to 40°C into the polynomial expression of the Constantan alloy (A-Alloy) strain gauge. Since the CTE of steel material of the pipeline test rig was assumed to be similar to the strain gauge CTE, no reference specimen was prepared.

S3 shows a good linear thermal strain expansion as the temperature increases from room temperature until reaching 40°C. The CTE of the test rig which shows the average value of 12.25×10^{-6} /°C is equivalent to the carbon steel 1018 CTE which has the value of $11 \sim 13 \times 10^{-6}$ /°C (ASM International, 2002).

5.5.3 Investigation of shear strain in the thermal expansion experiment

It is interesting to investigate the behaviour of the anisotropic composite material when it is being heated up, as referred to in the study in the previous section. However, the presence of shear strain which may adversely affect the thermal strain readings will be properly addressed. The reason for this analysis was to determine the relative shear strain using Mohr's Circle theory in the anisotropic Triaxial Woven Fabric (TWF) composite due to the temperature change.

The following equations were used in this study;

$$\text{Average Strain } (\varepsilon ave) = \frac{\varepsilon 21 + \varepsilon 23}{2} \qquad \text{(Equation 5.2)}$$

$$\gamma 22 = 2 \text{ x } \varepsilon 22 - (\varepsilon 21 + \varepsilon 23) \qquad \text{(Equation 5.3)}$$

$$R = \sqrt{\left(\frac{\varepsilon 21 - \varepsilon 23}{2}\right)^2 + \left(\frac{\gamma 22}{2}\right)^2} \qquad \text{(Equation 5.4)}$$

$$\text{Tan} 2\theta = \frac{\frac{\gamma 22}{2}}{(\varepsilon 21 - \varepsilon 23)} \qquad \text{(Equation 5.5)}$$

Maximum principal strain $\varepsilon 1$

$$\varepsilon 1 = \frac{1}{2}(\varepsilon 21 + \varepsilon 23) + \frac{1}{2}\sqrt{(\varepsilon 21 - \varepsilon 23)^2 + (2 \text{ x } \varepsilon 22 - \varepsilon 21 - \varepsilon 23))^2} \quad \text{(Equation 5.6)}$$

Where;

ε_n = strain reading of each element; where n = 21, 22, and 23

ε_1 = Maximum principal strain

γ = Shear strain

R = Mohr Circle Radius

Θ = Shear angle

Table 5.1: The strain readings after the 4th layer (at the defect area)

Temperature (°C)	ε21	ε22	ε23	εave	R
24	0	0	0	0	0
25	1.30E-05	1.30E-05	4.93E-06	8.94E-06	5.68E-06
26	2.39E-05	2.49E-05	1.29E-05	1.84E-05	8.55E-06
27	3.19E-05	3.59E-05	2.18E-05	2.68E-05	1.03E-05
28	3.98E-05	4.78E-05	2.88E-05	3.43E-05	1.46E-05
29	4.68E-05	5.98E-05	3.47E-05	4.07E-05	2.00E-05
30	5.37E-05	7.08E-05	4.17E-05	4.77E-05	2.39E-05
31	6.27E-05	7.97E-05	4.96E-05	5.61E-05	2.45E-05
32	7.16E-05	8.67E-05	5.66E-05	6.41E-05	2.38E-05
33	7.96E-05	9.26E-05	6.35E-05	7.16E-05	2.26E-05
34	8.75E-05	9.96E-05	7.05E-05	7.90E-05	2.23E-05
35	9.35E-05	1.10E-04	7.74E-05	8.55E-05	2.54E-05
36	1.00E-04	1.21E-04	8.44E-05	9.24E-05	2.92E-05
37	1.11E-04	1.30E-04	8.94E-05	1.00E-04	3.11E-05
38	1.19E-04	1.38E-04	9.43E-05	1.07E-04	3.40E-05
39	1.26E-04	1.47E-04	9.82E-05	1.12E-04	3.78E-05
40	1.33E-04	1.54E-04	1.02E-04	1.18E-04	3.98E-05

Table 5.2: The analysis of results after the 4th layer (at the defect area)

Temperature (°C)	ε1	ε2	γ22	Max Shear Strain (2R)	Θ in radians
24	0	0	0	0	0
25	1.46E-05	3.27E-06	8.03E-06	1.14E-05	22.5
26	2.69E-05	9.83E-06	1.31E-05	1.71E-05	24.9
27	3.72E-05	1.65E-05	1.81E-05	2.07E-05	30.5
28	4.89E-05	1.97E-05	2.71E-05	2.93E-05	33.9
29	6.07E-05	2.08E-05	3.81E-05	4.00E-05	36.2
30	7.16E-05	2.39E-05	4.62E-05	4.77E-05	37.7
31	8.06E-05	3.17E-05	4.72E-05	4.89E-05	37.3
32	8.79E-05	4.03E-05	4.52E-05	4.76E-05	35.8
33	9.41E-05	4.90E-05	4.22E-05	4.51E-05	34.6
34	1.01E-04	5.67E-05	4.12E-05	4.46E-05	33.7
35	1.11E-04	6.00E-05	4.83E-05	5.09E-05	35.8
36	1.22E-04	6.32E-05	5.62E-05	5.84E-05	37.0
37	1.32E-04	6.93E-05	5.82E-05	6.22E-05	34.7
38	1.41E-04	7.29E-05	6.31E-05	6.79E-05	34.1
39	1.50E-04	7.44E-05	7.03E-05	7.57E-05	34.1
40	1.58E-04	7.79E-05	7.33E-05	7.96E-05	33.5

From Tables 5.1, 5.2 and Figure 5.14, the value of the maximum strain in the transverse direction in the anisotropic composite shows very good agreement with the maximum principal strain. McElroy et al. (1988) and Hartwig (1988) also report the coefficient thermal expansion was higher in perpendicular or transverse than in the parallel or longitudinal direction of the fibres. This is because the restraining action of the fibre – either glass or carbon – does not occur in the perpendicular direction.
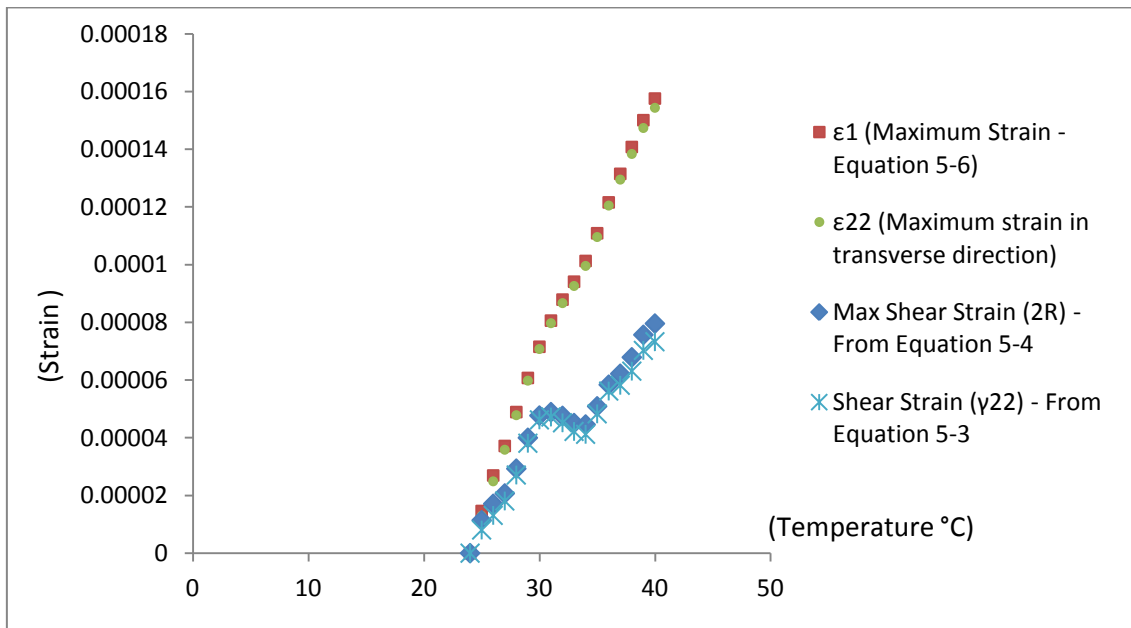
Figure 5.14: The effects of shear strain with the increasing temperature in the first four layers at the defect area

The shear strain and maximum shear strain measured in the first four layers of the composite repair increase as the temperature increases and decrease slightly between 30°C and 35°C and increase again linearly until 40°C. A maximum shear strain of almost 80 microstrain was recorded at 40°C.

From Tables 5.3, 5.4 and Figure 5.15, again, the value of maximum strain in the transverse direction shows very good agreement with the maximum principal strain. At the outermost layer of the composite repair (i.e. eight layers), the shear strain and

maximum shear strain increase as the temperature increases up to 179 microstrain and become constant between 30°C and 35°C. After that, they slightly decrease down to 172 microstrain at 40°C. This result shows that the eight layers of composite experience higher transverse and shear strain than half of the composite thickness (i.e. four layers).

Table 5.3: The strain readings after the 8th layer (at the defect area)

Temperature (°C)	$\varepsilon 21$	$\varepsilon 22$	$\varepsilon 23$	εave	R
24	0	0	0	0	0
25	6.896E-06	8.117E-05	1.894E-05	1.29E-05	6.85E-05
26	1.582E-05	9.211E-05	3.088E-05	2.34E-05	6.92E-05
27	2.572E-05	1.171E-04	4.981E-05	3.78E-05	8.02E-05
28	3.564E-05	1.370E-04	6.274E-05	4.92E-05	8.88E-05
29	4.457E-05	1.490E-04	7.468E-05	5.96E-05	9.06E-05
30	5.349E-05	1.599E-04	8.762E-05	7.06E-05	9.10E-05
31	6.540E-05	1.768E-04	1.035E-04	8.45E-05	9.43E-05
32	7.833E-05	1.857E-04	1.125E-04	9.54E-05	9.19E-05
33	9.127E-05	1.977E-04	1.224E-04	1.07E-04	9.22E-05
34	9.818E-05	2.096E-04	1.383E-04	1.18E-04	9.35E-05
35	1.061E-04	2.185E-04	1.483E-04	1.27E-04	9.37E-05
36	1.170E-04	2.304E-04	1.672E-04	1.42E-04	9.18E-05
37	1.250E-04	2.424E-04	1.764E-04	1.51E-04	9.52E-05
38	1.349E-04	2.533E-04	1.851E-04	1.60E-04	9.66E-05
39	1.518E-04	2.632E-04	1.940E-04	1.73E-04	9.27E-05
40	1.607E-04	2.711E-04	2.099E-04	1.85E-04	8.93E-05

Table 5.4: The analysis of results after the 8th layer (at the defect area)

Temperature (°C)	ε1	ε2	γ22	Max Shear Strain (2R)	Θ in radians
24	0	0	0	0	0
25	8.14E-05	-5.56E-05	1.37E-04	1.37E-04	-25.38
26	9.25E-05	-4.58E-05	1.38E-04	1.38E-04	-41.87
27	1.18E-04	-4.25E-05	1.59E-04	1.60E-04	-40.69
28	1.38E-04	-3.97E-05	1.76E-04	1.78E-04	-40.61
29	1.50E-04	-3.10E-05	1.79E-04	1.81E-04	-40.22
30	1.62E-04	-2.04E-05	1.79E-04	1.82E-04	-39.60
31	1.79E-04	-9.84E-06	1.85E-04	1.89E-04	-39.17
32	1.87E-04	3.53E-06	1.81E-04	1.84E-04	-39.64
33	1.99E-04	1.47E-05	1.82E-04	1.84E-04	-40.14
34	2.12E-04	2.47E-05	1.83E-04	1.87E-04	-38.80
35	2.21E-04	3.35E-05	1.83E-04	1.87E-04	-38.5
36	2.34E-04	5.03E-05	1.77E-04	1.84E-04	-37.07
37	2.46E-04	5.55E-05	1.83E-04	1.90E-04	-24.86
38	2.57E-04	6.34E-05	1.87E-04	1.93E-04	-27.13
39	2.66E-04	8.02E-05	1.81E-04	1.85E-04	-24.98
40	2.75E-04	9.60E-05	1.72E-04	1.79E-04	32.53
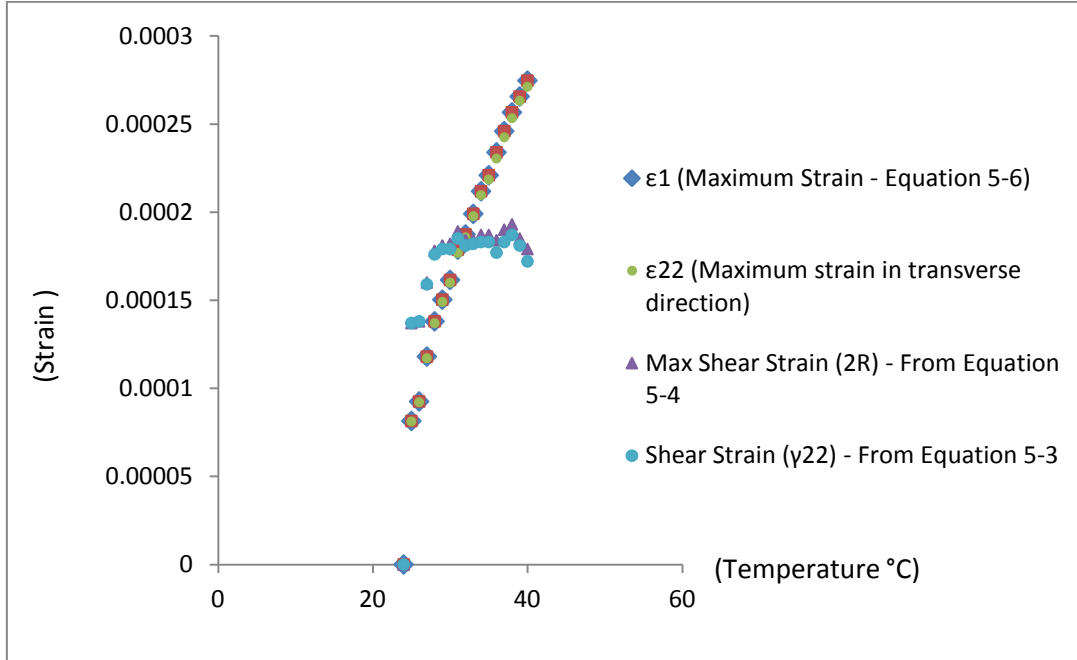
Figure 5.15: The effects of shear strain with the increasing temperature in the eight layers at the defect area

The above results show that shear strain between laminates is solely induced by temperature variations. However, before these laminates are induced by any external factors, in this case temperature, Billoet and Cherouat (1999) mention that the woven fabrics which are impregnated with resin actually already have complex internal microstructures and present anisotropic behaviour due to the directions of the fibres. In this study, when this anisotropic composite is subjected to temperature variations, according to Schwarz et al. (1991) the expansion behaviour of the fibre composites is then determined by fibre expansivity, the fibre arrangement and the matrix. In fact, there are two main factors responsible for the thermal expansion of composites. The first is the thermal expansion of the fibre itself and the second is the contribution resulting from the internal shear stresses which are a function of the fibre angle, the ratio of the moduli of fibre and matrix, and of the fibre anisotropy.

Schwarz et al. (1991) also mention that the effect of internal stresses is much greater, often resulting from a higher fibre modulus of elasticity. For example, carbon fibre that has a high modulus of elasticity does not only have high internal shear stress but also high internal shear strain. In Harding and Li's (1992) research in the determination of interlaminar shear strength for glass epoxy and carbon epoxy laminates at impact rates of strain, they found that the interlaminar shear stress is directly proportional to the average interlaminar shear strain. Therefore, it can be concluded here that measuring the CTE of composite at different layers, as referred to in Figure 5.12, is more practical for glass epoxy than the carbon epoxy composite. This is because using carbon fibre which has a higher fibre modulus and internal shear stress and strain than glass fibre would then lead to greater errors.

The detailed study of shear behaviour of woven composite fabrics such as shear force, shear angle and shear rate can be referred to in Wang et al. (2006). They have developed a predictive model of shear behaviour of textile composites to replace time consuming material characterisation tests. Lee et al. (1990) also present the same study but use bias-extension tests instead. They have managed to show how the shear angle properties of glass fabrics are determined and predicted when subjected to tensile bias testing. According to them, there are three main methods to determine shear angle. The

189

first is to calculate the shear angle using the theoretical equation based on the kinematic analysis of the bias-extension test. The second is to draw straight lines along the yarns for various images from the bias test. The third method is to use a series of images obtained from the test along with soft image correlation software. However, all these approaches carried out by the above researchers cannot be used for the woven composite that is wrapped round the pipe. The only way to measure the shear angle, strain and others due to thermal expansion is to apply Mohr's Circle theory using a strain gauge and surface temperature detector.

5.6   Summary and Conclusions

From the above results, from this experimental approach of using the surface temperature detector, it is possible to measure the CTE of the test material on site provided the measurement is carried out at proper locations; it also provides an alternative method to the bonded temperature sensor which may involve extra cost and time. For unreachable locations, for example, between layers of the composite repair, the temperature sensor has to be bonded next to the bonded strain gauge so that more accurate readings can be obtained. From these experimental results also, it can be concluded that the CTE measurement using this simple approach produced is acceptable and practical in this composite based pipeline repair. However, this approach produces better and accurate result in the isotropic material (i.e. steel) than in the anisotropic material (i.e. composite).

The results of maximum thermal strain at both layers (fourth and eight layers) show that the thermal strain is directly proportional to the temperature increase. In the investigation of shear strain in the thermal expansion experiment, the shear strain is found to be higher at the eighth layer (i.e. 172 microstrain) compared to the fourth layer of composite (i.e. 73.3 microstrain). However, at the eighth layer, the shear strain was nearly constant as temperatures increased. Therefore, the CTE readings at C3 and C4 (both at the eighth layer) as illustrated in Figure 5.12, were much closer to each other if compared to C1 and C2 (at the fourth layer) which were less apparent. This shows that

shear strains becomes more stable at the outer layers than the inner layers of the composite repair. This study concludes that maximum thermal and shear strain are not only influenced by the temperature but also thickness.

The values of shear angle at both fourth and eight layers show inconsistency as the temperature increases from 25 ℃ to 40 ℃. Again, this concludes that in the thermal expansion of the composite material, thermal strain and shear strain are the function of thickness and temperature of the material. But shear angle is less predictable and an accurate relationship cannot be easily established in this anisotropic composite.

6 CONCLUSIONS AND RECOMMENDATIONS

6.1 Introduction

The work presented in the previous five chapters presents investigations into the integrity of bonding in a composite-based pipeline repair using the integrated approach of structural health monitoring. This chapter summarises the content of these five chapters and salient points are addressed. It draws conclusions from the results of this research work and ends with some recommendations for future research to build on the current Study.

6.2 Summary and Conclusions

An overview of the pipeline integrity management programme that involves four main components, namely Assessment, Monitoring, Mitigation and Life Extension, was presented. This management programme covers all the aspects of structural pipeline integrity, especially for ageing pipelines that are subject to several damages. In the process of mitigating these damages, the composite repair has provided to be a reliable and economic solution in extending the life of these ageing pipelines. An integrated SHM that mainly involves FEA (ABAQUS) and experimental work which is represented as an integrated pipeline repair system (i.e. Figure 1.2) have been carried out in the current work. This system interfaces all the above four main components with the main aim of encompassing a reliable and cost-effective life extension programme. The objectives and contributions of this Study were also presented in Chapter 1.

In Chapter 2, a thorough literature review that was intended to give the background to the significance of the study in the field of pipeline integrity was carried out. It is important to really understand the scenario of pipeline damage and condition assessment, such as inspection, monitoring and reliability of information, so that enough data information of the damaged pipeline are obtained before making any decision on corrective and preventive actions in pipeline repair. Therefore, cost effective strategies

for future safe design and operation can be achieved. In this chapter, the composite repair was shown to be one of the reliable methods in the life extension of ageing pipelines.

However, without SHM, the aim of successfully achieving the life extension programme may be difficult. Some SHM literature related to numerical and experimental works were further discussed in depth in this chapter. Despite optical fibre sensors having many advantages over electrical strain gauges, Rectangular Strain Gauge Rosettes were used for this study. Some preliminary studies on this type of sensor were carried out first based on many references, such as from literature, recommendations and advice from manufacturers, etc. prior to the final decision being made. The lack of a report or information on the integrity of the bonding study on composite-based pipeline repairs and the unpredictable quality of the installation of glass epoxy composite (wet wrap application) in the pipeline repair are among the key factors that motivated this PhD study.

In Chapter 2 also, the previous and current researches show that stress concentrations in the pipelines refer to various discontinuities and defect geometries. However, none of the studies focus on the circumferentially arc-shaped defect on the pipeline. Hence, after comprehensive numerical works, the final half pipe model with a circumferentially arc-shaped defect has been selected and represents the actual pipe specimen. Stress and strain concentration factors based on a pipe with and without composite repairs were studied and analysed in Chapter 3.

One of the significant deliverables of this Study is the establishment of a Pipeline Repair Index (PRI) which was studied in Chapter 3. Through the comprehensive study of stress distribution in the composite-based pipeline repair, the PRI is shown to be very useful in the design optimisation of these repairs. The optimum length of repair obtained from the PRI has been compared and validated analytically with ASME PCC-2 2006 and it can be concluded that the shorter the defect the better the design optimisation will be. Through the numerical strain distribution study, the reduction of strain concentration factor percentage (SCFI %) was analysed and the results were

influenced by biaxial effects in the structural response. Overall, the main findings of the Chapter 3 can be concluded as;

- Any increasing pressure in the elastic working region has no influence on the increment of stress concentration values.

- The longer the arc defect length, the higher the hoop stress concentration will be.

- Poisson's ratio has a lesser influence on stress concentration as the length of the arc shaped defect is increased.

- The hoop stress is directly proportional to the length of the defect and inversely proportional to the thickness of the repair. However, axial stress is inversely proportional to both defect length and repair thickness.

- Stress concentration factor is not the function of the composite repair length neither thickness but the length of the defect instead. However, from the simulation works, it is clear that the stress concentration factor at the defect in the pipe with the composite repair is lower than at the defect without the repair.

- The optimum length of composite repair for the defect width of 40 mm is 160 mm as compared against the recommended length given by the manufacturer which is 240 mm. With this PRI study, nearly 20% of stress loading has been transferred in the circumferential direction and nearly 38% in the longitudinal direction.

As discussed in the earlier chapters, the FEA results that have been presented in Chapter 3 have to be validated experimentally. In order to do that, the experiment itself had to be carried out based on proper guidelines and standards so that the experimental results are correct and anticipate fewer errors. The selection and installation of sensors must be correct so that data acquisition can produce sensible results. The technique of installing the composite is also crucial because often the pipeline repairs are of the wet type rather than the cured type. In other words, the installation work usually relies on the skill of the applicator in ensuring the effectiveness of the fibre reinforcement after it

has been fully cured. Poor surface preparation and failing to follow the manufacturers'
guidelines may result in failures such as delamination etc. All the above requirements
have been fulfilled using the right methodology. The important findings of Chapter 4
can be summarized as:

- Yielding as a demarcation point in the study of bonding integrity between the
  reinforced material (steel substrate) and reinforcing material (composite) by
  previous researchers is arguable. Most of the repaired pipelines do not yield and
  there is a lack of analytical information about how well load is being transferred
  from the defect steel into the composite material in the elastic working region.
  Therefore, Chapter 4 has proved that it is possible to carry out this study
  provided all the above requirements have been followed correctly.

- The technique of installing strain gauges at the arc-shaped defect area is
  important because different orientation has produced different result. From this
  study, it is recommended to adopt the orientation technique that is similar to that
  of S3 since this technique has produced the most steady reduction of strain
  readings. About 14.25% load is transferred in the hoop and 23.5% in axial
  directions.

- All the manual calculation, numerical and experimental hoop stresses and strains
  and axial stresses show a very good agreement at the defect and nominal areas.
  However, axial strain correlation is much less apparent. This is attributed to
  mass and pressure loading differences between numerical and experimental
  system and lack of better complex analytical expressions in the manual
  calculation.

- In terms of the load transfer in the composite repair, the highest hoop load
  transfer between the composite layers occurs at the defect area but for the axial
  load transfer, it occurs at the nominal area. The error of 4.17% between the
  numerical and experimental hoop strains at the defect area could have been
  further improved had the accurate elastic constant values been obtained. This

small error confirms that the predicted elastic constant values used in the lamina type composite material in the modelling was correct and acceptable.

In Chapter 5, the experimental work using a strain gauge and temperature surface detector has shown that this methodology which was used in this thesis is feasible and acceptable to measure the CTE of test material (i.e. composite and steel). Since the composite used in this study was anisotropic and usually has high shear strain, the behaviour of the thermal strain is unpredictable. However, for isotropic material (i.e. steel), better results have been produced. In order to produce better CTE readings, there have been several suggestions for improvements and these are discussed in the following section. In summary, the main important findings can be concluded as:

- The behaviour of Maximum thermal strain shear strains were studied and can be concluded that they are not only influenced by the temperature but also by the thickness of the composite material. The inconsistency of shear angles values shows that shear angle is less predictable and the prediction of this behaviour in a quantitative manner is complicated and has therefore not been attempted here.

- Despite the fact that this approach has produced better and accurate result in the isotropic material (i.e. steel) than in the anisotropic material (i.e. composite), yet the CTE measurement using this simple and very cost effective approach is still acceptable and practical to be adopted in monitoring the thermal expansion of the composite repair with some improvements in the future.

6.3 Primary PhD Achievements

The earlier section presented the summary and conclusions achieved from the work carried out in this research. A list of main contributions is given here.

- Composite repair using the wet wrap application is shown to be an effective technique in reducing the SCF due to defects. The technique is cost effective and can increase the life of existing pipelines with defect, eliminating the need for replacing the pipeline.

- Effects of the number of layers on SCF

- Effects of defect length, repair length and etc on SCF.

- A complete methodology of the integrated Structural Health Monitoring (SHM) approach using simulation and experiment has provided an overview of the pipeline integrity management programme and assessed the integrity of bonding between the pipeline and composite repair in the economic and effective way.

- In practice, no model can claim to produce exact behaviours of this stress strain distribution without a proper validation from experiments. But this research has proven that this can be accurately achieved if sensible procedures and guidelines are properly planned and established.

- A simple method to study the thermal strain in the pipeline repair has been developed. This method demonstrates the easiest way to determine the coefficient of thermal expansion of the anisotropic composite and the isotropic steel without applying the standard laboratory procedures which are more expensive and complicated.

- The pressure and temperature interchangeable test rig developed in this experiment can be used as an example of a versatile product demonstrator in the future. With the same specifications, the composite manufacturer can fabricate a similar structure and specifications, and apply the same numerical and

experimental methodologies as discussed in this thesis so that the quality and reliability of their composite product can be verified at any time prior to site installation. Therefore, the design and cost of the repairs can be optimised with greater confidence.

- Finite Element Analysis (ABAQUS CAE) has provided a good tool in the study of stress and strain distribution before and after the composite repair as well as proving that the composite repair is one of the reliable and effective corrective and preventive solutions for ageing pipelines.

6.4 Recommendations for Future Work

In Chapter 3, the stress and strain concentration factors were studied based on the circumferentially arc-shaped notch at variable length and constant defect depth only. There would be another novelty if other researcher can establish the database of stress and strain concentration factors based on several types of notches with different length and depth for the pipeline with and without composite repair.

As discussed in Chapters 3 and 4, the current study on the integrity of bonding between reinforced material (i.e. steel) and reinforcing material (i.e. composite) relies on the composite repair model that was developed based on a macro-scale level only. Despite the theory of homogenisation being applied and rules of mixture being used in this development, the final result might have been more accurate if separate mechanical tests could have been carried out on the exact type of composite used in the study so that the precise elastic constant values could have been determined. This is because the predicted elastic constant values in the current work were mainly based on assumptions. In these two chapters also, simulation and experiments were carried out on the pipe specimen that was subjected to internal pressure tests only. Therefore, future work should involve internal pressure, bending and tension tests in order to produce more fruitful results. However, some modifications to the test rig would be required in order to make these tests possible.

In Chapter 5, the CTE was determined by experimental method only and it would be more convincing if these experimental results could be compared against the numerical results as well in the future. Therefore, the future work will be more challenging and interesting if ABAQUS or other FEA software can work with the model that is subjected to temperature load rather than pressure only. In terms of instruments used in the current work, it would be more realistic if the temperature surface detector were to be used together with the bonded temperature sensor so that the data from these two can be compared against each other. Hence, better results can be produced in the future.

In Chapter 5 also, some limitations were addressed. One of them was the use of a home oven as a heating oven. Based on the difficulties in controlling the temperature properly, it is recommended that a properly controllable heat oven be used to measure the thermal output in future research. Therefore, a proper thermal output experiment can be carried out in the future. Another possible reason why the CTE value at the fourth layer was very low may be because of the thermal residual strain effects. The thermal strain will be more accurate and sensible if the net thermal strain is produced after deducting not only thermal output but also residual strain. However, in the current work, this thermal residual strain was assumed to be negligible.

REFERENCES

ABAQUS Inc and DS (2007), "ABAQUS CAE User Manual", in 6.7th ed, Abaqus Inc, DS, United States of America.

AEA Technology Consulting (2001), *Temporary / permanent pipe repair guidelines - Health and Safety Executive,* Crown, Aberdeen. Scotland.

Alexander, C. (2009a), Assessing the state of composite repair systems, *Pipeline and Gas Technology*, *July Iss*.

Alexander, C. (2009b), Developing standards for composite repair systems, *Pipeline and Gas Technology, Oct. Iss.*

Alexander, C., (2009c), Evaluating the effects of wrinkle bends, *Pipeline and Gas Technology*, *Sept. Iss.*

Alexander, C. (2008a), "Strain based design methods for composite repair systems", *Proceedings of IPC2008, 7th International Pipeline Conference,* September 29-October 3, Calgary, Alberta, Canada.

Alexander, C. (2008b), "Using testing methods to evaluate pipeline mechanical integrity", *7th International Pipeline Conference,* 29 September - 3 October , Alberta Canada, ASME.

Alexander, C. and Worth, F. (2006), "Assessing the use of composite materials in repairing mechanical damage in transmission pipelines", *Proceedings of IPC2006, 6th International Pipeline Conference,* 25-29 September, Calgary, Alberta, Canada.

Alexander, C. (2007a), "Evaluating the use of composite materials in reinforcing offshore risers using full scale testing methods", *Proceedings of Conference ASME International Offshore Pipeline Forum,* 23 -24 October , Houston, Texas, USA.

Alexander, C. R. (2007b), *Development of a composite repair system for reinforcing offshore risers* (unpublished Doctor of Philosophy thesis), Texas A&M University, Texas.

Alexander's Gas & Oil Connections, (January 17, 2005), Petra Perdana believes oil and gas sector is bright, Volume 10, Issue 1 ed., *Star Publications*, http://www.gasandoil.com/goc/company/cns50323.htm.

Apicella, A., Del Nobile, M. A., Mensitieri, G., Montanino, M. and Stupak, P. R. (1994), "Thermal, mechanical and rheological evolution during the processing of multilayer thermosetting composite structures", *Composite Structures,* vol. 27, pp. 121-127.

ASM International (2002), "Thermal Expansion in Chapter 2", in *Thermal Properties of Metal*.

ASME (2010), *Repair of Pressure Equipment and Piping - PCC-2 2008*.

ASTM International (2009a), *ASTM D3171-09-Standard test methods for constituent content of composite materials*.

ASTM International (2009b), *ASTM D6856-03-Standard guide for testing fabric reinforced textile composite materials*.

Avram, J.B. (2001), *Fatigue response of thin stiffened aluminium cracked panels repaired with bonded composite patches,* Dept of the Air Force Air University, Air Force Institute of Technology, Ohio USA.

Azzi, V. D. and Tsai, S. W. (1965), "Anisotropic strength of composites", *Experimental Mechanics,* , pp. 283-288.

Bahai, H. (2001), "A Parametric Model for Axial and Bending Stress Concentration Factors in API Drillstring Threaded Connectors", *Pressure Vessels and Piping,* vol. 78, pp. 495-505.

Bahai, H. and Esat, I. I. (1994), "A Hybrid Model for Analysis of Complex Stress Distribution in Threaded Connectors", *Computers and Structures,* vol. 52, no. 1, pp. 79-93.

Barucci, M., Bianchini, G., Del Rosso, T., Gottardi, E., Peroni, I. and Ventura, G. (2000), "The expansion and thermal conductivity of glass fibre reinforced nylon at low temperature", *Cryogenics,* vol. 40, pp. 465-467.

Becht IV, C. and Sims, J. R. (2006), "Development in post construction codes and standards in the United States", *Failures*.

Beden, S. M., Abdullah, S., Ariffin, A. K., Rahman, M. M. and Al-Asady, N. A. (2008), "Effect of mesh size of finite element analysis in fatigue life assessment for pipe elbows", Azami Zaharim et al. (eds.), in: *Seminar on Engineering Mathematics,* Engineering Mathematics Group, Malaysia, .

Benham, P. P., Crawford, R. J. and Armstrong, C. G. (1996), *Mechanics of Engineering Materials,* 2nd ed, Pearson Prentice Hall, England.

Bergman, M. (1995), "Stress intensity factors for circumferential surface cracks in pipe", *Fatigue and Fracture of Engineering Materials,* vol. 18, pp. 1155-1172.

Billoet, J. L. and Cherouat, A. (1999), "Meso Structural Behaviour of Composite Fabric for the Simulation of Manufacturing of Thin Composite by Shaping Process", *12th International Conference on Composite Materials (ICCM-12),* July, Paris France.

Birchmeier, M., Gsell, D., Juon, M., Brunner, A. J., Paradies, R. and Dual, J. (2009), "Active fibre composites for the generation of Lamb waves", *Science Direct,* vol. 49, pp. 73-82.

Blanas, P., Wenger, M., Rigas, E. and Das Gupta, D. (1999), "Active Composite Materials as Sensing Elements for Fiber Reinforced Smart Composite Structures", *Smart Structures and Integrated Systems, Proceedings of SPIE,* Vol. 3329, p. 482.

BMT Fleet Technology (2005), *Pipeline Structural Integrity Assessment,* Business Briefing: Exploration & Production: The Oil & Gas Review 2004, Touch Briefings, http://www.touchbriefings.com/download.cfm?step=3&fileID=3550.

Brennan, F. P. (2008), *Structural Integrity Session 2b:Fatigue,* 2, Cranfield University, Bedfordshire, UK.

Brennan, F. P. (2007), "Stress Monitoring of Civil and Mechanical Engineering Infrastructure", *4th International Conference on Condition Monitoring,* 11 - 14 June, Harrogate, UK.

Brennan, F. P., Ngiam, S. S. and Lee, C. W. (March 2007), "An experimental and analytical study of fatigue crack shape control by cold working", *Science Direct Engineering Fracture Mechanics,* [Online], vol. 75, April 2009-pp.355-363 available **at:** www.sciencedirect.com.

Brennan, F. P., Paik, J. K., Carlsen, C. A., Daley, C., Garbatov, Y., Ivanov, L., Rizzo, C. M., Simonsen, B. C., Yamamoto, N. and Zhuang, H. Z. (2006), "Committee V.6: Condition Assessment of Aged Ships", *16th International Ship and Offshore Structures Congress,* Vol. 2, 20 - 25 August 2006, Southampton UK, p. 265.

Brennan, F. P., Wang, G., Boon, B., Ji, C., Garbatov, Y., Parunov, J., Rizzo, C. M., Rahman, T. A., Yamamoto, N., Rouhan, A. and Shin, C. H. (2009), "Committee V.6: Condition of Assessment of Aged Ships and Offshore Structures", *17th International Ship and Offshore Structures Congress,* Vol. 2, 16 - 21 August 2009, Seoul, Korea, pp. 309.

Britto, A. J., De Almeida, A. T. and Mott, C. M. M. (2010), "A multicriteria model for risk sorting of natural gas pipelines based on ELECTRE TRI integrating Utility Theory", *European Journal of Operational Research,* no. 200, pp. 812-821.

Brownlee, K. and Alexander, C. (2007), "Methodology for assessing the effects of plain dents, wrinkle bends, and mechanical damage on pipeline integrity", *NACE International Corrosion 2007 Conference & Expo,* March 11-15, 2007, Nashville, Tennessee.

Bruno, T. V. (2008)*, The Causes and Prevention of Pipeline Failures*, available at: http://www.metallurgical.com/Publications/ (accessed December 2009).

Bucinell, R. B. (2001), *Calculating principal Strains using a Rectangular Strain Gage Rosette,* Union College*,* New York, US.

Canaway, R.T. (2011), *RBI in Major Plants*, Suregrove Ltd.

Car, E., Oller, S. and Onate, E (2001), "Strain Plasticity Model for Anisotropic Materials - Composite Materials Application", *International Journal of Plasticity,* vol. 17, pp. 1437-1463.

Carpinteri, A. and Brighenti, R. (1998), "Circumferential surface flaws in pipes under cyclic axial loading", *Engineering Fracture Mechanics,* vol. 60, pp. 383-396.

Carpinteri, A., Brighenti, R. and Vantadori, A. (2004), "Circumferentially notched pipe with an external surface crack under complex loading", *Full, International Journal of Mechanical Sciences,* vol. 45, pp. 1929-1947.

Chawla, K. K. (1998), "Experimental determination of fiber properties", in *Fibrous material,* University of Alabama pp. 234-253.

Chen, Z., Cudney, H., Giurgiutiu, V., Rogers, C., Quattrone, R. and Berman, J. (1997), "Full-Scale Ferromagnetic Active Tagging Testing of C-Channel Composite Elements", *Smart Systems for Bridges, Structures, and Highways, Proceedings of SPIE,* Vol. 3043, p. 169.

Chung, D.D.L. (2001), "Structural Health Monitoring by Electrical Resistance Measurement", *Full,* vol. 10, no. Smart Mater. Struct; pp. 624-634.

Citadel Technologies (2007), *Carbon Composite Wraps for Pipeline Repair*, available at: http://www.cittech.com/products.html (accessed April 2009).

Clausard, C. (2006), *Pipeline integrity Management Strategy for Aging Offshore Pipelines*, Pigging Products and Services Association., http://www.ppsa-online.com/papers/2006-Aberdeen-7-Clausard.pdf.

CLOCK SPRING Company L.P. (January 8, 2005)*, Installation Guide Pipe Support*, available at: http://www.clockspring.com/PDF/Pipe%20Support%20Manual.pdf (accessed December 27, 2008).

Coenen, E. W. C., Kouznetsova, V. G. and Geers, M. G. D. (2010), "Computational homogenization for heterogeneous thin sheets", *International Journal for Numerical Methods in Engineering,* vol. 83, pp. 1180-1205.

Compere, G., Remacle, J. F., Jansson, J. and Hoffman, J. (2010), "A mesh adaptation framework for dealing with large deforming meshes", *International Journal for Numerical Methods in Engineering,* vol. 82, pp. 843-867.

CorroDefense LLC (2005), *The AquaWrap Solution for Civil Structure or Pipeline Reinforcement & Protection*, available at: http://www.corrodefense.com/ (accessed April 2009).

County of Santa Barbara (2009), *North County Oil and Gas Facility Sitting and Planning Analysis - Existing Infrastructure and Production Setting*, available at: http://www.countyofsb.org (accessed April 2009).

Creager, M. and Paris, P. C. (1967), "Elastic field equations for blunt cracks with reference to stress corrosion cracking", *International Journal of Fracture Mechanics,* vol. 3, no. 4, pp. 247-252.

Culshaw, B. (1984), "Fibre Optic Sensing Technique", in Sharpe, R. S. (ed.) *Research Techniques in Non Destructive Testing Volume 7,* Academic Press, London.

Da Costa Mattos, H. S., Reis. J.M.L., Sampaio,, R. F. and Perrut,, V. A. (2009), "An alternative methodology to repair localized corrosion damage in metallic pipelines with epoxy resins", *Materials and Design,* vol. 30, pp. 3581-3591.

Daniel, I. M. and Ishai, O. (2006), *Engineering Mechanics of Composite Materials,* Second Edition, Oxford University Press, New York.

De Carvalho, E. A. (2005), "Stress concentration factors for an internally pressurized circular vessel containing a radial U-notch", *International Journal of Pressure Vessels and Piping -Science Direct,* vol. 82, pp. 517-521.

De Leeuw, B. and Brennan, F. P. (2009), "Structural integrity monitoring index (SIMdex): a methodology for assessing structural health monitoring technologies", *J.AerospaceEngineering,* vol. 223, no. 392, pp. 515-523.

Denso North America, Inc. (2009), *Leaders in Corrosion Prevention and Sealing Technology*, available at: http://www.densona.com/DensoPetrolatumTapes.htm (accessed April 2009).

Department of Resources (2010), *Northern Territory Oil and Gas Pipelines*, available at: http://www.nt.gov.au/d/Minerals_Energy/ (accessed April 2010).

DeVries, N. A., Shivanna, K. H., Ta depalli, S. C., Magnotta, S. V. and Grosland, N. M. (2009), "IA-A FEMesh: Anatomic FE Models - A Check of Mesh Accuracy and Validity", *The Iowa Orthopaedic Journal,* vol. 29, pp. 48-54.

Dinovitzer, A., Lazor, R., Caroll, L. B. and Zhou, J. (2002), "Geometric Dent Characterization", *Proceedings of IPC 2002: International Pipeline Conference,* 29 September - 3 October 2002, Alberta Canada.

Dover, W. D., Brennan, F. P. and De Leeuw, B. (2001), "ACSM Stressprobe: A new Non Contacting Stress Measurement Technique for the Offshore Industry",

Proceedings of OMAE'01 20th International Conference on Offshore Mechanics and Arctic Engineering, 3 - 8 June, 2001, Rio De Janeiro, Brazil.

Ecke, W. (2008), *Application of Fibre Bragg Grating Sensors,* OFS-19 Tutorial, Institute of Photonic Technology (IPHT) Jena, Germany.

Efunda, I. (2011)*, Efunda: The ultimate online reference for engineers*, available at: http://www.efunda.com/formulae/solid_mechanics/plates/theory.cfm.

Elvin, N. and Leung, C. (1997), "Feasibility of Delamination Detection with Embedded Optical Fibres", Regelbrugge, M. E. (ed.), in: *Smart Structures and Integrated Systems, Proceedings of SPIE,* Vol. 3041, 1997, p. 627.

Emslie, C. and Gibson, K. (2010), *Risk Based Inspection in Asset Integrity Management*, Technical Article.

Enduro Pipeline Services (2009)*, Magnetic Flux Leakage and Multiple Data Set Inline Inspection*, available at: http://www.enduropls.com/articles.jsp (accessed April 2009).

Energy Workforce Sdn Bhd (2011)*, Alternating Current Field Measurement*, available at: http://www.energyworkforce.net (accessed April 2011).

ERSG Ltd. (2009), *Pipeline Risk Assessment*.

ETD Ltd. (2003), *Guidelines for Inspection, Monitoring, Repair and Maintenance of HRSGs - Based on Review of Worldwide Plant and Research Experience*.

Farrar, C. R. and Worden, K. (2007), "An introduction to structural health monitoring", *Philosophical transactions.Series A, Mathematical, physical, and engineering sciences,* vol. 365, no. 1851, pp. 303-315.

Fixter, L. and Williamson, C. (2006), *State of the Art Review - Structural Health Monitoring,* Qinetic/S&DU/T&P/E&M/TR0601122, Qinetic and SMART.mat, http://amf.globalwatchonline.com.

Foedinger, R., Rea, D., Sirkis, J., Troll, J., Grande, R. and Vandiver, T. L. (2000), *Structural Health Monitoring and Impact Damage Detection for Filament Wound*, Stanford University, Palo Alto, California.

Forsyth, D. S. (1998), "An Evaluation of Probability of Detection Statistics", *Airframe Inspection Reliability under Field / Depot Conditions,* 13 -14 May 1998, Brussels, Belgium, p. 1.

Fouladi, E., Fayazbakhsh, K. and Abedian, A. (2010), "Patch materials selection for ageing metallic aircraft structures using digital quantitative materials selection methods", *27th International Congress of the Aeronautical Sciences*, ICAS 2010, www.icas-proceedings.net.

Francini, B. and Alexander, C. (2006), "State of the art assessment of composite systems used to repair transmission pipelines", *Proceedings of IPC2006, 6th International Pipeline Conference,* 25 -29 September, Calgary, Alberta, Canada.

Frassine, R. (1997), "Long-Term Performance of a Polymer Composite Repair System for Gas Pipelines", *Advances in Polymer Technology,* vol. 16, no. 1, pp. 33-43.

Freire, J.L.F., Vieira, R.D. and Benjamin, A.C. (October 2006), *Part 2: Experimental strain analysis of metal loss defects in pipeline*, Society for Experimental Mechanics.

Freire, J.L.F., Vieira, R.D. and Benjamin, A.C. (August 2006), *Part 1: Experimental techniques in the field of pipeline integrity*, Society for Experimental Mechanics.

Fries, T. P. and Belytschko, T. (2010), "The extended/generalized finite element method: An overview of the method and its applications", *International Journal for Numerical Methods in Engineering,* vol. 84, pp. 253-304.

Frost, S. R. (2010a)*, Solving integrity management problems using Technowrap composite repairs*, available at: www.wtr.uk.com/docs/WTR-Petroleum-africa.pdf.

Frost, S. R. (2010b), *Technical data on Triaxial woven fabric composite*, Walker Technical Resources Ltd., Aberdeen, Scotland.

Frost, S. R. (2009), *Technowrap 2K Technical database report*, Walker Technical Resources Ltd., Aberdeen, Scotland.

Frost, S. R. (2008), "Operational guidelines for the use of the composite repairs", *ACORES*.

Furrow, P. C., Brown, R. T. and Mott, D. B. (2000), "Fiber Optic Health Monitoring System for Composite Bridge Decks", Liu, S. C. (ed.), in: *Smart Systems for Bridges, Structures, and Highways, Proceedings of SPIE,* Vol. 3988, Newport Beach, California, p. 380.

Gedeon, G. (2001), *Gulf of Mexico Oil and Gas Pipeline Installation, Impact and Mitigation*, OCS report MMS 2001, www.cedengineering.com.

Georgia Institute of Technology (March 2010)*, Electrical Resistance Strain Gauge Circuits; AE3145 Resistance Strain Gage Circuits*, available at: www.pdfqueen.com/pdf/st/strain-gauge-bridge-circuit (accessed May 2010).

Georgiou, G. A. (2006), *Probability of Detection (POD) Curves - Derivation, applications and limitations,* 454, Health and Safety Executive, London.

Gilbert, S. and Fix, G. (1973), *An Analysis of the Finite Element Method,* Prentice Hall, England.

Greenwood, R. (2002), *UKOPA Pipeline Fault Database,* R 4798, Advantica, Newcastle UK.

Gregory, O., Euler, W., Crisman, E., Mogawer, H. and and Thomas, K. (1999), "Smart Optical Waveguide Sensors for Cumulative Damage Assessment", *Smart Structures and Materials1999: Smart Systems for Bridges, Structures, and Highways Proceedings of SPIE,* Vol. 3671, p. 100.

Gunalton, Y., Courtois, G. d. and Cavalier, B. (2008), *Qualifications of Composite Systems for the Repair of Pipelines and Risers,* Indocoat 2008, Total, Jakarta Indonesia.

Habib, S. S. and Nahas, M. N. (1998), "Measurement of Fatigue Crack by Nondestructive Testing", *Engineering Science,* vol. 10, no. 2, pp. 65-67.

Hallen, J. M., Caleyo, F., Gonzalez, J. and Lagos, F. F. (2003), "Probabilistic Condition Assessment of Corroding Pipelines in Mexico", *111-Pan American Conference for Nondestructive Testing,* 2 - 6 June 2003, Rio De Janeiro, PANNDT, Brazil.

Hamila, N. and Boisse, P. (2009), "A semi-discrete shell finite element for textile composite reinforcement forming simulation", *International Journal for Numerical Methods in Engineering,* vol. 79, pp. 1443-1466.

Han, S., Brennan, F. P. and Dover, W. D. (2002), "Development of the alternating current stress measurement model for magnetostriction behaviour of mild steel under orthogonal magnetic fields for stress measurement", *Journal of Strain Analysis,* vol. 37, no. 1, pp. 21-31.

Harada, Y., Maruyama, Y. and Maeda, A. (1999), "Effect of Microstructure on Failure Behaviour of Light Water Reactor Coolant Piping under Severe Conditions", *Journal of Nuclear Science and Technology,* vol. 36, no. 10, pp. 923-933.

Harding, J. and Li, Y. L. (1992), "Determination of interlaminar shear strength for glass/epoxy and carbon/epoxy laminates at impact rates of strain", *Composite Science and Technology,* vol. 45, pp. 161-171.

Hartwig, G. (1988), "Thermal expansion of fibre composites", *Cryogenics,* vol. 28.

Herszberg, I., Bannister, M. K., Li, H., Thomson, R. S. and White, C. (2007), "Structural health monitoring for advanced composite structures", *The Sixteenth International Conference on Composite Materials,* 8 - 13 July, Japan.

Inaudi, D. and Glisic, B. (2006), "Distributed fiber optic strain and temperature sensing for structural health monitoring", *The Third International Conference on Bridge Maintenance, Safety and Management,* 16-19 July 2006, IABMAS, Porto, Portugal.

Inaudi, D. and Glisic, B. (2005), "Development of distributed strain and temperature sensing cables", *17th International Conference on Optical Fibre Sensors,* Bruges, Belgium.

Ito, T., Suganuma, T. and Wakashima, K. (1999), "Glass fiber polypropylene composite laminates with negative coefficients of thermal expansion", *Journal of Materials Science,* vol. 18, pp. 1363-1365.

Jaske, C. E., Vieth, P. H. and Beavers, J. A. (2002), "Corrosion 2002", April 7 - 11, Denver, Co.

Jenson, F., Iakovleva, E. and Reboud, C., (2009), *Modelling II: Evaluation of POD Curves Based on Simulation Results*, European Commission Joint Research Centre.

Kaminski, C. (2005), *Stress Analysis and Pressure Vessels,* University of Cambridge, UK.

Kaminskii, A. A. and Bastun, V. N. (1997), "Methods of Determining the Stress-Strain State and Fracture Toughness of Gas and Oil Line Pipe", *International Applied Mechanics,* vol. 33, no. 8, pp. 595-618.

Khan, A. S. and Hsiao, C. (1984), "Strain field in straight cylindrical shells due to applied forces on an attached shell", *Journal of Strain Analysis,* vol. 19, no. 4.

Kharionovski, V.V. (2006), "Express-method helps evaluate remaining gas pipeline life", *Gas Industry of Russia*,1st *Quarter 2011 Iss.*

Khazhinskii, G. M. (2005), "Approximate evaluation of stresses in dents of cylindrical shells", *Chemical and Petroleum Engineering,* vol. 41, no. 3-4, pp. 122-125.

Kim, Y. J. and Son, B. G. (2004), "Finite element based stress concentration factors for pipes with local wall thinning", *International Journal of Pressure Vessels and Piping - Science Direct,* [Online], vol. 81, November 2009- pp. 897-906 available at: www.elsevier.com/locate/ijpvp.

Kim, Y. J., Song, T. K., Kim, J. S. and Jin, T. E. (2007), "Limit Loads and Approximate J Extimates for Axial Through-Wall Cracked Pipe Bends", *Int J Fract - Springer,* vol. DOI 10.1007/s10704, no. 007-9166-2, pp. 249-264.

Knoxville, W. (2009), *Finite Element Analysis, Then and Now*, Amazines.com, CA, USA.

Kosai, M., Shimamoto, A., Yu, C. T., Kobayashi, A. S. and Tan, P. W. (1999), "Axial Crack Propagation and Arrest in a Pressurized Cylinder: An Experimental-numerical Analysis", *Full,* vol. 39, no. 4, pp. 256-264.

Kotrechko, S. A., Krasovskii, A. Y., Meshkov, Y. Y., Mettus, G. S., Polushkin, Y. A. and Torop, V. M. (2002), "Influence of Long Term Operation on the Toughness of 17GS Pipeline Steel", *Strength of Materials,* vol. 34, no. 6, pp. 541-547.

Kueh, A. and Pellegrino, S. (2007), "Triaxial weave fabric composites", *European Space Energy Contractor Report.*

Kueh, A., Soykasap, O. and Pellegrino, S. (2005), "Thermo mechanical behaviour of single ply Triaxial Weave carbon fibre reinforced plastic", NASA Astrophysics Data System (ed.), in: *European Conference on Spacecraft Structures, Materials & Mechanical Testing 2005,* 10-12 May, Netherlands.

Kulkarni, S. and Alexander, C. (2008), "Evaluating the effects of wrinkle bends on pipeline integrity", *Proceedings of IPC2008 7th International Pipeline Conference,* September 29 – October 3, 2008, Alberta, Canada.

Lebedev, A. A., Muzyka, N. R., Volchek, N. L. and Nedoseka, S. A. (2003), "Monitoring of Current State of Pipe Metal in Active Gas Pipelines - Experimental Method and Results", *Strength of Materials,* vol. 35, no. 2, pp. 122-127.

Lee, S., Munro, M. and Scott, R. F. (1990), "Evaluation of three in-plane shear test methods for advanced composite materials", *Composite,* vol. 21, no. 6, pp. 495-502.

Lee, O. S. and Pyun, J. S. (2002), "Failure Probability of Corrosion Pipeline with Varying Boundary Condition", *KSME International Journal,* vol. 16, no. 7, pp. 889-895.

Lesmana, D.S. (2010), High pressure gas transmission pipeline repair using Clock Spring composite sleeve in Indonesia, *Pipeliner*, *July Iss*.

Linton, V. (September 2008), *Stress Corrosion Cracking in Gas Transmission Pipelines; Understanding Crack Extension by Fatigue,* 13, University of Adelaide, Australia.

LIOS Technology Inc (2010)*, Distributed Temperature Sensing System*, available at: www.lios-tech.com (accessed February 2010).

Littell, J. (2008), *The experimental and analytical characterization of the macromechanical response for triaxial braided composite materials,* The University of Akron, Oh. US.

Lloyds Register (2011)*, Asset Management and Safety Assurance for the UK Energy Industry*, available at: www.llyodsregister.co.uk (accessed January 2011).

Longest, P. W. and Vinchurkar, S. (2007), "Effects of mesh style and grid convergence on particle deposition in bifurcating airway models with comparisons to experimental data", *Medical, Engineering and Physics,* vol. 29, pp. 350-366.

Lotsberg, I. (2008), "Stress concentration factors at welds in pipelines and tanks subjected to internal pressure and axial force", *Marine Structures,* vol. 21, pp. 138-159.

Lukacs, J., Nagya, G., Toroka, I., Egertb, J. and Pereb, B. (2010), "Experimental and Numerical Investigations of External Reinforced Damaged Pipelines", *Procedia Engineering,* vol. 2, pp. 1191-1200.

Mahgerefteh, H. and Atti, O. (2006), " Modelling Low Temperature - Induced Failure of Pressurized Pipelines ", *AIChe Journal,* vol.52, No.3, pp. 1248-1256.

Mahgerefteh, H. and Abbasi, M.U. (2007), "Modelling Blow Down of Pipelines under Fire Attack", *AIChe Journal,* vol.53, No.9, pp. 2443-2450.

Malcolm, J. (2009), *To replace or to wrap - the standardisation of composite repair*, Reinforced Plastics.com.

Martineau, R. and Romero, C. (1996), *Response of a stainless steel cylinder with elliptical ends subjected to an-off center blast load*, Los Alamos National Laboratory, US.

Matelect Ltd. (2004), *The Potential Drop Technique & Its Use in Fatigue Testing,* FPD04, Matelect Ltd, London.

McElroy, D. L., Weaver, F. J. and Bridgman, C. (1988), "Thermal expansion of epoxy fibre glass composite specimens", *International Journal of Thermophysics,* vol. 9, no. 2.

McGraw-Hill (2003), "McGraw-Hill Dictionary of Scientific & Technical Terms", The McGraw-Hill Companies, Inc.

Measurements Group (2000)*, Strain Gage Rosettes – Selection Application and Data Reduction;*, available at: http://www.measurementsgroup.com/guide/tn/tn515/515intro.htm (accessed April 2010).

Michalopoulos, E. and Babka, S. (2000), *Evaluation of Pipeline Design Factors,* 7094, Gas Research Institute, Hartford, Ct, US.

Moerman, W., Taerwe, L., De Waele, W., Degrieck, J. and Baets, R. (2000), *Remote Monitoring of Concrete Elements by Means of Bragg Gratings*, Stanford University, Palo Arto, California.

Mohitpour, M., Golshan, H. and Murray, A. (2003), *Pipeline design and construction : a practical approach,* 2nd ed, ASME Press, New York.

Mousavi, S. E., Xiao, H. and Sukumar, N. (2010), "Generalized Gaussian quadrature rules on arbitrary polygons", *International Journal for Numerical Methods in Engineering,* vol. 82, pp. 99-113.

Murad, M. A. (2009), "The Development of Structural Health Monitoring (SHM) Procedures for the Structural Integrity and Maintenance Repair of Offshore Ageing Pipelines", *European-American Workshop on Reliability of NDE,* June 24 – 26, 2009, Berlin Germany.

Murad, M. A. and Brennan, F. P. (2010), "Simulation of Blunt Defect and Behaviour in a Thin Walled Cylinder for the Development of Structural Health Monitoring Techniques for Pipeline Repairs ", *4th International Conference on Advanced Computational Engineering and Experimenting,* 8 - 9 July, Paris, France.

Murad, M. A., Brennan, F. P. and Frost, S. R. (2011), "The study on the bonding integrity between the reinforced steel pipeline and reinforcing composite wraps (Technowrap) using Structural Health Monitoring Technique", *5th International Conference on Composite Testing and Model Simulation,* 14 - 16th February, Lausanne, Switzerland.

NASA (1996), *Fiber reinforced polymer composite material selection*.

National Instruments Measurement (2011)*, What is Compact Rio?*, available at: www.ni.com (accessed November 2011).

National Instruments Measurement (2001)*, Measuring Strain with Strain Gages*, available at: http://ni.com/legal/termsofuse/unitedstates/us (accessed March 2009).

Ochoa, O. O. and Alexander, C. (2007), *Composites Repair Methods for Steel Pipes,* 12/07A184, Offshore Technology Research Center, Texas.

O'Donoghue, P. E. and Zhuang, Z. (1999), "A finite element model for crack arrestor design in gas pipelines", *Fatigue Fracture Engineering Materials Structure,* [Online], vol. 22.

Osmont, D., Dupont, M., Gouyon, R., Lemistre, M. and Balageas, D. (2000), "Damage and Damaging Impact Monitoring by PZT Sensors-Based HUMS", *Smart Structures and Materials 2000: Sensory Phenomena and Measurement Instrumentation, Proceedings of SPIE,* Vol. 3986, p. 85.

Ostsemin, A. A. and Saidov, G. I. (2004), "Evaluation of the Crack Resistance and Mechanical Properties of the Metal of Large Diameter Pipes under Static and Dynamic Loads", *Strength of Materials,* vol. 36, no. 4, pp. 391-400.

Palmer, A. C. and King, R. (2008), "Inspection and Monitoring", in *Subsea Pipeline Engineering,* Penwell CNP, Oklahoma USA, pp. 477-478.

Palmer, R. and Paisley, P. (2000), "Repairing integral corrosion defects in pipelines - A case study", *4th International Pipeline Rehabilition and Maintenance Conference,* September 2000, UK.

Park, G. and Inman, D. J. (2007), "Structural health monitoring using piezoelectric impedance measurements", *Philosophical transactions.Series A, Mathematical, physical, and engineering sciences,* vol. 365, no. 1851, pp. 373-392.

Parvin, A. and Wu, S. (2008), "Ply angle effect on fiber composite wrapped reinforced concrete beam–column connections under combined axial and cyclic loads", *Composite Structures,* vol. 82, pp. 532-538.

Pederson, K. A. (2008)*, FEA Mesh Architecture - KAP's Corner*, available at: www.capinc.com (accessed November 2010)

Performance Composites Ltd (2009)*, Mechanical properties of carbon fibre composite materials, fibre / epoxy resin (120 Deg cure)*, available at: http://www.performance-composites.com/carbonfibre/mechanicalproperties_2.asp (accessed January).

Peterson, R. E. (1953), *Stress Concentration Design Factors,* 1st ed, John Wiley & Sons, Inc, England.

PICA Corp (2011)*, Direct Condition Assessment*, available at: www.picacorp.com (accessed January 2011).

Pilkey, W. D. (1997), *Peterson's Stress Concentration Factors*, John Wiley & Sons, Inc.

Pipeline Monitoring Ltd (2011)*, Pipeline Monitoring*, available at: www.pipelinemonitoring.com (accessed March 2011).

Polak, J. (1983), "Stress and Strain Concentration Factor Evaluation Using the Equivalent Energy Concept", *Materials, Science and Engineering,* vol. 61, pp. 195-200.

Pople, J. (1992), "Gauge installation and protection in hostile environments", in *Strain Gauge Technology,* second ed, Springer, p. 104.

Qian, J., Wang, W., Lewis, A. C., Qidwai, M. A. S. and Geltmacher, A. B. (2010), "Quality improvement of non-manifold hexahedral meshes for critical feature determination of microstructure materials", *International Journal for Numerical Methods in Engineering,* vol. 82, pp. 1406-1423.

Radaj, D. and Zhang, S. (1996), "Stress concentration at fictitiously rounded sharp notches in shear loading", *Engineering Fracture Mechanics,* vol. 55, no. 4, pp. 675-676.

Raju, I. S. and Newman, J. C. (1986), "Stress intensity factors for circumferential surface cracks in pipes and rods under tension and bending loads", in Underwood, J. H., Chait, R., Smith, C. W. (eds.) *Fracture Mechanics,* ASTM, Philadelphia, pp. 789-805.

Rao, M. B., Bhat, M. R., Murthy, C. R. L., Madhav, K. Y. and Asokan, S. (2006), "Structural Health Monitoring (SHM) Using Strain Gauges, PVDF Film and Fiber Bragg Grating (FBG) Sensors: A Comparative Study", *Proc. National Seminar on Non-Destructive Evaluation,* Dec 7 - 9, 2006, Hyderabad India, Indian Society for Non-Destructive Testing, p. 333.

Reboud, C., Pichenot, G., Paillard, S. and Jenson, F. (2010), "Statistical Study of ECT Detection around Fasteners using Simulation Based POD Curves", *American Institute of Physics,* vol. 29.

Rinehart, A. J. (2003), *Effects of Localized Geometric Imperfections on the Stress Behavior of Pressurized Cylindrical Shells* (unpublished Doctor of Philosophy thesis), Texas A&M University, Texas USA.

Rizkalla, S., Benmokrane, B. and Tadros, G. (2000), "Structural Health Monitoring Bridges with Fibre Optic Sensors", *European COST F3 Conference on System Identification and Structural Health Monitoring,* 2000, Madrid Spain, p. 501.

Roctest Ltd. (2011)*, Pipeline Monitoring Systems*, available at: www.roctest-group.com (accessed April).

Rosas, M.A., Vieira, R.D. and Freire, J.L.F. (December 2007), Use of small scale pipeline specimens to test a steel adhesive repair system, *Experimental Techniques,* Vol. 31, Iss. 6, pp 64-72 Nov/Dec

Satpathi, D., Victor, J., Wang, M., Yang, H. and and Shih, C. (1999), "Development of a PVDF Film Sensor for Infrastructure Monitoring", *Smart Structures and Materials 1999: Smart Systems for Bridges, Structures, and Highways, Proceedings of SPIE,* Vol. 3671, pp. 90.

Schwarz, G., Krahn, F. and and Hartwig, G. (April 1991), "Thermal expansion of carbon fibre composites with thermoplastic matrices", *Cryogenics,* [Online], vol. 31.

Scrivner, R. and Alexander, C. (2008), "Element of an engineering based integrity management program", *Proceedings of IPC2008 7th International Pipeline Conference,* September 29 – October 3, 2008, Alberta, Canada.

Shin, C. S. (1986), "A discussion on various estimations of elastic stress distributions and stress concentration factors for sharp edge notches", *Int J Fatigue,* vol. 4, no. 8, pp. 235-237.

Simola, K., Cronvall, O., Mannisto, I., Gunnars, J., Alverlind, J., Dillstrom, P. and Gandossi, L. (2009), *Studies on the effect of flaw detection probability assumptions on risk reduction at inspection,* NKS-208, Denmark.

Sinha, D. N. (2005), *Acoustic Sensor for Pipeline Monitoring,* LA-UR-05-6025, Los Alamos National Laboratory.

Smart Pipe Company, I. (2008)*, A New Life for Aging Pipelines*, available at: http://www.smart-pipe.com/index.php?id=3 (accessed April 2009).

Smith, K., Thompson, B. and Brasche, L. (2004)*, Model Based POD: Success and Opportunities*, available at: www.cnde.iastate.edu/MAPOD (accessed April 2009).

Smojver, I. and Ivancevic, D. (2010) "Coupled Euler Lagrangian Approach Using Abaqus /Explicit in the Bird Strike Aircraft Damage Analysis", *SIMULIA customer conference*.

Sohn, H. (2007), "Effects of environmental and operational variability on structural health monitoring", *Philosophical transactions.Series A, Mathematical, physical, and engineering sciences,* vol. 365, no. 1851, pp. 539-560.

Sohn, H., Farrar, C. R., Hemez, F. M., Shunk, D. D., Stinemates, D. W. and Nadler, B. R. (2003), *A Review of Structural Health Monitoring Literature: 1996–2001,* LA-13976-MS, Los Alamos National Laboratory, University of California.

Sosnovskii, L. A. and Vorob'ev, V. V. (2000), "The Influence of Long Operation on Fatigue Strength of Pipe Steel", *Strength of Materials,* vol. 32, no. 6, pp. 523-529.

Staten, M. L., Kerr, R. A., Owen, S. J., Blacker, T. D., Stupazzini, M. and Shimada, K. (2010a), "Unconstrained plastering—Hexahedral mesh generation via advancing-front geometry decomposition", *International Journal for Numerical Methods in Engineering,* vol. 81, pp. 135-171.

Staten, M. L., Shepherd, J. F., Ledoux, F. and Shimada, K. (2010b), "Hexahedral Mesh Matching: Converting non-conforming hexahedral-to-hexahedral interfaces into conforming interfaces", *International Journal for Numerical Methods in Engineering,* vol. 82, pp. 1475-1509.

Student, O. Z., Sijacki-Zeravcic, V., Skrypnyk, I. D., Nykyforchyn, H. M. and Lonyuk, B. P. (1999), "Distinctive Features of Fatigue Crack Growth in 14MoV63 Pipe Steel After Service", *Materials Science,* vol. 35, no. 3, pp. 381-388.

SWComposites/Eng-Tips Forums, (2010), *Elastic Constant Values*. Online Discussion Forum / Blogs.

Tennyson, R. C. and Mufti, A. A. (2000), "Monitoring bridge structures using fibre optic sensors", *European COST F3 Conference on System Identification and Structural Health Monitoring,* Madrid Spain, p. 511.

Thien, A. B., Chiamori, H. C., Ching, J. T., Wait, J. R. and Park, G. (April 2007), "The use of macrofibre composite for pipeline structural health assessment", *Full,* vol. Struct. Control Health Monit. 2008;15:43–63, no. DOI: 10.1002/stc.203.

Thodi, P., Khan, F. and Haddara, M. (2008), "The Selection of Corrosion prior Distributions for Risk Based-Integrity Modeling", *Stoch Environ Res Risk Assess-Springer,* vol. DOI 10.1007/s00477, no. 008-0259-X, pp. 1-17.

Tian, Z., Liu, J. and Yey, L. (1997), "Studies of stress concentration by using special hybrid stress elements", *International Journal for Numerical Methods in Engineering,* vol. 40, pp. 1399-1411.

Tippler, P. A. and Mosca, G. P. (eds.) (2007), *Physics for scientists and engineers,* W.H.Freeman.

Todd, M. D., Nichols, J. M., Trickey, S. T., Seaver, M., Nichols, C. J. and Virgin, L. N. (2007), "Bragg grating-based fibre optic sensors in structural health monitoring", *Philosophical transactions.Series A, Mathematical, physical, and engineering sciences,* vol. 365, no. 1851, pp. 317-343.

Tootkaboni, M. and Brady, L. G. (2010), "A multi-scale spectral stochastic method for homogenization of multi-phase periodic composites with random material properties", *International Journal for Numerical Methods in Engineering,* vol. 83, pp. 59-90.

University of Alberta (Nov 2002), *FEM Convergence Testing,* ANSYS Tutorials, University of Alberta, www.mece.ualberta.ca/tutorials/ansys/UT/Converge/Print.html.

Uribe, D. C. and Neugebauer, C. J. (2002), "Sharp error bounds for the Trapezoidal rule and Simpson's rule", *Journal of Inequalities in Pure and Applied Mathematics,* vol. 3, no. 4, pp. 1-22.

Vel, S. S. and Batra, R. C. (2001), "Exact solution for cylindrical bending of laminated plates with embedded piezoelectric shear actuators", *Smart Materials and Structures,* vol. 10, pp. 240-251.

Verhoosel, C. V., Remmers, J. J. C., Gutierrez, M. A. and De Borst, R. (2010), "Computational homogenization for adhesive and cohesive failure in quasi-brittle solids", *International Journal for Numerical Methods in Engineering,* vol. 83, pp. 1155-1179.

Vijayakumar, K. and Atluri, S. N. (1981), "Embedded elliptical crack in an infinite solid subject to arbitrary crack face tractions", *Journal of Applied Mechanics,* vol. 48, pp. 88-96.

Vishay Micro Measurements (2007), *Measurement of thermal expansion coefficient using strain gage*.

Vishay Micro Measurements (4 February 2005), *Strain Gage Selection-Criteria, Procedures, Recommendation,* Tech Note TN-505-4.

Walker Technical Resources (2009), *TechnoWrap2K*.

Walz, J. E., Fulton, R. E. and Cyrus, N. J. (1968), "Accuracy and Convergence of Finite Element Approximations", *NASA Langley Research Centre, Full,* vol. 150, no. AFFDL-TR-68-150, pp. 995-1027.

Wan, C., Mita, A. and Kume, T. (2008), "An Automatic Pipeline Monitoring System Using Sound Information", *Structural Control and Health Monitoring,* vol. DOI: 10.1002/stc.295.

Wang, C. S., Wu, F. and Chang, F. K. (2001), "Structural Health Monitoring from fibre-reinforced composites to steel-reinforced concrete", *Institute of Physics Publishing, Smart Mater. Struct.,* [Online], vol. 10.

Wang, J., Harrison, P., Long, A. C. and Clifford, M. J. (2006), "Prediction and Characterization of the Shear Behaviour of Viscous Woven Textiles Composites", *The 8th International Conference on Flow Processes in Composite Materials (FPCM8),* 11 – 13 July, Douai, France.

Wayman, M., (2008), *Non Intrusive Pipeline Condition Assessment*, Advanced Engineering Solutions Ltd.

Weese, R. K., Burhanm, A. K. and Fontes, A. T. (2005), "An Investigation of Coefficient of Thermal Expansion, Decomposition Kinetics, and Reaction to Various Stimuli", *36th International Annual Conference of ICT & 32nd International Pyrotechnics Seminar, Karlsruhe, Germany,* 28 June - 1 July, Lawrence Livermore National Laboratory.

Weymouth, L. J., Starr, J. E. and Dorsey, J. (1979), "Chapter 2: Bonded Resistance Strain Gages", in Strain Gauge Technology, pp. 112-120.

WrapMaster, Inc. (2009)*, Composite Solutions for Pipelines and Structures*, available at: http://www.wrapmaster.us (accessed April 2009).

www.dnvsoftware.com (2006)*, ORBIT Pipeline Integrity*, available at: http://www.dnv.com/binaries/orbit+pipelineintegrity_brochure_tcm4-159685.pdf (accessed December 2008).

Xue, L., Widera, G. E. O. and Sang, Z. (2005), "Application of FEM analysis methods to a cylinder-cylinder intersection structure", *18th International Conference on Structural Mechanics in Reactor Technology (SMiRT 18),* 7 - 12 August, Beijing China.

Yang, Z., Cho, C., Kim, C. B. and Beom, H. G. (2008), "The effect of biaxial load on stress and strain concentrations in a finite thickness elastic plate containing a circular hole", *International Journal for Numerical Methods in Engineering,* vol. 75, pp. 103-126.

You, L. H. (2004), "An efficient method for thermal analysis of composites containing anisotropic continuous fibers and arbitrary number of interfacial layers", *Computational Materials Science*, pp. 49-66.

You, X. C., Zhuang, Z., Huo, C. Y., Zhuang, C. J. and Feng, Y. R. (2003), "Crack Arrest in Rupturing Steel Gas Pipelines", *International Journal of Fracture,* vol. 123, pp. 1-14.

Zhang, Y. and Yan, G. (2007), "Detection of gas pipe wall thickness based on electromagnetic flux leakage", *Russian Journal of Non Destructive Testing,* vol. 43, no. 2, pp. 123-132.

Zostrich Geotechnical Ltd, (2001), *Pipeline Routes - Ground Motion Monitoring OTDR.*

APPENDIX 1 - RESULTS OF DETAILED CALCULATION FOR PRESSURE VESSEL AND DEVELOPMENT OF TEST RIG

General Technical Specifications:

The Maximum Allowable Operating Pressure (MAOP)

Or Design Pressure   = **53.5 Bar (775.75 Psig)**

The Maximum Allowable Working Pressure (MAWP)   = **90.50 Bar (1147.74 Psig)**

Material standards :   API 5L Grade B (equivalent to ASTM A 53 or ASME B31.3)

Material   :   Carbon Steel Pipe

Pressure Rating   :   Class 300

Fluid Service   :   Normal (cold water)

Pipe Dimension   :   Outer Diameter 219.1 mm (NPS 8")

Pipe Thickness   :   8.18 mm

Flange Type   :   Weld Neck (WN) Forged Flanges

Material standard   :   ASTM A105N–ASME B16.5, Material Group 1.1

Note: *The above pressure values are only based on the calculations of Pipe No 2 and 3 (i.e. Pipes that contain the defect depth of 3.5 mm). For further details of calculations and technical information, please refer to AS BUILT Report (The Development of Piping System for PhD Experimental Works; Ref: Prof Feargal Brennan)*

IMPORTANT ATTENTION:

For Temperature Test Application (as referred to ASME B31.3):

Standard Design Temperature: 300º F (149º C)

Standard Design Pressure: 655 Psig (45.17 Bar)

Maximum Operating Temperature: 140º F (60º C)

Maximum Operating Pressure: 72.5 Psig (5 Bar)

For Pressure Test Application (as referred to ASME B31.3):

Standard Design Pressure: 740 Psig (51.03 Bar)

Standard Design Temperature: 100º F (38º C)

Maximum Operating Pressure: 725 Psig (50 Bar)

Maximum Operating Temperature: 77º F (25º C) – Room Temperature

Note: *In order to perform a pressure test, Pipe No 5 **MUST BE DISMANTLED** first. This will ensure the heating element inside Pipe No 5 is safe and not damaged since the maximum withstand pressure of the heating element is **10 Bar ONLY**.*

Actual Hydrostatic Test value that was obtained on 7/08/2009 is **68.10 Bar.**

Pneumatic and Hydrostatic (HT) Test Report (All data required for ASME B31)

TEST NUMBER: 01	PROJECT NO: 1	PAGE 1 OF: 1
PROJECT NAME: Pneumatic and hydrostatic tests for Experimental Piping System		

TEST INFORMATION

SYSTEM DESCRIPTIONS: This structure will be solely used in the lab of Cranfield University UK and just for the purpose of research works (structural pipeline integrity)

DESCRIPTION OF TEST BOUNDARIES:

The test was carried out in an isolated area (closed warehouse) for safety reasons.

DESIGN TEMPERATURE: 148.9º C	DESIGN PRESSURE: 45.17 Bar
TEST METHOD: [√] HYDROSTATIC: 68 Bar	[√] PNEUMATIC: 14 Bar
TEST FLUID: Normal water	APPLICABLE CODE: N.A

TEST REQUIREMENTS (FOR HT)

REQ TEST PRESSURE: 68.10 Bar	TEST FLUID TEMPERATURE: 27º C
REQ TEST DURATION: 30 mins (HT)	AMBIENT TEMPERATURE: 27º C

TEST RESULTS

TEST DATE : 7 AUG 2009 (PNEUMATIC TEST)	START TIME	[√] AM 12:30	[ ] PM
	FINISH TIME	[√] AM 05:40	[ ] PM
TEST DATE: 7 AUG 2009 (HYDROTEST)	START TIME	[√] AM 07:10	[ ] PM
	FINISH TIME	[√] AM 07:40	[ ] PM

ACTUAL GAUGE PRESSURE	68 Psig (Bar)

TEST EQUIPMENT

TYPE		RANGE	CAL DATE	CAL DUE
Pressure Gauge - Parker (Brand new)		0 - 70 Bar	(New-Factory setting)	N.A

REMARKS:
Pneumatic:
Leaks at nipple joints / blind flanges. Immediate reworks were carried out using SMAW and Dye Penetration (NDT) at the weldment.
Hydrostatic:
The result was O.K and successful. No indication of water leakage especially at the welding areas No plastic deformation occurred during and after the test.

TEST ACCEPTANCE

CARRIED OUT BY: (Ir Mahadi Abd Murad)	DATE: 07-Aug-09
APPROVED BY: (Prof Engr Dr Feargal Peter Brennan)	DATE: 25–Sept-09

Photos of the Design and Build of the piping system

Figure 1: Shop drawings were displayed in the workshop for references – Design Stage
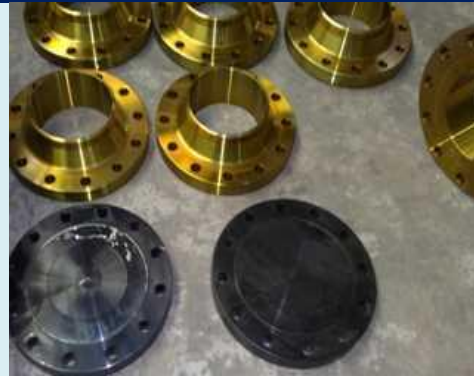

Figure 2: Materials used such as 300 Lbs Weld Neck and Blind Flanges

Figure 3: A dial gauge used in controlling the tolerance – before, during and after defect machining

Figure 4: The defect length of 40 mm and depth of 3.75 ± 0.25 mm were measured using a digital calliper – Final profile of artificial corrosion

Figure 5: Welding works on all five pipe segments using simple and reliable jig and fixture.

Figure 6: A pipeline was properly tightened prior to Hydrostatic Test

APPENDIX 2 – COMPOSITE WRAP PROCESS (PHOTOS)

Composite Installation Process using Technowrap2K Technology

Figure 1: Mechanical cleaning using power brush

Figure 2: Degreasing the uncoated metal surface using Acetone

Figure 3: Heating up the compound

Figure 4: Weighing up the material

Figure 5: Weighing mixtures of Parts A and B

Figure 6: Stirring up Part A and Part B for two minutes

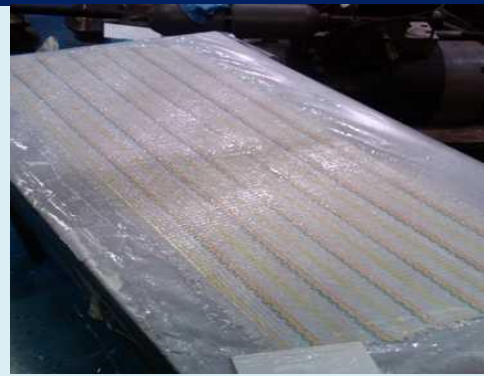Figure 7: Impregnating epoxy into the fibre glass
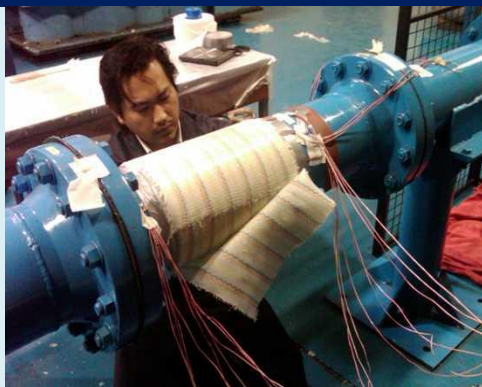

Figure 8: Fully impregnated composite ply

Figure 9: Composite hand-wrapping

Figure 10: Strengthening the wraps with stricture banding – Green pull ply was put between wet composite and stricture banding

Figure 11: The wrapped composite was left for 24 hours (Normal curing)

Figure 12: Fully cured composite wraps

APPENDIX 3 – STRAIN GAUGE INSTALLATION PROCESS (PHOTOS)

Figure 1: Pipe specimen before the surface cleaning

Figure 2: Hand Brush kits were used in the surface cleaning

Figure 3: A cleaned surface area yet to be scrubbed with Silicon Carbide Paper 220-grit and Conditioner A

Figure 4: Cleaning the surface using Neutralizer 5A and cotton swab

Figure 5: Cleaning the surface area with CG6-Isopropyl Alcohol (solvent degreaser) using gauze sponges

Figure 6: Neutralizing the back of tool case using Neutralizer 5A and gauze sponges

Figure 7: Mylar tape was stuck onto the strain gauge. The back of tool case was really helpful in this process

Figure 8: Positioning the gauge onto the steel surface using a Mylar tape

Figure 9: The bottom surface of strain gauge was smeared with M200 Catalyst
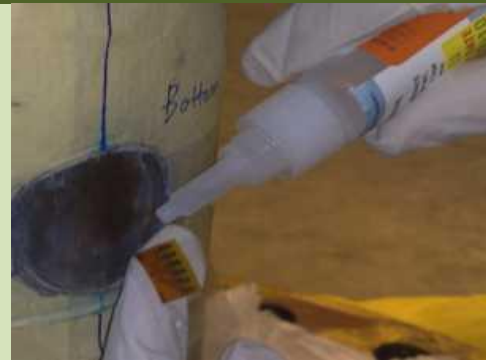

Figure 10: Then a drop of M-200 adhesive was applied at the bottom edge of strain gauge

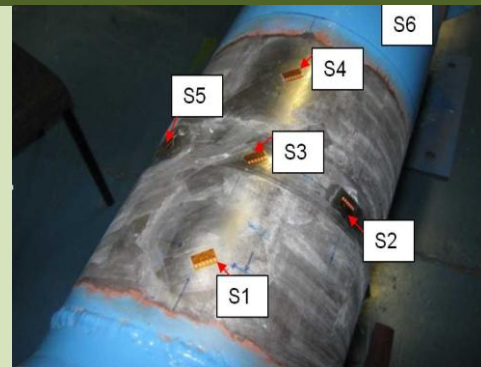Figure 11: A finger pressing for 2 minutes was gently applied on the strain gauge - ensuring a full bonding

Figure 12: The completed installation of strain gauges at different locations (all have a same resistance of 120 Ohm

Figure 13: Soldering the rectangular strain gauge to leadwires using Vishay Soldering Unit

Figure 14: Flushing out the flux residues right after soldering work using Rosin solvent

Figure 15: M Coat A was smeared onto the strain gauge - to prevent any moisture penetration

Figure 16: A complete strain gauges installation with leadwires

Figure 17: 1 and 5 % Accuracy test – Shift in grid resistance was less than 2% (means acceptable)

Figure 18: Leakage to ground testing – More than 20 000 MegOhm (means good installation)

Figure 19: Repeating the above procedures (surface preparation) on the composite material

Figure 20: Repeating the above procedures (coating and protection) on the composite material. For 4th and 8th. layers of composite wraps
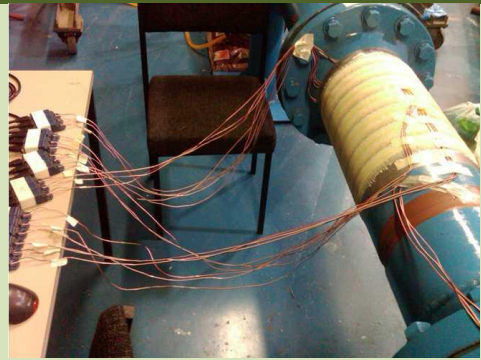

Figure 21: Data acquisition was carried out after the 4th. layer of the composite repair
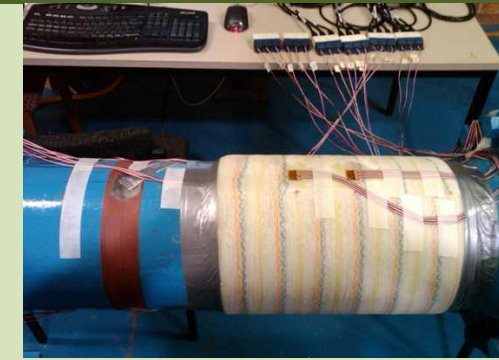

Figure 22: Data acquisition was carried out after the 8th. Layer of the composite repair
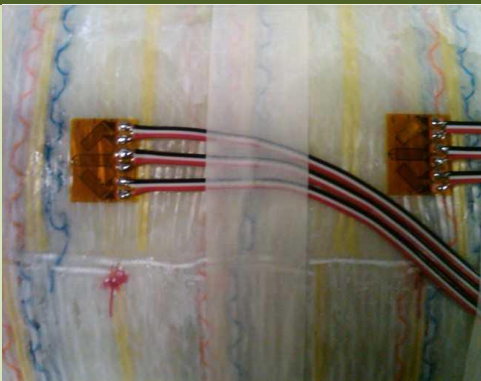

Figure 23: A close view of bonded Rectangular strain gauge rosettes on the composite material

Figure 24: A complete strain gauge tool kits was essentially required in order to produce a good strain measurement result

1) Electrical Insulation Test Results (Strain gauge type CEA-06-120CZ-120)

Location and Position (on steel pipe – 120 Ohm)		1% (actual)	1% (Manufacturer's spec)	Leakage to Ground
S1	S1a1	-0.12 %	± 0.4%	>20 GOhm
	S1a2	-0.02 %	± 0.4%	>20 GOhm
	S123	-0.08 %	± 0.4%	>20 GOhm
S2	S1b1	-0.2 %	± 0.4%	>20 GOhm
	S1b2	+0.1 %	± 0.4%	>20 GOhm
	S1b3	-0.24 %	± 0.4%	>20 GOhm
S3	S1c1	+0.1 %	± 0.4%	>20 GOhm
	S1c2	-0.04 %	± 0.4%	>20 GOhm
	S1c3	-0.03 %	± 0.4%	>20 GOhm
S4	S21	-0.06 %	± 0.4%	>20 GOhm
	S22	-0.04 %	± 0.4%	>20 GOhm
	S23	-0.26 %	± 0.4%	>20 GOhm
S5	S31	-0.12 %	± 0.4%	>20 GOhm
	S32	-0.06 %	± 0.4%	>20 GOhm
	S33	-0.14 %	± 0.4%	>20 GOhm
S6	Sd1	-0.24 %	± 0.4%	>20 GOhm
	Sd2	-0.06 %	± 0.4%	>20 GOhm
	Sd3	-0.06 %	± 0.4%	>20 GOhm

2) Electrical Insulation Test Results (Strain gauge type CEA-06-250UR-350)

Location and Position (on composite – 350 Ohm)		1% (actual)	1% (Manufacturer's spec)	Leakage to Ground
C1	C1a1	-0.2 %	± 0.4%	>20 GOhm
	C1a2	+0.02 %	± 0.4%	>20 GOhm
	C123	-0.06 %	± 0.4%	>20 GOhm
C2	C2b1	-0.08 %	± 0.4%	>20 GOhm
	C2b2	+0.09 %	± 0.4%	>20 GOhm
	C2b3	+0.1 %	± 0.4%	>20 GOhm
C3	C3c1	+0.03 %	± 0.4%	>20 GOhm
	C3c2	-0.03 %	± 0.4%	>20 GOhm
	C3c3	-0.24 %	± 0.4%	>20 GOhm
C4	C4d1	-0.04 %	± 0.4%	>20 GOhm
	C4d2	-0.06 %	± 0.4%	>20 GOhm
	C4d3	-0.15 %	± 0.4%	>20 GOhm